Nationaal Lucht- en Ruimtevaartlaboratorium
National Aerospace Laboratory NLR

Executive summary

Wind criteria due to obstacles at and around airports

Problem area
Wind, wake and turbulence induced by obstacles may affect the flight handling and performance of aircraft during take-off and landing. Therefore wind disturbance criteria are required. Because aircraft are much more vulnerable to disturbed wind velocity profiles during the final stage of the approach than during take-off the focus of the study was aimed on landing aircraft. Within the frame work of the wind disturbance study three altitude bands were defined according to their threat to safety:
Firstly, height between 0ft and 200ft. In this region flare, de-crab and high speed roll out takes place. Apart from prevailing gust and turbulence due to general surface characteristics, stand alone obstacles may play a dominant role in this part. From a safety point of view this is a critical phase.
Secondly, height between 200ft and 1000ft. Gust/turbulence levels due the build up area affecting the landing zone are dominant in this segment. Speed deficits and accompanying turbulence due to "stand alone" obstacles are submerged. From a safety point of view this phase is less critical.
Thirdly, height above 1000ft.
From a safety point of view wind disturbance above 1000ft is not considered a threat for flight safety.

Description of work
The investigation is focused on the effects of wind disturbances on the flight handling and landing performance of aircraft. This has been done by means of offline mathematical simulations. Two

Report no.
NLR-TP-2010-312

Author(s)
A.M.H. Nieuwpoort
J.H.M. Gooden
J.L. de Prins

Classification report
Unclassified

Date
July 2010

Knowledge area(s)
Veiligheid (safety & security)
Vliegoperaties
ATM & Airport operaties
Vluchtnabootsers

Descriptor(s)
Simulation
Safety
Meteorology
Flight Mechanics
Handling Qualities
Landing performance

aircraft types were chosen at the high and low end of the aircraft weight and inertia range viz. B747 and Fokker 100. A limited number of piloted moving base simulations has been executed to validate the offline results. Based on the simulations applicable wind disturbance criteria were defined.

Results and conclusions

The conclusions of the study for the defined segments can be summarized as follows:
For the segment that covers the approach flight phase from 1000ft AGL to 200ft AGL it appeared both from the offline and piloted simulations that the obstacle clearance planes defined by ICAO Annex 14 give sufficient protection with respect to wind disturbances due to “stand alone obstacles”.
For the segment that covers the landing phase from 200ft to touch down and the high speed roll out it was established that wind disturbance criteria are necessary that are more stringent than the “Annex 14” planes. The segment where the wind disturbance plane is restrictive is bounded by a disk-shaped segment with origin in the center of the runway threshold and radii of approximately 1200m (perpendicular to runway centerline) and 900m in front of the runway threshold. In order to cover the high-speed roll out the 1:35 plane is extended up to 1500m aft of the runway threshold.
The study also revealed a strong relation between surface roughness, reference wind speed and gust/turbulence levels. Surface roughness and reference wind speeds selected for the simulations lead to gust and turbulence levels varying from medium to severe.

Applicability

Legislation of planned constructions at and in the vicinity of airports.

Nationaal Lucht- en Ruimtevaartlaboratorium, National Aerospace Laboratory NLR

Anthony Fokkerweg 2, 1059 CM Amsterdam,
P.O. Box 90502, 1006 BM Amsterdam, The Netherlands
Telephone +31 20 511 31 13, Fax +31 20 511 32 10, Web site: www.nlr.nl

Nationaal Lucht- en Ruimtevaartlaboratorium
National Aerospace Laboratory NLR

NLR-TP-2010-312

Wind criteria due to obstacles at and around airports

A.M.H. Nieuwpoort, J.H.M. Gooden and J.L. de Prins[1]

[1] Aerospace Software & Technologies Institute

Customer	DGTL
Contract number	05.004873
Owner	DGTL
Division	IVW
Distribution	Unlimited
Classification of title	Unclassified
	July 2010

Approved by:

Author	Reviewer	Managing department
ND 8/7/10	10-8 2010	b.a. 8/7-2010

Summary

This report deals with the effects of wind disturbances behind obstacles on a landing aircraft. Because aircraft are much more vulnerable to disturbed wind velocity profiles during the final stage of the approach than during take-off ([9] only the effects on approaching aircraft have been considered.
Based on the investigation wind disturbance criteria have been defined.

To limit the scope of the study two ground segments were defined in which obstacles may affect the handling and performance of an aircraft on the glide path. The glide path parts covered by these two ground segments range from 1000ft AGL to 200ft AGL and from 200ft AGL to touch down. For altitudes above 1000ft AGL it is assumed that wind disturbances from a safety point of view present no direct hazard to an approaching aircraft. The area which covers the height band above 1000ft is indicated yellow in the figure below.

1. **Planned constructions in the vicinity of the runway threshold.** Wind disturbance will be caused by the speed deficit and induced turbulence as result of the shading of a "stand alone" obstacle in combination with the prevailing gust/turbulence conditions. The effect of this is perceptible during the last part of the final approach (below 200 ft), during the flare and the high-speed roll out. This sector is defined in the figure below as the **green** area.

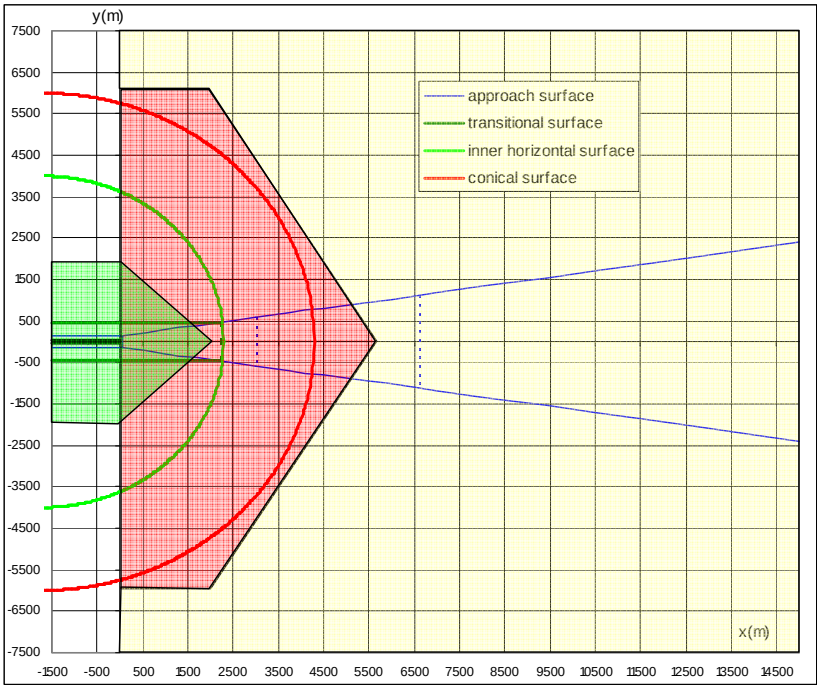

2. **Planned constructions in a sector outside the above-mentioned area**. Wind disturbances then are not directly caused by the wake induced by a “stand alone” obstacle but are the result of the prevailing turbulence intensity due to the build up area that affects the runway threshold zone. The turbulence intensity is a function of the surface roughness parameter (z0) and a reference wind speed. The effects of this are perceptible during final approach in the altitude band of 200ft to 1000 ft. This sector is defined in the figure as the **red** area.

In the figure also the ground projection of the various obstacle clearance intersection lines defined in ICAO Annex 14 ([11] is drawn.

The investigation is aimed at the effect of wind disturbances (wind, shears, gusts and turbulence) on the response and landing performance of aircraft. This was done mainly by means of offline mathematical simulations. Two aircraft types have been used at the high and low end of the aircraft weight and inertia range viz. a Boeing 747 and a Fokker 100. A limited number of piloted moving base simulations with the B747 have been performed to validate the offline results by means of pilot ratings.

The National Aerospace Laboratory (NLR) and the Aerospace Software & Technologies Institute (ASTI) of Delft University of Technology (TUD) have performed the work in response to the DGTL call for tender presented in ([1].

The study was able to refine the above-mentioned segments and to define wind disturbance planes, which are in the immediate vicinity of the runway more restrictive than the ICAO Annex 14 obstacle clearance planes.

The conclusions of the study for the considered glide path segments can be summarized as follows:

- **The variation in mean wind speed due to wind disturbing structures must remain below 7 knots <u>along the aircraft trajectory</u> at heights below 200ft. The speed deficit change of 7 knots must take place over a distance of at least 100m.**
- **The variation in mean wind speed due to wind disturbing structures must remain below 6 knots <u>across the aircraft trajectory</u> at heights below 200ft. The speed deficit change of 6 knots must take place over a distance of at least 100m.**

This results in the following guidelines as far as obstacles are concerned:

1. **The glide path segment that covers the approach from 1000ft AGL to 200ft AGL**.
   a. <u>"Stand alone" obstacle.</u>
      No distinct effect of "stand alone" obstacles on the aircraft handling and performance could be established in this height range. The effect is submerged in the overall surface characteristics of the build up area affecting the runway. The offline and piloted simulations showed that the obstacle clearance planes defined by ICAO Annex 14 give sufficient protection to wind disturbances as result of "stand alone" obstacles. No specific wind disturbance planes are required for this segment.
   b. <u>Surface roughness.</u>
      In this altitude range the wind disturbance effect on the aircraft is defined by the turbulence intensity applicable for build up area affecting the runway. It is a function of the surface roughness and a reference wind speed.
      The offline and piloted simulations showed that RMS values of the turbulence intensity in excess of 5kts (heavy turbulence) sometimes lead to too large glide path deviations as result of gust and wind shear phenomena.
2. **The glide path segment that covers the landing phase from 200ft AGL to touch down and the high speed roll out.**
   a. <u>"Stand alone" obstacle.</u>
      In this height range a distinct effect of "stand alone" obstacles on the aircraft handling and performance could be established.
      For this segment wind disturbance criteria are necessary that are more stringent than the ICAO "Annex 14" planes. It appeared that "stand alone" obstacles in a disk-shaped area with origin in the center of the runway threshold and radii of approximately 1200m (perpendicular to runway centerline) and 900m in front of the runway threshold and not protruding an imaginary plane with a slope of 1:35 with the extended runway centerline as base did not affect the response and performance of the aircraft significantly. In order to cover the high speed ground roll the 1:35 plane is also applicable up to 1500m beyond the runway threshold.
   b. <u>Surface roughness.</u>
      Also in this height range the aircraft handling and performance is affected by the turbulence intensity applicable for the build up area preceding the runway on which the aircraft lands.
      The offline and piloted simulations showed that RMS values of the turbulence intensity less than 4kts (medium/heavy turbulence) due to the surface roughness in the vicinity of the landing area in combination with the speed deficit and induced speed gradients of "stand alone" obstacles limited by the 1:35 plane did not lead to unacceptable aircraft handling and landing performance.

Because the 1:35 plane is a practical interpretation of the 7kts criterion this means that the study has reconfirmed the 7kts criterion for “stand alone” obstacles. However, in the Annex 14 obstacle clearance planes the criterion only has to be applied to a defined area in front and aft of the runway threshold. Outside this area no specific wind disturbance criteria for “stand alone” obstacles are required.
In addition to the 7kts criterion, this research has formulated the gust/turbulence levels at which aircraft handling and landing performance will be significantly deteriorated.

The segment where the wind disturbance plane is restrictive for “stand alone” obstacles is shown as the **green** area in the figure shown hereafter.

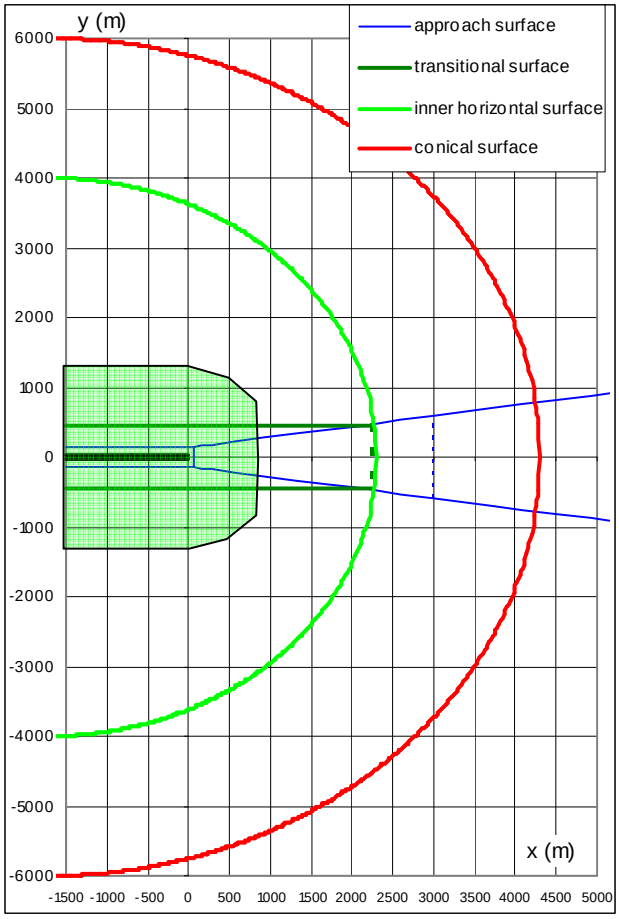

Contents

List of figures

List of tables

Abbreviations

AGL	Above Ground Level
ANOVA	Analysis of Variance
AOM	Aircraft Operating Manual
AP, A/P	Autopilot
APP	Approach
AQAP	Allied Quality Assurance Publication
ASTI	Aerospace Software & Technology Institute
ATS, A/T	Auto throttle
AWO	All Weather Operations
b	Aircraft span [m]
CAS	Calibrated airspeed
CG	Centre of Gravity
C-H, C/H	Cooper-Harper
CL	Centre line
DGTL	Directoraat Generaal Luchtvaart (Dutch Directorate General of Civil Aviation)
DLTA	Aileron deflection [deg]
DLTR	Rudder deflection [deg]
DME	Distance Measuring Equipment
DNW	Duits Nederlandse Windtunnel
ESDU	Engineering Science Data Unit
FAA	Federal Aviation Administration
FAS	Final approach speed in IAS [knots]
Fav	Average acceleration in shear intensity curve [g]
g	Acceleration of gravity [m^2/s]
GA	Go-Around
G/S	Glide slope
GRACE	Generic Research Aircraft Cockpit Environment
Hobst	Height of obstacle [m]
Href	Height above ground were reference wind speed is measured [m]
HRW	Height of CG above the ground [ft, m]
IC	Initial Condition
ICAO	International Civil Aviation Organization
IVW	Inspectie Verkeer en Waterstaat (Transport and Water Management Inspectoraat)
ILS	Instrument Landing System

ISO	International Standard Organization
Ixx, Iyy, Izz	Aircraft inertias (kgm2)
Ixz, Ixy, Iyz	Aircraft products of inertia (kgm2)
JAA	Joint Aviation Authorities
JAR	Joint Aviation Requirements
KNMI	Koninklijk Nederlands Meteorologisch Instituut
LDG	Landing
LIB	Luchthaven Indelings Besluit
LOC	Localiser
LST	Low Speed Tunnel
Mph	Miles per hour
NASA	National Aeronautics and Space Administration
NAV	Navigation
NLR	National Aerospace Laboratory NLR
OLS	Obstacle Limiting Surfaces
OWE	Operational Weight Empty
p	Effective porosity of obstacle (- , %)
PAPI	Precision Approach Path Indicator
PDP	Proef Draai Plaats (Engine test run facility)
PFD	Primary Flight Display
PSD	Power Spectral Density
PHI	Bank angle [deg]
RFP	Request for proposal
RMS	Root Mean Square, Standard deviation
SD	Standard Deviation
Sgmu, Sgmv, Sgmw	Standard deviation of turbulence in three directions (kts)
LU, LV, LW	Scale lengths of turbulence in three directions (m)
TAS	True airspeed (m/s, knots)
T,t	time [sec]
T/H	Threshold of runway
TD	Touch Down
TSO	Technical Standard Order
TUD	Technical University of Delft
Vgust	Gust speed (knots)
VMC	Visual Meteorological Conditions
V/S	Vertical speed of aircraft [ft/sec]
VHF	Very High Frequency
Vwind	Wind speed at height HRW

Vwind ref	Reference wind speed at 10m height (knots)
Vs	Stall speed
V20	Reference wind speed at 20ft height
V10	Wind speed at 10m height
VOR	VHF Omni-directional Range
Vw	Mean wind speed at specific height in boundary layer
WP	Work package
Xa	Distance to runway threshold (m)
XPATHN	Distance downstream, normal to the obstacle, measured parallel to the ground [m]
XRW	X-coordinate in runway axes system along extended runway centerline with origin on the runway T/H and positive in runway direction [m,ft]
YPATHN	Lateral distance measured along obstacle [m]
YRW	Y-coordinate in runway axes system, lateral deviation from runway centerline, positive in right-hand direction [m,ft]
ZPATHN, HRW	Height of CG above the ground [m, ft]
z0	Average surface roughness parameter for site terrain, average over some km's upstream of obstacle

Greek symbols:

$\sigma_u, \sigma_v, \sigma_w$	Standard deviation of u,v,w-component of turbulence, [m/s]

1 Introduction

This report deals with the effects of wind disturbances caused by man made structures (in this report called obstacles) on aircraft during approach and landing. Because aircraft are much more vulnerable to disturbed wind velocity profiles during the final stage of the approach than during take-off ([9] the study focused on the approach and landing phase.
Based on the investigation wind disturbance criteria have been defined.

Based on ([1] two areas have been selected in which buildings or obstacles may affect the handling and performance of landing aircraft.

1. Constructions in the vicinity of the runway threshold. Here in addition to the prevailing gust/turbulence level wind disturbances may be enlarged by “stand alone” obstacle shading and the evoked increase in gust/turbulence levels. The effect of this is perceptible during the last part of the final approach (below 200ft), during the flare and the high-speed roll out. The sector in which “stand alone” obstacles may produce wind disturbances that affect the aircraft handling and performance significantly below 200ft is shown schematically in Figure 1-1 as the ***green*** area.
2. Constructions in a sector outside the above mentioned area. Wind disturbances due to obstacles situated in this sector are mainly the result of the turbulence intensity, which is a function of the so-called surface roughness parameter (z0) and a reference wind speed. Effects due to “stand alone” obstacle shading in this area submerge in the overall surface characteristics. This area produces wind disturbances, which affect aircraft on a higher part of the glide path, viz. between heights of 200ft to 1000ft. It is shown in Figure 1-1 as the ***red*** area.

Outside the ***green*** and ***red*** area (***yellow*** area in Figure 1-1) wind disturbances due to buildings/obstacles affect aircraft on the glide path above a height of 1000 ft. Wind disturbances due to buildings/obstacles are considered not critical with respect to aircraft safety above this height. The area which covers the height band above 1000ft is indicated yellow in Figure 1-1. The subdivision of the segments presented in Figure 1-1 is based on simple geometry and is only a first estimation of the areas in which obstacles may affect the handling and performance of aircraft on the glide path. Results from the study will be used to refine the mentioned sectors.

The core of the investigation is aimed at the effect of wind disturbances (wind, shears, gusts and turbulence) on the response and performance of landing aircraft. This is done mainly by means of offline mathematical simulations. Two aircraft types have been used at the high and low end of the aircraft weight and inertia regime viz. the Boeing B747 and Fokker 100.

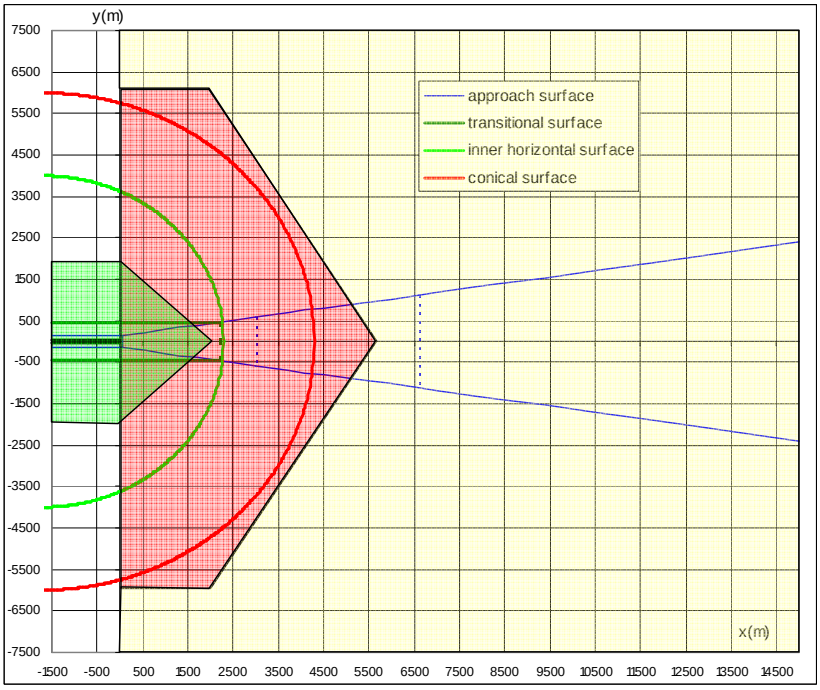

Figure 1-1: Definition of sectors in which wind disturbance affects landing aircraft

A limited number of piloted moving base simulations have been performed with the B747 to validate the offline results by means of pilot ratings.
By combining the objective (recorded data) and the subjective data (pilot comments) a more balanced conclusion has been obtained.

Both the wind disturbance field in the direction of flight (wind shear phenomena) and perpendicular to the direction of flight (crosswind deviations) as well as the impact of gust and turbulence on aircraft handling and performance has been taken into account.

In ICAO Annex 14 ([11] obstacle clearance surfaces are defined to reduce the collision probability of aircraft with obstacles in the vicinity of a runway.

The Annex 14 surfaces mentioned in Figure 1-1 are defined as follows:

Inner horizontal surface

This is a surface located in a horizontal plane above an airport and its environment.

Transitional surface

This is a complex surface along the side of the strip and part of the side of the approach surface that slopes upwards and outwards to the inner horizontal surface.

Approach surface

This is an inclined plane preceding the threshold.

Approach surface
This is an inclined plane preceding the threshold.

The data for the dimensions and slopes corresponding to the above-mentioned planes are presented in Table 1–1 for an aero plane reference field length of more than 1800m and a 45m width runway.

Table 1–1: Dimensions and slopes of obstacle limitation surfaces (landing & approach)

	non-instrument runway	non-precision approach	precision approach cat I	precision approach cat II + cat III
inner horizontal	height: 45m radius: 4000m	height: 45m radius: 4000m	height: 45m radius: 4000m	height: 45m radius: 4000m
transitional	slope: 14.3%	slope: 14.3%	slope: 14.3%	slope: 14.3%
approach	length of inner edge: 150m distance from threshold: 60m divergence (each side): 10% length: 3000m slope: 2.5%	length of inner edge: 300m distance from threshold: 60m divergence (each side): 15% length: 3000m slope: 2.0%	length of inner edge: 300m distance from threshold: 60m divergence (each side): 15% length: 3000m slope: 2.0%	length of inner edge: 300m distance from threshold: 60m divergence (each side): 15% length: 3000m slope: 2.0%

The ground projection of the various obstacle clearance intersection lines defined in Annex 14 is included in Figure 1-1.

The aim of this investigation is to define planes from a perspective of the wind disturbance hazard in addition to the obstacle clearance planes. If constructions are planned within the defined wind disturbance planes then no problems in aircraft handling are expected. However if proposed constructions exceed a minimum width and protrude the wind disturbance planes a potential problem may arise. Through simulation and testing it must then be demonstrated that e.g. because of a more refined shape of the construction the evoked wind disturbance does not violate the acceptance criteria as derived for the worst-case block-shaped obstacle with height limited by the wind disturbance plane used for the norm definition.

References ([3] to ([9] are NLR documents that yield earlier research related to crosswind operations and wind climates.

The investigation comprehended six successive work packages, which are described in ([2]:

- WP1: Inventory
- WP2: Modeling wind disturbances due to obstacles
- WP3: Offline computer simulations
- WP4: Correlation of results
- WP5: Validation of wind disturbance criteria on GRACE
- WP6: analysis and reporting

NLR divisions that participated in the research have ISO 9001/AQAP 110 standards approval. The National Aerospace Laboratory (NLR) and the Aerospace Software & Technology Institute (ASTI) of Delft University of Technology (TUD) have performed the work in response to the DGTL call for tender presented in ([1].

The report is organized as follows. In section 2 the scope of the investigation is defined into more detail. Section 3 gives an overview of the wind, gust and turbulence characteristics in the earth boundary layer. The wind climate models behind obstacles required for the simulations are discussed in section 4. Section 5 deals with acceptance criteria required for the offline and piloted simulations. The offline simulations performed with the Fokker 100 and Boeing B747 aircraft are described in section 6. The simulator experiment with the B747, which was carried out on NLR's six degrees of freedom research flight simulator GRACE in March 2006, is presented in section 7. The results and proposed wind disturbance criteria are presented in section 8. Finally conclusions and recommendations are given in section 9.

2 Scope of the investigation

2.1 Introduction

The approval procedure for planned constructions at or in the vicinity of airports takes place according to several guide lines and recommendations.
The position and height of the planned construction is verified with the so-called “Obstacle Limitation Surfaces (OLS)” laid down in ICAO Annex 14, Aerodromes ([11].
During the assessment of a planned building also arrival and departure procedures applicable for the airport are considered. This because planned buildings may not interfere with electronic and visual landing aids and beacons such as ILS and VOR/DME. Finally the minimum flight safety altitude within the vicinity of the airport has to be addressed when assessing a new construction proposal.
For Schiphol and the vicinity of the airport the height restrictions of buildings are laid down in chapter 8 of the aviation law called “Luchthaven indelings besluit (LIB)”.
Wind disturbances due to (new) constructions are not part of this legislation. However the Schiphol legislation will be re-assessed. Part of this re-assessment is to see if the obstacle clearance planes have to be adapted for wind disturbances.
It is known from pilot reports that in certain meteorological conditions, constructions meeting the obstacle limitation surfaces but located nearby the approach paths of aircraft can cause wakes, vortices and turbulence that are disturbing to air traffic. The consequence may be the execution of a missed approach or in general will have a negative effect on aircraft safety.
At this moment the so-called 7-knots criterion is used for the approval procedure of planned constructions. In practice it means that buildings protruding an imaginary plane with a slope of 1:35 with the extended runway centerline as base are submitted to further investigations. The foundation for the criterion however is small because it is based on a relatively small number of pilot incident reports.
Therefore a need is present to qualify and quantify the wind disturbance more clearly such that it can be part of the evaluation procedure in addition to the existing ICAO guidelines.
Consequently IVW-DL chartered by DGTL issued a RFP for an investigation to formulate wind disturbance criteria due to structures planned at and around airports.
The investigation based on this RFP has been done by means of available mathematical models of representative aircraft in offline computer simulations. In addition a moving base flight simulator experiment was executed to verify the offline results.
From the offline computations the most safety critical cases were determined, hereby reducing the number of pilot-in-the-loop simulations.

2.2 Existing criteria

2.2.1 Introduction

Wind disturbance due to structures (obstacles) and the effect of this on the handling and performance of aircraft did not get much attention because structures were located far away from the runways. Because of the increasing expansion of airport related activities more and more obstacle congestion occurs near and at airfields. Although construction height restrictions apply by law, in recent years the number of buildings situated relatively close to active runways has increased substantially.

2.2.2 7kts criterion

In the Netherlands the cause for a number of tests and studies related to wind disturbances due to structures near runways has been an engine test run facility for wide body aircraft located on Amsterdam Airport Schiphol. This facility is situated close to the threshold of runway 27 and 22. A plan view is shown in Figure 2-1.

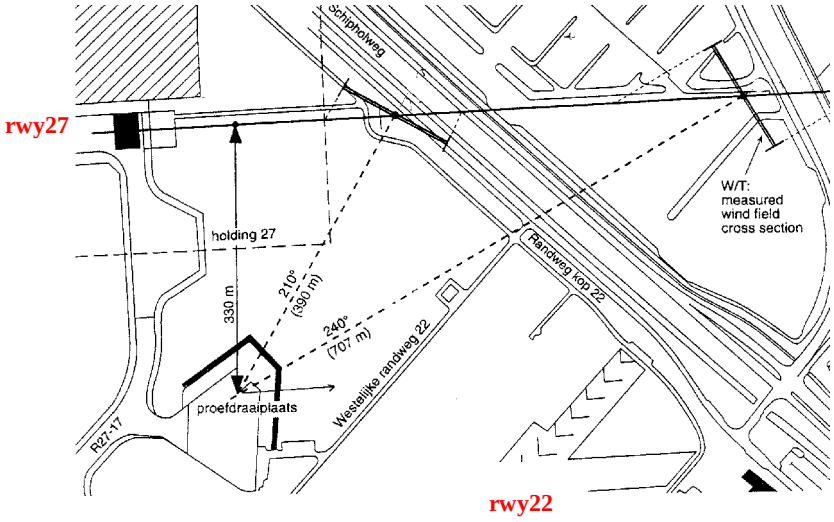

Figure 2-1: Position of PDP near runway 27 and 22

A number of pilots reported heavy disturbances at low heights under strong south-westerly winds landing on these runways. Studies performed in ([5], ([6] and ([7] lead to the conclusion that the main problem was caused by the strong viscous wake behind the facility in which the wind speeds were reduced significantly. Also the variation in cross wind during the last stage of the approach appeared to be a significant disturbing factor to aircraft. At present there is no generally accepted criterion, which describes the allowed distortions in the wind field behind buildings located close to runways. For authorities it is therefore difficult to assess the effect of the wind flow around obstacles in relation to possible effects on flight safety. Based on the

limited amount of pilot reports, wind tunnel and simulator tests ([6] NLR was able to draft a pragmatic solution, which was called the 7kts criterion. It is related to the maximum lateral wind speed defect that occurs behind an obstacle and is defined as follows:

"The difference in wind velocity perpendicular to the aircraft over a short interval may not exceed 7kts"

The wind speed defect in longitudinal direction is not included in this criterion. Also the shape and the width of the wake are not accounted for. Furthermore nothing is said about the corresponding gust and turbulence levels that obviously will affect aircraft handling. Therefore it was recognized that more study was required to obtain better insight into the phenomena, which would lead to a more balanced and well-founded criterion. From the investigation a new criterion could evolve but also an adaptation or a reconfirmation of the present 7kts criterion is possible.

2.3 Objectives

The objectives of the work described in this report are:

- To collect objective performance data during offline simulated auto land approaches flown in strong gusting crosswind conditions with and without the presence of obstacles.
- To collect objective performance data and pilot subjective workload data and acceptance ratings during a limited number of pilot-in-the-loop approaches flown in strong gusting crosswind conditions with and without the presence of obstacles.
- To arrive at a criterion for planned buildings/structures, based on the offline simulations and the assessment of five highly qualified pilots, whether the changed wind climate due to an obstacle is acceptable or not from a flight technical point of view.

2.4 Boundaries and limitations

Through this study more insight is obtained into the controllability and safety of an aircraft during landing under the influence of obstacles.
However, in order to focus the investigation a number of choices were required to complete the investigation in limited time. It is expected that these choices resulted in the worst-case situation and will not further limit the obstacle planes. In consultancy with the contractor, the following limitations to the investigation have been made:

- Tail wind components are not present.
- The wind direction is perpendicular towards a "stand alone" obstacle. Thus effects due to a non-perpendicular wind flow are no part of this investigation. Through this assumption symmetric flow patterns streaming from the obstacle can be postulated.
- Turbulence and wind shear are dependent on the ***total*** wind speed.

- The F100 offline simulations and piloted B747 simulations only address generic “worst-case” block-shaped obstacle characteristics in which variations in the wind field at the two corners of the obstacle are taken into account. The offline B747 simulations also encompassed simulations in which less critical “regular” block-shaped obstacles were implemented.
- A “worst case” obstacle width is assumed.
- No mechanical failures (e.g. engine) are introduced to the aircraft during the approach/landing.
- Only dry runway conditions are considered.
- Good visual conditions (20 miles) prevailed during the piloted simulations.
- Maximum cross wind in the investigation is limited to 20 knots.
- The work is tailored to two jet aircraft equipped with conventional controls. Propeller driven aircraft and Fly-By-Wire aircraft as well as Very Large Aircraft have not been evaluated. However in section 9 possible consequences are elaborated on.
- The results apply to a neutral atmosphere including strong winds in excess of 15 knots. Convective effects as result of the local heating of the earth surface by the sun have not been taken into account.
- High speed roll out, take-off and go-around were no part of the investigation.

3 Wind, gust and turbulence in the earth boundary layer

3.1 Introduction

Wind phenomena can be divided into a number of categories: mean wind, wind shear, discrete gusts and turbulence. Mean wind and turbulence are statistical parameters that are related to each other. Gust is defined as a discontinuous momentary change in wind speed and direction. Turbulence is characterized by very irregular wind flows. The following graph shows the wind phenomena as function of their frequency in relation to their effect on an aircraft.

Increasing frequency →			
Mean Wind	**Wind shear**	**Gust**	**Turbulence**
Performance	Performance Controllability	Controllability	Nuisance
	Structural loads	Structural loads	Fatigue

In this section the atmospheric conditions present in the earth boundary layer will be addressed, whereas section 4 deals with the specific wind climate behind an obstacle.

3.2 Mean wind

The wind at heights well above the surface of the earth is directed along lines of equal pressure. This is called the gradient wind and its magnitude is unaffected by the roughness of the earth's surface. At the surface of the earth horizontal drag forces, induced by ground obstacles, are exerted on the wind flow causing it to slow down. This force decreases with increasing height above the ground and becomes negligible at the gradient height where the wind speed first reaches the gradient wind value. For strong winds the gradient height depends on terrain roughness and the strength of the wind. It can vary from about 250m over smooth terrain to 400-500m over an extremely rough city terrain. This is shown in Figure 3-1 for a common gradient wind of 100 mph (86 knots).

The region between the ground and the gradient height is known as the atmospheric boundary layer in which the wind speed progressively increases with height. The variation of the mean wind speed from the ground to the gradient height can be approximated by a number of mathematical expressions of which the power law and logarithmic law are well known ([23]. They are valid for strong winds associated with fully developed weather systems in which the assumption of a neutrally stable atmosphere is valid.

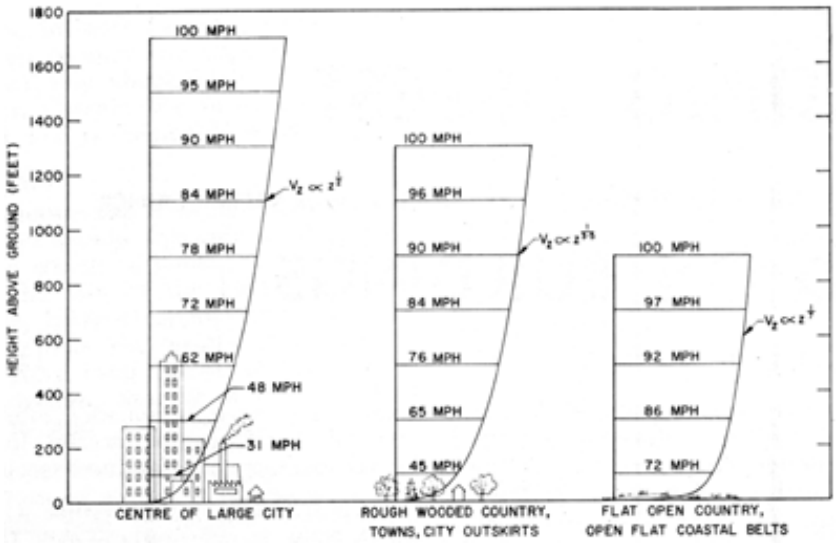

Figure 3-1: Mean wind speed profiles for three surface roughness parameters

The logarithmic law is of the form:

$$Vw = Vwref * \frac{\left[\ln(h/z0) + fctgrd\right]}{\ln(Href/z0)} \qquad (3.1)$$

In (3.1) "$Vwref$" is the mean wind speed at a defined reference height "$Href$". "$z0$" is the surface roughness length which is a measure of the retarding effect that the surface has on the wind speed near the ground. The parameter "$fctgrd$" in (3.1) is included to make the wind speed constant at the gradient height ([24].

Mean wind speed profiles according to (3.1) are plotted in Figure 3-2 for three surface roughness values. They are related to a runway scenario of a fixed cross wind of 20kts at $Href$ =10m.

"$z0$" values representative for various surface conditions are presented in Table 3–1 ([24]. The $z0$ band of interest for aircraft operations considered in this investigation is framed in red. According to this source the surface roughness for runway areas at airports lies between .003m and .004m.

The wind profiles depicted in Figure 3-2 apply to surface roughness values defined in Table 3–1 viz. **flat desert (z0 =.001m), open farmland (z0 =.01m**) and **hedged farmland (z0 =.1m)**.

As can be observed from (3.1) and Figure 3-2 the wind profiles for all three surface roughness lengths correspond to a mean wind speed (23 knots) at the reference height ($Href$ =10m).

In addition to the mean wind speed also the X-wind and head wind component are plotted in Figure 3-2. At the reference height a head wind component of 12kts can be observed.

As shown the wind profiles in Figure 3-2 are linked to the wind speed present at the reference height. Consequently at the gradient height, different wind speeds result for different z0 values.

Table 3–1: Overview of values of surface roughness z0 ([24]

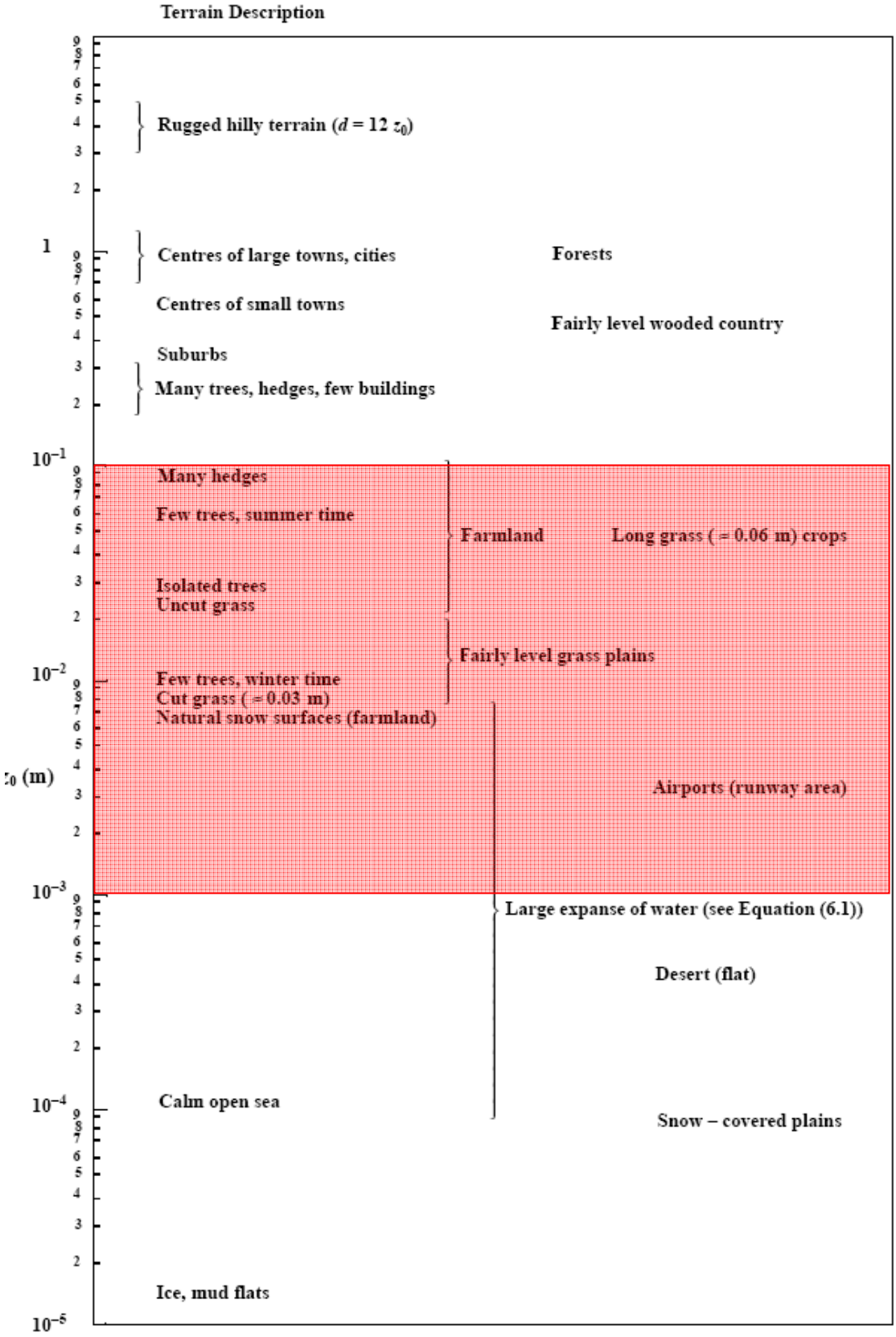

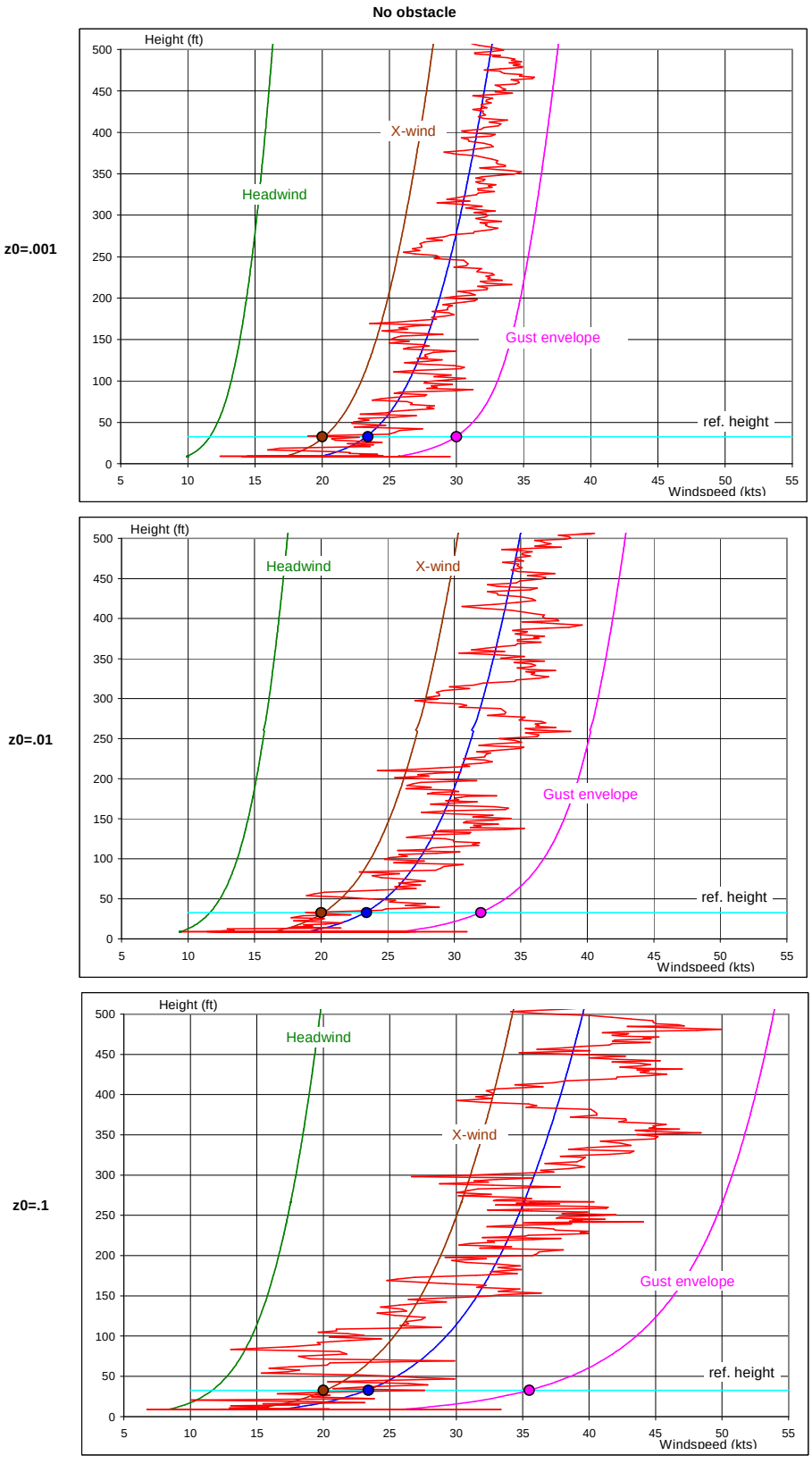

Figure 3-2: Wind profiles for 3 surface roughness parameters

This is contrary to the profiles shown in Figure 3-1 which originate from a common wind speed at the gradient height. In this study the modeling according to 3.1 is used because of the relevance of the measured reference wind speed near the runway threshold, which is radioed to the pilots during their final approach.

3.3 Gust and turbulence

The velocity of near surface winds is constantly changing. Fluctuations in direction and in speed occur every minute. Consequently the mean wind flow is accompanied by varying amounts of shears as the wind is broken up by the surface roughness into gusts and turbulence. As with the mean wind speed the turbulence depends on the type of terrain and is greater in urban areas than in open country. From measurements it appears that the magnitude of the gusts increases with the mean wind speed.

Theoretically the gust/turbulence due to the shearing effect becomes negligible at the gradient height. However the intensity of the turbulence is also affected significantly by the thermal stability of the air. Cold surface air tends to damp out mechanical turbulence. Heated surface air tends to rise and to increase turbulence. When the wind is strong, the air near the surface becomes thoroughly mixed and the thermal stability becomes neutral. Under these conditions temperature differences are such that they neither damp out nor increase the mechanical turbulence caused by surface roughness.

The mean wind is constant for the wind averaged over a specified period of wind measurement. The error in the mean wind is defined as turbulence. The characteristics of turbulence are determined by scale length (band width) and standard deviation (intensity). The turbulence intensity is defined as the quotient of the standard deviation (root mean square) and the momentary mean wind speed. The **turbulence intensity** is not constant because of the change in mean wind speed with height. The **turbulence intensity** is also reflected in the variations in wind direction. In smooth terrain the wind direction fluctuates through ±20dg typically and ±40dg maximum. In rough city terrain the fluctuation is ±60dg typically and peak fluctuations correspond to a complete reversal of the wind flow direction.

In ([25] a gust speed envelope is derived based on the **turbulence intensity** and the so-called **peak factor**. The **turbulence intensity** is dependent on the surface roughness length (z0) and the height above the ground. The **peak factor** is a function of height, gust duration and the observation period over which the wind speed is measured.

The ratio between the maximum gust speed (envelope) and the mean wind speed is called the gust factor. In ([25] the **gust factor** is defined as follows:

$$\textbf{Gust factor} = \textbf{Vgust/Vwind} = 1 + \textbf{peak factor} \times \textbf{turbulence intensity} \qquad (3.2)$$

The maximum gust profile (gust envelope) is also shown in Figure 3-2. It must be realized that this is a profile of the envelope of peak gust speeds rather than the profile at a particular time. Instantaneous wind speed profiles including gust/turbulence as function of height might evolve as is shown in Figure 3-2 (red curve).
For a fixed reference wind speed[1)], Figure 3-2 clearly shows the substantial effect of the surface roughness parameter on the mean wind speed profile and the corresponding gust envelope.
Table 3–2 shows wind speeds and corresponding gust factors obtained from Figure 3-2 applicable for a height of 200 ft.

Table 3–2: Wind speeds as function of surface roughness

Values at 200 ft **Mean wind: 23 knots**	z0 (m)	Mean wind speed (knots)	Max. gust speed (knots)	Gust factor (-)
flat desert	.001	28.5	35	1.23
open farmland	.01	30	39	1.3
hedged farmland	.1	33	48	1.45

Figure 3-2 shows large shear effects as function of height for the wind speed profile corresponding to the "**hedged farmland**".

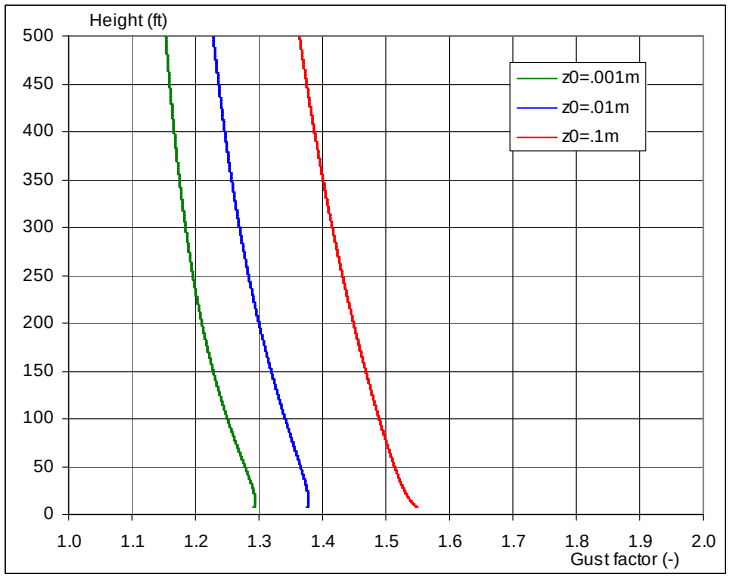

Figure 3-3: Gust factor as function of height (no obstacle)

For the wind profiles in Figure 3-2 **gust factors** as function of height are presented in Figure 3-3. Gust factor values range from approximately 1.15<->1.36 at a height of 500ft to values of

[1)] The reference wind speed is measured at a height of 10m and is representative for the threshold area of the runway

1.3<->1.5 close to the ground. In strong, turbulent wind conditions, **gust factors** are typically 1.3 over open sea, 1.6 over open country and 2 or greater over very rough terrain.
When the wind has blown over a fetch of at least 100km of uniform terrain the boundary layer is in equilibrium with the underlying surface i.e. the wind and gust profile does not change with increasing distance. However it is exceptional that a sufficiently long upwind fetch of uniform terrain occurs for an equilibrium boundary layer to exist. Examples are open sea, large plains and extensive forests.
Immediately downwind of a change in terrain roughness, such as the edge of a town, a new internal layer starts to grow. This is schematically shown in Figure 3-4. Within this new layer the flow is not in equilibrium and the wind profile and its turbulence characteristics change as the distance behind the change in terrain roughness increases. Above the internal layer it can be assumed that the wind profile is independent again from the distance and equal to the value just upwind of the roughness change. A change in surface roughness causes changes in the profiles of mean wind speed and gust/turbulence. Consequently the gust speed also changes with the distance downwind of the roughness change up to a particular distance where equilibrium conditions are again established.
The change in surface roughness shown in Figure 3-4 introduces an increase in wind shear effects and turbulence levels.

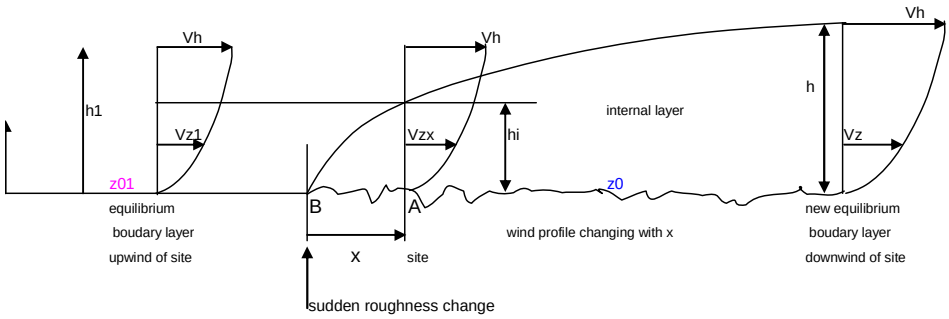

Figure 3-4: Wind profile as function of distance behind change of surface roughness

3.4 Wind shear

Air flow in the boundary layer is normally turbulent to some degree but such turbulence does not significantly alter the aircraft's flight path. Practically all turbulence hazardous to flight is a result of **wind shear**, a sudden *"variation in wind along the flight path of a pattern, intensity and duration that displaces the aircraft abruptly from its intended path."* The **shear is the rate of change of wind speed and direction** and its effect on flight can range from inconsequential to extremely hazardous.

The wind shear hazard arises from:

Vertical shear which is the change in horizontal wind velocity with height. i.e. as the aircraft is climbing or descending.

Horizontal shear is the change in horizontal wind velocity (i.e. speed and/or direction – gusts and lulls) with distance flown.

Horizontal speed defects, up draughts and downdraughts will impact the angle of attack of an aircraft flying into them. A horizontal speed defect in combination with a vertical downdraught can cause an aircraft to sink rapidly and can also impose high structural loads on the aircraft. If such gusting/turbulence occurs when an aircraft is flying near the surface, particularly in take-off and landing, it may place the aircraft in a dangerous situation. The closer to the surface that the shear occurs the more hazardous it will be for aircraft, particularly for aircraft with low momentum. The shear may be large and rapid enough to exceed the airspeed safety margin and the aircraft's capability to accelerate or climb.

3.5 Effects on aircraft response

Frequencies affecting flight handling range between .5 and 2.5 rad/sec (.08 and .4 Hz). Consequently scale lengths of turbulence defined by this frequency range are important for aircraft control issues.
At lower frequencies the effect on control becomes less prominent, however then aircraft performance becomes affected. In this lower frequency band wind shear phenomena play an important role. Wind shear in the horizontal plane is characterized as a change in speed of 20 knots or more for a time period of at least 5 seconds.
From a flight handling point of view near the vicinity of the ground unique and complex flight conditions occur. Just before and during the flare accurate control of the flight path is required because the width of the runway is small whereas large changes in both strength and direction of the wind may occur. In addition precise control of the roll attitude of the aircraft is required. In particular this applies to large wing-mounted engine configurations where a nacelle ground-strike is possible. Therefore both handling and performance are at stake during final approach in strong wind conditions.
As has been discussed a number of variables are present in the models describing the characteristics of the atmosphere in the boundary layer. Key parameters are the wind speed at the reference height (Vwind ref), the surface roughness (z0), the standard deviation of the turbulence (related to the turbulence intensity) and the scale length. Figure 3-5 shows the relationship between the surface roughness and the standard deviation of horizontal turbulence (sgmu, sgmv) as function of the wind speed at the reference height according to Appendix B.

The same relationship is found from ([25]. Also indicated in the figure are values of correlated turbulence intensities.

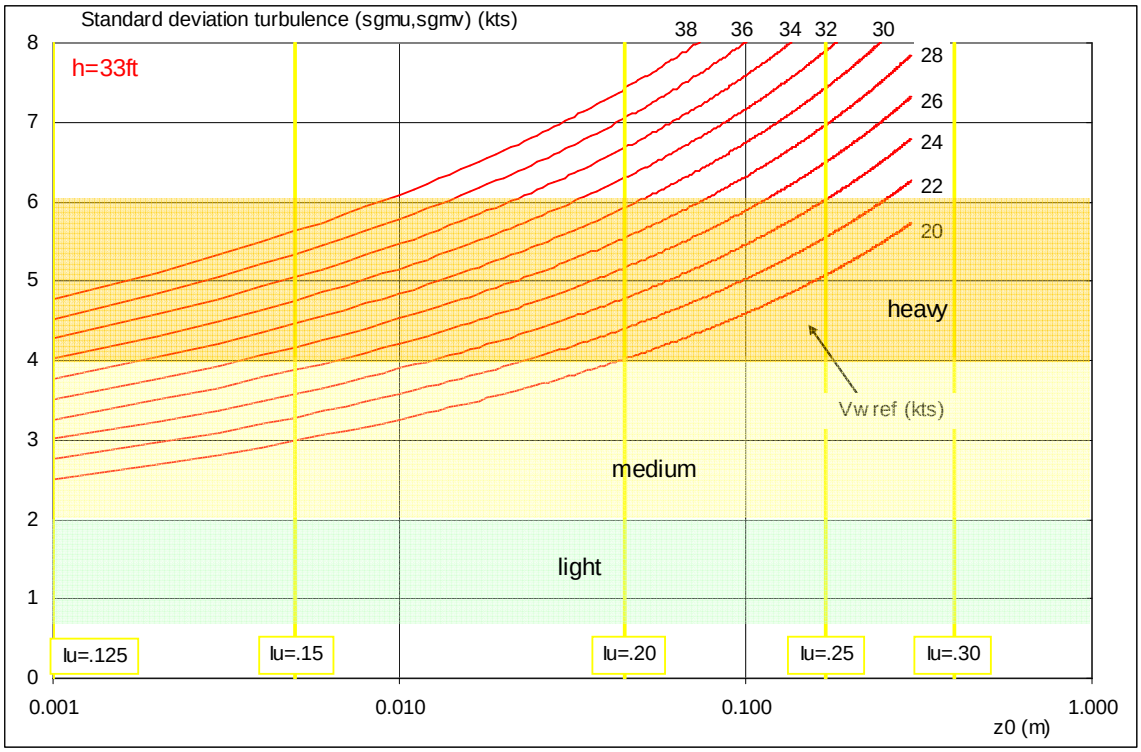

Figure 3-5: Standard deviation of horizontal turbulence as function of z0

JAR-AWO ([10] has defined atmospheric models applicable for low altitude (<2000ft) which are used amongst others for the certification of autoland systems. In this document JAR-AWO also defines various levels of turbulence which are given in the next table.

Table 3–3: JAR-AWO definition of turbulence levels

Standard deviation (kts)	Light	Medium	Heavy
Sgmu = Sgmv	1.5	3.0	5.0
Sgmw	.75	1.5	2.5

In the atmospheric models the standard deviation of the vertical turbulence (sgmw) is correlated to the horizontal turbulence components. Figure 3-6 shows this relationship as function of height according to JAR-AWO ([10] and ESDU ([25]. It can be observed from the figure that the JAR-AWO standard deviation of the vertical turbulence is equal to the horizontal component at a height of 1000 ft or more and decreases to a half near the ground. ESDU shows

a similar relationship, only very close to the ground the standard deviation (Sgmw) decreases to zero.

The three turbulence levels mentioned in Table 3–3 are schematically depicted in Figure 3-5 as three separate bands. It can be observed that a range of surface roughness magnitudes are able to create heavy turbulence. For instance a z0 value of .001m causes heavy turbulence (standard deviation 4.3 knots) at an extreme reference wind speed of 35 knots.

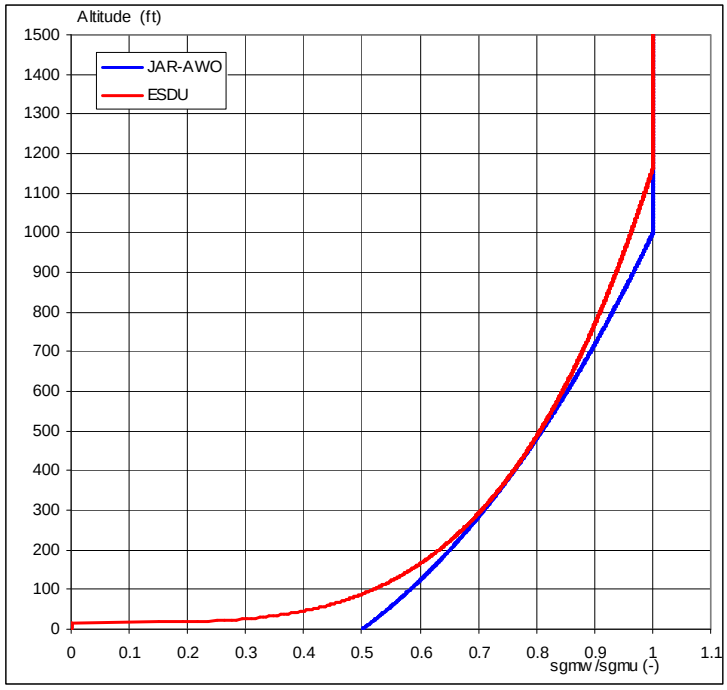

Figure 3-6: Relationship of vertical turbulence and horizontal turbulence as function of height

However the same standard deviation results from a surface roughness of .03m and a reference wind speed of 23 knots. Turbulence intensity however is quite different for the two cases and ranges from .125 to .18.

ICAO has defined turbulence levels in terms of g-variations with respect to the normal 1g load on the aircraft. These are presented in the next table.

Table 3–4: Turbulence levels according to ICAO

Very low	below .05 g	Light oscillations
Low	0.05 to 0.2 g	Choppy; slight, rapid, rhythmic bumps or cobble stoning
Moderate	0.2 to 0.5 g	Strong intermittent jolts
Severe	0.5 to 1.5 g	Aircraft handling made difficult
Very severe	above 1.5 g	Increasing handling difficulty, structural damage possible

Figure 3-7 presents maximum normal loads in the height band of 50ft to 200ft experienced during 100 auto land approaches with the F100 in varying turbulence conditions. During the approaches no “stand alone” obstacle was present. The turbulence characteristics are completely determined by a build up area. From the individual plots in this figure it can be observed that when the standard deviation of the horizontal gust (sgmu) is increased from 1.0 knot to 7.4 knots the maximum normal load that can occur increases from 1.1 g to 1.65 g. In the plots the surface roughness and reference wind speed is shown which leads to the sgmu range presented. For reference in Figure 3-7 also the boundaries for low and moderate turbulence as defined in Table 3–4 have been indicated.
Figure 3-7 shows that sgmu values in excess of approximately 6 knots may lead to severe turbulence conditions according to ICAO standards. According to JAR-AWO this is designated as heavy turbulence.

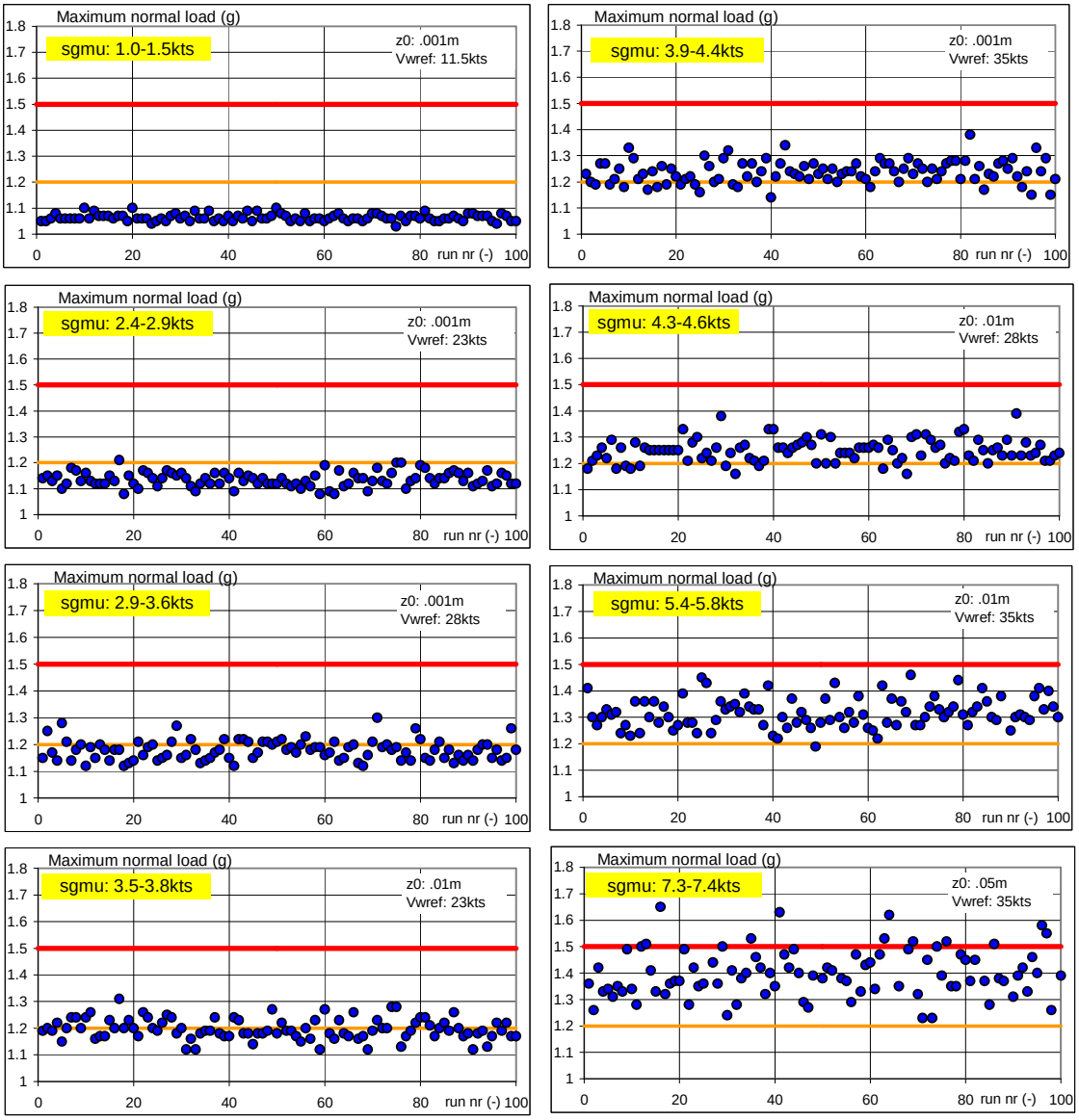

sgmu (kts)	1.0-1.5	2.4-2.9	2.9-3.6	3.5-3.8	3.9-4.4	4.3-4.6	5.4-5.8	7.0-5.9
	.001 11.5	.001 23	.001 28	.01 23	.001 35	.01 28	.01 35	.05 35
mean (g)	1.06	1.14	1.18	1.20	1.24	1.25	1.32	1.40
stdev (g)	0.01	0.03	0.04	0.04	0.04	0.04	0.06	0.09
max (g)	1.10	1.21	1.30	1.31	1.38	1.39	1.46	1.65
min (g)	1.03	1.08	1.12	1.12	1.14	1.16	1.19	1.23

Figure 3-7 Maximum normal load as function of sgmu standard deviation

In Appendix A it is shown that g-variations of .32g and .36g occur for the B747 and F100 respectively when flying in “heavy” turbulence conditions defined by JAR-AWO”. In ICAO standards this condition is labeled as moderate turbulence (Table 3–4).

It can be demonstrated that the low altitude atmospheric model of JAR-AWO is valid for only **one** surface roughness length viz. z0=.046m. As can be observed from Figure 3-5 this corresponds to a turbulence intensity of .2.

From Figure 3-5 it appears that heavy turbulence in the JAR-AWO model (z0=.046m) can be created by reference wind speeds ranging from 20 knots to 30 knots.

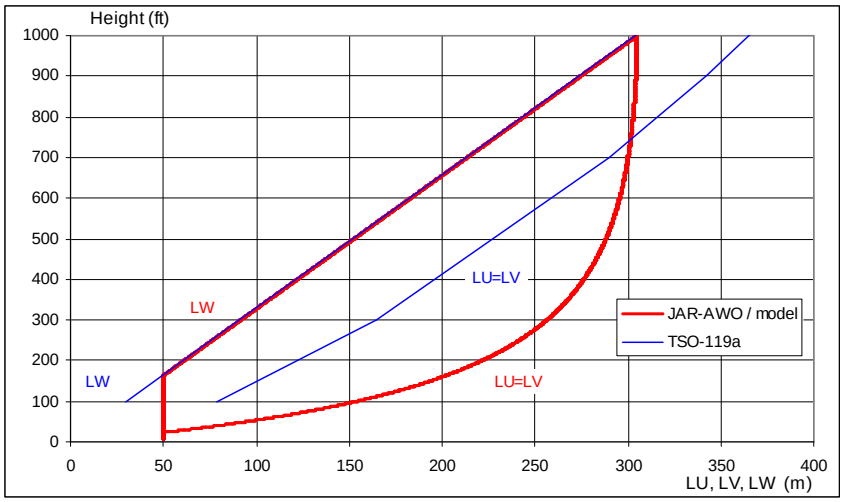

Figure 3-8: Definition of scale lengths

Figure 3-8 shows the scale lengths LU, LV and LW applicable for horizontal turbulence (sgmu, sgmv) and vertical turbulence (sgmw) as defined by JAR-AWO and MILSPEC. They are tailored to the frequency range of interest viz. flight handling and performance at low altitude (<2000ft). Also plotted are the scale lengths defined by TSO-117A ([13], which specifies criteria for wind shear alerting systems. Both for the offline and online (pilot in the loop) simulations the scale lengths as defined by JAR-AWO/MILPSEC are used in the atmospheric model. As can be observed from Figure 3-8 the scale lengths range from a constant value of 1000ft above a height of 1000 ft to 50m near the ground.

4 Wind climate behind a “stand alone” obstacle

4.1 Introduction

The present study takes a parametric variation of several wind related parameters as a starting point to evaluate where undesired wind conditions start to occur. Moreover, a real time piloted flight simulator test was part of the research, which requires short wind field calculation times. Both requirements made the use of very sophisticated wind field calculation methods or the use of experimental data obtained in a wind tunnel and subsequent interpolation less attractive. Therefore a simple analytic calculation method was developed that fulfilled the requirements. The method was based on widely accepted modelling of wakes behind wind breaks and was further improved by means of wind tunnel data in wakes behind building structures as are typical for Schiphol and also on wind tunnel data on the PDP. The method is described in detail in Appendix B. During the piloted simulator tests, the wind field generated in this way was considered very realistic by the pilots. First a general picture of the wind flow around obstacles will be sketched.
Furthermore results will be shown of the boundary layer wind field including a stand alone obstacle with a limited width.

4.2 General description

The airflow around a generic block shaped construction is described in ([26], ([27] and ([28]. It is schematically shown in Figure 4-1.

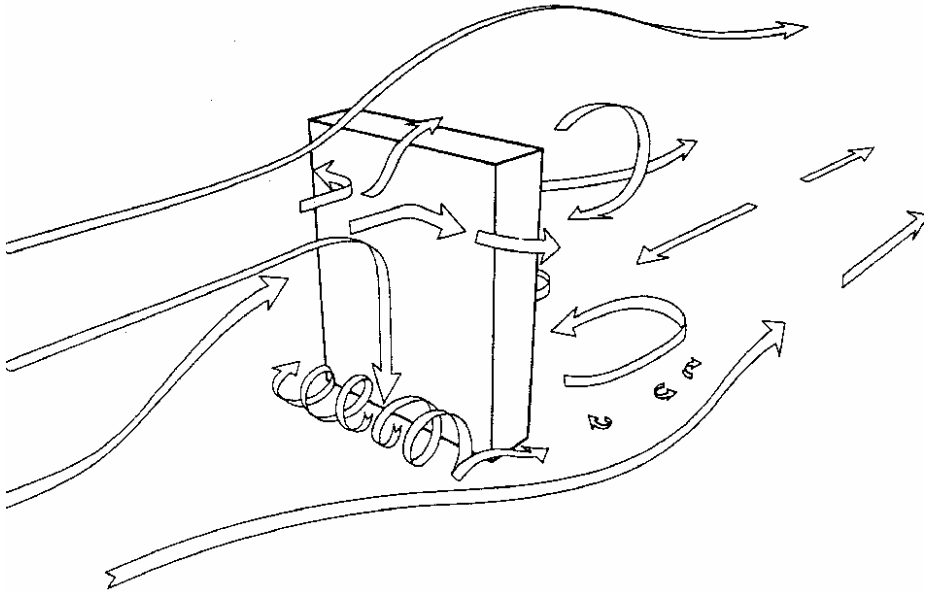

Figure 4-1: Schematic airflow around building

The airflow depends on the characteristics of the approaching wind and on the size and shape of the building itself. Due to the surface roughness the wind speed increases with the height of the

building. When the wind reaches the obstacle the wind gradually diverges until at the stagnation point at three-quarter of the building height an upward and downward flow occurs. Below this height air flows downwards and outwards reaching the windward corners. The accelerated air streams pass around the corners of the building where two jets of air are formed in lob-like areas that stretch downwind for a considerable distance. In particular for long slender obstacles high speeds may evolve. The corner streams are usually indicated as the corner effect and are able to create wind shear like phenomena.
As the wind flows around the obstacle it creates pressures above or below local atmospheric conditions. Pressures over most of the “wall towards the wind” are above atmospheric. The maximum occurs at the stagnation point, where the air is brought to rest. The contours follow a well-defined shape around this centre. Close to the corners accelerating flow produces small areas where the pressure is below atmospheric (suction areas). The sidewalls, roof and “wall on the leeside” all experience suction. At the “wall on the leeside” an upward flow occurs towards the region of high suction on the roof. Close to the sidewalls and the roof air flows in a reverse direction back towards the front where it separates from the surface of the building. The air motion over the top of the building creates an upward flow that only at a respectable distance behind the building reverts to a downward flow.

The area behind the building is known as the wind shade or wake area. In the wake relative slow wind speeds are present. The area is characterized by its high turbulence levels that can be observed at quite a distance behind the building. This is caused by the transformation of high energy available in the airflow into gust/turbulence when the airflow is slowed down significantly. Changes in wind direction up to 180 degrees may occur in this area. In general the wake behind the building extends to 4 to 5 times the building height. However this does not mean that behind the wake the original undisturbed speed profile immediately is restored. Wind tunnel tests have shown that the disturbances may extend to more than 15-20 times the building height.
The wake and corner streams are two phenomena related to each other. As result of the corner speeds and the wake, whirls will develop starting from the corners of the building. Due to these whirls air is dragged along at the edges of the wake area. The air supply for this comes from larger distances behind the obstacle where speeds gradually decrease and the pressure slowly increases. As result of this a flow will evolve in an opposite direction towards the building.
This leads to the formation of two large stationary whirls around a vertical axis in the wake area. The faster moving and smaller whirls are present between the fast airflow outside the wake and the mentioned larger stationary whirls. Due to the wake a site downwind from the obstacle will be shielded from the wind for a considerable distance. In practice this shielding depends on the height of the obstacle and the distance of the site downwind. The shielding effect will vary with

height above the site surface and the net result is usually to produce a distorted wind speed profile such as given in Figure 4-2.
Also indicated in Figure 4-2 is the boundary of the internal layer that develops behind the building. In the internal layer wind speeds less than that would occur in the undisturbed flow are present. Above the internal boundary the undisturbed wind speed profile is valid.

It is assumed that the incoming airflow is perpendicular to the front side of the building. This means that a symmetrical air flow can be adopted, which is favorable for the mathematical wind flow modeling behind the building. This is not the case when wind approaches the building from an oblique direction. Then conical whirls are created on the rooftop and sides of the obstacle leading to an asymmetrical flow pattern. The conical eddies are transported with the upward airflow and can be active at a large distance behind the obstacle. The wake area in the case of an oblique airflow is smaller than for perpendicular flow.

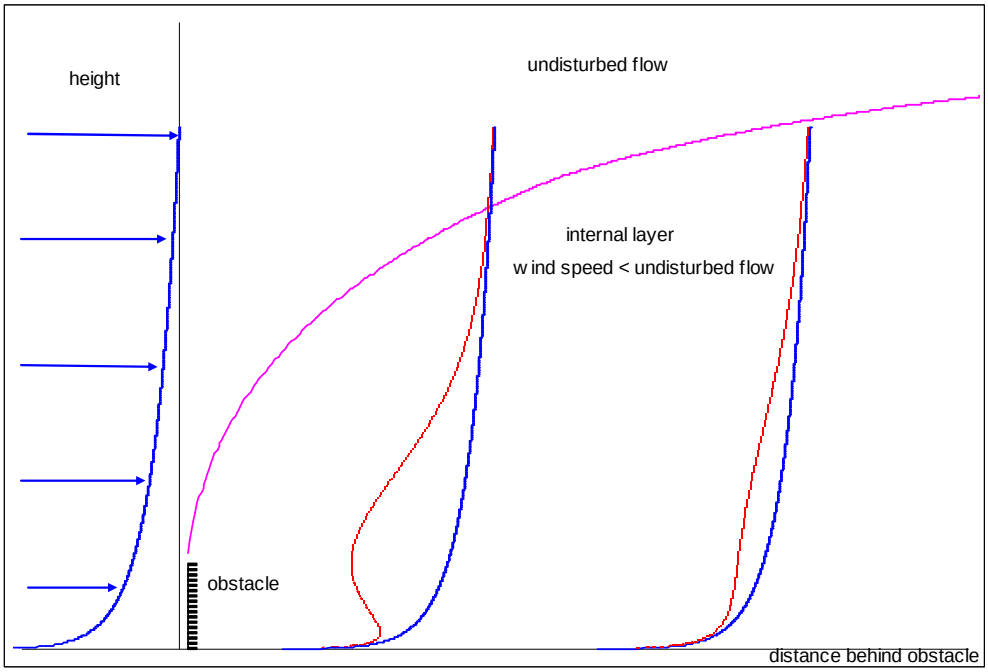

Figure 4-2: Air flow pattern behind obstacle

Consequently parameters that affect the airflow around and behind an obstacle significantly are:

1. Height

When the height of an obstacle is increased the basic airflow patterns around the obstacle don't change very much. However a taller obstacle increases the airflow around the sides of the obstacle significantly. Because of the increased corner streams the height of an obstacle has a significant effect on the wake area. The taller the obstacle the larger the reverse flow area will be.

2. Width

An increase in obstacle width at constant height and depth has a large effect on the magnitude of the wake area. There appears no limit value for this phenomenon. Consequently an increase in obstacle width will automatically lead to a larger wake area.

3. Depth

When the depth of an obstacle is large in relation to the width and height of the obstacle a smaller wake area will develop. This situation arises when the depth is more than two times the building height. Consequently a thin obstacle creates a wake area with larger whirls and more reverse airflow.

4. Airflow direction

When a corner of an obstacle is directed towards the wind direction (oblique flow) this may lead to the creation of strong conical “corkscrew like” whirls that can be transported by the airflow over a large distance behind the obstacle. Very complex and asymmetric flow patterns may result. In general an oblique airflow leads to a smaller wake area.

5. Shape

The shape of an obstacle strongly affects the airflow patterns and the resulting wake characteristics. If an obstacle diverges from the “block shaped” form as is discussed here wake characteristics can deteriorate substantially. An increase in roof inclination enlarges the wake area. Also the roof and roof edge shape define the possibility of the creation of strong conical eddies. Smooth and rounded shapes are favorable in this respect because the lower probability on whirls. An abrupt change in shape creates strong airflows and eddies. As result of the U-shape of the construction this situation occurred at the engine test run facility (PDP) mentioned in section 2.2.2. Characteristics of such an obstacle are defined as “worst case” in the offline and online simulations. Therefore to avoid high-speed airflows the pressure differences must be kept as low as possible. Consequently gradual changes in geometry must be aimed at. If the shape of an obstacle deviates from the rectangular form usually wind tunnel or flow calculations are required.

4.3 Wind climate modelling behind infinitely long (2D) obstacle

The model for the wake behind an infinitely long obstacle placed perpendicular to the wind is studied extensively in the past and well-documented. Although this type of obstacle is not of interest in the study at hand, it serves as the basis for determining the wake behind obstacles of finite width and the PDP. The wake model is the same as used for the FLYLAND study ([9]. This is a modified ESDU-model ([18] with improved fits to the experimental data. A detailed description of the model is given in Appendix B.

4.4 Wind climate modelling behind obstacle with limited width

The 2D wind break model has been extended to include the end effects for wind breaks or buildings of finite width in order to generate a realistic, although generic building wake. Verification of the results was done using the results of wind tunnel measurements. Figure 5-3 shows a comparison between the results of the model used and the wind tunnel for a wind field at 400m behind a building complex. It is seen that the comparison between the wind velocity defects is very acceptable, certainly if the generic wake properties (width, gradients and depth) are considered.

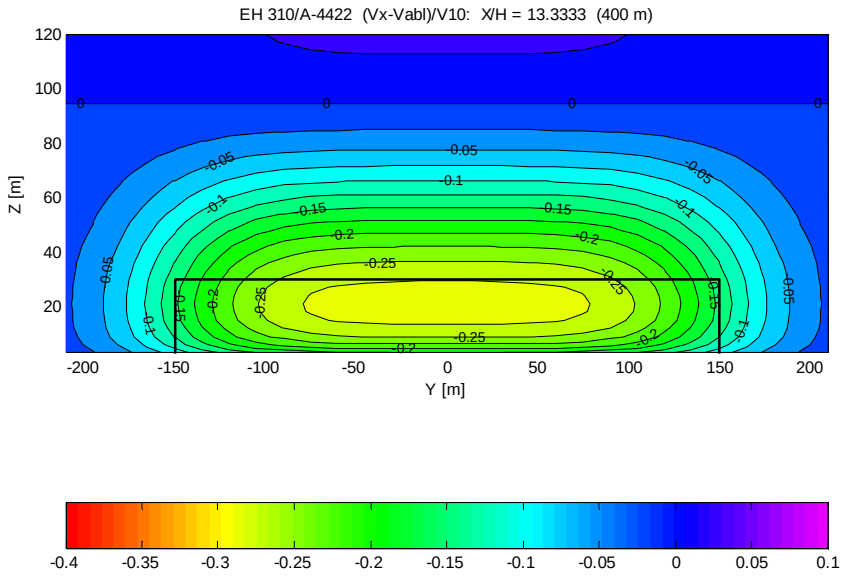

a) Results of wind tunnel model

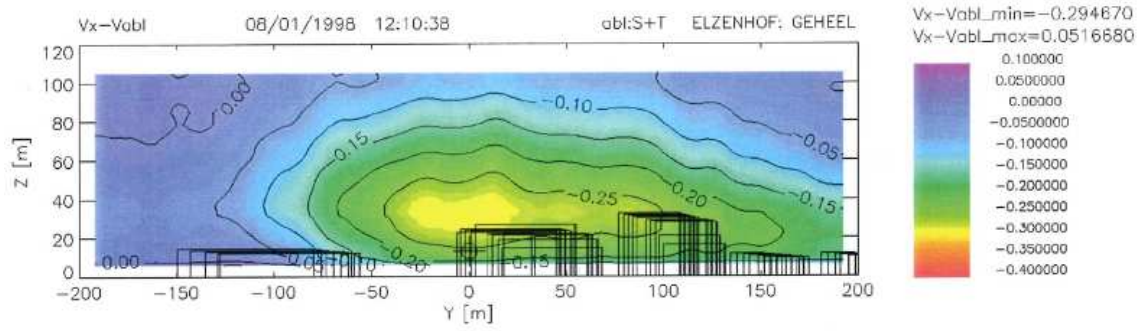

b) Data from wind tunnel experiment

Figure 4-3: Wind velocity decrease behind building complex

4.5 Wind climate modelling behind PDP facility

The calculation of the wind field behind the PDP involved a more complicated model as the strong vortices shed by the PDP had a dominating effect on the vertical position of the wake. Besides, the wake of the PDP was exceptionally deep due to the unfavourable shape of the facility. This combination caused a deep wake to be lifted to the height of the approach trajectory for runway 27 (Figure 4-4).

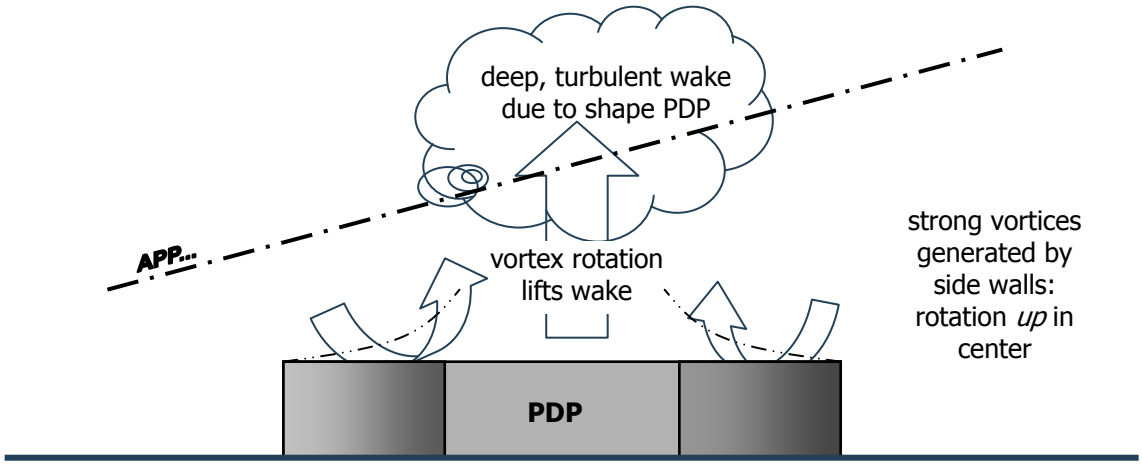

Figure 4-4: Schematic of vortex wake lifting mechanism behind PDP

It was this wake that lay on the basis of the original 7 knots criterion. Figure 4-5 shows the results of the wind tunnel measurements translated into the actual wind conditions that occurred at the times of the approaches that resulted in pilot reports. On one day the wind direction was 220° with 22 knots and on the other day it was 240° with 30 knots. The cross wind components in both cases reach 7 knots as is seen in the figure.

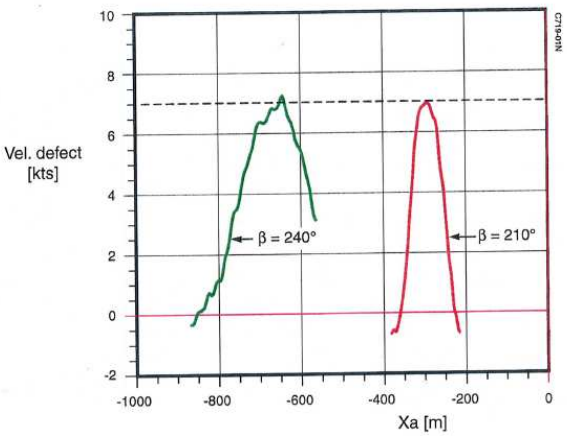

Figure 4-5: The 7 knot cross wind velocity variation behind PDP (pilot report conditions)

The rationale behind the simple criterion was as written in ([5]:

1. "The magnitude of the velocity defect in case of cross wind conditions will determine the magnitude of the side slip disturbance effects,
2. For a wake of given width, the maximum velocity defect is proportional to the gradients experienced by the aircraft;
3. The larger the gradients, the larger also the (aerodynamic) turbulence levels in the wake."

However, as was stated in the same reference, the criterion clearly lacked a more sound basis e.g. to make more clear statements on the width of the wake that also determine the gradients, apart from being 'of the order of the width of the PDP-wake'. The present study is intended to shed more light on that question.

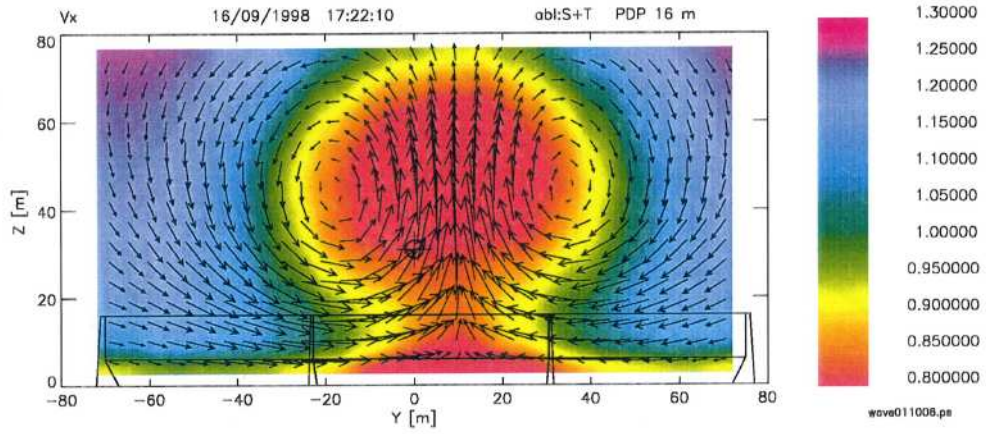

a) Measurement DNW-LST ([5].

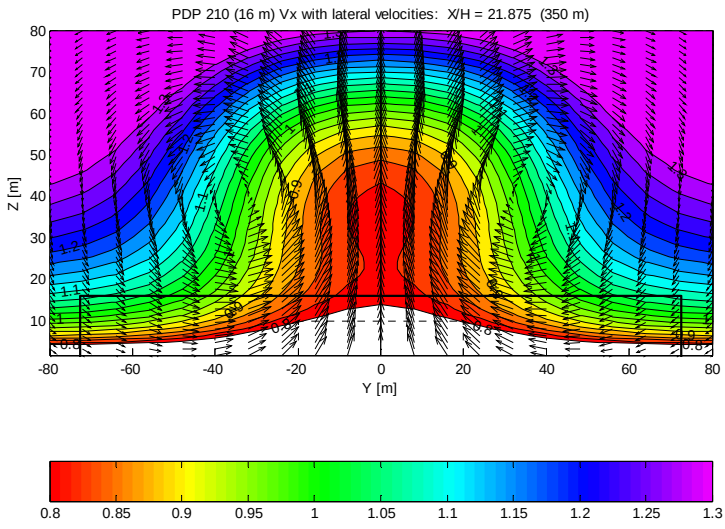

b) Result of PDP wind model at x=350m.

Figure 4-6: Wind field behind the PDP for wind direction 210° (colors give velocity magnitude (V/V_{10}) in wind direction, vectors are velocities normal to the wind direction)

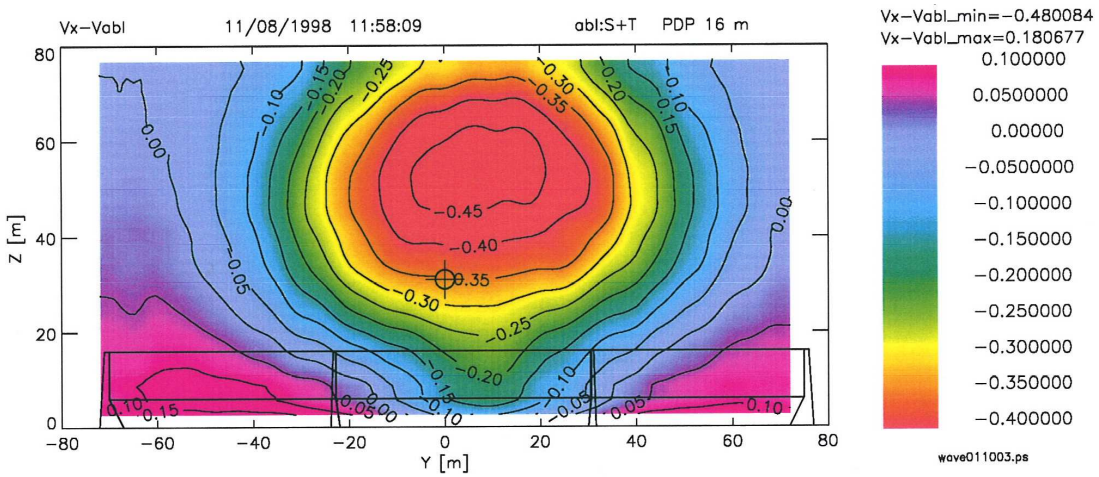

a) Measurement DNW-LST ([5].

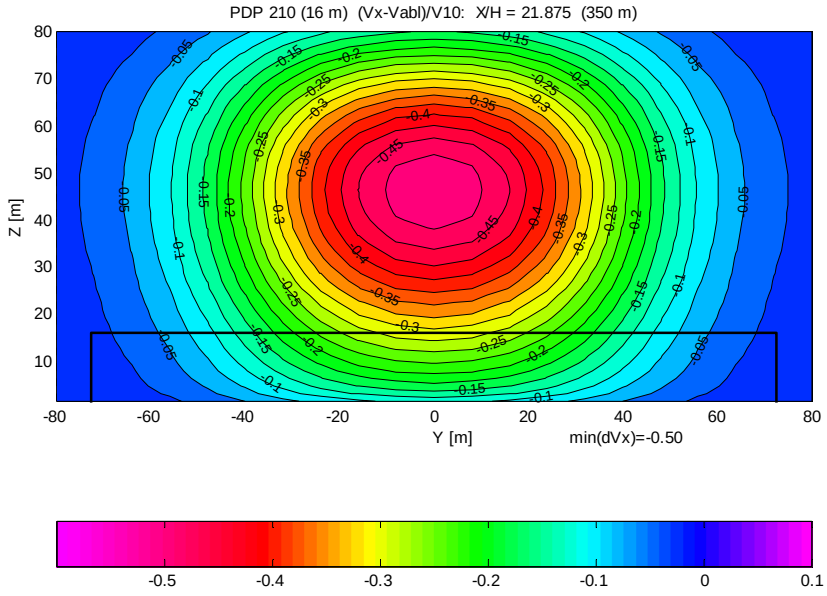

b) Result of PDP wind model at x=350m.

Figure 4-7: Wake behind the PDP for wind direction 210°).

The wake including cross flow velocities, as measured in the wind tunnel, is shown in Figure 4-6 in comparison with the results of the calculation method, adapted for the PDP-situation. Dimensionless wake velocities as obtained from wind tunnel data and the PDP wind model are presented in Figure 4-7 . As can be observed for both data sets the position and depth of the wake show a good agreement.

Turbulence levels were also measured in the LST-test. Figure 4-8 shows the turbulence level distribution behind the PDP at z = 46 and 22m in the same cross section as above. The calculation results were adapted in these graphs, to reflect the lower undisturbed atmospheric boundary layer turbulence levels that were present in this wind tunnel test.

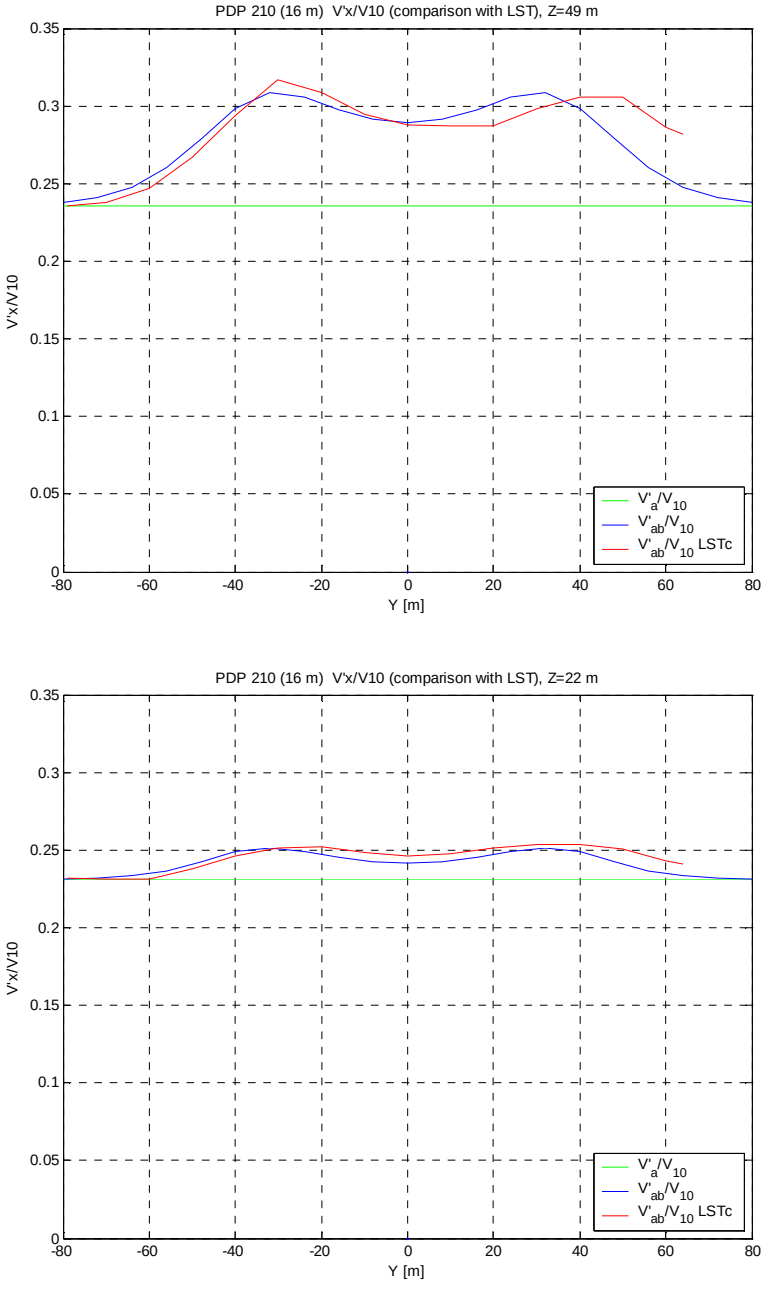

Figure 4-8: Calculated turbulence levels behind the PDP for wind direction 210° (blue line) compared to the DNW-LST wind tunnel results (red line)

4.6 Atmospheric model examples

The effect of the wake behind a “worst case” obstacle on the wind speed profile is presented in Figure 4-9. For the same three surface roughness parameters shown in Figure 3-2 (z0=.001m, .01m and .1m) the wind speed distortion is presented. The speed defect corresponds to an obstacle at a position of 400m before the threshold and a lateral offset of 700m with respect to the runway centerline. Dimensions of the obstacle are a height of 45m and a width of 250m. It can be observed that for these conditions the speed defect occurs between a height of 150ft and 250ft. The maximum speed defect varies from 10kts to 14kts depending on the surface roughness.

It can be expected that the speed defect in combination with the mean wind speed profile and the stochastic gust/turbulence variations leads to smaller or larger shear effects, depending on the sign of the gusts near the speed deficit. Thus situations are possible in which the combined effect of the speed defect and gusts partly cancel out. This means that the mutual effect of the wind disturbance due to the obstacle on the aircraft performance is minor. However also a worst case scenario may arise if circumstances are against all the odds and both wake and gust enhance each other.

Obviously in the crosswind landings that are considered in this study both the head wind and crosswind component are affected by the speed defect. Figure 4-9 shows the head and cross wind components when the mean wind direction is assumed constant with height and making an angle of 60 degrees with the runway centerline. The wind velocity is taken such that the cross wind at the reference height of 10m corresponds to 20 knots.

The speed deficit in the headwind (along track) can be labeled as a performance decreasing wind shear phenomenon, whereas the sudden lull in the crosswind (cross track) may lead to disturbing roll deviations and to an offset in the localizer track.

Just as in Figure 3-2 the gust envelope profile is include in Figure 4-9. It can be observed that the gust speed envelope becomes smaller in the same height range where the speed deficit occurs. However still higher gust factors are experienced in this area as is shown in Figure 4-10. Depending on surface roughness the gust factor is increased with 30<->35 % due to the presence of the obstacle.

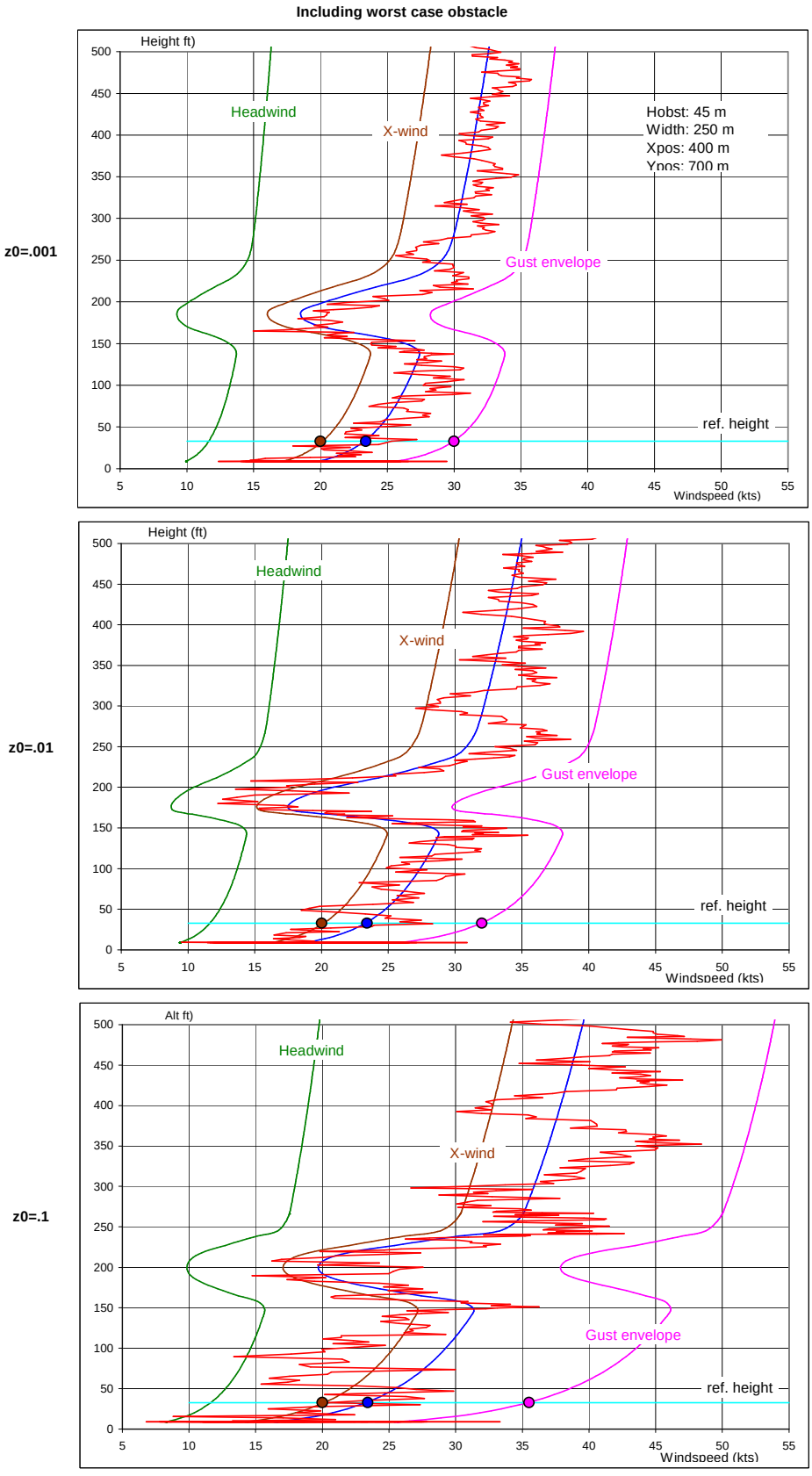

Figure 4-9: Wind profiles including nearby obstacle for 3 surface roughness parameters

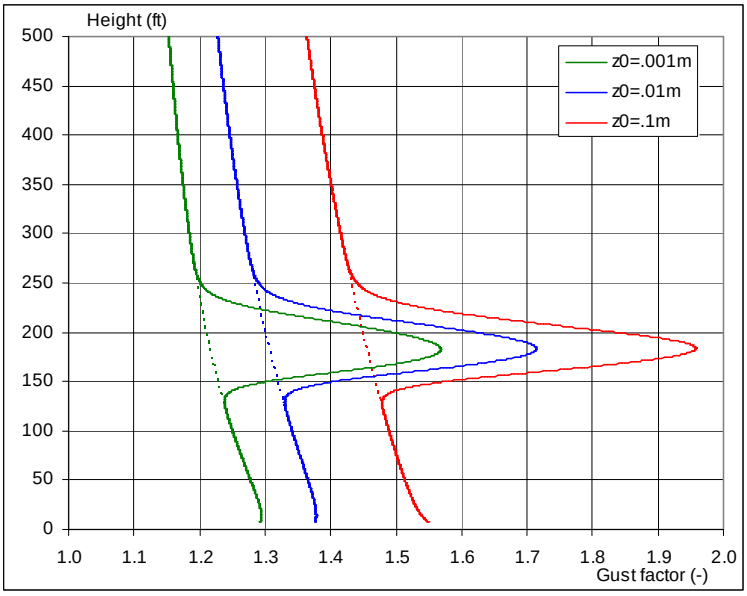

Figure 4-10: Gust factor as function of height with obstacle included

5 Acceptance criteria for non-piloted and piloted simulations

5.1 Introduction

To decide whether the flyability during approach, landing and flare in the presence of obstacles is acceptable or not acceptance criteria are established. These acceptance criteria have been applied both to the objective data gathered during the offline (non-piloted) and online (piloted) simulation runs and to the subjective ratings of the project pilots during the piloted simulations. Although not used as an acceptance criterion also the sink rate at main gear touch down is discussed.

5.2 Objective acceptance criteria

The objective acceptance criteria are related to the following items:

1. Applicable to **piloted** simulations
   - The number of go-around's in the piloted simulations
     a. Due to a longitudinal/lateral speed defect
     b. Due to turbulence
2. Applicable to **non-piloted** simulations
   - The number of crossings of the critical F-factor in the offline simulations in the altitude band of 50ft to 450ft.
     a. Due to a longitudinal speed defect
     b. Due to turbulence
3. Applicable to **piloted** and **non-piloted** simulations
   - The vertical speed during final approach (<200ft)
     a. Due to a longitudinal speed defect
     b. Due to turbulence
   - The touchdown dispersion
     a. Due to a longitudinal/lateral speed defect
     b. Due to turbulence
   - The bank angle at the runway threshold (F100 simulations only)
     a. Due to a lateral speed defect
     b. Due to turbulence
   - The bank angle at touchdown.
     a. Due to a lateral speed defect
     b. Due to turbulence

5.2.1 Critical F-factor

A wind speed defect along the approach path of an aircraft can be seen as a wind shear encounter. Due to a number of accidents in the USA in which wind shear was the main cause, wind shear alerting systems have been developed. In order to certify these systems Technical Standard Orders (TSO) have been issued by the FAA. An important parameter that evolved from NASA studies ([12] with respect to this subject is the so-called F-factor expressed in g. It describes the wind shear impact on the climb angle with respect to the ground. The F-factor is defined as:

$$FFACT(g) = \frac{\dot{U}_x}{g} - \frac{w}{TAS} \qquad (5.1)$$

where $\dot{U}_x$ is the Lagrangian derivative of the horizontal wind, g is the gravitational acceleration, w is the vertical wind component and TAS is the aircraft's true airspeed. The first term on the right side represents the **horizontal shear** component and the second the **vertical shear** component as mentioned in section 3.4.

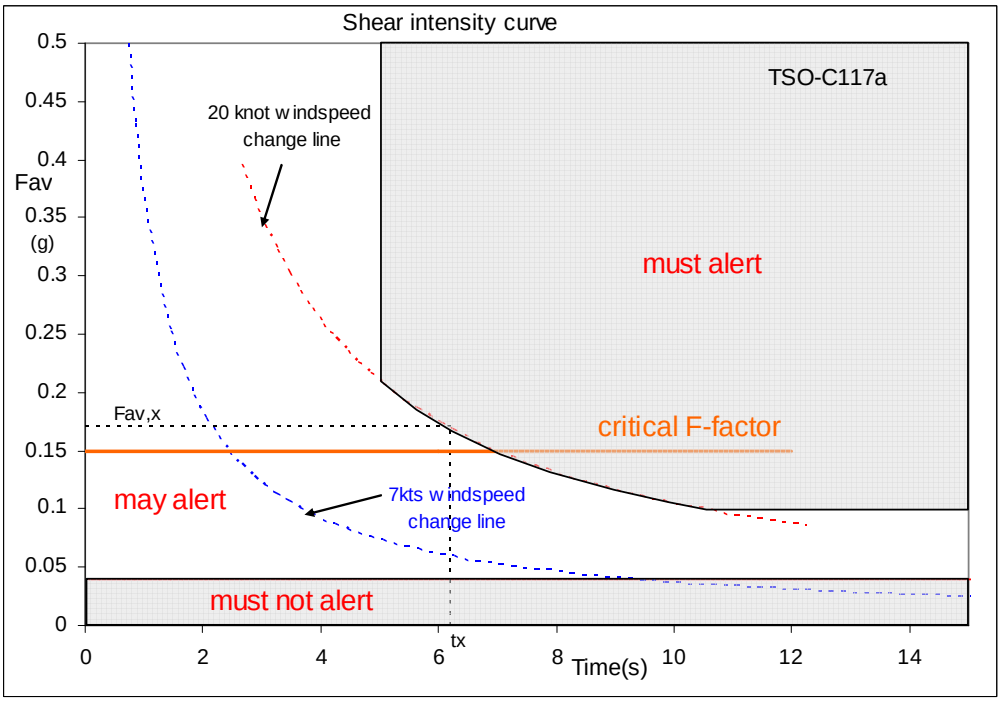

Figure 5-1: Wind shear intensity curve and critical F-factor

In TSO –C117 ([13] trip levels for these systems are defined. In Figure 5-1 the so-called "**shear intensity curve**" is shown in which these trip levels are indicated. As an example in the plot the parameter **Fav, x** is the average shear intensity, which results in a 20-knot wind speed change

after **tx** seconds. According to this TSO then a wind shear alert must occur. Also in the graph the line corresponding to a 7 knot wind speed defect is plotted.
In this investigation a critical F-factor value of .15g is chosen as longitudinal criterion. This F-factor value frequently is used in NASA studies and is also plotted in Figure 5-1 as well.
For the offline simulations the crossing of the critical F-factor below 200 ft is considered as an "alternative" go-around parameter.
The critical F-factor can be triggered by a speed defect as result of e.g. obstacle shading but also in turbulent conditions in which shear phenomena may be present.

5.2.2 Vertical speed during final approach (below 200ft)

5.2.2.1 Due to a longitudinal speed defect

A descent rate of 1000 ft/min or more is considered unacceptable during final approach. If such an event is encountered in this stage operational procedures prescribe the initiation of a go around. Consequently this event is used as an acceptance criterion in this study. To evaluate the amount of longitudinal speed defect behind an obstacle which causes a descent rate exceeding 1000 ft/min., open loop simulations with the F100 model were performed. Vertical speed loss due to various combinations of the strength of a longitudinal wake versus endurance of the wake was evaluated.
In the performed simulations it is assumed that the event can evolve unattended for a time period of 3 seconds before pilots will react to the situation. Consequently the descent rate due to the longitudinal speed defect was recorded after 3 seconds. As an example a time trace of a maximum speed defect of 8 knots in a time period of 4 seconds is presented in Figure 5-2. The overall results of the evaluation are presented in Figure 5-3. Herein the descent rate after 3 seconds is depicted as function of the maximum speed defect (wake) encountered and endurance of the speed defect. The descent rate according to the ILS glide path is indicated as well. From the figure it can be observed that wakes with a maximum of 8 knots or more and lasting more than 4 seconds lead to a descent rate in excess of 1000 ft/min.

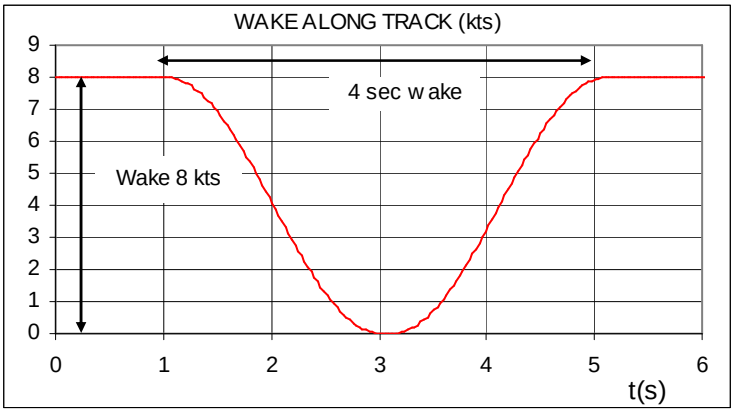

Figure 5-2: Maximum longitudinal speed defect of 8kts in 4 seconds

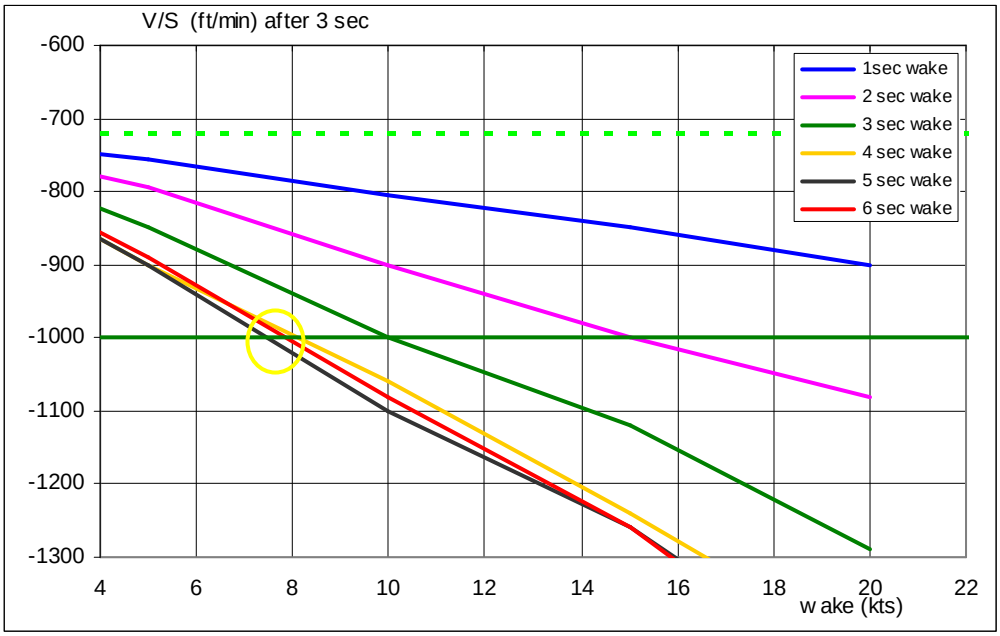

Figure 5-3: Descent rate as function of speed defect characteristics

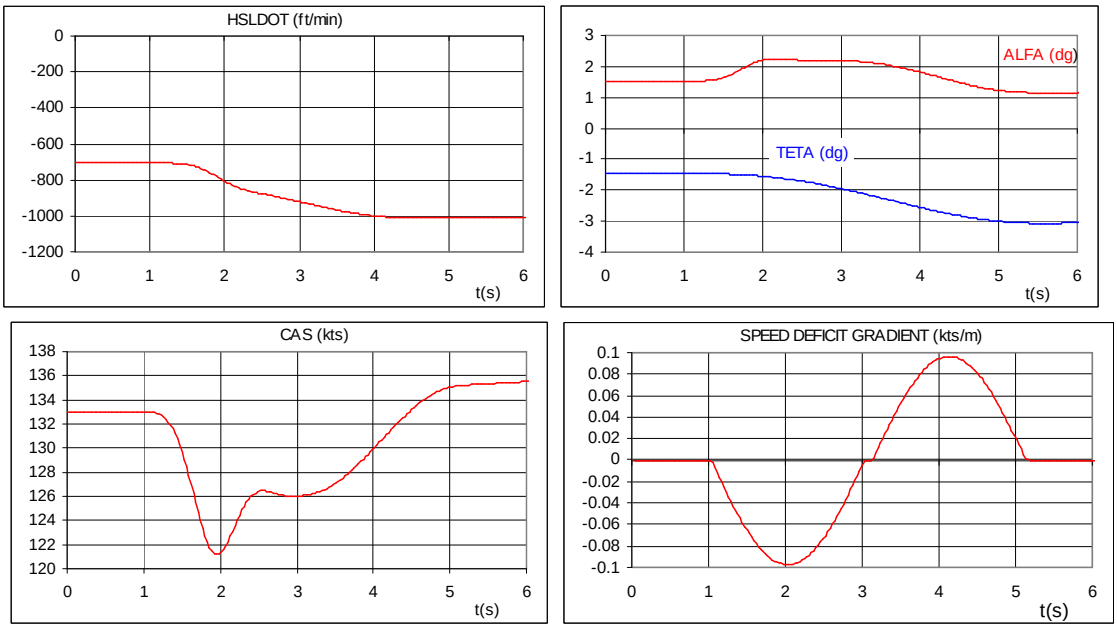

Figure 5-4: Longitudinal time histories corresponding to a along track speed deficit of 8 knots

Time histories of vertical speed, CAS, angle of attack/Pitch attitude and the speed deficit gradient as result of the along track speed defect in Figure 5-2 are shown in Figure 5-4.
The along track speed defect shown in Figure 5-4 can be considered as a condition in which a wind shear occurs. This is illustrated in Figure 5-4 by the time history of the airspeed (CAS). The speed deficit gradient attains a peak value of .1 kts/m., which corresponds to a 8kts speed defect over a distance of 80m.

5.2.2.2 Due to turbulence

Apart from a speed defect due to shading of a “stand alone” obstacle also gust/turbulence is able to create vertical speed s in excess of 1000 ft/min. This is illustrated in Figure 5-5 in which the minimum vertical speed in the altitude band of 50ft to 200ft is depicted encountered during 100 auto land approaches with the F100 aircraft in varying turbulence conditions. During the approaches no “stand alone” obstacle was present..

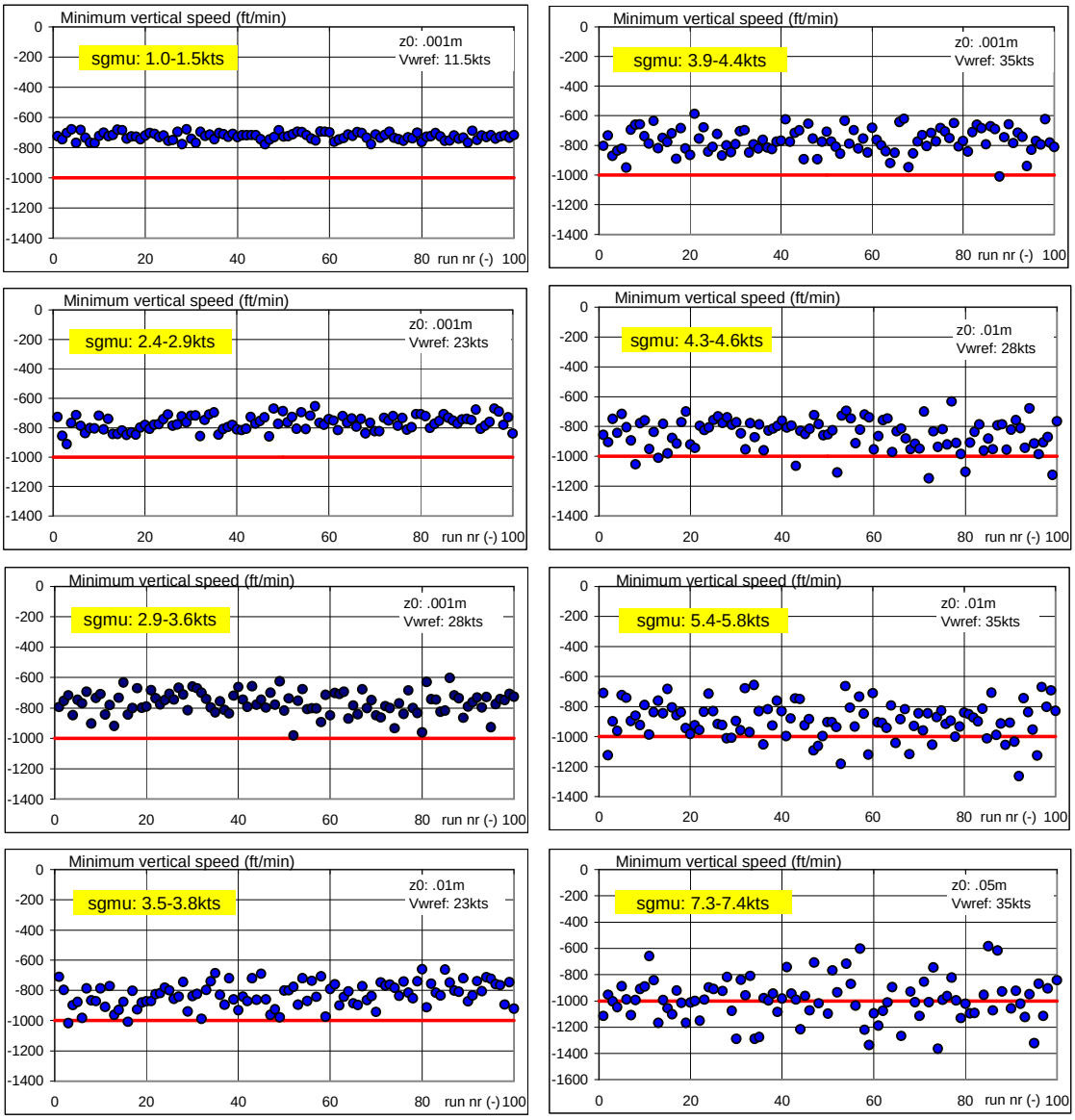

sgmu (kts)	1.0-1.5	2.4-2.9	2.9-3.6	3.5-3.8	3.9-4.4	4.3-4.6	5.4-5.8	7.0-5.9
	.001 11.5	.001 23	.001 28	.01 23	.001 35	.01 28	.01 35	.05 35
mean (ft/min)	-726	-768	-768	-828	-768	-852	-891	-992
stdev (ft/min)	24	51	75	81	83	103	122	160
max (ft/min)	-678	-654	-602	-660	-586	-632	-657	-583
min (ft/min)	-778	-911	-981	-1016	-1009	-1147	-1264	-1364

Figure 5-5: Minimum vertical speed as function of sgmu below 200ft

From the individual plots in this figure it can be observed that when the standard deviation of the horizontal gust (sgmu) is increased from 1.0 knot to 7.4 knots the minimum vertical speed that can occur decreases from approximately -780 ft/min to -1360 ft/min.
In the plots the surface roughness and reference wind speed is shown which leads to the sgmu range presented.
For reference in Figure 5-5 the 1000 ft/min descent rate has been indicated.
Figure 5-5 shows that standard deviations of horizontal turbulence (sgmu) in excess of approximately 4 knots may lead to busts of the 1000 ft/min descent rate

5.2.3 Vertical speed at touch down

The vertical speed at the moment of touch down was monitored and evaluated, but it was not used as an acceptance criterion. The reason for this is that vertical touchdown speeds in simulators generally appear to be larger than in real landings. This is created by a number of limitations inherent to piloted simulation such as lack of periphery and small time lags between visual and mathematical model parameters. Both for offline and online simulations limitations in the models representing the ground effect and the dynamics of wheel spin up are restrictive.

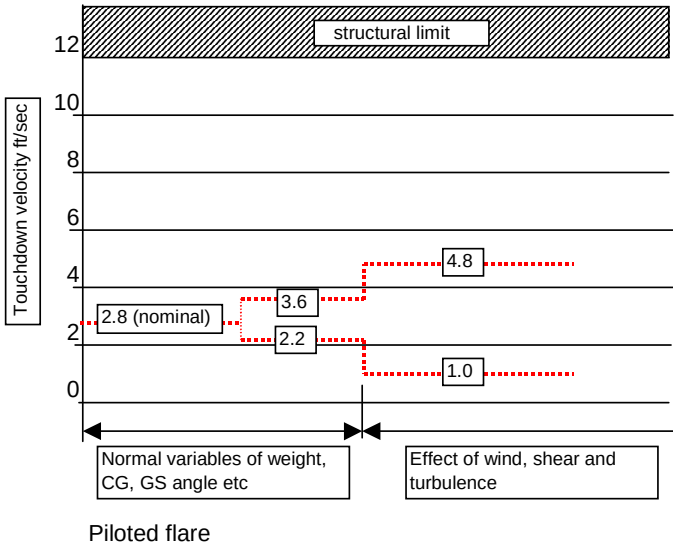

Figure 5-6: Touch down velocities

Figure 5-6 indicates the dispersion in touch down velocities for B747 aircraft around the nominal 2.8 ft/sec as experienced during normal landings and landings in adverse weather conditions such as strong winds, shears and turbulence.
A cumulative probability plot of B747 touch down data is shown in Figure 5-7. It reveals that for 99.5% of the landings a vertical velocity at touch down of 6 ft/sec or less is experienced. Therefore a touch down sink speed of 6 ft/sec is adopted as a reasonable boundary for this study.

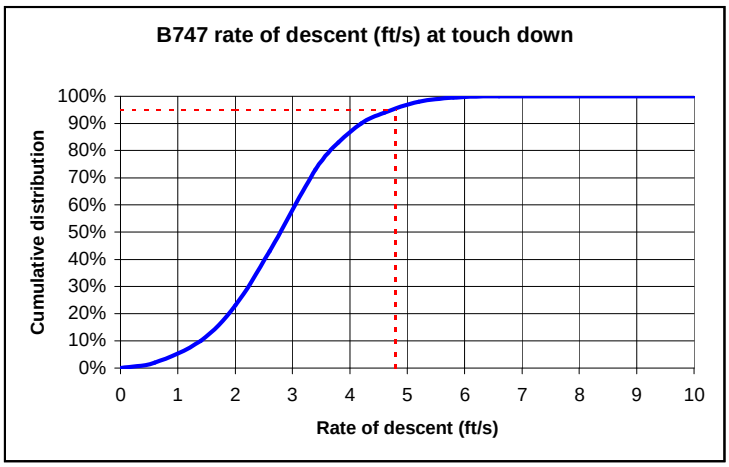

Figure 5-7: Cumulative distribution of B747 touch down descent rates

5.2.4 Touch down dispersion

The required touch down position is defined by JAR-AWO document section 131 ([10]. This document yields criteria for performance demonstration of automatic landings. The required touch down accuracy is shown in Figure 5-8, which applies to the aircraft's center of gravity position relative to the runway.

The box is symmetric with respect to the centerline of the runway, because it is the aim of pilots to have main gear touch down near the centerline. From a cockpit perspective this means (in particular for large aircraft) that during flare and landing the cockpit position is on the upwind part of the runway. Because of the difference in wheel track between the B747 and Fokker 100 both aircraft have different allowable center of gravity touch down zones.

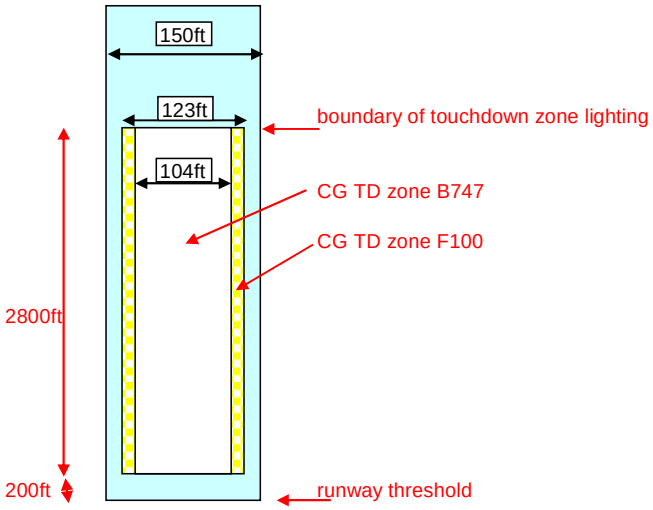

Figure 5-8: Required touch down zone

The touch down dispersion is influenced both by the turbulence conditions prevailing during the final approach as well as by the influence of a “stand alone” obstacle creating both a speed defect and an increase/decrease of the turbulence conditions.

5.2.5 Bank angle limits below 200ft (including T/H and touch down)

5.2.5.1 Introduction

Lateral directional acceptance criteria have been defined from wake vortex research. Here it was investigated which roll angle disturbance due to a wake encounter was accepted as function of height. Work done in this area is described in ([14], ([15] and ([16]. Figure 5-9 shows the magnitude of the roll angle as function of height above the ground that was still considered as non-hazardous. Figure 5-9 was derived for a four-engine Boeing B-707 aircraft. It can be observed from the plot that at heights below 200 ft the tolerated roll angle varies from approximately 10 degrees (200 ft) to 6 degrees (50 ft).

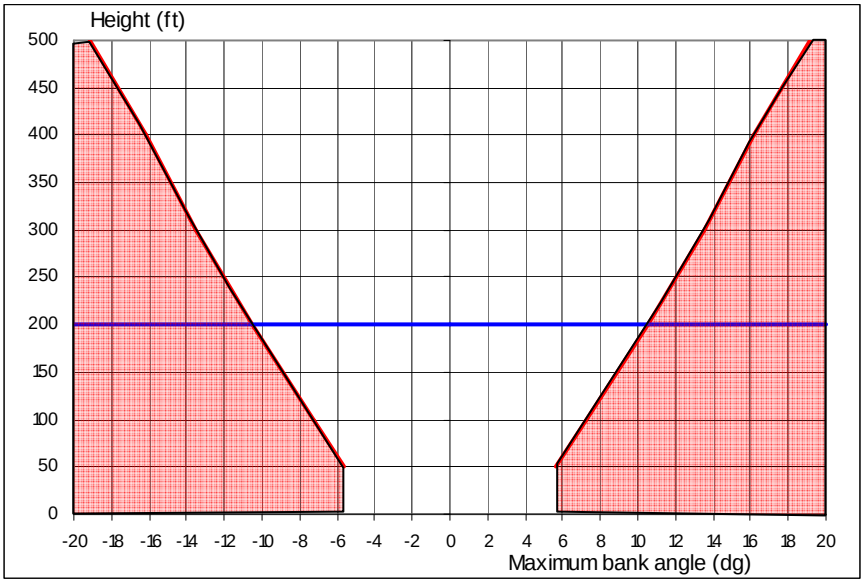

Figure 5-9: Boundary between hazardous and non-hazardous bank angles

5.2.5.2 Bank angle limit due to a lateral speed defect

To evaluate the amount of lateral speed defect behind an obstacle which causes a bank angle exceeding the values presented in Figure 5-9, open loop simulations with the F100 model were performed. Bank angle excursions were recorded resulting from a matrix in which the maximum strength of a wake versus endurance of the wake was varied. Hereby it is assumed that the event can evolve again unattended for a time period of 3 seconds before pilots will react to the situation. Consequently the bank angle change due to the speed defect was recorded after 3 seconds. As an example a time trace of a maximum lateral speed defect of 12 knots in a time

period of 4 seconds is presented in Figure 5-10. The overall results of the evaluation are presented in Figure 5-11. Herein the bank angle after 3 seconds is depicted as function of maximum lateral speed defect (wake) and endurance of the speed defect.

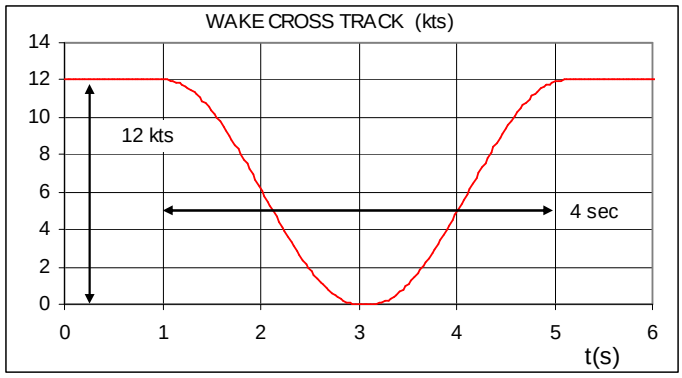

Figure 5-10: Time history of a lateral speed defect as function of time

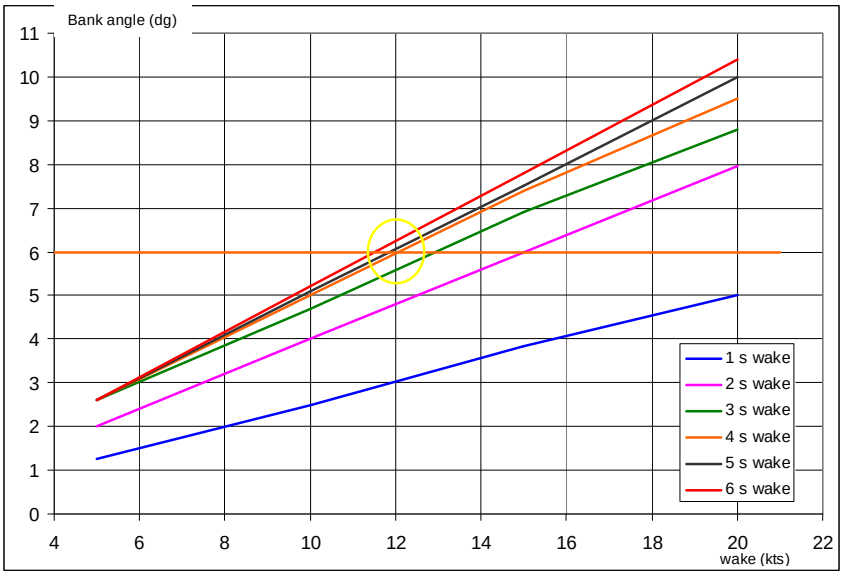

Figure 5-11: Bank angle limits as function of wake strength and wake endurance

From the figure it can be observed that wakes of 12 knots or more lasting more than 4 seconds lead to a bank angle in excess of 6 degrees. Time histories of side slip angle, bank angle, roll rate and roll acceleration and heading/track as result of the lateral speed defect in Figure 5-10 are shown in Figure 5-12. Furthermore in the figure the speed deficit gradient (kts/m) is presented. A peak value of .15kts/m can be observed. This means that with this gradient the 12 knots speed deficit is reached after a distance of 80m.

The lateral speed defect shown in Figure 5-10 can be considered as a condition in which the crosswind momentarily drops off. This is illustrated in Figure 5-12 by the time histories of

heading (PSI) and track (TRACK). Initially an offset between the two variables is present as result of the left-hand crosswind.

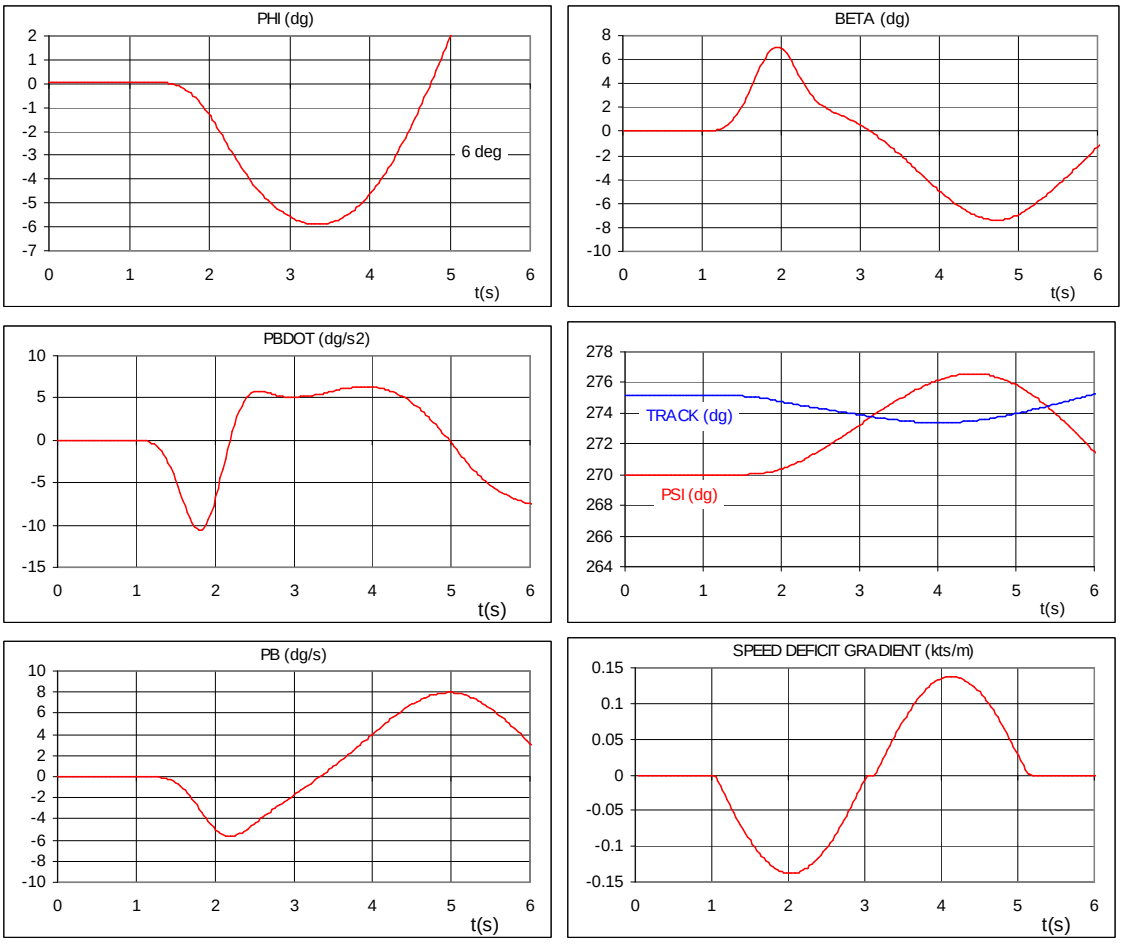

Figure 5-12: Lateral time histories corresponding to a lateral speed defect of 12kts

When passing the obstacle shading the cross wind falls of and track and heading come together leading to perturbations in side slip angle and roll. Due to the so called dihedral effect of the wing the lateral speed defect initially results in a positive side slip angle and left wing down roll acceleration.

5.2.5.3 Due to turbulence

Apart from a lateral speed defect also turbulence is capable of upsetting the aircraft during final approach. This is illustrated in Figure 5-13 in which the maximum bank angle in the altitude band of 50ft to 200ft is depicted encountered during 100 auto land approaches with the F100 aircraft in varying turbulence conditions. During the approaches no “stand alone” obstacle was present. From the individual plots in this figure it can be observed that when the standard deviation of the horizontal gust (sgmu) is increased from 1.0 knot to 7.4 knots the absolute

maximum bank angle excursion that can occur increases from approximately 1.6 degree to 8.3 degrees.

In the plots the surface roughness and reference wind speed is shown which leads to the sgmu range presented.

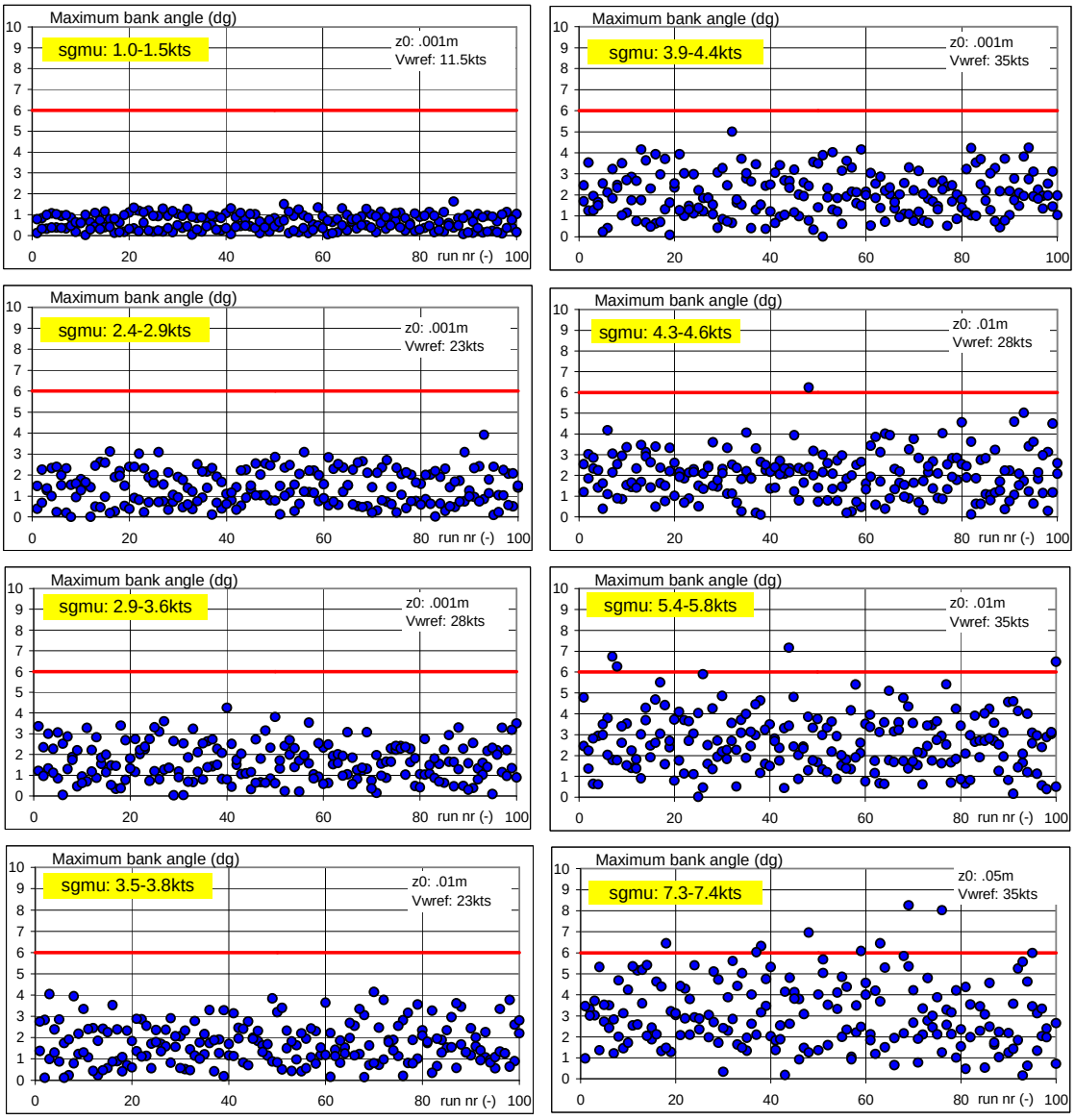

sgmu (kts)	1.0-1.5	2.4-2.9	2.9-3.6	3.5-3.8	3.9-4.4	4.3-4.6	5.4-5.8	7.0-5.9
	.001 11.5	.001 23	.001 28	.01 23	.001 35	.01 28	.01 35	.05 35
mean (g)	0.63	1.39	1.64	1.71	2.01	2.02	2.63	3.06
stdev (g)	0.36	0.82	0.90	0.95	1.01	1.06	1.35	1.59
max (g)	1.63	3.92	4.25	4.15	5.01	6.24	7.16	8.26
min (g)	0.02	0.00	0.03	0.11	0.01	0.10	0.02	0.16

Figure 5-13: Maximum bank angles as function of sgmu below 200ft

For reference in Figure 5-13 the 6 degrees bank angle limit applicable at the runway threshold and at main gear touch down has been indicated.

Figure 5-13 shows that standard deviations of horizontal turbulence (sgmu) in excess of approximately 4.5 knots may lead to a condition in which the absolute bank angle exceeds 6 degrees.

5.3 Subjective acceptance criteria

Subjective criteria for the piloted simulations have been based on Cooper-Harper and mental workload rating scales. Examples of these rating scales are presented in Appendix C. Although not used as a criterion the rating scale for assessing the control effort of selected parameters during a specific task is presented in this appendix also.

Albeit related to each other, approach and landing are different phases of flight for pilots with different performance criteria. Therefore in the piloted simulator experiment two phases have been defined for which pilot ratings have been collected.

Table 5–1: Acceptance criteria for pilot ratings

		approach (1000ft-200ft)	**landing (200ft-TD)**	**take-off**
longitudinal	**desired**	less than 1/2 dot	40-100ft over T/H	------
	adequate	less than 1 dot	100-150ft over T/H	------
lateral	**desired**	less than 1/2 dot	less than 30ft from CL	less than 10ft from CL
	adequate	less than 1 dot	less than 60ft from CL	------

First the ***'approach phase'*** which covered the height range from 1000ft to 200ft and the actual ***'landing phase'*** from 200ft to touch down including de-crab and flare. To assist the pilot in keeping consistent C-H ratings during the experiment for both phases different performance criteria have been used. These criteria are presented in Table 5–1.

The pilots were briefed to base the decision to either continue or abort the landing on:

- The interpretation of the basic flight instruments such as speed, speed trend, climb/sink rate, altitude, ILS deviations and wind vector display.
- The perceived hazard of the situation.

5.4 Summary of acceptance criteria

The following acceptance criteria have been defined for the offline/online simulation runs:

- Acceptance criteria on **objective** data
  i. For the **piloted simulations** the presence of a "stand alone" obstacle may not lead to an increase in the number of go-around's.
  ii. For the **offline simulations** the presence of an obstacle may not lead to a substantial increase in the number of crossings of the critical F-factor below 450 ft.
  iii. The touch down point of the aircraft's center of gravity must fall within the box defined in Figure 5-8.
  iv. Below 200 ft the maximum bank angle in the simulation runs may not exceed the values as indicated in Figure 5-9.
  v. No single landing may experience a bank angle at touch down exceeding the value corresponding to a nacelle or wing tip ground strike.
  vi. Descent rate below 200ft may not exceed 1000ft/min
- Acceptance criteria on **subjective** data (piloted simulations only)
  Cooper-Harper rating of less than or equal to 5 must be obtained for both the approach and landing phase.
  A C-H rating in excess of 5 indicates moderate deficiencies in flying qualities.
  Furthermore the mental workload must be no more than in between "*Demanding of pilot attention, skill or effort"* and "*very demanding of pilot attention, skill or effort"*.

6 Non-piloted F100 and B747simulations

6.1 Introduction

To extract valid conclusions from the offline simulations, validated flight simulator mathematical models are required in which the responses of an aircraft in reaction to atmospheric disturbances (including mean wind, shears, gusts and turbulence) are modeled with sufficient accuracy.
With the validated models offline auto land simulations can be performed in various atmospheric wind fields. For the purpose of this investigation two types of aircraft have been chosen each representing a specific aircraft class viz. a Boeing B747 and Fokker 100.
The objective of the offline auto land simulations is to find wind disturbances which are critical from an aircraft response and performance point of view.
Obviously handling qualities are difficult to predict when performing simulations in which the pilot is not participating in the control loop. However by means of a Monte Carlo like approach prediction of aircraft landing performance is possible with offline simulations.
In the simulations it is assumed that nominal conditions exist. This means that the following assumptions have been made:

- ILS precision approaches are performed.
- A maximum crosswind of 20 knots (excluding gusts) at the reference height of 10m is selected. The consequences of increasing the maximum crosswind to 25 knots (excluding gusts) are discussed in section 9.
- The high speed ground roll is part of the Fokker 100 **offline** simulations, because in high crosswind conditions the high-speed ground part of the landing is crucial. However because of the limited accuracy of the mathematical models describing the interaction of the aircraft, landing gear and runway surface results must be evaluated carefully.
- In the **piloted** simulations the high-speed ground part of the landing is not taken into account.

The F100 offline simulations have been performed by NLR whereas the Boeing B747 offline evaluation was done by the Aerospace Software & Technology Institute (ASTI) of TUD.

6.2 Wind conditions

The maximum crosswind/tailwind levels in which take-off and landing runways still can be used are very important. It determines the orientation of the main runways and can lead to specific requirements for necessary runways under crosswind conditions. The quadrangle in the wind rose shown in the left part of Figure 6-1 shows the implication of a number of requirements for runway 27 of Schiphol airport. It presents the boundaries for a crosswind of 20 knots (lines parallel to the runaway track), a tail wind of 10 knots (right line perpendicular to

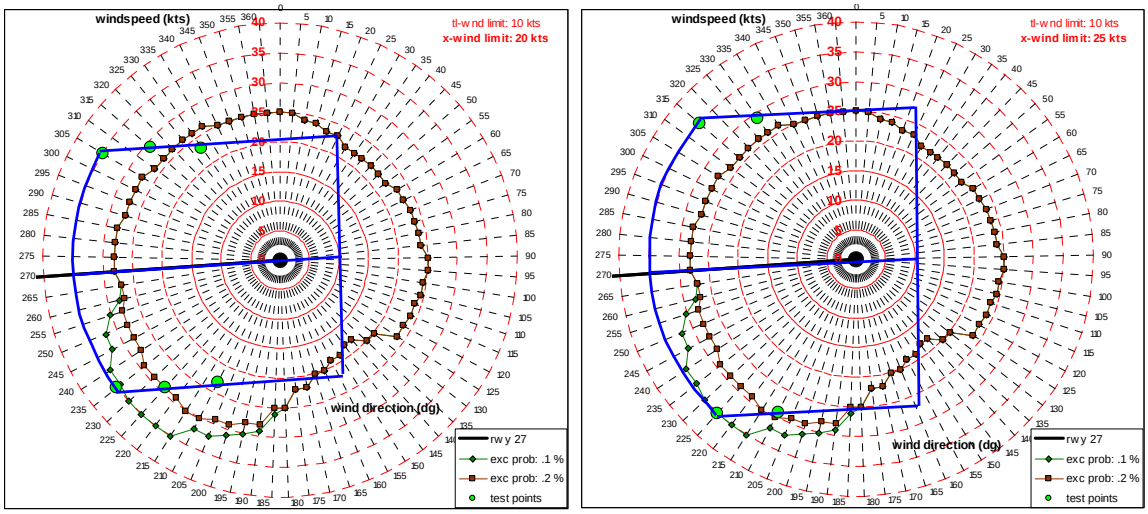

Figure 6-1: Wind rose for Schiphol airport in relation to runway 27

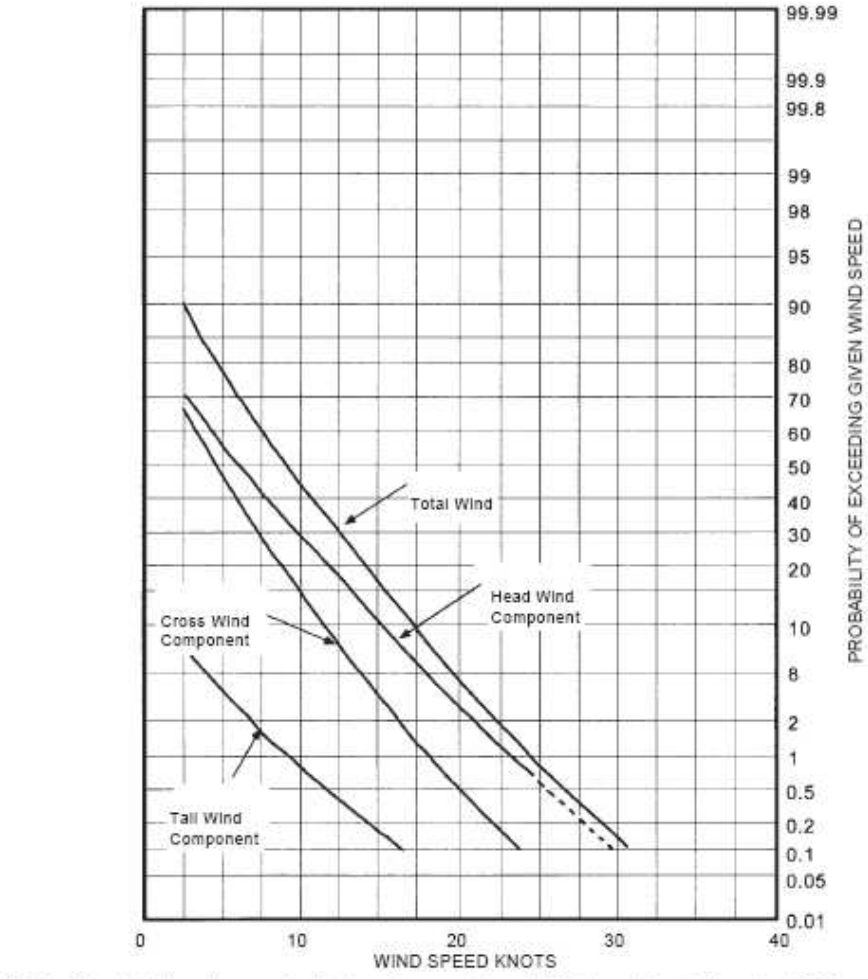

NOTE: This data is based on world-wide in-service operations of UK airlines (Sample size about 2000)

FIGURE 1 Cumulative probability of reported Mean Wind and Headwind, Tailwind and Crosswind Components when landing

the runway track) and a wind speed of 35 knots (arc at left). The right part of the figure shows the same boundaries for a crosswind of 25 knots, a tail wind of 10 knots and a wind speed of 35 knots. The wind rose also includes wind speed distributions for Schiphol as function of wind direction with a .1% and .2% exceeding probability. As can be observed from the plots maximum wind speeds of 35 knots with a .1% exceeding probability from south western directions can be encountered at Schiphol Airport.
For runway 27 the permissible wind directions without exceeding the specified wind limits can be found directly from the plots. From Figure 6-1 test points (green dots) have been determined for both the offline and online simulations.
The figure on page 63 labelled “FIGURE 1” is obtained from a JAR-AWO document ([10] and shows the probability of exceeding a given mean wind speed magnitude based on world-wide in-service operations of UK airlines. From this plot it appears that a 30kts mean wind has a probability of occurrence of .1%. However as is shown in Figure 6-1 for Schiphol 35kts wind speeds occur with a .1 % probability. Consequently there is a higher probability to encounter 30kts mean wind speeds or more at Schiphol airport.

6.3 Comparison between B747 and F100 aircraft

Table 6–1 shows a comparison of the B747 and F100 geometrical, inertial and flight condition-dependent parameters.
The table clearly shows the difference in aircraft proportions. In particular the difference in aircraft inertias is appealing and indicates why these two aircraft have been chosen for the simulations. It can be noted that the roll inertia of the B747 is almost 60 times the inertia of the Fokker 100, whereas the airspeed only is 1.2 times larger than the Fokker 100. Obviously this has impact on the lateral/directional flight dynamics.

Table 6–1: B747 and F100 aircraft data for approach/landing

		B747	F100	B747/F100
Parameter	**Unit**			
Wing area	m2	510.97	93.5	5.5
Mean aerodynamic cord	m	8.324	3.833	2.2
Span	m	59.643	28.076	2.1
Center of gravity range	% mac	14.5-32	7-35	
Mass	kg	240000	33000	7.3
Inertia moment Ixx	kgm2	18700000	320000	58.4
Inertia moment Iyy	kgm2	41000000	1800000	22.8
Inertia moment Izz	kgm2	56000000	2000000	28.0
Inertia moment Ixz	kgm2	1100000	90000	12.2
Flap setting	deg	30	42	
Gear position		dwn	dwn	
Reference speed	kts IAS	141	118	1.2

Aircraft parameters for the simulations such as landing mass and flap setting have been based on a light aircraft weight. Light aircraft weights are chosen because then reference speeds are lowest, which from a flying qualities point of view are more critical.
Recommended flap settings and speeds result from the manufacturer's operational manual (AOM) of the two aircraft (see Table 6–2).

Table 6–2: B747 and F100 reference data

F100 (off line simulations)				B747 (piloted simulations)			
	mass CG	32860 kg 21.7% mac			mass CG	240000 kg 25 % mac	
APP/LDG	Vref	129 kts	flap 25	APP/LDG	Vref	148 kts	flap 25
APP/LDG	Vref	118 kts	flap 42	APP/LDG	Vref	141 kts	flap 30

To bring the dimensions of the two aircraft in perspective Figure 6-2 shows the front view of the B747 and F100 in relation to an obstacle height of 25m.

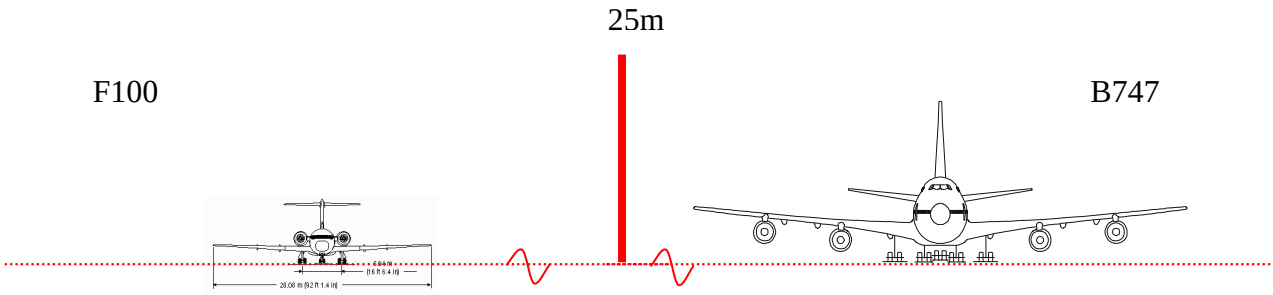

Figure 6-2: Aircraft dimension related to an obstacle height of 25 m

The crosswind landing technique of the B747 and F100 is different. The B747 normally is traverse landed in a nominally wings level condition. Too large control wheel inputs must be avoided because of the complicated lateral control system of the aircraft. At a certain level of wheel input also spoiler deflection is commanded which may lead to large drag increases not desirable during the final approach.
Contrary to the B747 the lateral flight control system of the F100 is much simpler and only commands aileron deflection. With the F100 a de-crab maneuver is initiated between 100-150ft AGL leading to a non-wings level condition during the flare with the upwind main gear touching first.

6.4 Fokker 100

6.4.1 Mathematical models

For the dynamic simulations of the ILS auto land approaches and landings in x-wind conditions use has been made of an offline simulation package based on the non-linear equations of motion ([30]. Beside the non-linear aerodynamic model and engine characteristics the package also contains the mass and inertia properties of the Fokker 100. Generic auto pilot and auto throttle control laws governing the control surfaces (ILS tracking) and throttles (airspeed) are incorporated in the simulation model.

6.4.1.1 Mass properties model

The mass and inertia properties of the Fokker 100 including fuel quantity and payload distribution are derived from data presented in ([41].

Table 6–3: Mass properties data of F100

Fuel (kg)	5010	Ixx (kgm2)	356920
Payload (kg)	3200	Iyy (kgm2)	1843450
OWE (kg)	24648	Izz (kgm2)	2111930
Aircraft mass (kg)	32858	Ixz (kgm2)	90260
Xcg (%mac)	21.7	Ixy (kgm2)	6930
Ycg (%span)	.06	Iyz (kgm2)	-145
Zcg (%mac)	6.8		

Table 6–3 gives an overview of the mass properties data used in the simulations.

6.4.1.2 Aerodynamic model

For the approach and land simulations use was made of the aerodynamic data base of the Fokker F100 as laid down in Fokker report L-28-336 ([42]. The aerodynamic database used for stability and control purposes is built up in two parts viz. LG100x.tab containing the longitudinal characteristics and DR100x.tab, which yields the lateral/directional data.

6.4.1.3 Engine model

The performance and transient characteristics of the Rolls-Royce TAY Mk650 engines used in the simulations are obtained from a technical design report.

6.4.1.4 Landing gear model

The offline simulation package also yields the dynamics of the undercarriage, including the tire and shock absorber characteristics of the F100 landing gear. The required data for the under carriage is obtained from ([41].

6.4.1.5 Flight control model

The F100 offline auto land simulations are governed by:

1. Auto pilot control laws which command the control surfaces of the aircraft to follow the ILS glide path and
2. Auto throttle control laws that command the engines to deliver thrust to maintain the commanded approach speed.
3. Flare and de-crab control laws that take over aircraft and thrust control at defined heights above the ground. Control surface and throttle commands line up the aircraft with the runway centerline bring the aircraft in a flare pitch attitude and close the throttles to idle.

These actions must be performed withstanding the wind disturbances that are present during the approach.

6.4.1.6 Wind climate model

6.4.1.6.1 Wake axes

In the wake behind an obstacle the average wind speed is reduced but mechanical turbulence is increased, because some of the velocity energy is converted to turbulence energy. Consequently intense intermittent gusts and matching lulls can be experienced on the lee side. Turbulent eddies may form in both the horizontal and vertical plane.

The mathematical model of the earth boundary layer and the disturbed wind speed profile behind a three dimensional obstacle is discussed in section 3 and section 4 respectively. The model described in section 4 (applicable to a generic block shaped obstacle with “worst case” wake characteristics) has been implemented in the offline simulation package of the Fokker 100.

The wind climate model and all variables related to it are valid in the so-called “***wake axes system***”, which is defined as follows:

Origin: Situated in the geometric center of the obstacle projected on the ground.

XPATHN-axis: Perpendicular to windward wall, positive in the direction of the wind vector.

YPATHN-axis: Perpendicular to the X-axis, positive to the left when looking in the positive X-direction

ZPATHN-axis: Perpendicular to the ground plane positive upwards

This axes system is presented in Figure 6-3 in blue.

However the position of the aircraft is presented in the "***runway axes system***", which is defined as:

Origin: On the runway centerline at runway threshold

XRW-axis: Along runway centerline positive in the direction of landing.

YRW-axes: Perpendicular to X-axis positive to the right as seen from the landing aircraft

HRW-axis: Perpendicular to the ground plane positive upwards

This axes system is presented in Figure 6-3 in red.

Figure 6-3 shows schematically the part of aircraft trajectory that is affected by the obstacle shading and also the positions where the landing aircraft may encounter vortices created by a PDP-like obstacle.

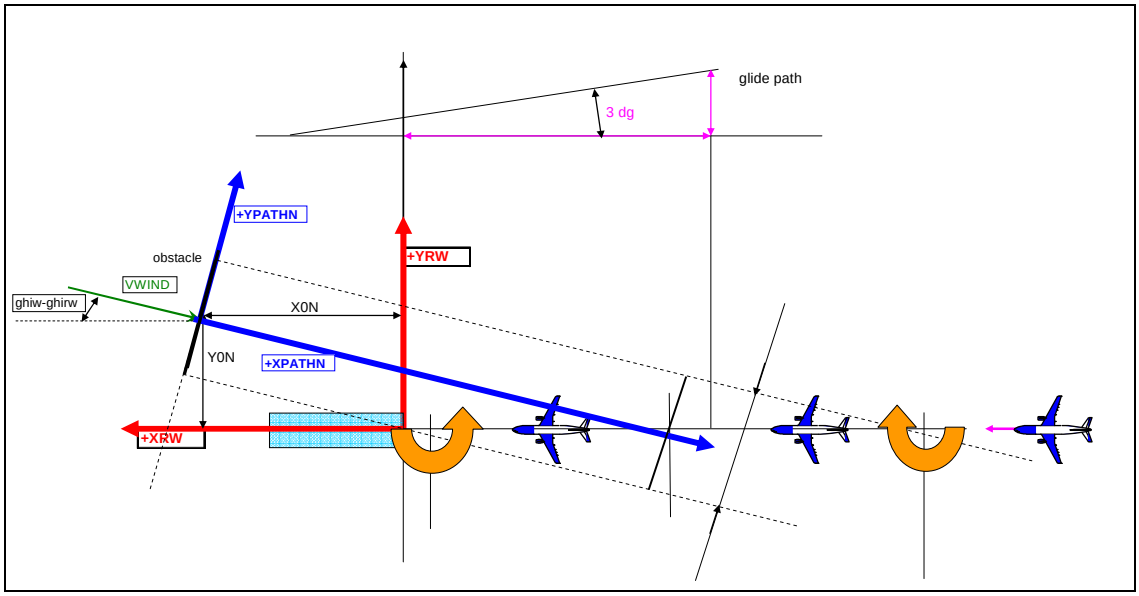

Figure 6-3: Conversion of wake to the runway axes system

6.4.1.6.2 Effect of wake vortices on F100 aircraft dynamics

As is elaborated in section 4 and Appendix B the strength of the vortices streaming from a PDP like structure can be estimated. This data is employed to calculate the resulting increments/decrements in the vertical force and rolling moment on a F100 wing platform crossing the vortex pair. The vortex model is based on the Rankine formulation ([43] and ([44].

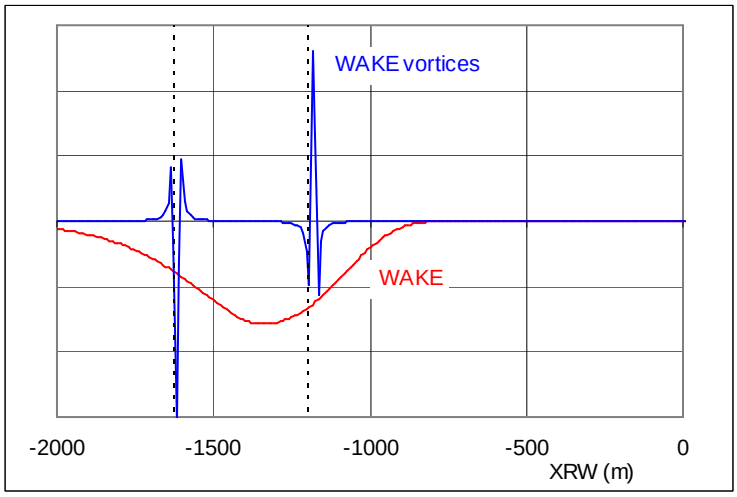

Figure 6-4: Position of obstacle vortices in relation to the wake

Figure 6-4 illustrates the position of the vortices with respect to the wake behind an obstacle. The wake is shown as function of the distance in front of the runway threshold. The wake characteristics correspond to an obstacle positioned 400m in front of the runway threshold with an offset to the runway centerline of 700m. The obstacle is block shaped with a width of 250m and a height of 45m. The wind speed at the reference height of 10m is 35kts.

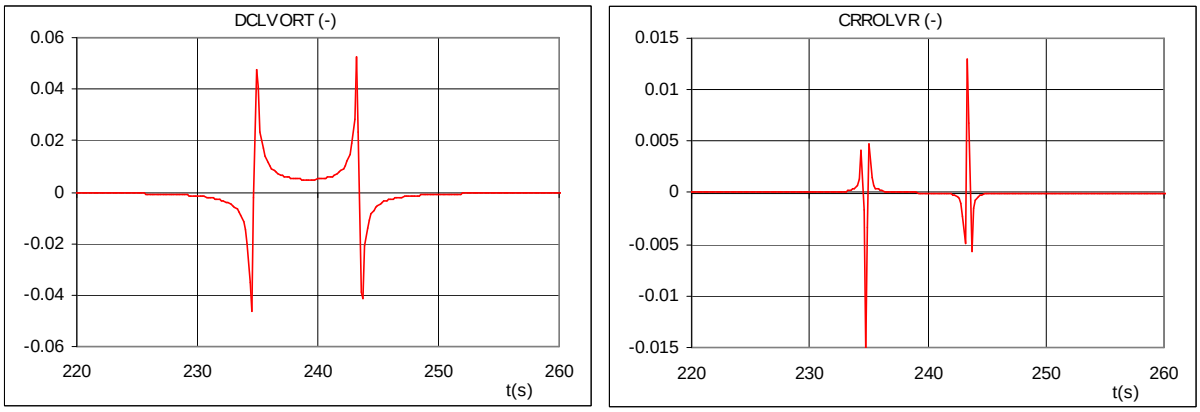

Figure 6-5: Delta lift and rolling moment due to wake vortices

Figure 6-5 shows the ensuing changes due to the vortices on the lift (DCLVORT) and rolling moment coefficient (CRROLVR) of the F100 aircraft.
The induced aircraft perturbations due to these change in lift and roll appear to be small as can be observed from Figure 6-6 and Figure 6-7. The plots show the response of the aircraft in terms of delta angle of attack (ALFVORT), roll rate and roll angle.

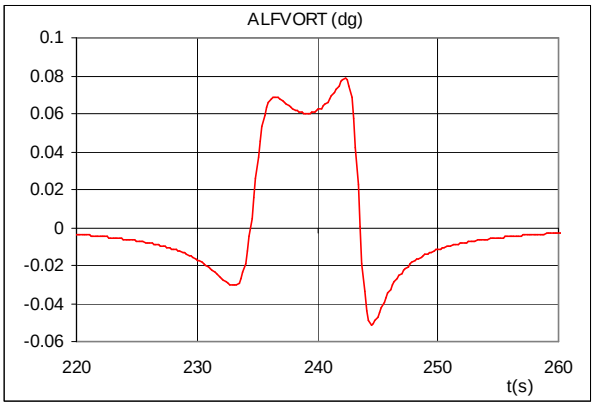

Figure 6-6: Delta angle of attack due to obstacle vortices

In section 4 and Appendix B it is shown that contrary to the wake vortices streaming from aircraft wings vortices due to obstacles are much smaller in strength. Consequently they are not capable to affect the attitude and performance of a landing aircraft significantly.

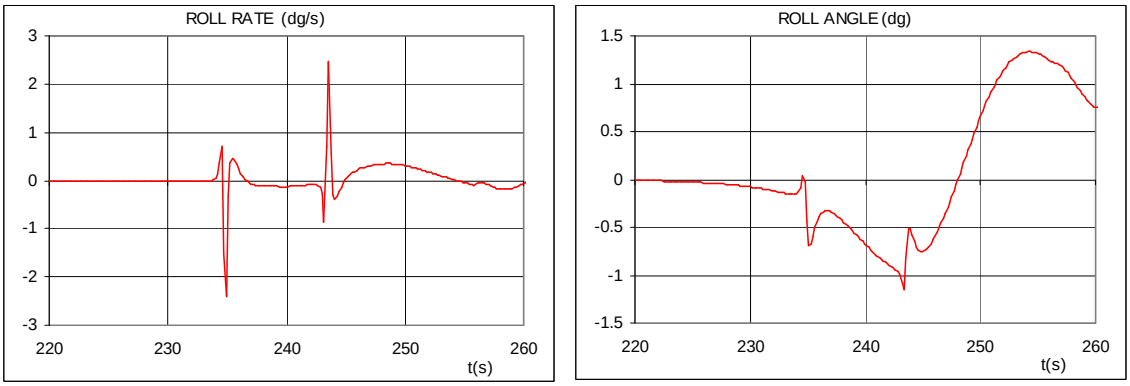

Figure 6-7: Lateral response due to wake vortex pair encounter

6.4.2 Model check out

Mean wind speed

Before the start of the simulations the implemented wind climate including the gust/turbulence models were compared with models available in the literature. Both MILSPEC MIL-F-8785C ([31] and JAR-AWO ACJ AWO 131 ([10] define mean wind speed models and turbulence spectra for low altitudes (<2000ft).

MILSPEC requires for the certification of Category C operations a low altitude disturbance model. Just as the JAR-AWO model the MILSPEC model is based on a logarithmic wind profile and a reference wind speed at a height of 20ft. The turbulence models are based on both the von Karman and Dryden form.

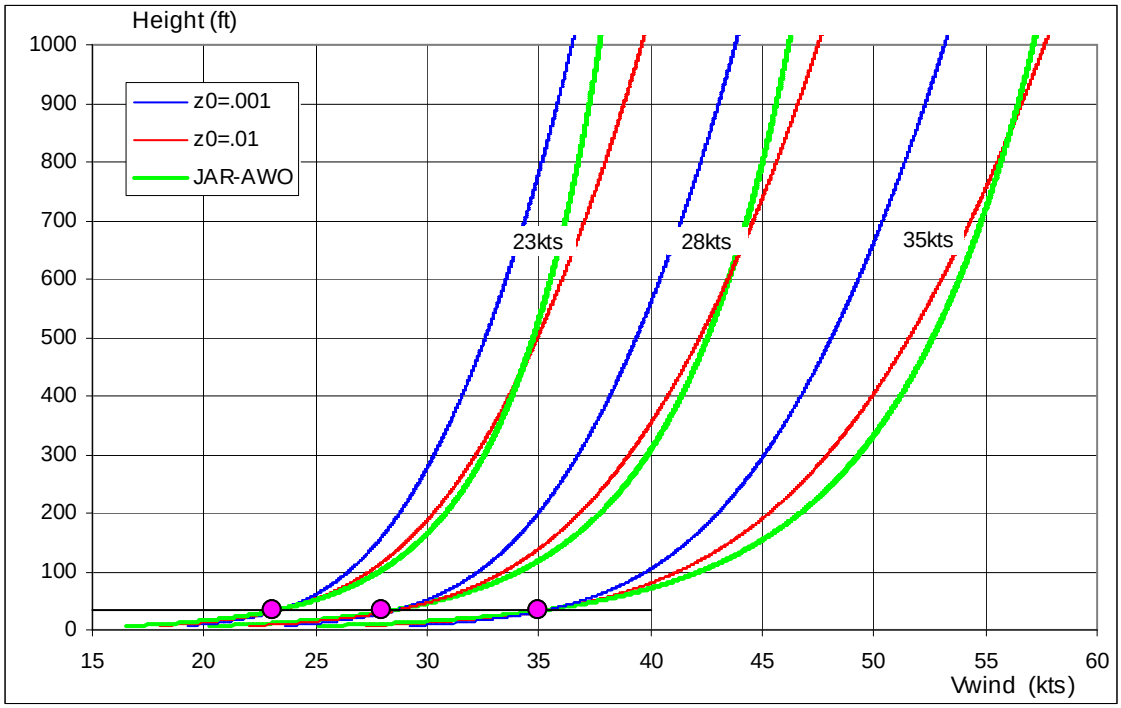

Figure 6-8: Comparison of wind profiles with JAR-AWO/MILSPEC data

Turbulence RMS intensities are defined. Scale lengths are the same as for JAR-AWO. Furthermore it can be shown that the mean wind speed model as specified by JAR-AWO is identical to the MILSPEC wind speed logarithmic profile if a value of .046m is chosen for the surface roughness parameter (z0).

Figure 6-8 shows mean wind speed profiles applicable for a reference wind speed (Vwind ref) of 23, 28 and 35 knots according to the JAR-AWO and MILSPEC (z0=.046m) model and the implemented wind climate model (z0=.001 and z0=.01) in the F100 simulation. It can be observed that the JAR-AWO wind profiles and the wind profiles used in the simulations corresponding to a z0 of .01m cover the same wind speed range.

RMS turbulence intensities

RMS values of horizontal turbulence intensities (sgmu, sgmv) as result of reference wind speeds of 23, 28 and 35 knots and surface roughness of .001 and .01m are depicted in Figure 6-9. Also the corresponding JAR-AWO/MILSPEC RMS values of the horizontal turbulence intensities are presented for the three mentioned wind speeds. Just as in Figure 3-5 also in Figure 6-9 the three turbulence level ranges as defined by JAR-AWO are indicated. It shows that the selected reference wind speeds and surface roughness lengths cover a large range of turbulence levels. Light to heavy turbulence is encountered. It can be observed that the JAR-AWO 'RMS' values lie between 'RMS' values corresponding to a z0 of .001m and .01m used in the simulations.

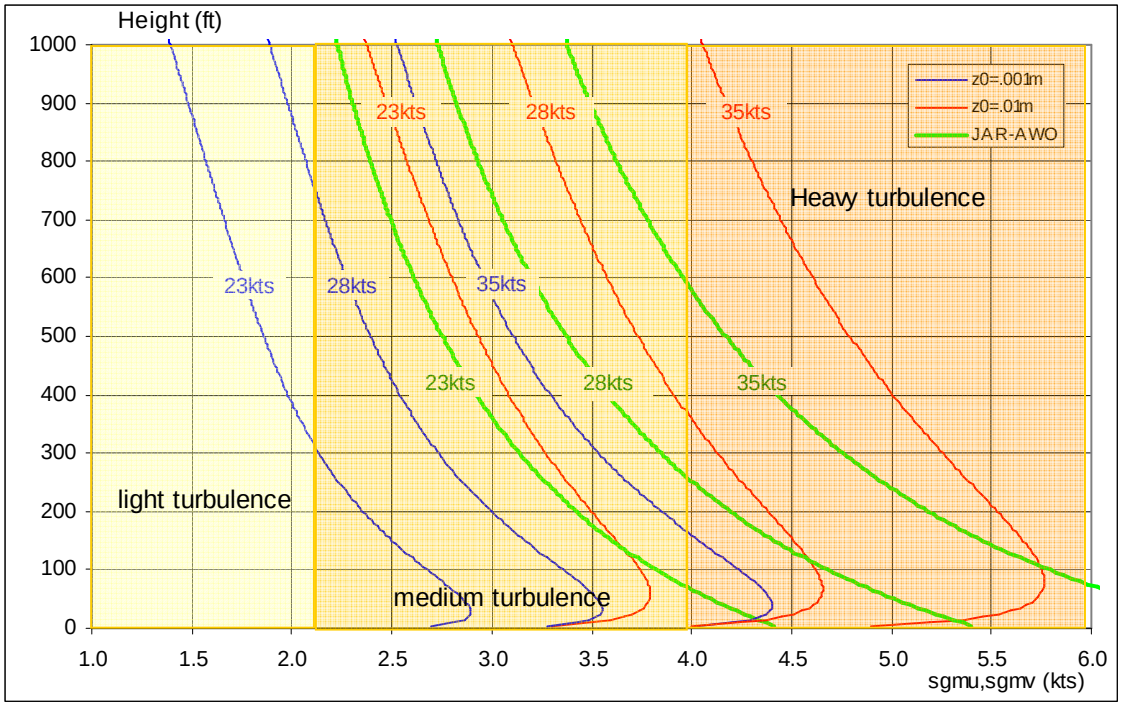

Figure 6-9: Comparison of RMS turbulence intensities with JAR-AWO/MILSPEC data

However standard deviations of turbulence exceeding approximately 6 knots result in large structural excitations on an airframe. This is illustrated by Figure 6-10 in which the normal load deviations due to turbulence on a F100 aircraft are shown as function of surface roughness (z0) and reference wind speed (Vwind ref). The normal loads shown are the average of the maximum/minimum normal load that occurred in samples of 100 approaches performed for a number of z0/Vwind ref combinations.

From the figure it can be observed that for a surface roughness of .001m maximum normal load varies between 1.15g and 1.25g. According to ICAO standards this corresponds to low-moderate turbulence. For a surface roughness of .01m normal load variations already lie between 1.22g and 1.35g which is characterized as moderate turbulence. JAR-AWO/MILSPEC turbulence (green ovals in Figure 6-10) leads to normal load values between 1.3g and 1.48g which can be considered as an upper limit (severe turbulence) to what is tolerable from a flying qualities point of view.

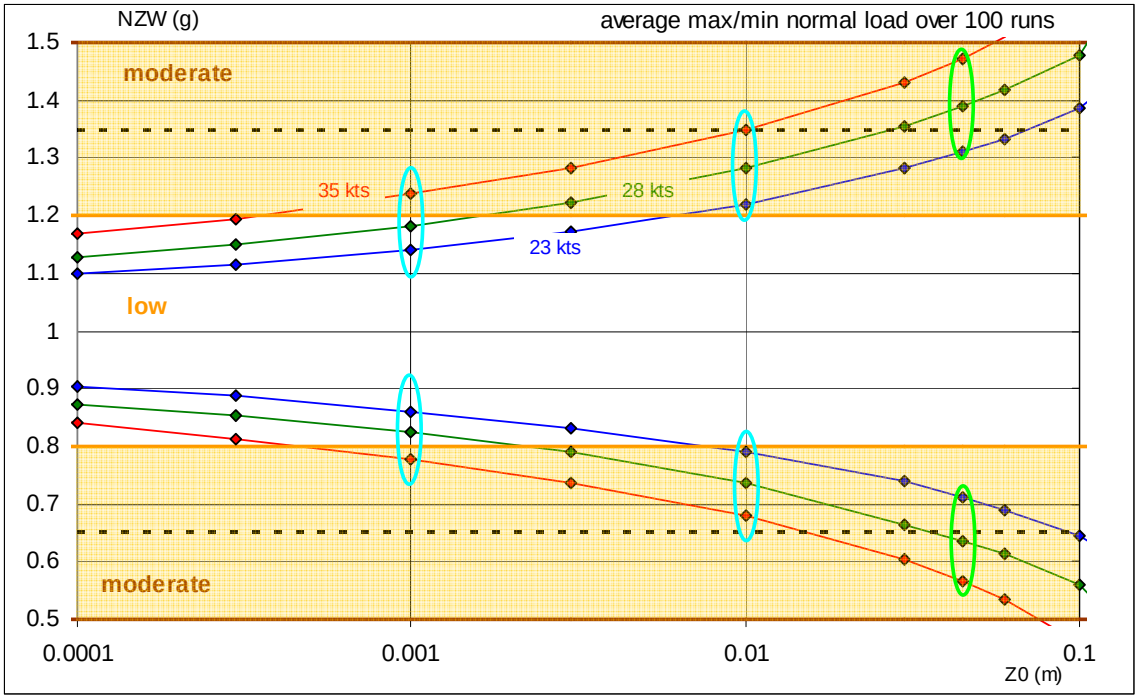

Figure 6-10: Normal load as function of surface roughness and wind speed

In Figure 6-10 lines corresponding to .35g variations are drawn. According to Table 3–4 this range is labeled as heavy turbulence by JAR-AWO standards.

Power spectrum density

Figure 6-11 shows power spectrum density (PSD) plots applicable to the model turbulence in three directions (Ugust, Vgust and Wgust). The data is recorded at airspeed of 66.9 m/s and applies to a scale length of 1000ft in each direction.

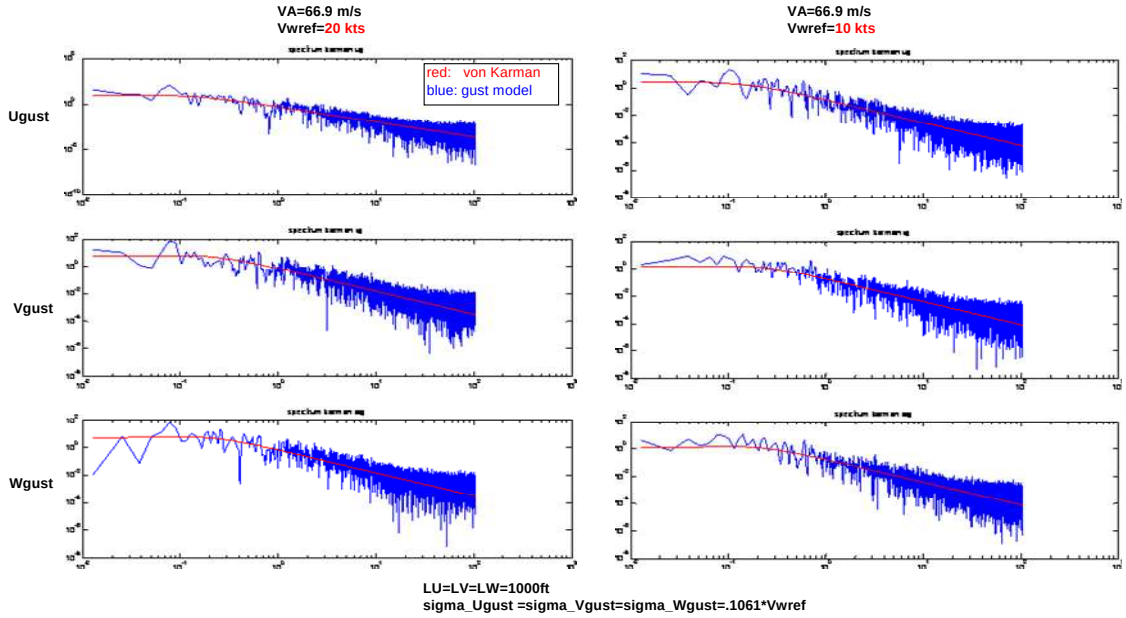

Figure 6-11: PSD plots of model turbulence in relation to the von Karman spectra

The model turbulence is compared with the von Karman spectra for two reference wind speeds viz. 10kts and 20kts. The RMS values of the turbulence depend on the reference wind speed and are chosen the same in the three directions. As can be perceived a good correspondence as function of frequency is obtained.
Finally the model turbulence data is compared with flight data from Fokker 70 crosswind certification trials performed at Keflavik airport (Iceland) ([22]. According to the turbulence scaling defined by ICAO (Table 3–4) the aircraft experienced heavy turbulence during these flight tests.

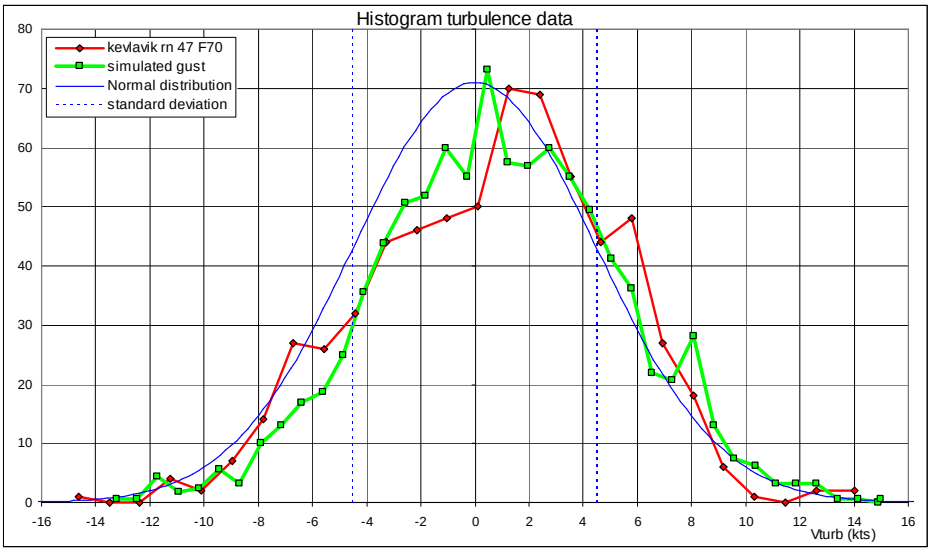

Figure 6-12: Histogram of turbulence data from flight and model

Figure 6-12 shows a histogram of the F70 Keflavik data corresponding to an approach towards runway 020. This approach resulted in a go-around initiated at approximately 100ft AGL.
In addition in the plot the corresponding RMS value of 4.3kts is indicated. Simulated model turbulence data with the same RMS value is represented by the green line. For reference the corresponding normal distribution is plotted as well.
Due to the stochastic behavior of the gust/turbulence every simulated approach is unique. However all samples are part of the envelope defined by the overall model parameters such as reference wind speed, surface roughness, RMS of the turbulence intensity, scale length and gust speed envelope. Figure 6-13 shows six samples of wind speed profiles corresponding to a wind speed of 35kts at the reference height (10m) and a surface roughness of .01m. For reference also the wind profile is plotted which was reconstructed from an approach and landing of a Boeing 757 aircraft in strong crosswind and turbulent conditions ([39].

Critical F-factor

As discussed in section 5 below a height of 450ft a critical F-factor of .15g is chosen as an acceptance criterion for the offline F100 simulations. Because of this, tests are performed to make sure that the algorithm in which the F-factor is calculated is a valid procedure.
The F-factor takes the effects of both performance decreasing horizontal shears and vertical shears into account.
Figure 6-14 (a) shows the airspeed decay as result of a performance decreasing wind deficit of 7kts, which occurs in a period of time of 5 seconds. Gust/turbulence is not present. This more or less represents the 7kts wind speed loss behind an obstacle. It can be observed that the F-factor (FFACT) reaches a maximum value of .11g too low to trigger the critical F-factor of .15g.
Figure 6-14 (b) shows the airspeed decay as result of a performance decreasing wind deficit of 20kts also taking place in five seconds. Now it is evident that the F-factor exceeds the critical F-factor after a time period of approximately 4.2 seconds.

A final test of the model wind shear logic comprises a simulation with a test case used for the certification of the F100 wind shear system ([46]. The horizontal (VWIND) and vertical (WEW) wind as function of time are presented in the left part of Figure 6-15. When turbulence with an RMS turbulence intensity of 2.6m/s (5.1 knots) and a scale length of 500ft in all three directions, is added to the wind profiles, time histories of the horizontal and vertical wind result as presented in the right part of Figure 6-15. Figure 6-16 shows the response of the F100 aircraft to the wind profile shown in the right part of Figure 6-15. Presented are the horizontal and vertical shear components that are part of the F-factor (section 5.2.1). Furthermore the decrease in performance is clearly visible through the loss in air (ground) speed. As can be observed airspeed even drops below the reference speed of 1.3 Vs. It must be mentioned though that in this simulation no throttle inputs are given. Normally the auto throttle will react to the speed loss by applying power.

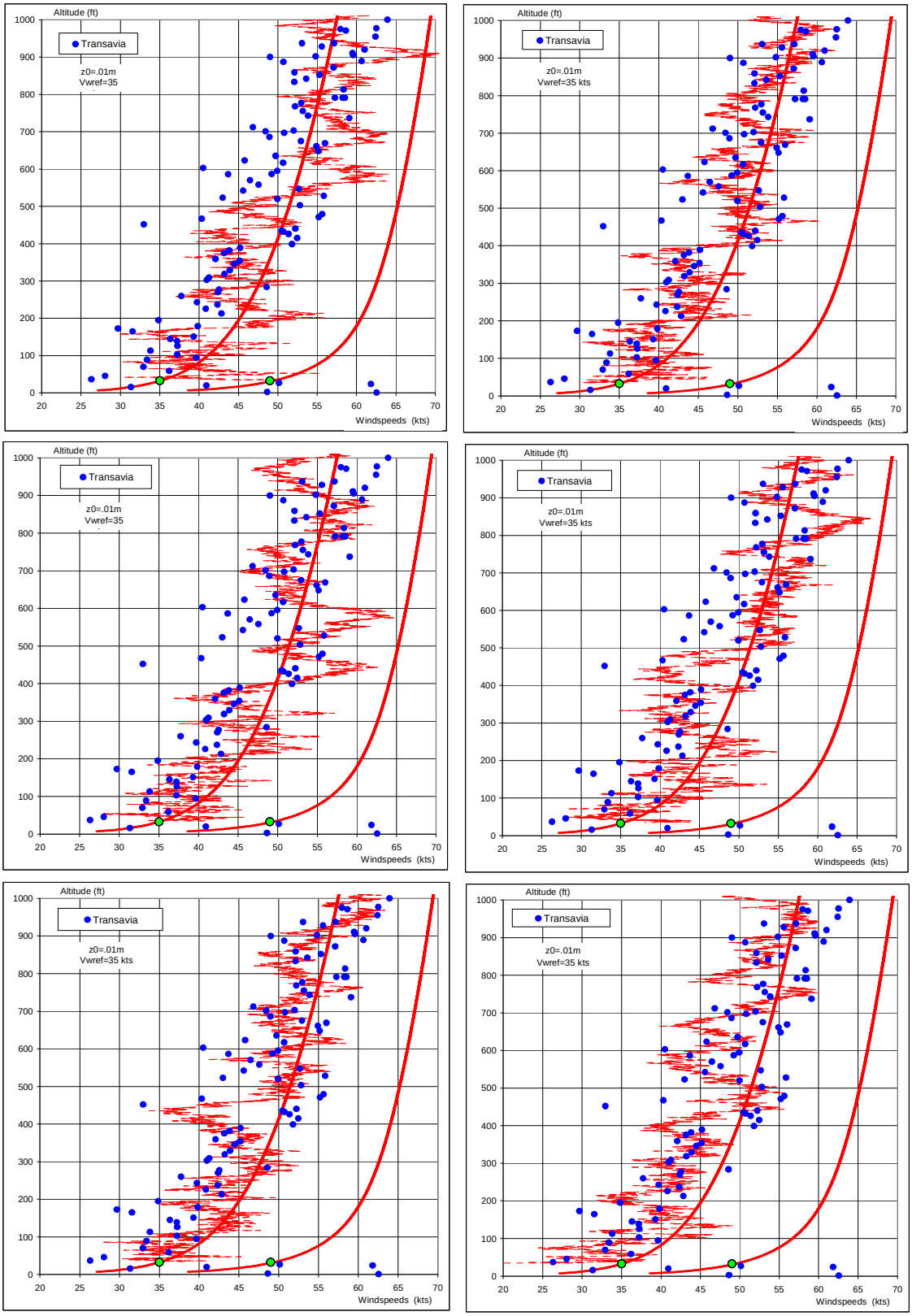

Figure 6-13: Model wind samples compared to wind profile from ([39]

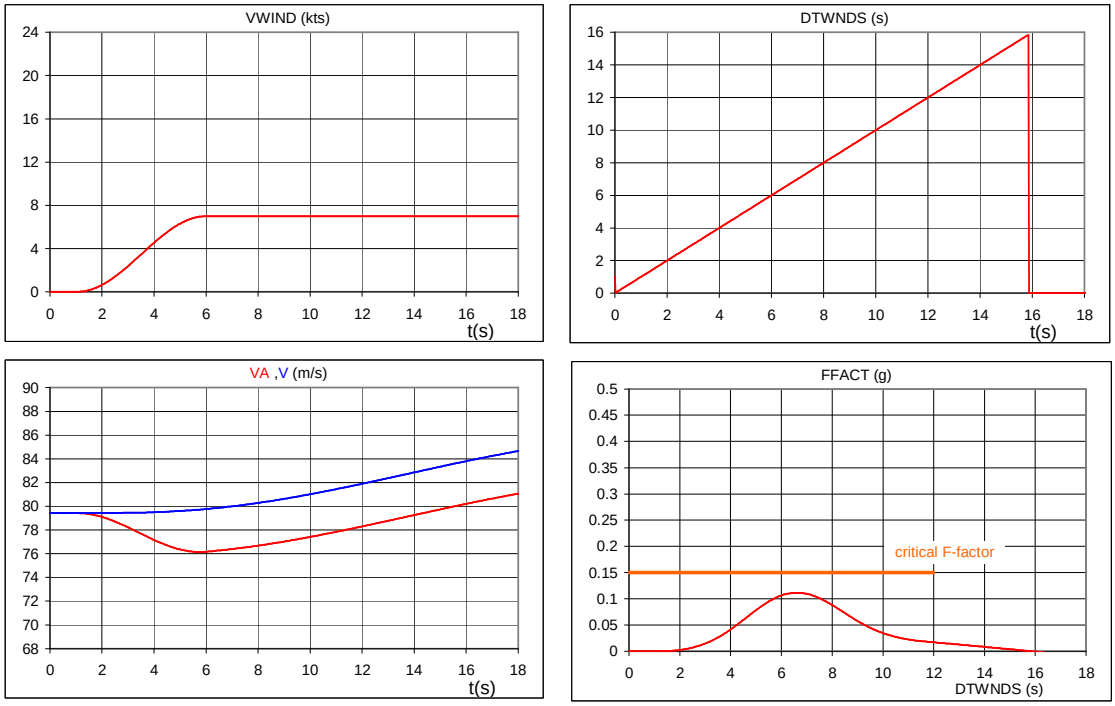

a) Speed deficit of 7kts

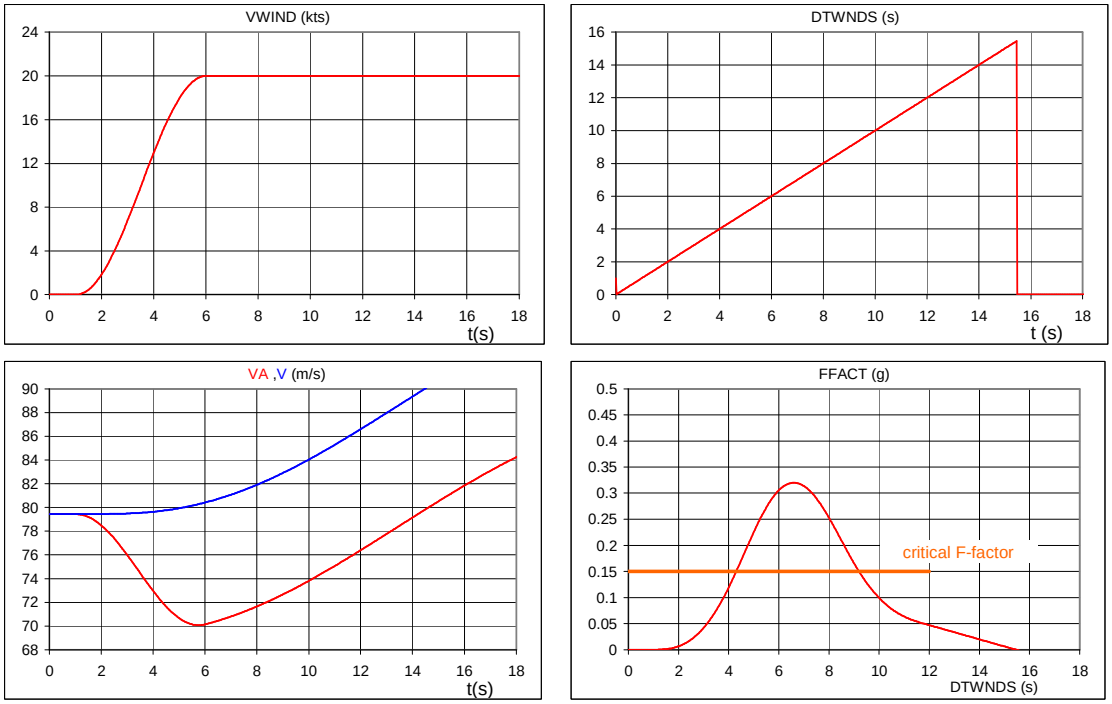

b) Speed deficit of 20kts

Figure 6-14: Speed deficit in relation to the "F-factor"

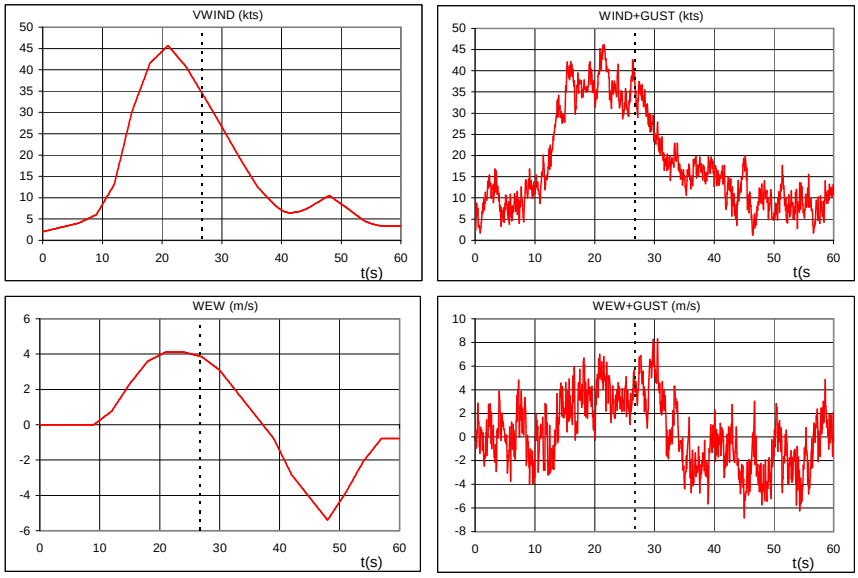

Figure 6-15: Wind shear profiles with and without turbulence

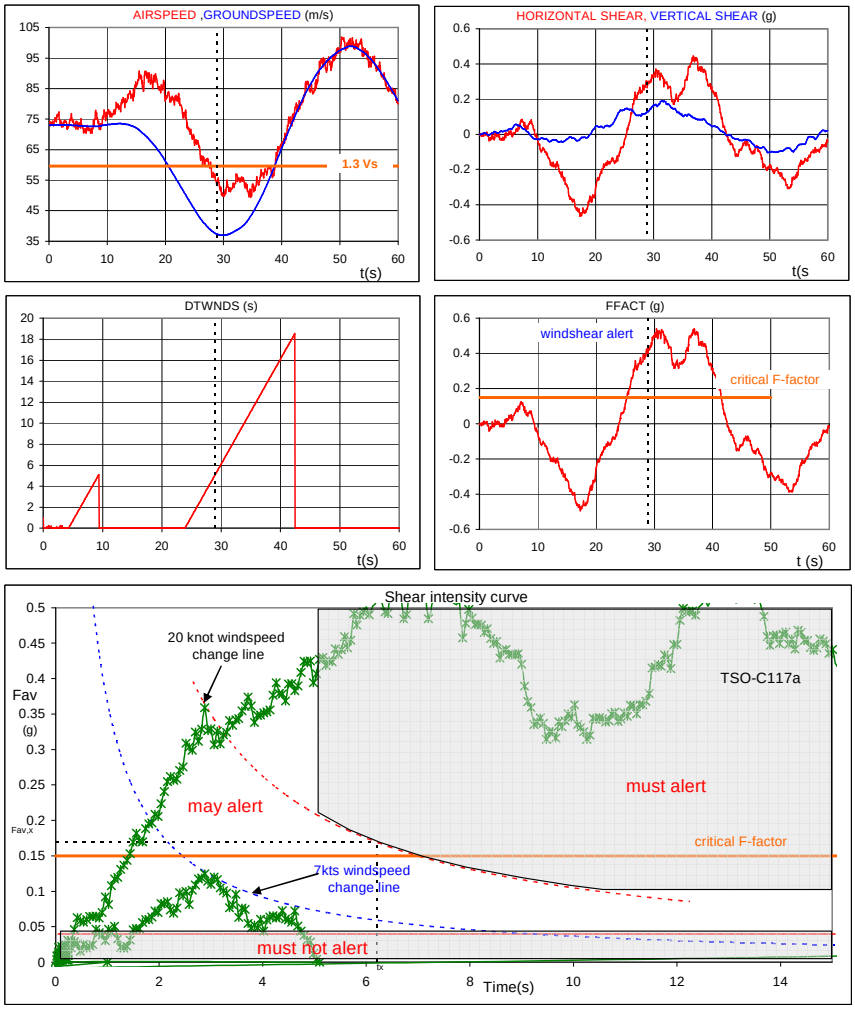

Figure 6-16: Wind shear test

From the plot in Figure 6-16 in which the F-factor (FFACT) is displayed it can be noted that a wind shear alert is generated after 29.6 seconds into the time history or 5 seconds after the system is armed (see DTWNDS parameter). This event is indicated in the other plots as well. In the "*shear intensity curve*" plot it can be observed that the real wind shear threat is triggered whereas smaller airspeed variations due to turbulence remain below the critical F-factor and trip levels of the wind shear alert logic.

6.4.3 Test matrix

The test matrix for the offline F100 simulations comprises a number of selected wind/gust/turbulence conditions in combination with a limited number of obstacle positions and obstacle dimensions in the sector defined as the ***green*** area in section 1. This is based on the observation that obstacles situated in this sector are able to affect the aircraft on the glide path below approximately 350ft. Obstacles positioned outside this sector affect the aircraft above 350ft. In addition it appeared from simulations that the effects of the wake outside the ***green*** area vanished and that the wake turbulence merged into the wind and gust/turbulence characteristics governed by surface roughness parameters. As was described they represent the combined wind disturbance effects of a much larger build up area.

Wind conditions selected

Wind conditions chosen for the F100 simulations to runway 27 of Schiphol Airport are applicable for a cross wind limit of 20kts without gusts as presented in Table 6–4.

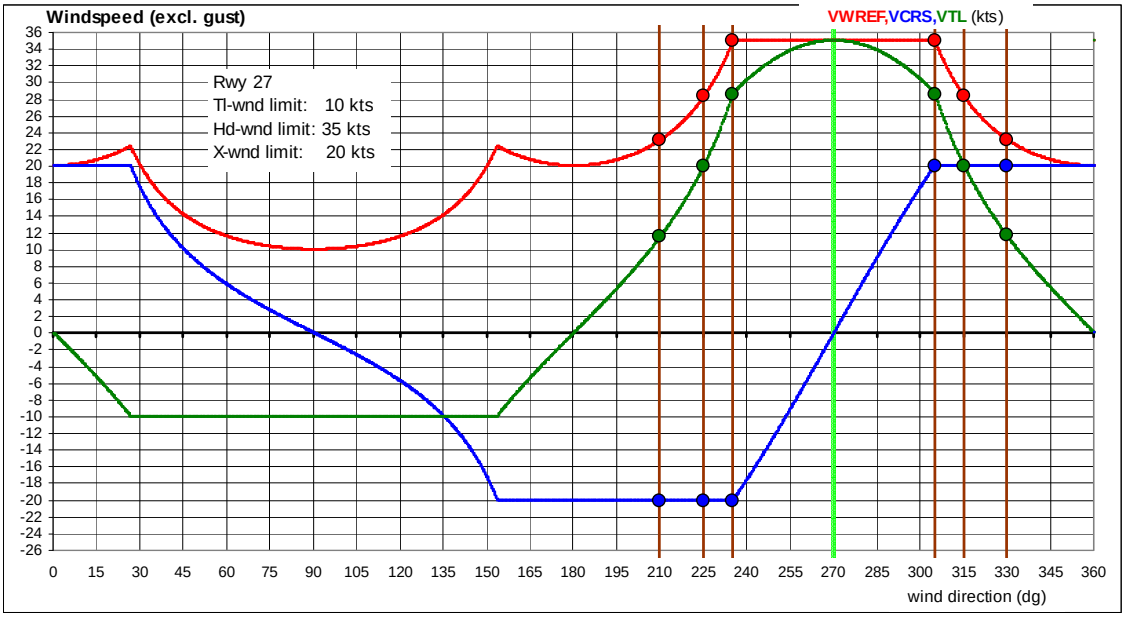

Figure 6-17: Wind speeds as function of wind direction

Table 6–4: Wind conditions for F100 offline simulations

Wind speed (kts)	Wind direction (dg)	Cross wind (kts)	Head wind (kts)
23	210/330	20	12
28	225/315	20	20
35	235/305	20	29

As can be observed from both crosswind from left and right have been included.
These wind conditions are obtained from the left wind rose shown in Figure 6-1 and are depicted in this plot by green dots. The selected wind conditions with respect to runway 27 are also presented in Figure 6-17, which shows the total mean wind speed (VWIND REF), the crosswind (VCRS) and headwind (VTL) components as function of wind direction. The maximum wind speed that is employed in the simulations is restricted to 35kts. From the wind rose shown in Figure 6-1 it can be noted that this wind speed from south western directions occurs at Schiphol airport with a .1% exceeding probability.

Obstacle dimensions and positions

The upper constraint posed on obstacle height is determined by the ICAO obstacle clearance planes as defined in ([11]. The upper left graph in Figure 6-18 shows the "Annex 14" maximum allowable height of a "stand alone" obstacle up to a maximum of 160m. In the plot the centers of the "stand alone" obstacles with the "Annex 14" height limit are distributed over a ground grid originating at the center of the threshold and extending 6000m in front of the threshold (X0) and 6000m perpendicular to the runway centerline (Y0). The lower plots in Figure 6-18 present the "*maximum speed defect*" and "*maximum RMS turbulence intensity*" that is experienced by an aircraft on the glide path when it encounters the wake of an "Annex 14 height limited" worst case block shaped obstacle positioned on the defined ground grid. The height of the glide path where this encounter occurs is presented in the upper right plot of Figure 6-18. The speed defect and RMS values presented in Figure 6-18 correspond to the following wind climate parameters:

1. Reference wind speed: 23 knots
2. Wind direction: 330 degrees
3. Surface roughness: .01m.
4. Porosity obstacle: -100% "Worst case"

According to Figure 3-5 this means that due to the overall surface roughness medium turbulence conditions are present.
From calculations it appears that critical wake characteristics occurred between an obstacle width of 200m and 300m. Smaller widths resulted in wakes that were too small in endurance to change the attitude and performance of the aircraft significantly. Larger widths did not aggravate the wake substantially further. Therefore both for the offline and online simulations a standard obstacle width of 250m has been adopted.

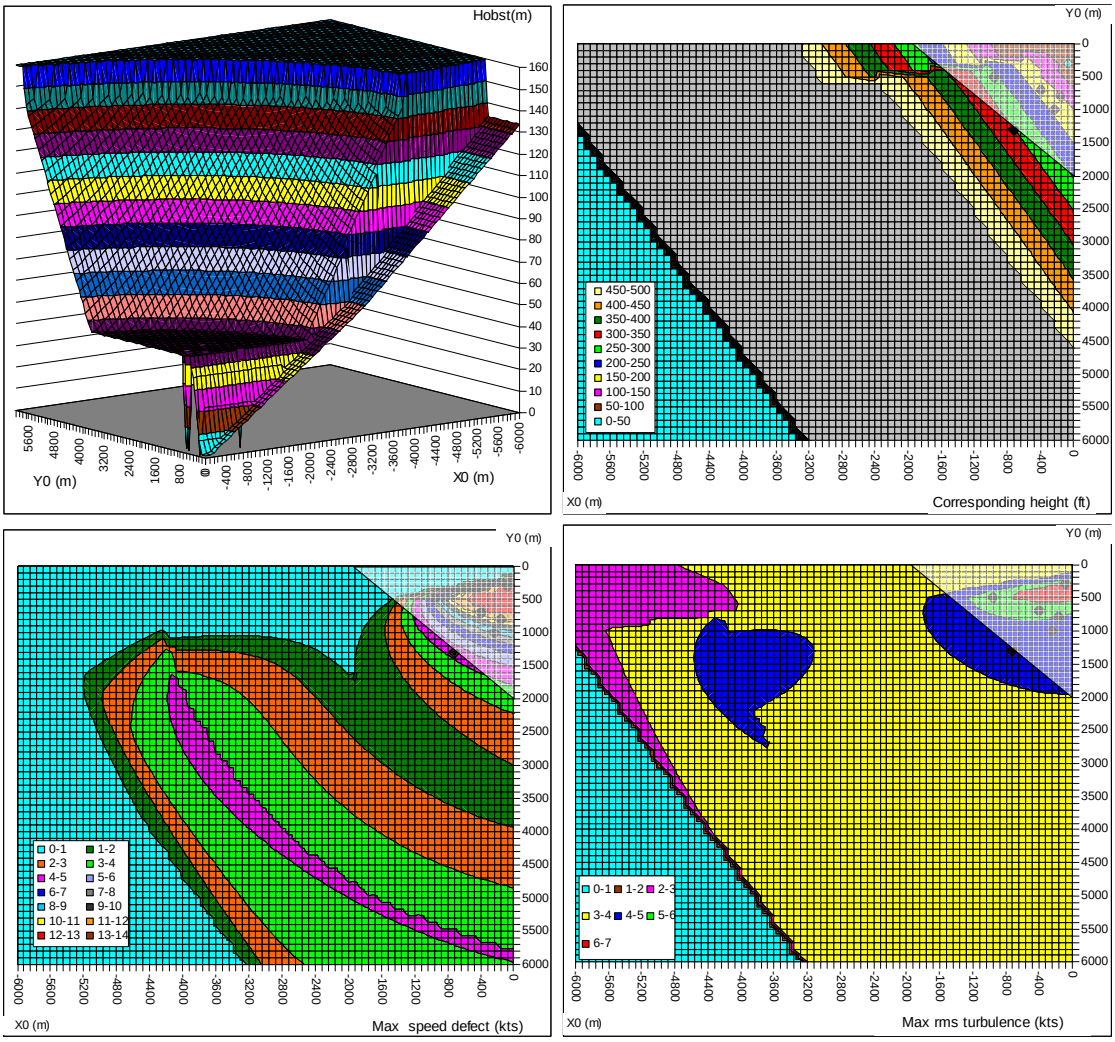

Figure 6-18: Speed defect and RMS turbulence intensity corresponding to annex 14 planes

A number of observations can be made from Figure 6-18:

- Speed defects up to 13 knots occur within a disk-shaped segment of 1000m (X0) x 1200m (Y0) with origin at the centre of the threshold.
- Corresponding RMS turbulence intensity values within this segment range from 4 to 7 knots.
- Glide path heights at which these speed deficits and RMS values occur, range from 0 to approximately 200ft.
- For the wind conditions simulated the upper right plot shows that the wind disturbance affect the aircraft below 350ft when obstacles are situated inside the triangle defined by the corner points X0=2000m and Y0=2000m. This is the **green** area defined in Figure 1-1 and is indicated in the plots by the semi permeable triangle.

It can be concluded that the Annex 14 height restriction leads to speed defects higher than 7kts and that these values are encountered in the **green** area as defined in Figure 1-1.
For reference in the semi permeable triangles the selected obstacle positions for the F100 offline simulations are indicated.
According to Table 3–4 the standard deviation of turbulence due the combined effects of a "stand alone" obstacle and a build up area is labeled as heavy to severe within the semi permeable triangle.

As has been illustrated in section 4 the height of an obstacle is a very important parameter with respect to wind disturbance. This is reflected in the practical translation of the 7kts criterion into a height restricted plane indicated as the "1:35" plane. It consists of an imaginary plane with a base that coincides with the extended runway centreline and has a slope of 1:35 upwards ([47]. After the introduction of the 7kts criterion (1:35 plane) no pilot reports on this issue have been received.
Consequently the investigation is started with a further evaluation of the 7kts criterion. Basically the 7kts criterion does not address the effect of wind shear, gust and turbulence although these phenomena affect the handling qualities and performance of an aircraft to a large extend. Therefore these aspects will be addressed specifically.

In section 6.4.2 it was demonstrated that a speed deficit of 7 knots alone does not reach critical F-factors and therefore is not an immediate danger to flight safety. However it was also shown in section 5.2.2 that a speed defect of approximately 8 knots was able to bring the F100 aircraft in a condition during final approach where it experiences a descent rate of more than 1000 ft/min.

> **Consequently it is postulated that a variation in mean wind speed due to a wind disturbing obstacle less than 7 knots along the aircraft trajectory below 200ft can be considered as a possible criterion with respect to flight safety.**
> **In addition gust/turbulence levels may not exceed a RMS value of 4 knots.**

To evaluate the impact of the 1:35 plane height restricted obstacles on the speed deficit and turbulence intensity RMS values the same calculations with the wind climate model were performed as done for the Annex 14 height restricted obstacles shown in Figure 6-18. The results are shown in Figure 6-19 for the same ground grid and wind climate parameters as were used for the "Annex 14" case.
For reference also in these plots the selected obstacle positions for the F100 offline simulations are indicated within the **green** area of Figure 1-1.

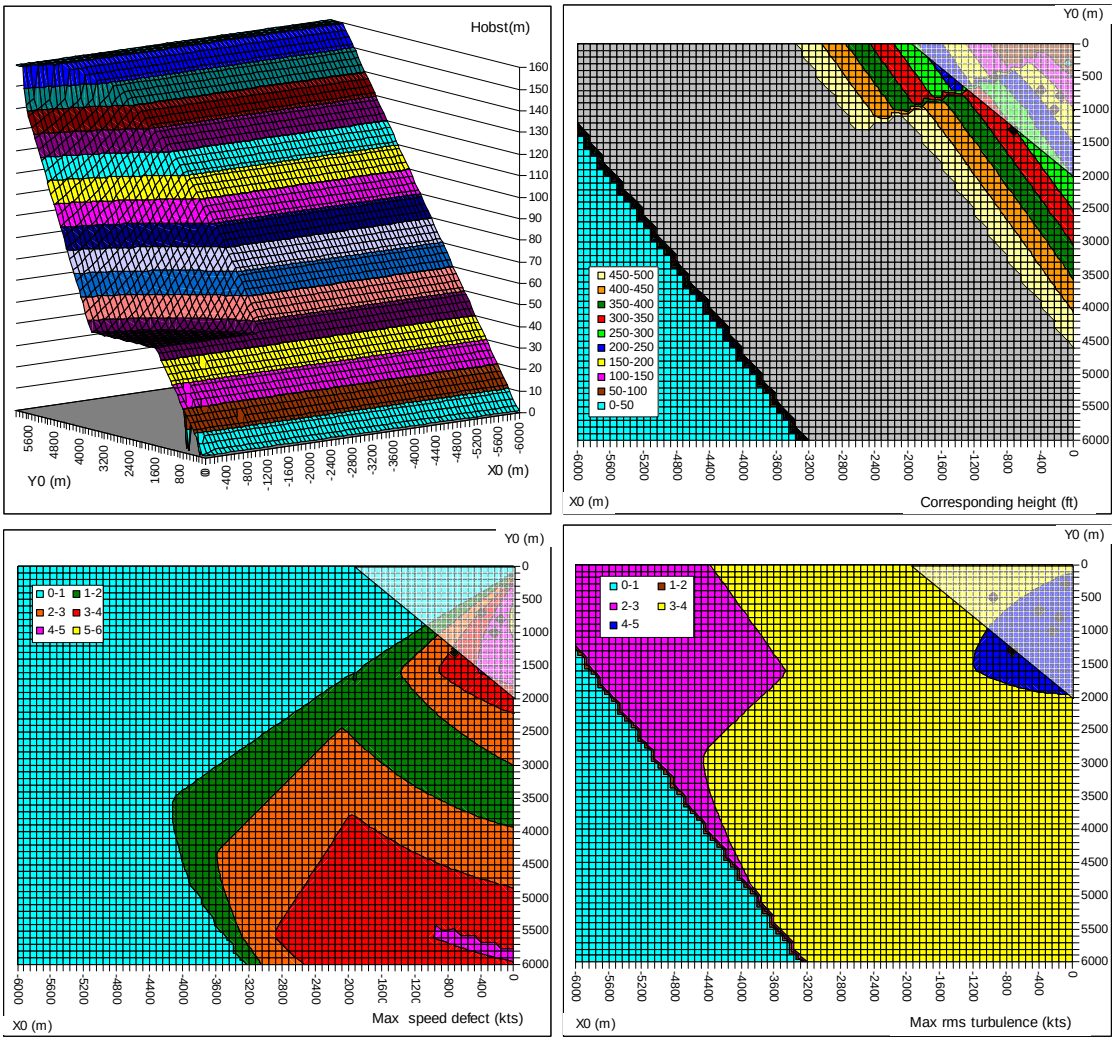

Figure 6-19: Speed defect and RMS turbulence intensity corresponding to 1:35 plane

Observations from Figure 6-19 are:

- From the "stand alone" obstacle height plot (upper left plot in Figure 6-19) it can be observed that between X0= 0<=>2000m and Y0=1500<=>5000m ICAO annex 14 obstacle clearance planes are more restrictive than the "1:35" plane.
- A small band exists where a maximum speed defect of 5-6 knots occurs. This band is situated close to the runway threshold (0-100m) at a distance from 500 to 1000m from the extended runway centerline.
- Corresponding RMS turbulence intensity values within this band range from 4 to 5 knots.
- Glide path heights at which these values are encountered comprise the same range as for the "Annex 14" case viz. 0 to approximately 200ft.

It can be concluded that the wind climate model predicts maximum speed defects smaller than 7kts with the 1:35 plane restriction and that these maximum values are encountered also in the **green** area as defined in Figure 1-1. According to Table 3–4 the standard deviation of

turbulence due to the combined effects of a “stand alone” obstacle and a build up area encountered in this region is labeled as medium to heavy. Consequently it can be concluded from this that despite the 1:35 height restriction turbulence levels are still high for the chosen combination of reference wind speed and surface roughness.

As has been mentioned based on this evaluation a number of obstacle positions have been determined indicated in Figure 6-18 and Figure 6-19. They are also presented by the red and blue marks in Figure 6-20. They are included in the offline test matrix defined hereafter.

In the left plot of Figure 6-20 the obstacle positions for the offline F100 simulations are projected symmetrically within the **green** area. The right part of the figure shows the height of the “stand alone” obstacle test points according to the “annex 14” obstacle clearance planes (purple shaded) and the “1:35” plane (green shaded). Also from this figure it appears that the “1:35” plane is more restrictive than the obstacle clearance plane only between a lateral offset of 200m and 1550m from the extended runway centerline.

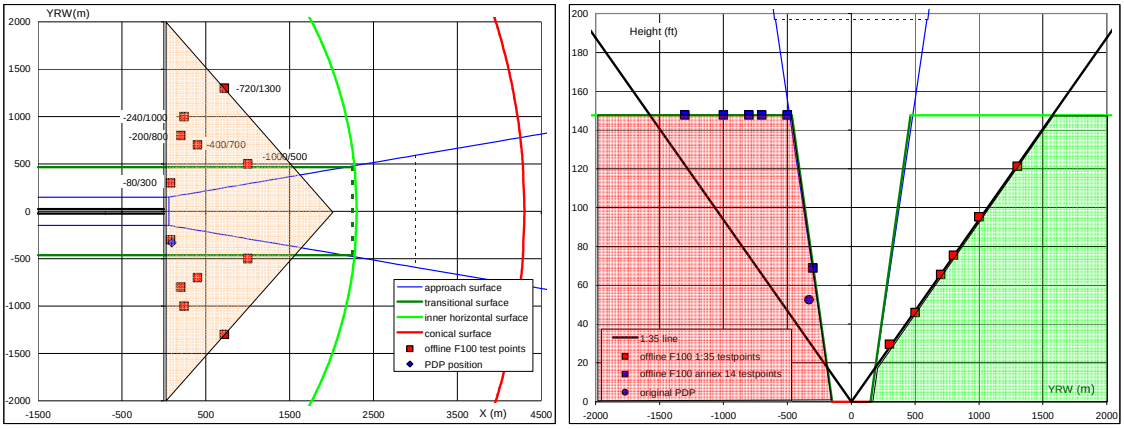

Figure 6-20: Test points situated in XY plane and YZ plane

The complete test matrix for the offline simulations is presented in Table 6–5.

It is split up in three parts, viz.:

1. **Session one** consists of simulations without the presence of a “stand alone” obstacle (POROS=100%) and simulations in which the original PDP configuration (POROS=-100%) is included. The simulations without a “stand alone” obstacle serve as a reference. Approaches and landings are made with three different reference wind speeds viz. 23, 28 and 35kts, a crosswind limit of 20kts and two surface roughness parameters (.001m and .01m). Fifty runs per surface roughness parameter are performed leading to a total of 100 runs per item. According to Figure 6-9 this means that in the simulations RMS turbulence intensities are encountered varying from light to heavy turbulence below 300ft.
2. **Session two** of the matrix consists of 100 simulations at a reference wind speed of 28kts and a cross wind limit of 20kts in which the height of the selected “stand alone” obstacles is

varied according to the "1:35" plane. Also here two surface roughness parameters (.001m and .01m) are considered. A "worst case" obstacle (POROS:-100%) with a width of 250m is simulated. According to Figure 6-9 this means that in the simulations RMS turbulence intensities are encountered varying from medium to heavy turbulence below 300ft.

3. **Session three** of the matrix consists of 100 simulations at a reference wind speed of 28kts and a cross wind limit of 20kts in which the height of the selected "stand alone" obstacles is varied according to the obstacle clearance planes defined in ICAO Annex 14. Again two surface roughness parameters (.001m and .01m) are considered. A "worst case" obstacle (POROS:-100%) with a width of 250m is simulated. According to Figure 6-9 this means that in the simulations RMS turbulence intensities are encountered varying from medium to heavy turbulence below 300ft.

Table 6–5: Offline test matrix for F100 simulations

sion 1 Landing rwy 27 Original PDP configuration worst case obstacles

mean wind speed (kts) excl gust	wnddir. (dg)	X-wind (kts)	Hd-wind (kts)	Turb (on/off)	Appr. spd flps 42 (kts)	nr of runs	Hobst (ft)	Z0 (m)	Width (m)	XRW/YRW-position (m)	POROS (%)	FILE
23	210/330	20	12	off	123	50/50	52	.001/.01	145	-93/332	100	ses1_0
23	210/330	20	12	on	133	50/50	52	.001/.01	145	-93/332	100	ses1_1
23	210/330	20	12	on	133	50/50	52	.001/.01	145	-93/332	-100	ses1_2
29	225/315	20	20	on	133	50/50	52	.001/.01	145	-93/332	100	ses1_3
29	225/315	20	20	on	133	50/50	52	.001/.01	145	-93/332	-100	ses1_4
35	235/305	20	29	on	133	50/50	52	.001/.01	145	-93/332	100	ses1_5
35	235/305	20	29	on	133	50/50	52	.001/.01	145	-93/332	-100	ses1_6

sion 2 Landing rwy 27 Height obstacles according to 1:35 plane worst case obstacles

mean wind speed (kts) excl gust	wnddir. (dg)	X-wind (kts)	Hd-wind (kts)	Turb (on/off)	Appr. spd flps 42 (kts)	nr of runs	Hobst (ft)	Z0 (m)	Width (m)	XRW/YRW-position (m)	POROS (%)	FILE
28	225/315	20	20	on	133	50/50	30	.001/.01	250	-80/300	-100	ses2_1
28	225/315	20	20	on	133	50/50	66	.001/.01	250	-400/700	-100	ses2_2
28	225/315	20	20	on	133	50/50	75	.001/.01	250	-200/800	-100	ses2_3
28	225/315	20	20	on	133	50/50	121	.001/.01	250	-720/1300	-100	ses2_4
28	225/315	20	20	on	133	50/50	46	.001/.01	250	-1000/500	-100	ses2_5
28	225/315	20	20	on	133	50/50	95	.001/.01	250	-240/1000	-100	ses2_6

sion 3 Landing rwy 27 Height obstacles according to annex 14 plane worst case obstacles

mean wind speed (kts) excl gust	wnddir. (dg)	X-wind (kts)	Hd-wind (kts)	Turb (on/off)	Appr. spd flps 42 (kts)	nr of runs	Hobst (ft)	Z0 (m)	Width (m)	XRW/YRW-position (m)	POROS (%)	FILE
28	225/315	20	20	on	133	50/50	69	.001/.01	250	-80/300	-100	ses3_1
28	225/315	20	20	on	133	50/50	148	.001/.01	250	-400/700	-100	ses3_2
28	225/315	20	20	on	133	50/50	148	.001/.01	250	-200/800	-100	ses3_3
28	225/315	20	20	on	133	50/50	148	.001/.01	250	-720/1300	-100	ses3_4
28	225/315	20	20	on	133	50/50	148	.001/.01	250	-1000/500	-100	ses3_5
28	225/315	20	20	on	133	50/50	148	.001/.01	250	-240/1000	-100	ses3_6

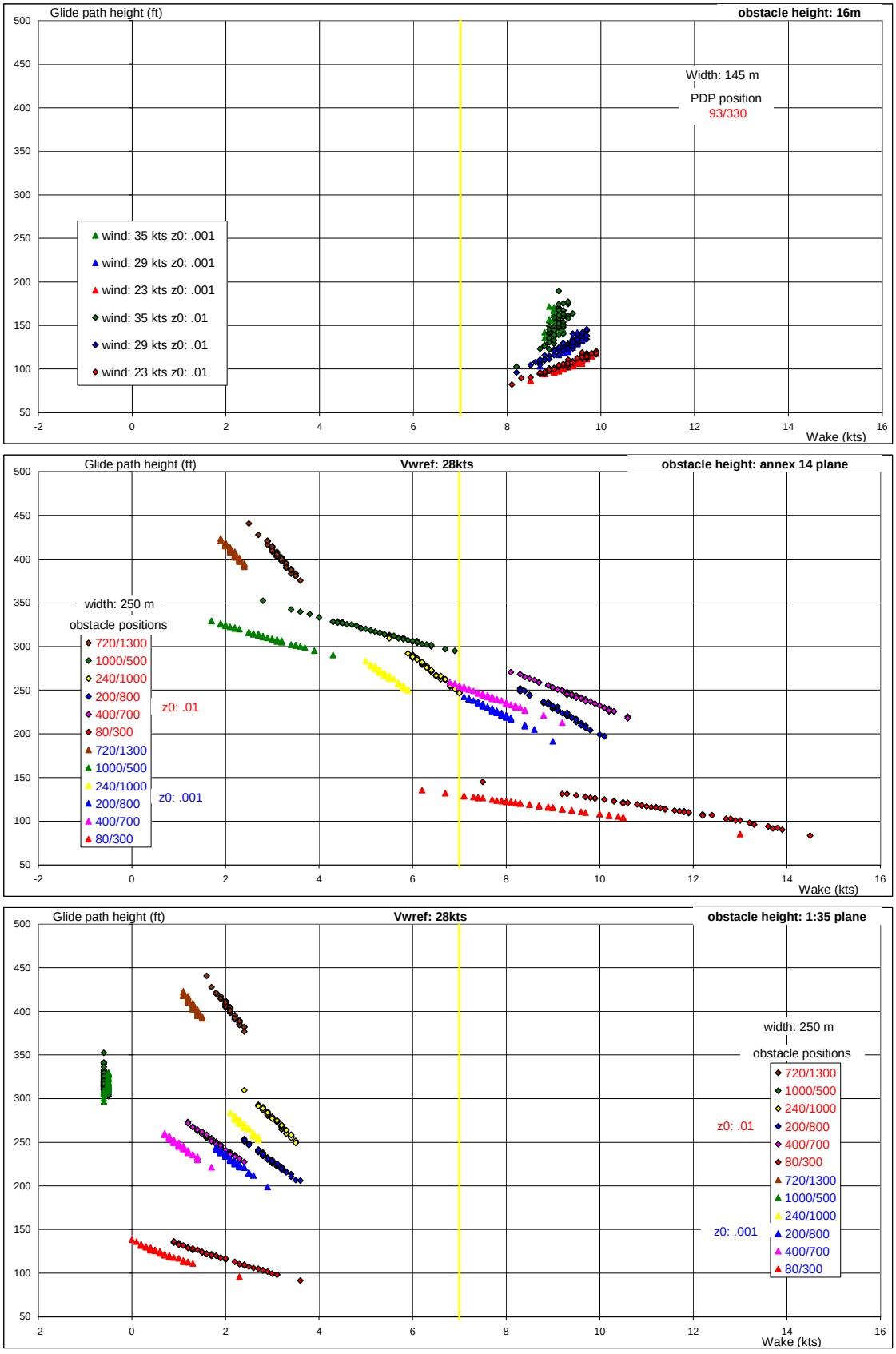

Figure 6-21: Wake height as function of obstacle position and obstacle dimension

The F100 wind correction applied to the approach speed depicted in Table 6–5 is derived from the F100 AOM. The approach speed (Vref+5) corresponds to a KCAS of 123kts for the aircraft mass and flap setting used. This speed is corrected for wind, including gusts as follows:

- Wind up to 10kt : no correction
- Wind (+gust) 10 – 20kts : add 5kts
- Wind (+gust) more than 20kts : add 10kts

The maximum wind correction with respect to Vref is 15kts.

The three sessions in the test matrix can be distinguished in terms of their wake characteristics. This is illustrated in Figure 6-21 where for the obstacle positions chosen (Figure 6-20) the maximum speed deficits behind the obstacle in wind direction are plotted for the performed approaches. This is done as function of height at which this maximum speed deficit encounters the aircraft. The 7kts speed deficit line is indicated in each plot for reference.

The first plot shows the wake corresponding to the runs performed in **session 1** of the test matrix. As can be observed the maximum speed deficit for the original PDP configuration amounts to 8-10 knots. The height at which the wake is encountered varies from 100ft to 200ft depending on the reference wind speed. Clearly this is a critical height regime because de-crab and flare take place in this height band.

The second plot in Figure 6-21 shows that “stand alone” obstacles with heights according to the Annex 14 obstacle clearance planes (**session 3**) produce much larger speed defects. However it is interesting to see that the speed deficit decreases quickly and encounters the aircraft at higher heights when the obstacle is positioned farther away from the threshold. Again most critical is the wake below 200ft where a speed deficit ranging from 6 to 14 knots is encountered.

Finally speed deficits due to “stand alone” obstacles with a height according to the “1:35” plane (**session 2**) are depicted in the third plot of Figure 6-21. The selected positions of the obstacle result in maximum speed defects between zero knots and 4 knots well below the 7kts reference. Due to the various positions of the obstacle the heights at which the aircraft traverses the wake become more dispersed. Heights where the wake is encountered ranges from 100ft up to 450ft.

6.4.4 Results

6.4.4.1 Introduction

In this section results will be presented obtained from the F100 offline simulations defined in the test matrix and performed with the F100 non-linear simulation package including the wind climate model derived in section 3 and 4. According to the offline test matrix numerous auto land like approaches have been performed with the F100 model. Results of simulations addressing the original PDP configuration (session 1) are presented in Figure 6-27 to Figure 6-31. Results from session 2 and 3 are shown in Figure 6-34 to Figure 6-35.

6.4.4.2 Example

First, as an example time histories are presented in Figure 6-22 and Figure 6-23 which are the result of a simulated auto land ILS approach with the F100 to runway 27 in atmospheric conditions determined by a reference wind speed of 23 knots, a wind direction preventing a X-wind exceeding 20kts at the reference height and a surface roughness of .01m. According to Figure 6-9 this means that medium turbulence is encountered. Both figures yield the same parameters as function of the distance to the threshold of the runway. The figures include the height of the CG of the aircraft with respect to the commanded glide path (HEIGHT), the wind including gust and wind without gust (WIND), the calibrated airspeed (KCAS), the lateral offset with respect to the runway centreline (YRW), the roll angle (ROLL ANGLE), the headwind component (HEADWIND), the distance of the aircraft with respect to the obstacle (DISTANCE TO OBSTACLE), the power setting (POWER) and the crosswind component (CROSSWIND).

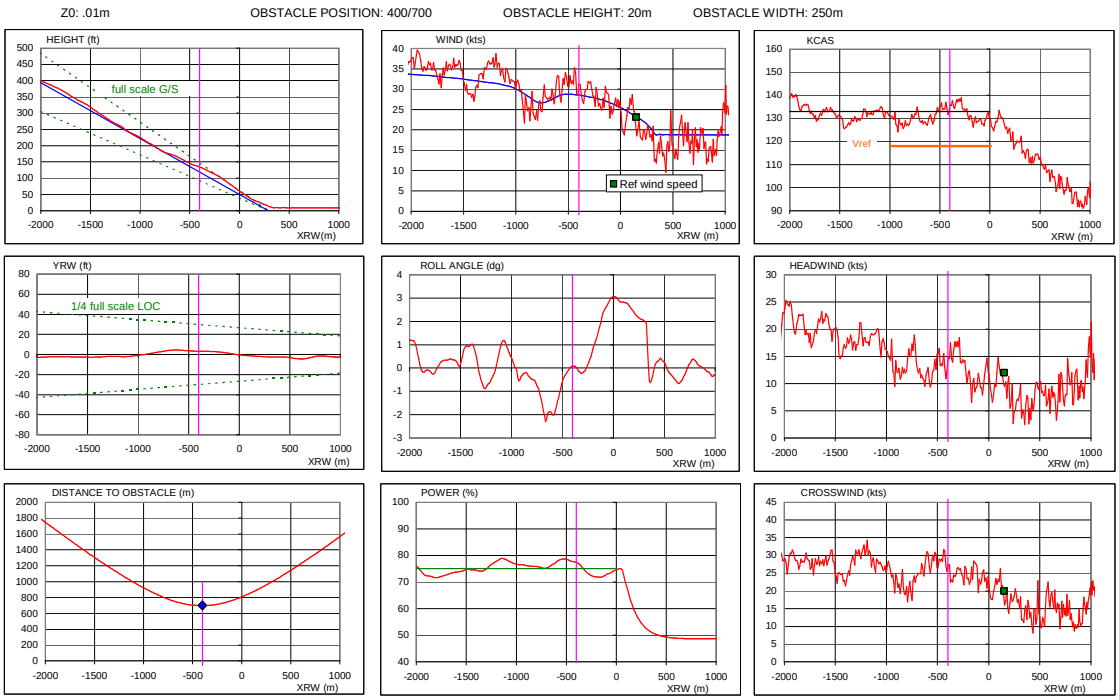

*Figure 6-22: Time histories of parameters recorded during offline F100 simulation (**case1**) wind speed: 23kts z0:.01m (medium turbulence)*

Figure 6-22 shows the results of an approach and landing when a “worst case” obstacle is positioned 400m in front of the runway threshold with an offset of 700m from the runway centreline (in short 400/700). Obstacle height is 20m (according to “1:35” plane) and obstacle width is 250m. It is referred to as **case1** hereafter.
Figure 6-23 shows the results of an approach with a “worst case” obstacle position of 240m in front of the threshold and a lateral offset of 500m (in short 240/500). Obstacle height now is 45m according to “Annex 14” and obstacle width is identical, viz. 250m. It is referred to as **case2** hereafter.

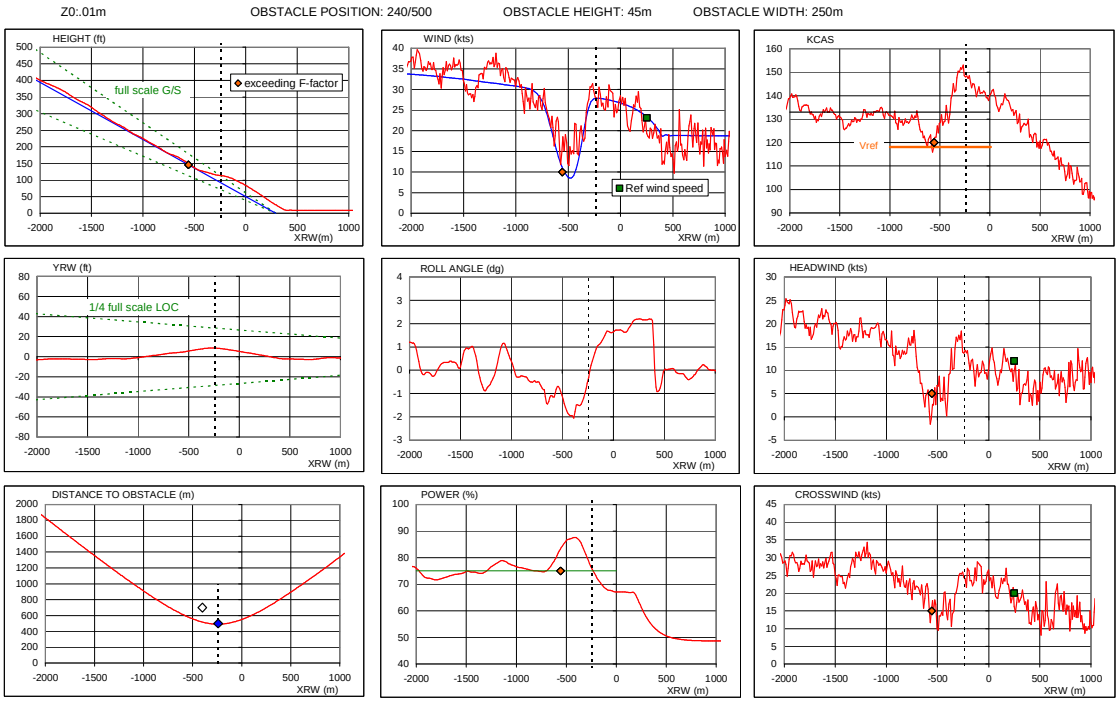

*Figure 6-23: Time histories of parameters recorded during offline F100 simulation (**case2**) wind speed: 23kts z0:.01m (medium turbulence)*

From a comparison of both figures it can be observed that the obstacle configurations yield a large difference in wake characteristics. In **case1** the maximum speed deficit is 3.1kts, whereas in **case2** a maximum speed defect of 19.5kts is experienced. The wake for **case1** affects the aircraft between heights of 150-250ft, whereas in **case2** the wake encounter occurs between altitudes of 100-200ft. The impact on the aircraft response for the two cases is quite different. In **case1** the headwind and crosswind component are not much changed by the obstacle shading. Consequently no large power and control corrections are required. In **case2** the opposite occurs. The headwind component completely drops off. The crosswind component is also affected severely with a decay of almost 15 knots. As result of the speed defect in the headwind, airspeed also decreases. To compensate for the imminent airspeed loss the auto throttle increases power as can be seen from the POWER parameter in Figure 6-23. However despite the application of

power the speed loss is large enough to reach the aircraft reference speed of 118 knots and to exceed the critical F-factor. As can be noted from the orange square in Figure 6-23 this occurs just before the largest speed defect. Obviously the shading from the wind by the obstacle is limited in time. After the largest speed defect has occurred the wind quickly reaches its original magnitude. However the auto throttle is not capable of reacting fast enough to this change. From the airspeed and height plot in Figure 6-23 it is can be observed what happens as result of this. Due to the sudden increase in wind and the surplus of thrust the aircraft accelerates and ascends above the glide path. The consequence may be a delayed touch down and/or a touch down at a too high airspeed.

Table 6–6: Overview of snapshots at wake height, at T/H and TD

	wake		at T/H		at TD	
	1:35	Annex 14	1:35	Annex 14	1:35	Annex 14
Wake (kts)	3.1	19.5				
Height of wake (ft)	150-250	100-200				
Position of wake in front of T/H (m)	-800	-518				
Offset from runway CL (m)			-0.5	5.2	-2.6	-1.5
X-Position of CG at TD (m)					323	384
Roll angle (dg)			3.1	1.7	1.9	2.1
Pitch angle (dg)			-0.6	-2.8	0.9	-1.2
Heading (dg)			275.4	276.8	272.2	272.2
Sink rate			760 ft/min	714 ft/min	6.5 ft/s	8.5 ft/s
Height (ft)			59	82		
Kcas			130	141	115	130

The initial decrease and subsequent increase in the crosswind also affects the lateral directional behaviour of the aircraft. Lateral/directional corrections are required to line up the aircraft with the runway centreline. However due to the fluctuating crosswind and headwind as result of the obstacle shading the de-crab and line up with the runway centreline quickly becomes a very demanding task certainly in combination with deteriorating longitudinal flying characteristics.

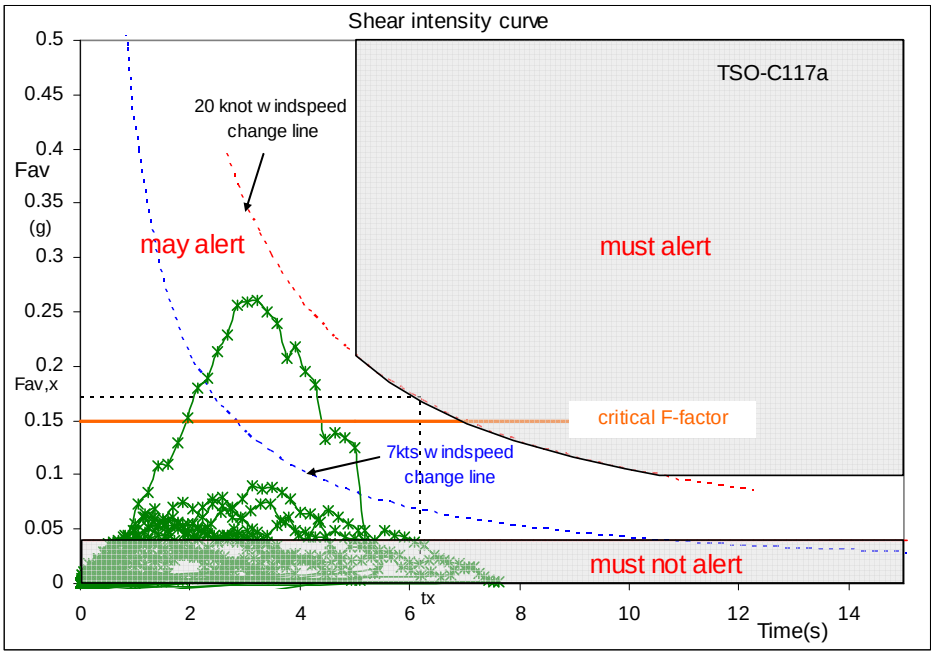

Figure 6-24: F-factor of case2 in shear intensity curve

The above described effects on the landing performance are illustrated in Table 6–6 in which snapshots are presented of **case2** (Annex 14) and **case1** (1:35) at the moment the aircraft passes the obstacle wake, crosses the runway threshold and at the moment the main gear touches the runway surface.

Figure 6-24 shows the F-factor plotted in the "*shear intensity curve*" as defined in TSO-117a. It appears that although the critical F-factor is exceeded the wake endurance is too short to reach the region in the plot where a wind shear alert should occur.

6.4.4.3 Height of CG at T/H, TD dispersion, Roll angle & Sink rate & Airspeed at TD

At first results from session 1 related to the PDP configuration will be discussed. In this batch of simulations the reference wind speed (23, 29 and 35 knots) and the surface roughness (.001m and .01m) were varied. In all runs gust/turbulence was included except for run nr 0 in which the turbulence models were switched off. The results for this case are presented in the plots with green diamond symbols.

In the plots the severity of the turbulence level is indicated as well. The classification is based on Table 3–3 and Table 3–4.

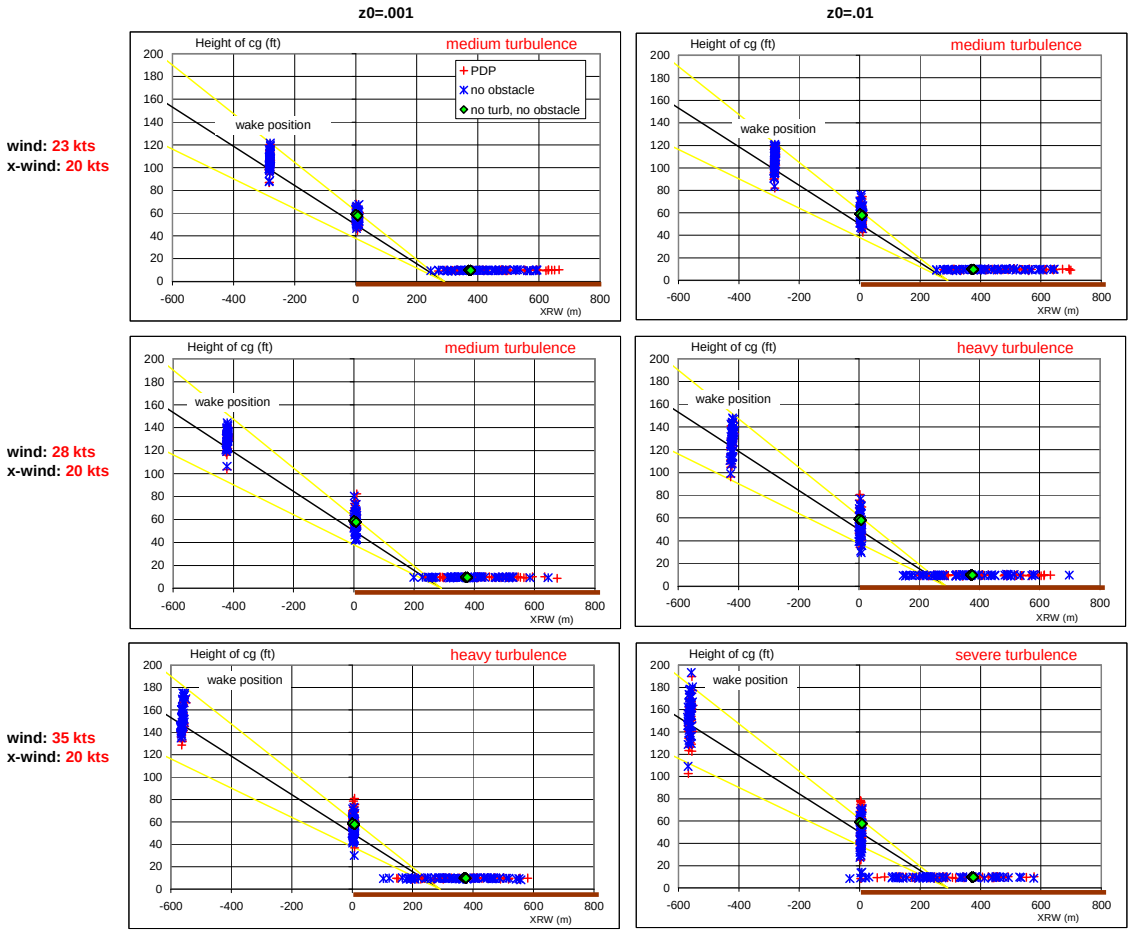

Figure 6-25: Height of cg during wake encounter, T/H and main gear touch down

Results are compared for two conditions, viz:

- No “stand alone” obstacle is included. Only turbulence characteristics due to build up area are included. This is labeled as the reference condition.
- A “stand alone” obstacle with PDP like characteristics is included positioned at 93m in front of the threshold with a lateral offset of 330m (93/330).

Figure 6-25 presents the wake position, threshold crossing and main gear touch down points of the performed approaches in session 1 with respect to the ILS glide path. It can be observed from Figure 6-25 that the position of the wake due to the PDP is influenced mainly by the reference wind speed. For a reference wind speed of 23kts the wake position lies at approximately 90-120ft, whereas for a reference wind speed of 35kts the wake position shifts to a height band of 120-180ft. Clearly noticeable is the increase in data scatter when the turbulence level increases. When severe turbulence is present shown in the lowest right plot of Figure 6-25 landing performance becomes unacceptable because a number of main gear touch downs occur in front of the runway threshold.

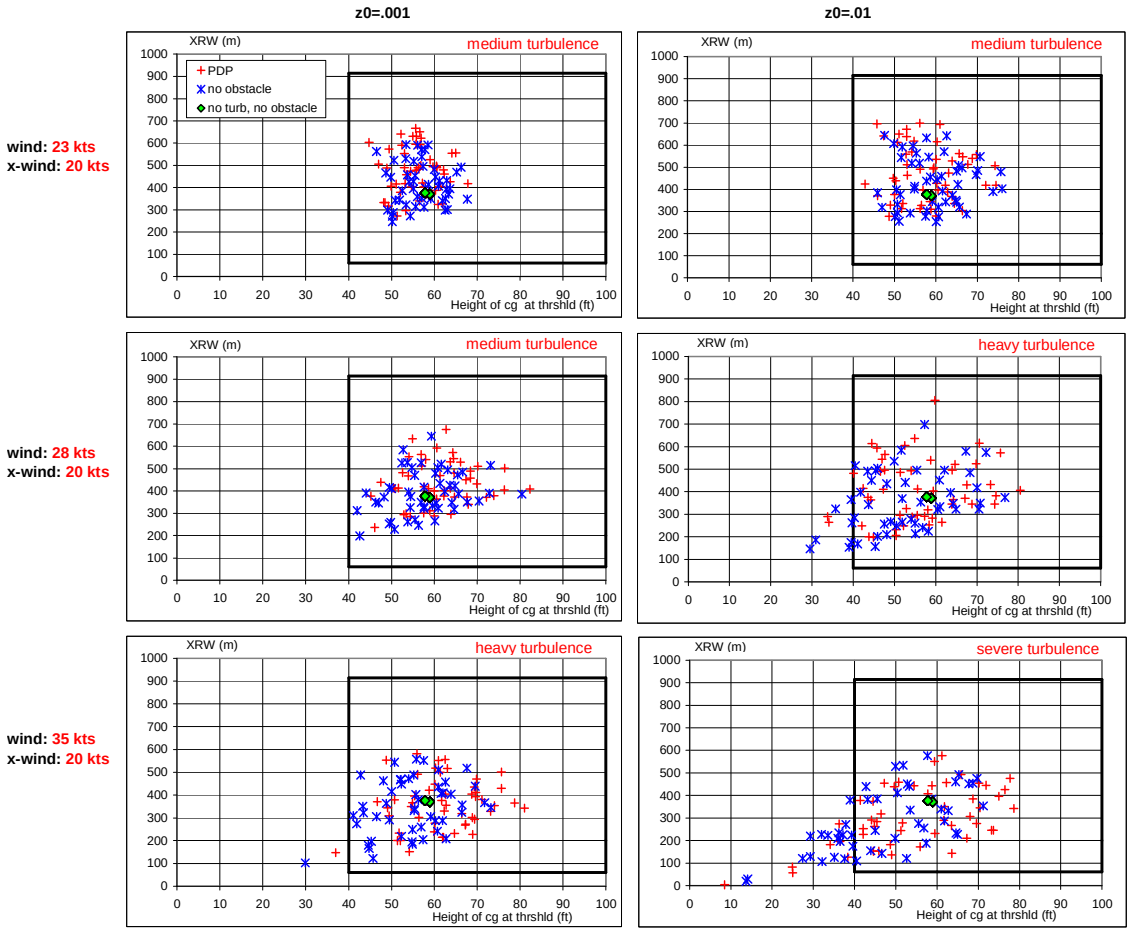

Figure 6-26: Height of cg at T/H versus main gear touch down

Figure 6-26 shows the height of the centre of gravity at the threshold versus main gear touch down as obtained from the runs of session 1. In fact this represents the airborne distance which is part of the landing performance. The box shown in the plots indicate the boundaries set for the main gear touchdown and runway threshold crossing. The following observations can be made from this figure:

- The plots show the large impact of the encountered turbulence level on the airborne distance performance. When encountering heavy/severe turbulence (RMS turbulence intensities in excess of 5kts) landing performance decreases substantially, noticeable by the low threshold passing and early main gear touch down.
- The effect of the presence of the PDP structure can be evaluated from Figure 6-26 as the difference between the data representing the runs in which the PDP structure was included and the runs where this was not the case. For low reference wind speeds and consequently low turbulence levels the data are closely correlated. This means that the data scatter is mainly caused by the turbulence characteristics of the earth surface in front of the runway.

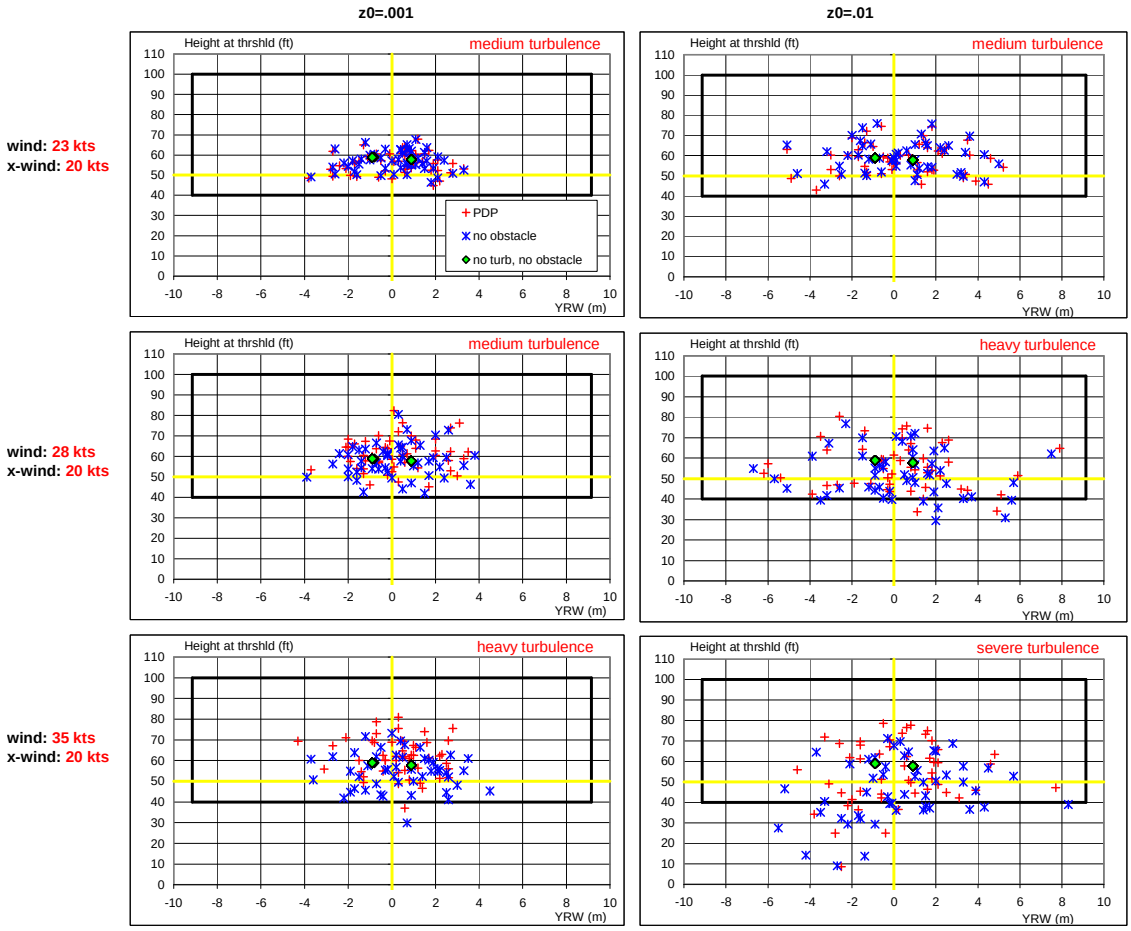

Figure 6-27: Height of CG at threshold

However with increasing reference wind speed and severity of the turbulence the difference between the two data sets becomes larger which is caused by the presence of the "stand alone" obstacle. The difference can be attributed to the already mentioned observation of additional power increase to absorb the momentary speed loss due to the PDP wake and the sub sequential height increase and delayed main gear touch down.

Figure 6-27 also presents snapshots taken in all performed approaches at the moment the aircraft passes the runway threshold, but now referred to the lateral deviation at the T/H. The data is referenced against a window that is based on the subjective acceptance criteria as defined in Table 5–1. At the threshold the centre of gravity of the aircraft should be at a height between 40ft and 100ft and within 30ft (9.1m) on either side of the runway centerline. Figure 6-27 shows that the lateral requirement is fulfilled for all cases.

However in the vertical plane landings with undershoots below 40ft occur. This is illustrated in Table 6–7 in which the percentage of landings that undershoots the threshold window as function of reference wind speed and surface roughness is presented. That undershoots below

40ft may occur is also found in ([48], in which a study is conducted using in-flight recorded data collected from day-to-day landing operations.
From this table the following observations can be made:

- The number of undershoots increases substantially when reference wind speeds and surface roughness are above 28kts and .01m respectively. As the table shows this corresponds to RMS turbulence intensity (sgmu) values of more than 4kts.
- Less undershoots occur when the PDP structure is included. This can be attributed to the application of power required to compensate initially for the speed loss due to the obstacle shading. As was observed from Figure 6-23 this results in a height increase just before landing.

Table 6–7: Survey of number of undershoots at threshold (T/H)

Windspeed (kts)	z0=.001 m Sgmu (kts)	Undershoot (%)	z0=.01 m Sgmu (kts)	Undershoot (%)	comment
23	----	0	----	0	no obstacle
23	2.4 – 2.9	0	3.5 – 3.8	0	no obstacle
23	2.4 – 2.9	0	3.5 – 3.8	0	PDP
28	2.9 – 3.6	0	4.3 – 4.6	6	no obstacle
28	2.9 – 3.6	0	4.3 – 4.6	4	PDP
35	3.9 – 4.4	2	5.4 – 5.8	34	no obstacle
35	3.9 – 4.4	2	5.4 – 5.8	14	PDP

Figure 6-28 shows the main gear touch down dispersion plotted against the TD box as defined for the F100 in Figure 5-8. In addition the position of the wake encounter projected into the ground plane is indicated for each case. It appears that the surface roughness does not effect the wake position very much. However, an increase in wind speed shifts the wake further away from the threshold and thus to a higher altitude (see also Figure 6-25). Figure 6-28 shows that only at a reference wind speed of 35kts and a surface roughness of .01m landings result in an undershoot. However it must be remarked again that at this wind speed severe turbulence is encountered.

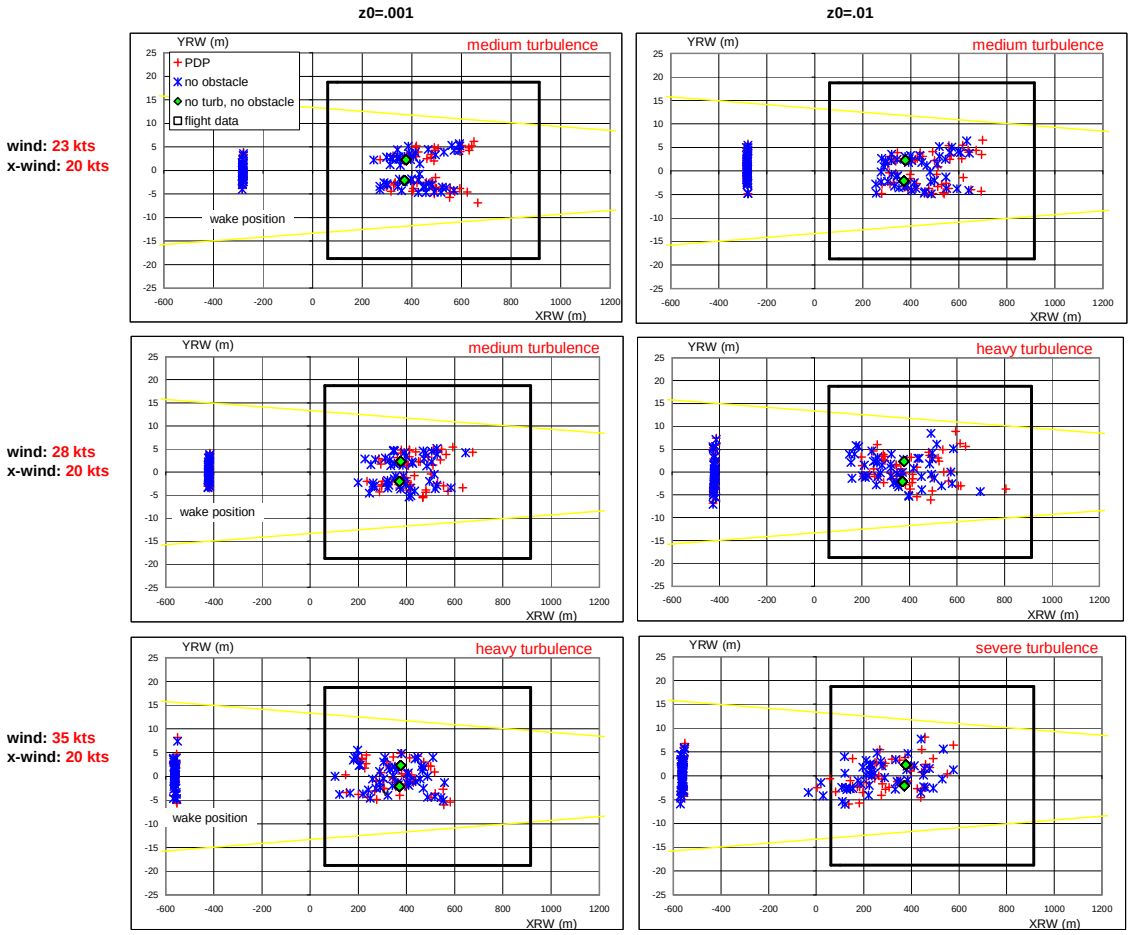

Figure 6-28: Main gear touch down dispersion

In Figure 6-29 the roll angle at the threshold and at main gear touch down is plotted for all cases. Also the roll angle boundaries as indicated in Figure 5-9 are included. Again the large increase in dispersion is noticeable when the turbulence levels are increased.
Magnitude of touch down roll angles remains within the boundary limits. However two landings at z0=.01m and 35kts wind speed (severe turbulence) result in a roll angle bust at the threshold.

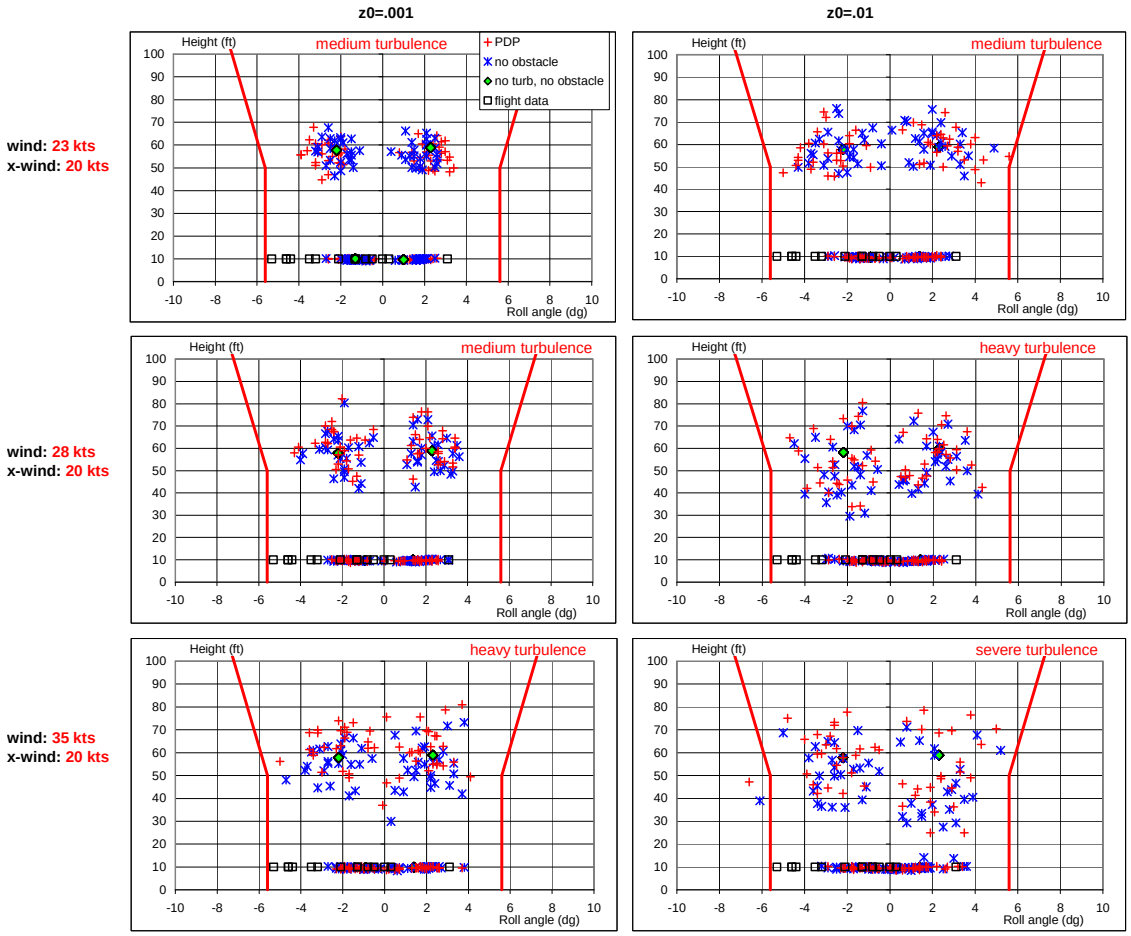

Figure 6-29: Roll angle at threshold and main gear touch down

Figure 6-30 and Figure 6-31 present the sink speed and airspeed respectively at main gear touch down versus the lateral position of the aircraft CG (YRW) at touch down with respect to the runway centerline. Table 6–8 shows the percentage of landings that resulted in a main gear touch down speed in excess of 6 ft/s.

Table 6–8: Survey of number of sink speeds at TD above 6 ft/s

Wind speed (kts)	z0=.001 m Sgmu (kts)	>6 ft/s (%)	z0=.01 m Sgmu (kts)	>6 ft/s (%)	comment
23	----	0	----	0	no obstacle
23	2.4 – 2.9	0	3.5 – 3.8	2	no obstacle
23	2.4 – 2.9	2	3.5 – 3.8	0	PDP
28	2.9 – 3.6	2	4.3 – 4.6	10	no obstacle
28	2.9 – 3.6	0	4.3 – 4.6	6	PDP
35	3.9 – 4.4	14	5.4 – 5.8	26	no obstacle
35	3.9 – 4.4	8	5.4 – 5.8	14	PDP

Also this table reveals the large impact on the landing performance of a wind speed increase in combination with an increase in turbulence level (surface roughness). It appears that at the higher wind speeds and higher turbulence levels the descent rate at main gear touch down associated with the PDP construction included becomes submerged in the atmospheric conditions created by the wind speed and gust/turbulence.

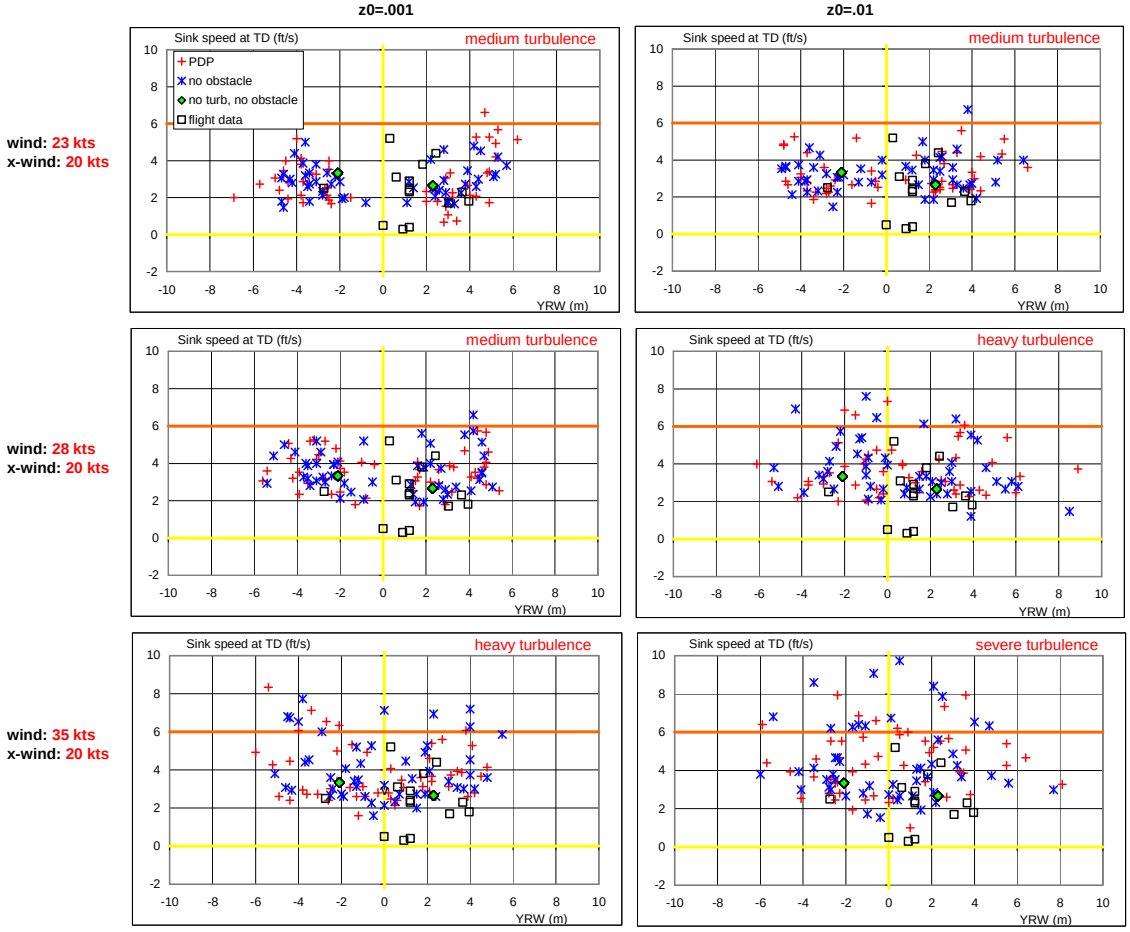

Figure 6-30: Sink speed at main gear touch down

Airspeed dispersion at main gear touch down (Figure 6-31) in particular is affected by surface roughness. In Figure 6-31 the employed approach speed, ref speed (1.23 Vs) and stall speed for the aircraft configuration simulated is indicated. It can be noticed that if no turbulence and/or "stand alone" obstacle is present the airspeed at main gear touch down is at the reference speed (green diamond symbols). As can be expected the data scatter around the ref speed increases when turbulence levels become higher. Airspeed increments/decrements up to 20kts at touch down can be observed. When severe turbulence is encountered the touch down airspeed in a number of cases is at or slightly below the stall speed.

In Figure 6-28 to Figure 6-30 available flight data of F100 landings from ([37] are plotted for comparison. It appears that these data are well situated within the dispersion of the simulation data.

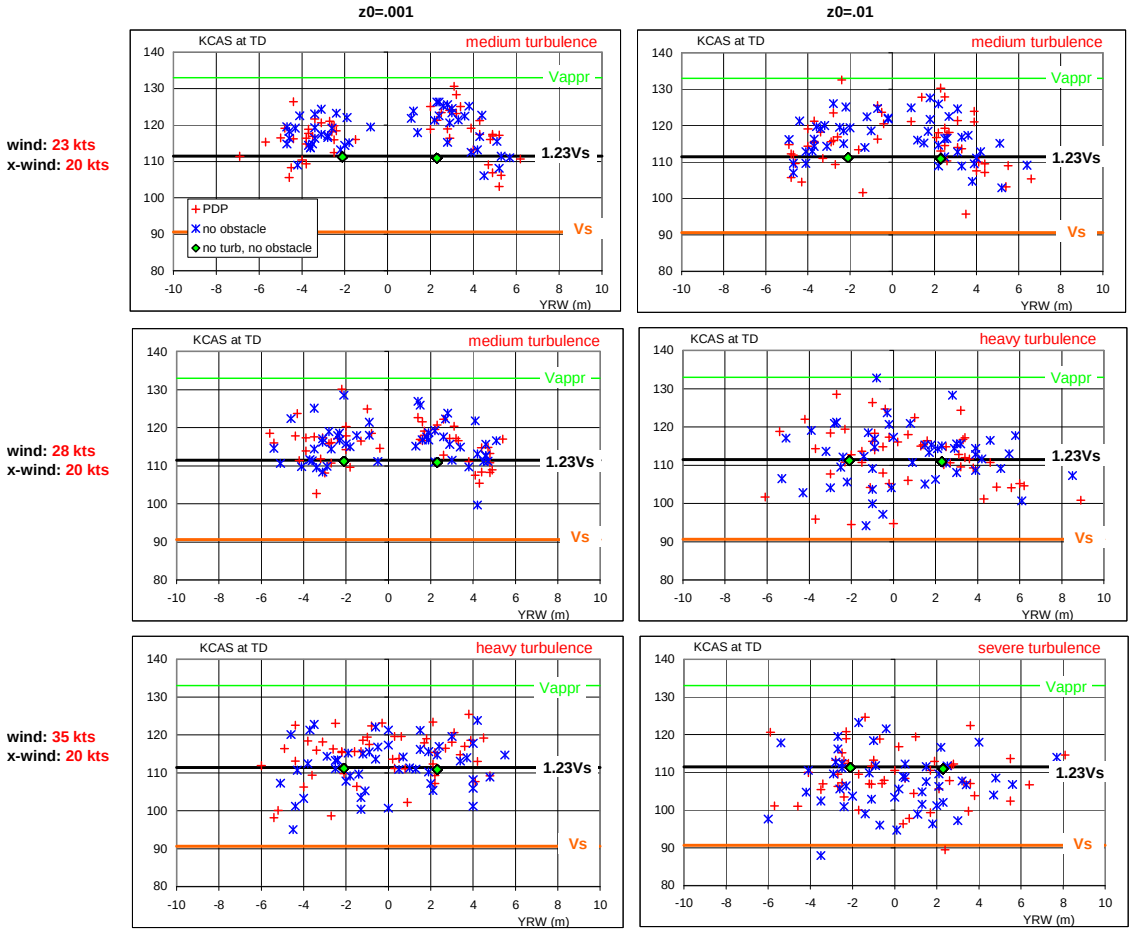

Figure 6-31: Airspeed at main gear touch down

Snapshot results at threshold and main gear touch down obtained from simulations according to conditions presented in session 2 and session 3 of the test matrix (Table 6–5) are presented in Figure 6-32 to Figure 6-35. Results from these sessions allow a comparison between the wind disturbance effects created by a generic block-shaped “worst case” stand alone obstacle with a height limited by the “1:35” plane and “Annex 14” planes. The width of the obstacle in all cases is 250m. The simulations are executed with a reference wind speed of 28kts and two surface roughness parameters viz. z0=.001m and z0=.01m.

- Figure 6-32 gives for all 6 considered obstacle positions and runs of the test matrix an overview of the position of the centre of gravity when the aircraft passes the wake, the runway threshold and the moment of main gear touch down. The left part applies to a surface roughness of .001m whereas the right part is valid for a z0 of .01m. Also from these plots it is clear that the wake position at the glide path is determined mainly by the obstacle position with respect to the runway threshold.

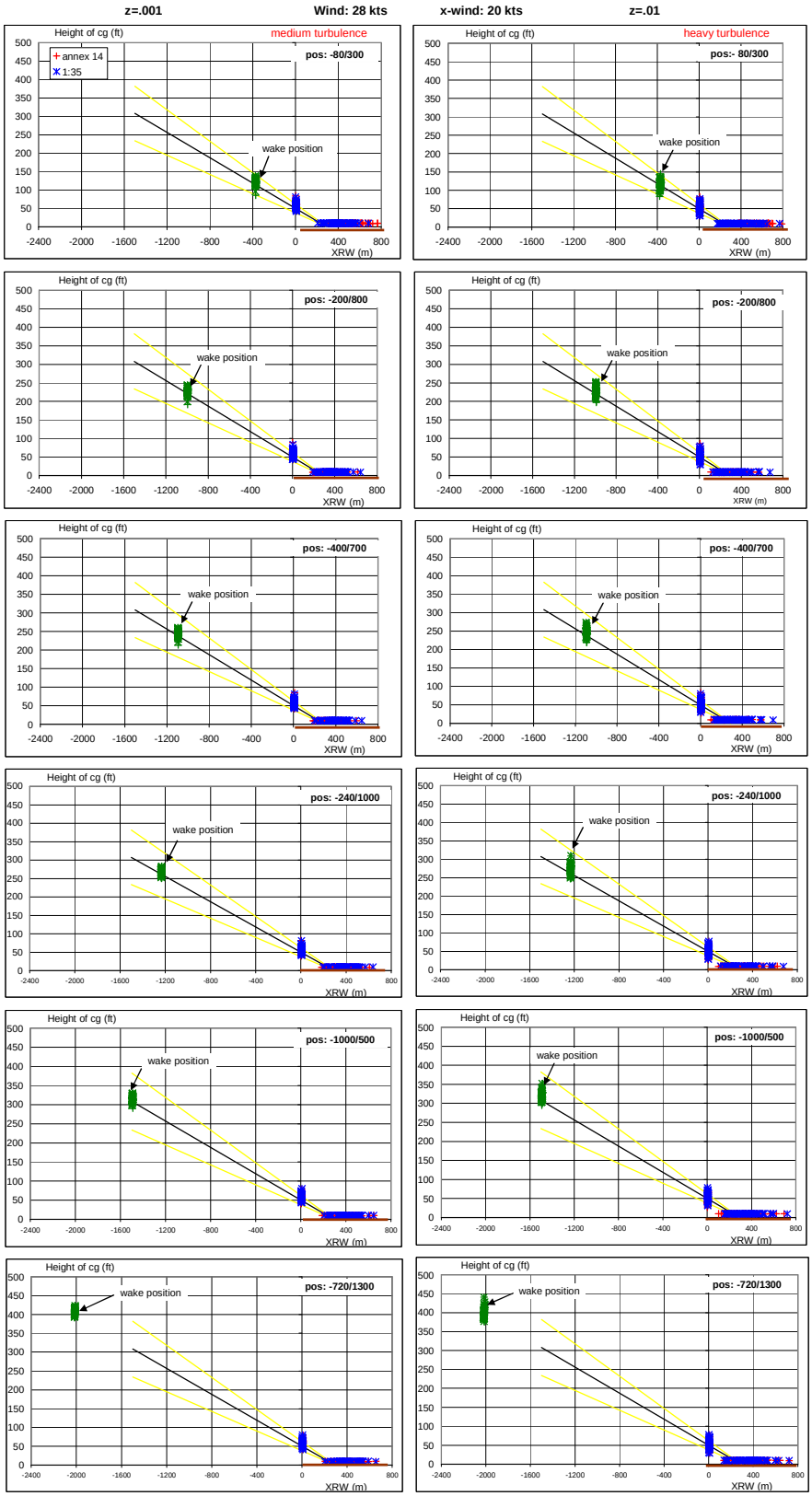

Figure 6-32: Height of cg during wake encounter, T/H and main gear TD

To illustrate the effects of a “stand alone” structure defined above on the aircraft landing performance two obstacles from Table 6–5 are compared, viz.:

- A stand alone obstacle positioned at 80m in front of the threshold with an offset of 300m from the runway centerline (in short 80/300), hereafter indicated as the “**nearby**” obstacle position (see first row plots of Figure 6-32).
- A stand alone obstacle positioned at 720m in front of the threshold with an offset of 1300m from the centerline (in short 720/1300), hereafter referred to as the “**far away**” obstacle position (see last row plots of Figure 6-32).

As mentioned obstacle height is varied according to the “1:35” plane and the obstacle clearance planes. The same set of parameters at the runway threshold and at the moment of main gear touch down as shown for the PDP configuration (Figure 6-27 to Figure 6-31) is presented in Figure 6-32 to Figure 6-35.

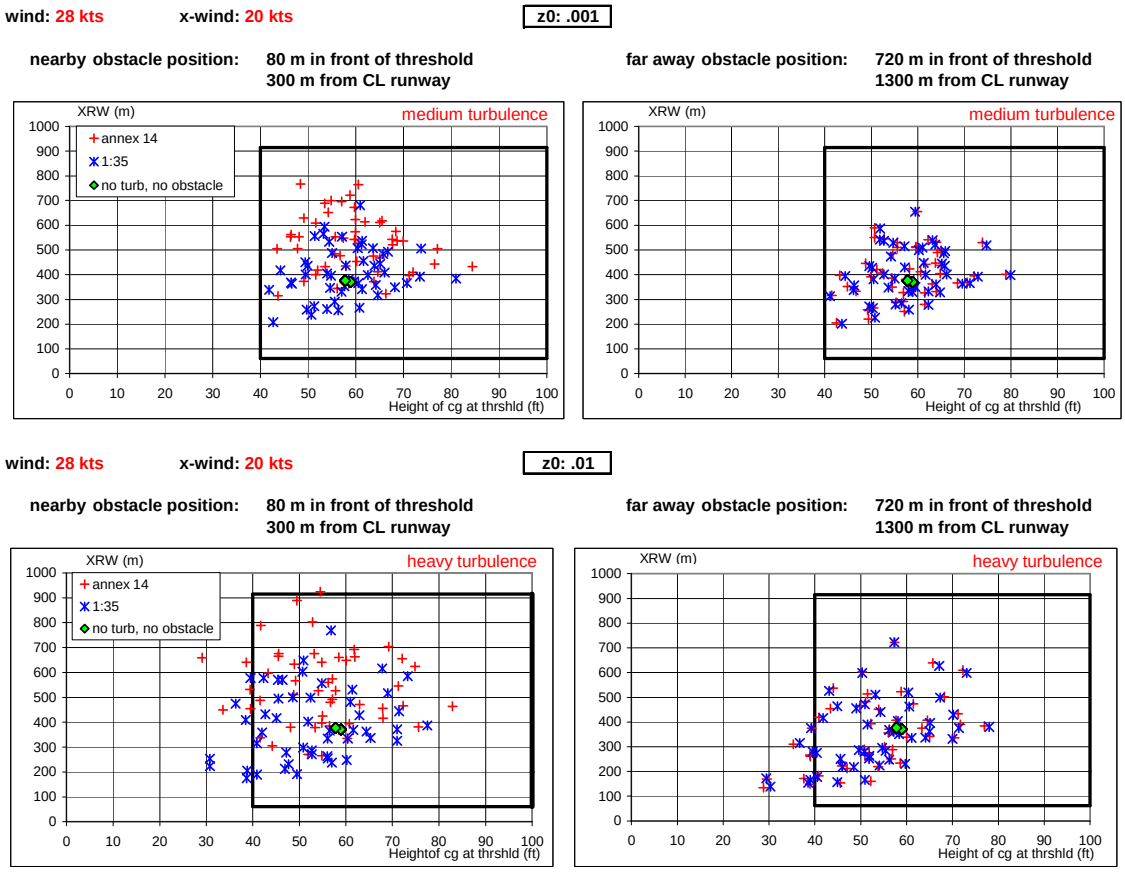

Figure 6-33: Height of cg versus main gear TD

Just as Figure 6-26 for the PDP, Figure 6-33 shows the airborne distance of the landing length defined by the height of the centre of gravity at T/H and main gear touch down. Two conditions are presented for each obstacle position, viz. a z0 of .001m and a z0 of .01m. In both cases the

reference wind speed is 28kts with a cross wind component of 20kts. The following observations can be made from this figure:

- The plots show the large impact of the encountered turbulence level on the airborne distance performance. When encountering heavy turbulence (RMS turbulence intensities in excess of 4kts) landing performance decreases substantially, noticeable by both by the low threshold passing and early main gear touch down.
- The effect of the presence of worst case stand alone obstacles can be evaluated from Figure 6-33 as the difference between the data representing the runs in which the stand alone obstacle is included and the runs where this is not the case. For the "**far away"** obstacle presented in the right hand plots of Figure 6-33 the data are closely correlated. This means that the data scatter is mainly caused by the turbulence characteristics as result of the surface characteristics. The wake and turbulence due to the "stand alone" obstacle however is not capable of affecting the landing performance significantly. The opposite occurs for the "**nearby"** obstacle presented in the left hand part of Figure 6-33. The difference between the two data sets is much larger clearly showing the impact of the "stand alone" obstacle on the landing performance.

By plotting the snapshot data for the two obstacle configurations, which are positioned far apart from each other and have different heights it is possible to evaluate what the effect on landing performance will be.

Figure 6-34, which is valid for a wind speed of 28kts and a surface roughness of .001m shows two sets of data. The left part applies to the "**nearby**" obstacle and the right part of the figure to the "**far away**" obstacle. For both "Annex 14" and "1:35" limited obstacle heights the following parameters are shown: the height of the CG at T/H, TD dispersion, roll angle at threshold and main gear touch down, sink rate at TD and the airspeed at touchdown. Figure 6-35 presents the same data only now applicable for a surface roughness of .01m. With a reference wind speed of 28kts medium turbulence is encountered in the auto land simulations with z0=.001m and heavy turbulence in the simulations with z0=.01m.

Also from Figure 6-34 and Figure 6-35 it can be observed that the "**far away**" obstacle data corresponding to the "1:35" height and "Annex 14" height are closely correlated. This means that the landing performance due to the "stand alone" obstacle is hardly affected. The landing dispersion is almost completely induced by the turbulence associated with the surface roughness. The opposite picture appears for the "**nearby**" obstacle. The dissimilarity between the two data sets has increased substantially and affects the landing performance of the aircraft. Figure 6-34 and Figure 6-35 again show the large impact of the turbulence level on the landing performance of the aircraft. However including a "**nearby**" obstacle aggravates the landing performance dispersion even more. For "Annex 14" limited height obstacles in heavy turbulence conditions the dispersion in a number of parameters becomes such that landing performance becomes unacceptable because roll angle limits are exceeded and sink rate and airspeed variations at touch down are too high.

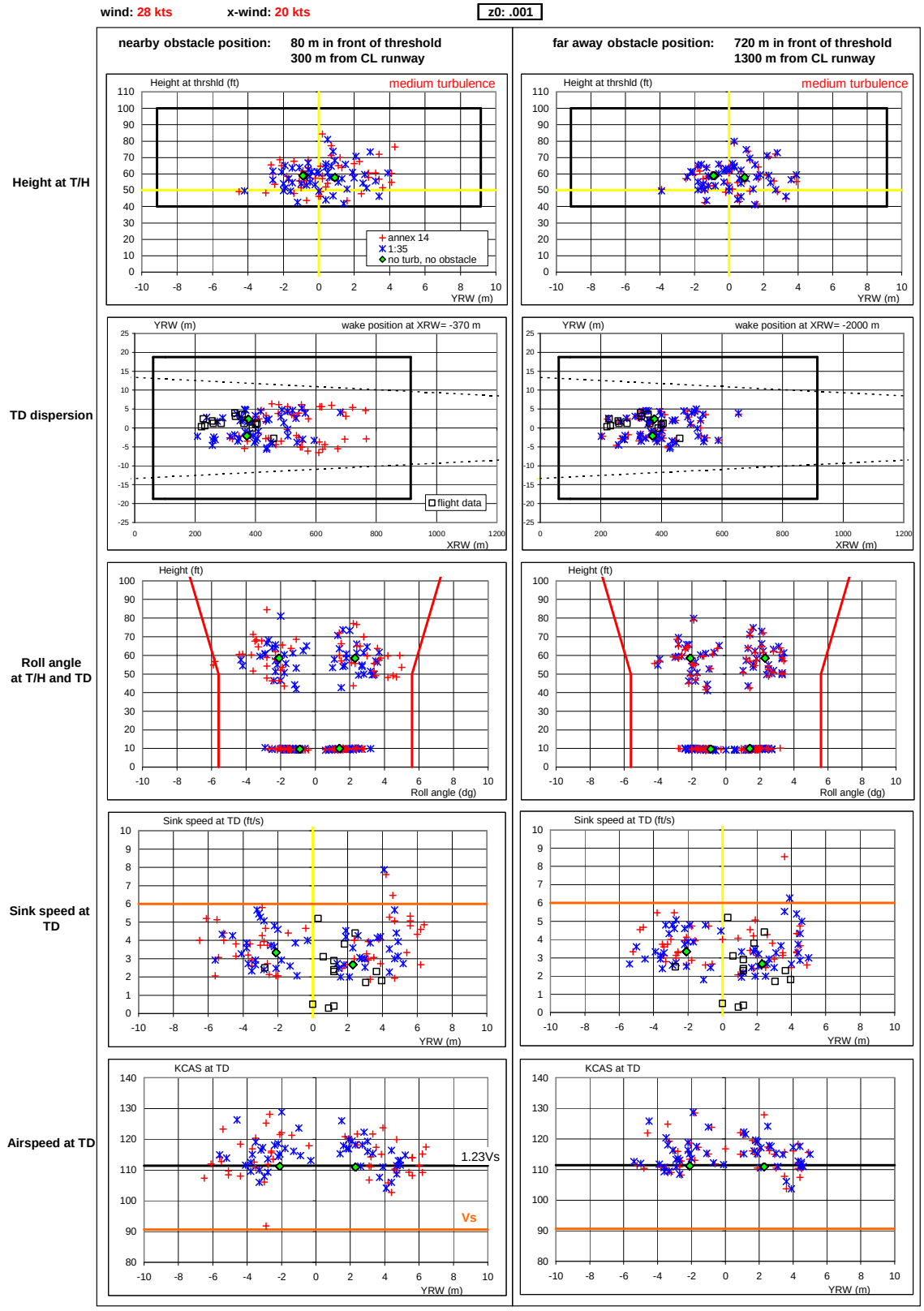

Figure 6-34: Comparison of parameters for obstacle nearby and far away for z0=.001

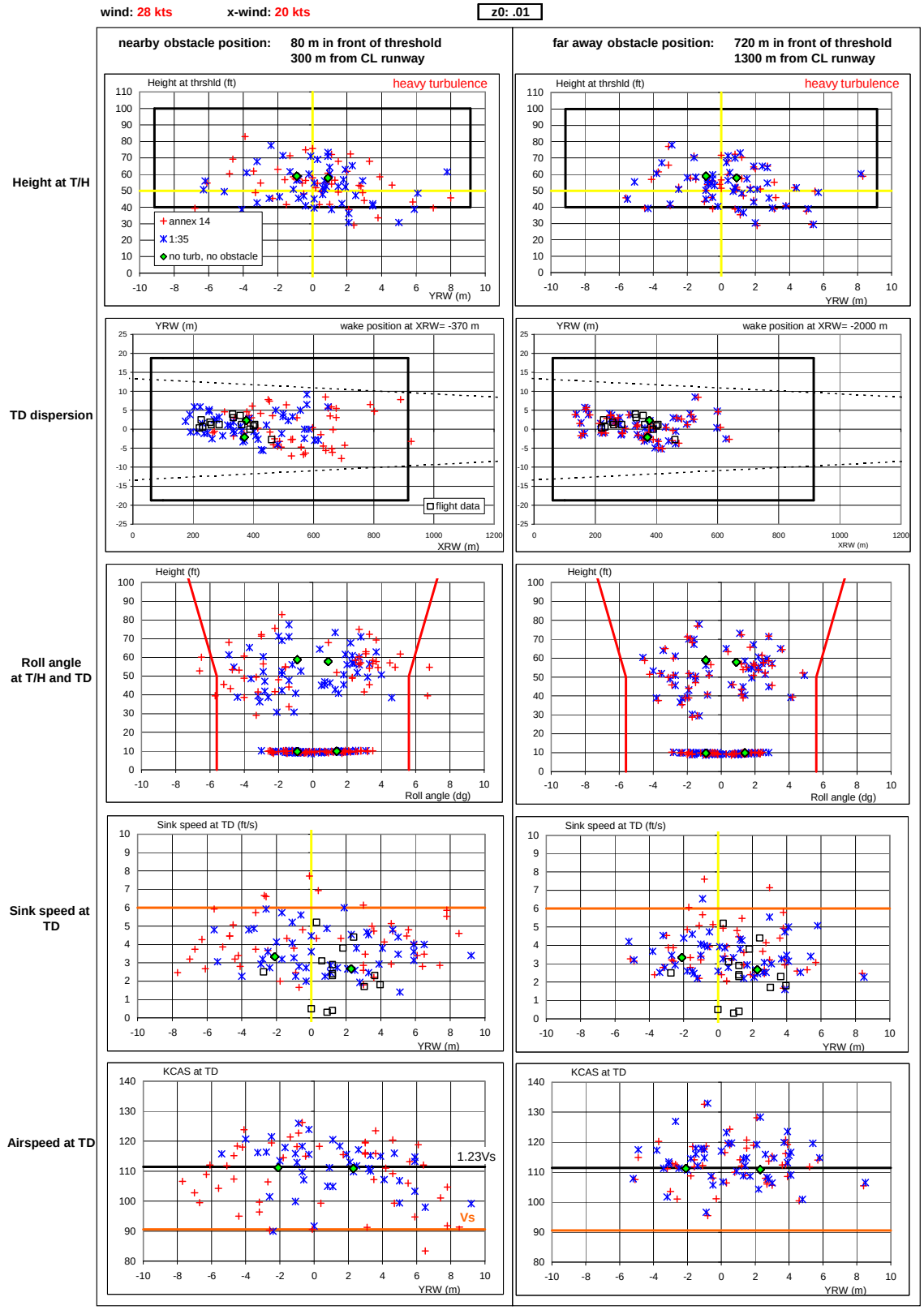

Figure 6-35: Comparison of parameters at threshold and TD for obstacle nearby and far away for z0=.01

6.4.4.4 Vertical speed below 200ft

As has been discussed in section 5.2.2 a descent rate of 1000 ft/min or more is considered unacceptable during final approach. Therefore during each approach to runway 27 of the performed offline auto lands, the minimum vertical speed below a height of 200ft occurring was logged. The results for the six considered obstacle positions in session 2 and session 3 are presented in Figure 6-36. Data related to the minimum vertical speed are shown for medium turbulence (z=.001m, red symbols) and heavy turbulence (z0=.01m, blue symbols) respectively. They apply for obstacles with height limited by the 1:35 plane (filled symbols) and obstacles limited by the Annex 14 obstacle clearance criteria (open symbols). As can be expected the crossing of the1000 ft/min line is strongly dependent on the amount of turbulence present during the approach and the position of the obstacle with respect to the runway threshold. It appears from the figure that heavy turbulence is able to create 1000ft/min busts independent of stand alone obstacle position and obstacle height. On the other hand if an obstacle according to Annex 14 is positioned close enough to the runway threshold also medium turbulence may lead to 1000ft/min busts.

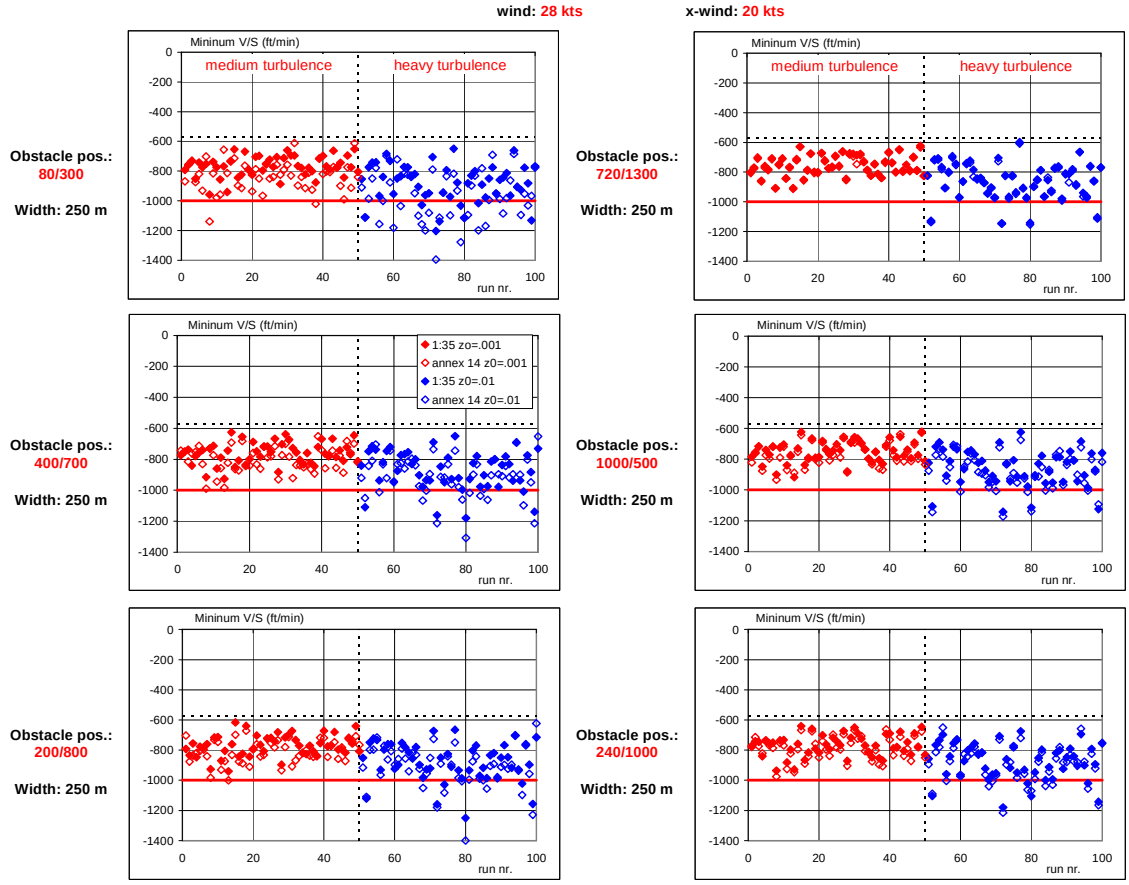

Figure 6-36: Minimum vertical speed as function of obstacle configuration and turbulence level

Medium turbulence did not lead to vertical speeds of -1000 ft/min or more during approaches with stand alone obstacles limited in height by the 1:35 plane.

6.4.4.5 Critical F-factor

The general conclusions drawn at the previous paragraphs are confirmed when looking at the number of critical F-factor crossings during the auto land simulations. According to the test matrix for each session number 100 auto lands have been simulated. They are divided in 50 runs with z0=.001m and 50 runs with z0=.01m. On the horizontal axis of each plot in Figure 6-37 to Figure 6-39 the number of simulations is presented. The first 50 simulations apply for a surface roughness of .001m whereas runs 50 to 100 apply for a surface roughness of .01m. On the vertical axis of each plot in Figure 6-37 to Figure 6-39 for each performed simulation run the height of the aircraft centre of gravity is presented at which the wake is encountered by the aircraft. For a given wind speed this height depends on the obstacle position and obstacle dimensions.

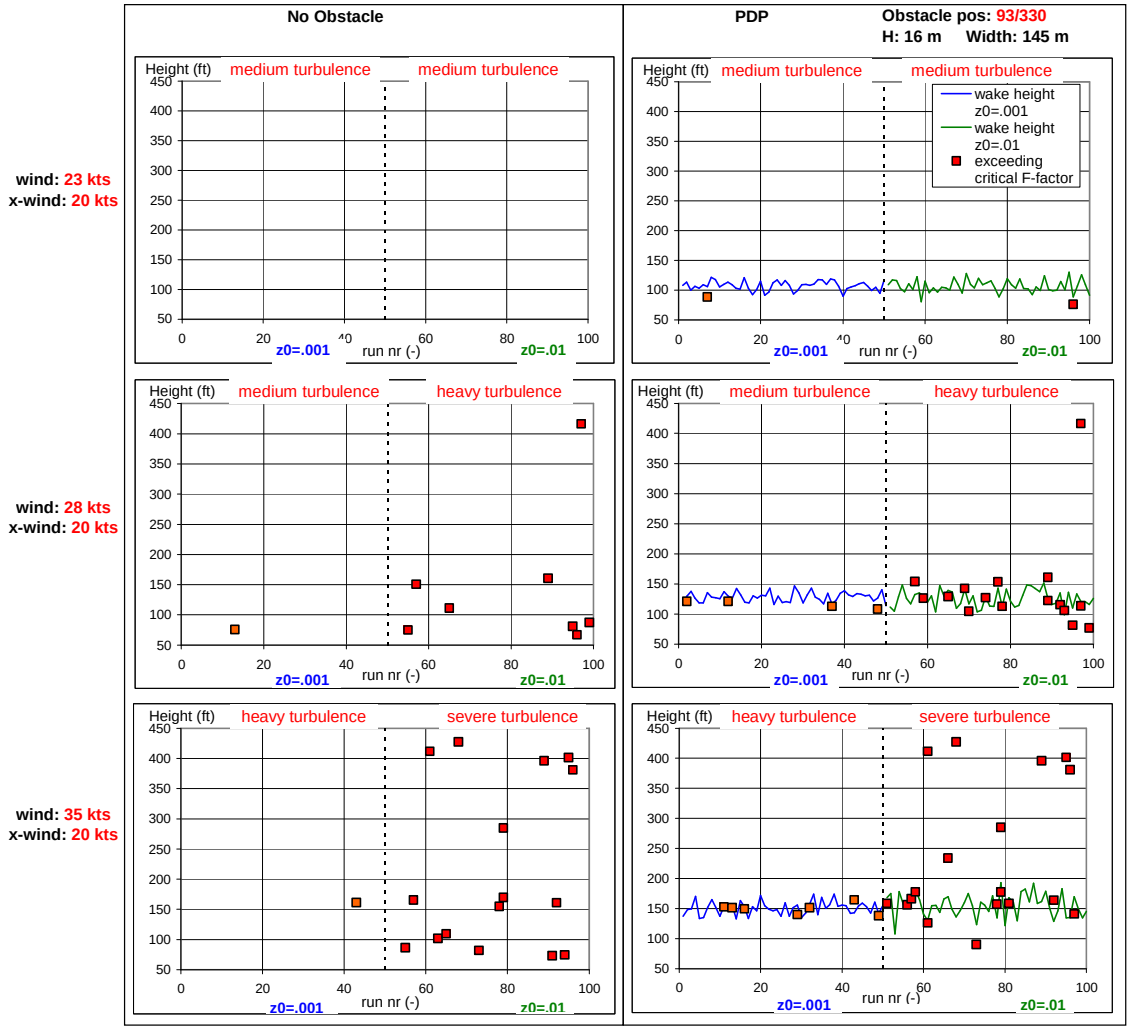

Figure 6-37: Critical F-factor exceeding for obstacle at PDP position

For the original PDP configuration (session 1) the results are shown in Figure 6-37. Figure 6-38 and Figure 6-39 yield the data corresponding to obstacle positions and obstacle height limits according to the “Annex 14” planes and the “1:35”plane (session 2 and 3).
In Figure 6-37 for three reference wind speeds (23, 28, 35kts) crossings of the critical F-factor are presented for the situation in which no “nearby” obstacle is present and the situation in which the PDP configuration is included. In each plot the turbulence level is indicated associated with the z0/Vwind ref combination.
The figure shows that at a reference wind speed of 23kts the height of the wake for the PDP configuration is situated at approximately 100 ft whereas at a wind speed of 35kts this height increases to 150 ft. The maximum strength of the wake for each case is approximately 9kts. The effect of the PDP obstacle is visible in Figure 6-37 by the number of critical F-factor crossings in the left part of the figure (no obstacle) and the right part (including PDP).
The following observations can be made from Figure 6-37:

- An increase in reference wind speed above 23kts in combination with an increase in surface roughness equal or above .01m or in other words a strong increase in turbulence level quickly deteriorates the atmospheric conditions to a level where gust/shear effects become prominent.
- If a PDP like obstacle is imbedded in the simulation it can be noted that at a wind speed of 28kts the number of critical F-factor crossings increases substantially around the height where the obstacle wake is encountered. Consequently due the wake and the gust and turbulence level, shear effects are increased at a height where flare and de-crab take place.
- At a wind speed of 35kts and surface roughness of .01m (severe turbulence) the increase in crossings due to the stand alone obstacle is less than noticeable at the wind speed of 28kts. This can be explained by the fact that due to the severe turbulence the effect of the standalone obstacle is submerged in the atmospheric conditions created by the high wind speed in combination with the larger surface roughness.

Table 6–9: Critical F-factor crossings for PDP

	no obstacle				PDP configuration			
	z0=.001		z0=.01		z0=.001		z0=.01	
wind speed	wake	F-factor crossings	wake	F-factor crossings	wake	F-factor crossings	wake	F-factor crossings
23 kts	0	0	0	0	9.4 kts	1	9.2 kts	1
28 kts	0	1	0	8	9.3 kts	4	9.2 kts	16
35 kts	0	1	0	16	8.9 kts	7	9 kts	18
total crossings		2		24		12		35
nr of landings		150		150		150		150
		1.3%		16.0%		8.0%		23.3%

The data presented in Figure 6-37 are summarized in Table 6–9. The table shows the number of crossings below 450ft.

Data presented for the PDP configuration in Figure 6-37 is also reproduced in Figure 6-38 and Figure 6-39 for six different stand alone obstacle positions. The figures show the results for the obstacle positions defined in session 2 of the test matrix with a height limited by the "1:35" plane (left part of Figure 6-38 and Figure 6-39) and session 3 with a height limited by "Annex 14"obstacle clearance planes (right part of Figure 6-38 and Figure 6-39). As can be observed from the test matrix the data apply for one reference wind speed only, viz. 28kts. Generic block-shaped "worst case" obstacles are considered with a width of 250m. A summary of the results shown in Figure 6-38 and Figure 6-39 is presented in Table 6–10.

As can be observed from the plots the height at which the wake is traversed by the aircraft varies from 125ft (position 80/300) to 400ft (position 720/1300).

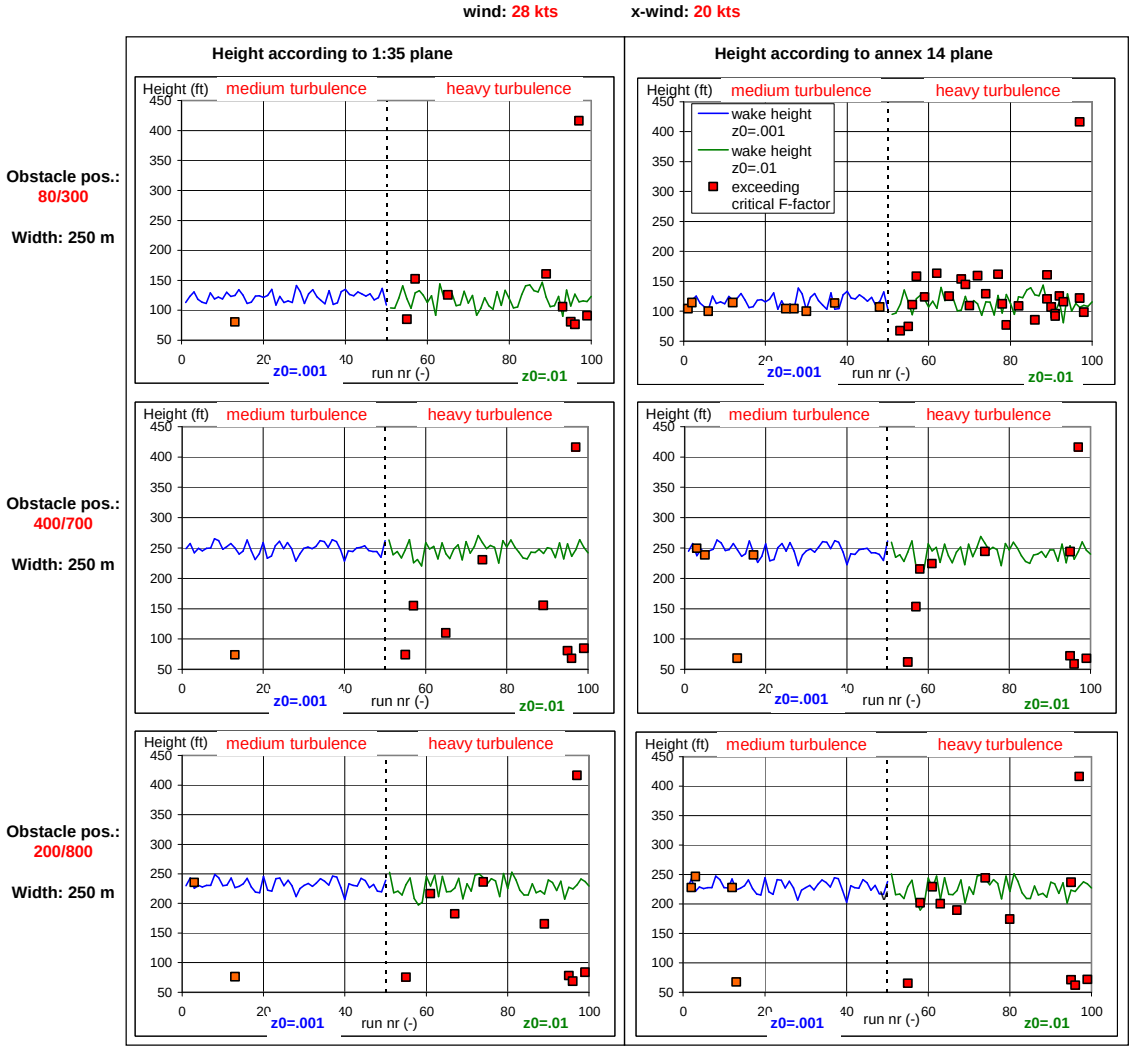

Figure 6-38: Critical F-factor exceeding for obstacles according to 1:35 and annex 14 plane

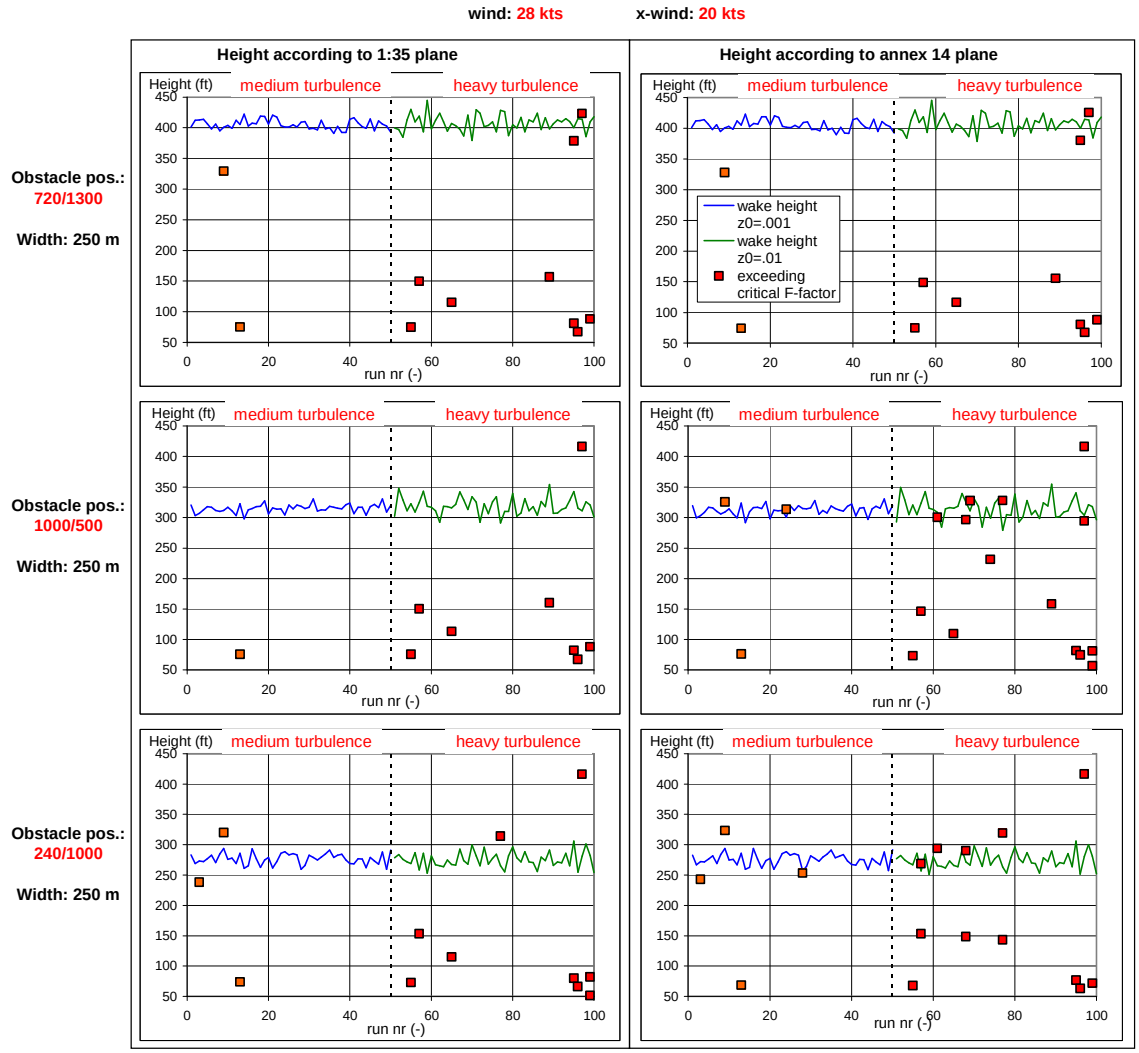

Figure 6-39: Critical F-factor exceeding for obstacles according to 1:35 and annex 14 plane

Table 6–10: Critical F-factor warnings for 1:35 and annex 14 planes

	height according to 1:35 plane				height according to annex 14 plane			
	z0=.001		z0=.01		z0=.001		z0=.01	
obstacle position	wake	F-factor crossings	wake	F-factor crossings	wake	F-factor crossings	wake	F-factor crossings
80/300	**0.6 kts**	**1**	**1.8 kts**	**9**	**8.7 kts**	**9**	**11.3 kts**	**27**
400/700	**0.9 kts**	**1**	**1.8 kts**	**9**	**7.5 kts**	**4**	**9.5 kts**	**10**
200/800	**2.1 kts**	**2**	**3 kts**	**9**	**7.6 kts**	**4**	**9.1 kts**	**12**
720/1300	**1.3 kts**	**2**	**2 kts**	**9**	**2.2 kts**	**2**	**3.1 kts**	**9**
1000/500	**-0.5 kts**	**1**	**-0.6 kts**	**8**	**2.7 kts**	**3**	**5.4 kts**	**15**
240/1000	**2.2 kts**	**3**	**3 kts**	**9**	**5.2 kts**	**4**	**6.4 kts**	**12**
total crossings		**10**		**53**		**26**		**85**
nr of landings		**300**		**300**		**300**		**300**
		3.3%		**17.7%**		**8.7%**		**28.3%**

From Figure 6-38, Figure 6-39 and Table 6–10 the following observations can be made:

- Maximum speed deficits in the wake for obstacles according to the 1:35 plane height limit are in the range of nil to 3 knots. This applies for both surface roughness parameters considered.
- Maximum speed deficits in the wake for obstacles according to the "Annex 14" obstacle clearance height limit are in the range of 2 to 11 knots. This applies for both surface roughness parameters considered.
- For a wind speed of 28kts and no "stand alone" obstacle the following conclusion can be derived from Table 6–9 :
    - For a surface roughness of .001m (medium turbulence) 2% of the approaches resulted in a crossing of the critical F-factor. For a surface roughness of .01m (heavy turbulence) the number of crossings is increased to 16%.
- If these numbers are compared with the results of Table 6–10 it follows for the number of critical F-factor crossings expressed in percentage of the total number of performed simulations:

Obstacle	Z0=.001m	Z0=.01m
No "stand alone" obstacle	2%	16%
According to 1:35 plane	3.3%	17.7%
According to Annex 14	8.7%	28.3%

From this table it can be observed that:

- Surface roughness (which can be translated into a certain turbulence level) has a large effect on the wind shearing in the lower atmosphere.
- The number of crossings when no "stand alone" obstacle is present appears to be of the same order as for the case in which obstacles are present according to the "1:35" plane height limit. This applies both for the surface roughness of .001m (2% versus 3.3%) and surface roughness of .01m (16% versus 17.7%)
- A substantial increase in crossings can be observed when the obstacle height is increased to "Annex 14" level. For a surface roughness of .001m a large increase can be noted. For a surface roughness of .01m the increase is smaller although still significant. The latter result is understandable because the wind shearing then is governed mainly by the increased surface roughness (turbulence). The stand alone obstacle becomes less prominent in these conditions.

6.4.4.6 Conclusions

Based on the offline F100 auto land simulations an area could be defined where "Annex 14" heights in combination with a certain turbulence level, created significant, undesired disturbance

on the final approach and landing performance. This disk-shaped shaded area valid for “worst case” obstacles is shown in Figure 6-40. It can be observed from the figure that the area covers four of the six tested obstacles configurations within the **green** area shown in Figure 1-1. All configurations within the defined area affect the aircraft on the glide path below 350ft and have maximum speed deficits of 6kts or more. However medium turbulence level (RMS turbulence intensity approximately 4 kts) or more may also lead to degraded landing performance within this area independent of “stand alone” structures.

After touch down the aircraft enters the high speed ground roll phase in which the aerodynamics still play an important role. Down to an airspeed of approximately 80 knots the aerodynamic control surfaces contribute substantially in the controllability of the aircraft. A conservative estimation obtained from the F100 simulations shows that this high speed ground roll in adverse weather conditions may consume up to 1500m of runway length. Therefore the area defined for the airborne phase is extended parallel to the runway centre line as indicated in Figure 6-40.

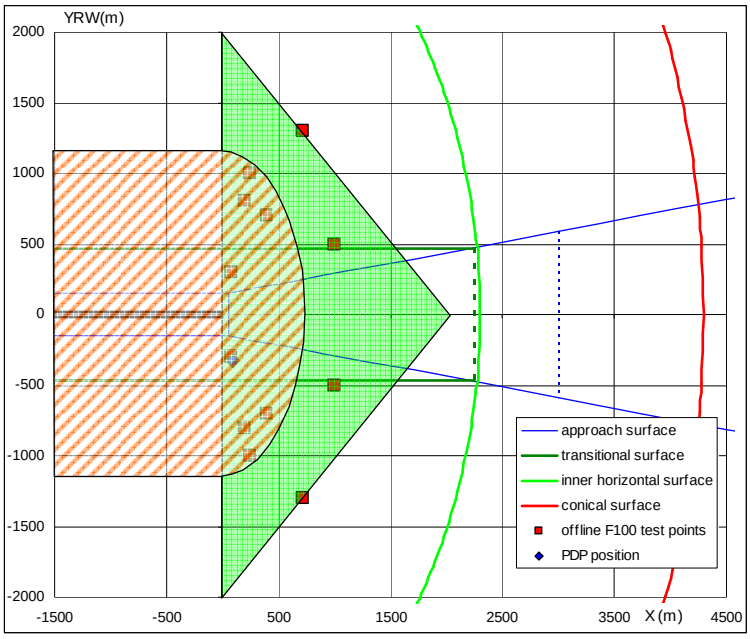

Figure 6-40: Disk shaped area in which 1:35 wind disturbance plane applies

6.5 Boeing B747

6.5.1 Aircraft model

The offline Monte Carlo simulations for a Boeing 747 type aircraft were performed with a six degree-of-freedom, non-linear model with the characteristics of a Boeing 747-200 equipped with four Pratt & Whitney JT9D-3 engines ([32]([33]. A summary of the B747, inertial and flight condition-dependent parameters can be found in Table 6–11. A light aircraft mass and an aft centre of gravity were chosen since this implies a low landing reference speed “Vref” which

offers the most critical flying qualities. The approach speed of 150kts was determined empirically through an analysis of the aircraft model's stall speed with the recommended flap setting of 30°, and includes a correction of 20kts for the expected longitudinal gusts.

Table 6–11: B747-200 inertial and flight condition parameters

Parameter	**Value**	**Unit**
Wing area S	510.97	m²
Mean aerodynamic chord (mac) $\bar{c}$	8.32	m
Wing span b	59.64	m
Position of centre of gravity	25	% mac
Mass	226,800	kg
Reference speed V_{ref}	150	kts IAS
Flap setting	30	deg
Gear position	DWN	-

A generic autopilot with auto-throttle system guides the aircraft along the ILS trajectory while holding the prescribed reference speed. More details on the functionality of the programmed autopilot are given in section 6.5.3. The aircraft equations of motions and the control system were updated at 50 Hz.

6.5.2 Atmospheric response model

Atmospheric turbulence is a random, stochastic phenomenon and can be decomposed in the gust velocities u_g, v_g and w_g. A random gust field is typically modeled by passing a white noise signal through a linear, rational filter which generates a colored output signal, the gust velocities ([34]. The transfer function of this forming filter should be defined such that the generated output seems to best fit the frequency characteristics (power spectral densities) of the available theoretical and experimental data on atmospheric turbulence.

The effect of turbulent air on aircraft behavior can be modeled as additional aerodynamic forces and moments acting on the aircraft. These extra forces and moments are then functions of the gust velocities u_g, v_g and w_g.

The aircraft response to atmospheric turbulence can be split up in a symmetric motion component and an asymmetric motion component.

The symmetric response of the aircraft, defined by the longitudinal forces X_g and Z_g, and the longitudinal moment M_g, only depends on the varying longitudinal gust components $\hat{u}_g$ and α_g acting in the centre of gravity. A gust velocity field that is encountered along the aircraft's flight path can be described with a one-dimensional turbulence model characterized by the known Dryden spectral densities.

The asymmetric aircraft motion is more complicated since the gust velocities u_g and w_g vary along the lateral axis resulting in a span wise distributed turbulence field that effects the rolling and yawing moments of the aircraft. Consequently, atmospheric turbulence now has to be considered as a two-dimensional process. The contribution of the side gust velocity v_g can still be evaluated in the center of gravity of the aircraft.
The gust model and the interaction with the aircraft dynamics are elaborated in more detail in Appendix D.

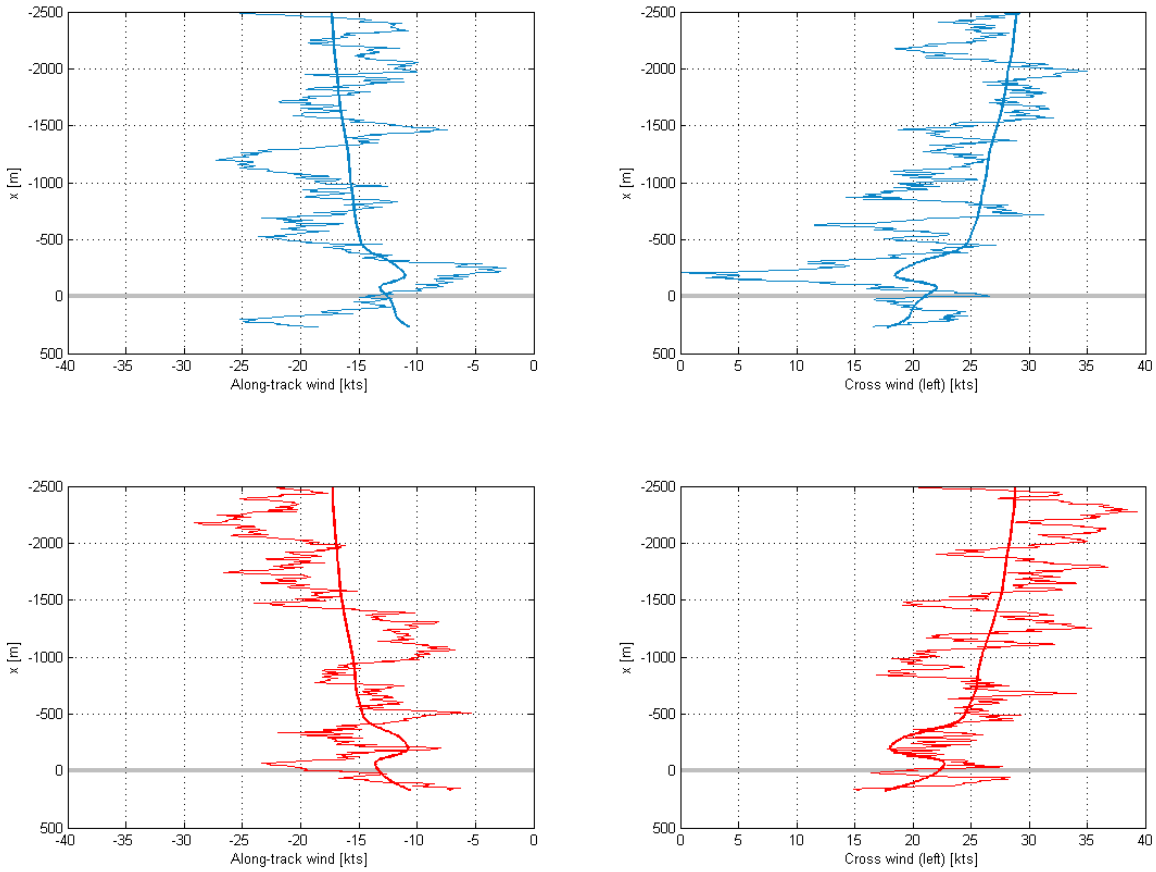

Figure 6-41: *Wind profiles for an approach through the wake of a generic obstacle*

The gust models and the models for the aircraft response to the created atmospheric turbulence are now combined with the wind climate model for the wake of an obstacle (section 4) to serve as an input for the offline simulation of the Boeing 747 approaches in the desired atmospheric conditions. A few examples of the created wind conditions are shown in Figure 6-41. Presented are mean wind profiles with superposed gust velocities as can be encountered during an approach through the wake of a “regular” block-shaped obstacle with height of 21m and width of 200m, located 300m next to the runway and 80m before the runway threshold (in short

80/300). The mean wind speed at 10m above the ground is 23kts coming from direction 210. The surface roughness is 0.03m. The horizontal gray line indicates the runway threshold.
In general, for the given environment conditions, additional gusts up to maximum 10-15kts are encountered additional to the mean wind velocity. Sometimes, the random atmospheric turbulence may cover up the presence of a wake as shown at the bottom. However there will also be situations where the gust peaks adds the effect of the wake. In the example at the top, the cross wind even suddenly drops from 25kts to nil when passing through the wake. Such scenarios will not contribute to a successful and safe landing.

6.5.3 Autopilot considerations

The designed autopilot offers vertical and lateral guidance of the aircraft along the ILS approach path. It consists of two uncoupled closed-loop control laws for, respectively, elevator and aileron control. The feedback loops use angular deviation and angular deviation rate with respect to the 3° ILS glide slope beam and the localizer beam for the vertical and lateral guidance, respectively. A yaw damper assists lateral motion of the aircraft through rudder deflection. An auto-throttle system controls the throttle setting in order to keep the predefined indicated airspeed during the approach.
Due to the highly turbulent atmospheric environment and strong wind shear conditions, the gains of the control laws were carefully tuned to increase its accuracy of guiding the aircraft to the touchdown zone. Open-loop de-crabbing has been added to compensate for the lateral drift just before touchdown caused by the vertical wind shear while keeping the wings almost level.

6.5.4 Test procedure and test matrix for “regular” obstacles

The Monte Carlo simulation focused on an objective analysis and comparison of B747 ILS approach trajectories to runway 27 disturbed by a wake originating from a building or obstacle in the vicinity of the runway threshold. The structure consists of “Annex 14” height limited obstacles and buildings with a height limit according to the “1:35” plane. For this comparison ‘regular’ block-shaped obstacles were chosen with a porosity factor *p* of 0.1 as mentioned in the wind climate modeling of section 4 and Appendix B. Simulated approaches through an atmosphere with only gust disturbances (thus no obstacle present) served as a baseline reference condition.
Each Monte Carlo run was performed with identical mean wind conditions corresponding to a maximum cross wind of 20kts at the reference height of 10m AGL. A related wind direction of 210 degrees was chosen, since this generates a wake disturbance as close as possible to touchdown which is the most critical stage of the landing. This results in a mean wind speed of 23kts coming from direction 210 (in short 210/23) at the reference height. The terrain surface roughness was fixed at 0.03m which according to ([23] is applicable for a runway-type

environment (i.e. flat land with only superficial vegetation (grass) and sometimes small obstacles, like runways, fallow farmland, etc).
Each experiment run started with the aircraft stabilized on the ILS path of runway 27 in complete landing configuration, i.e. flaps 30° and gear down. The initial altitude was set at 2000ft in order to allow complete aircraft stabilization by the autopilot and to provide adequate initialization time for the Dryden turbulence filter to output representative gust velocities.
Three independent variables were varied to obtain the test matrix of Table 6–12. First, the position of the obstacle, defined by the x- and y-coordinate of its centre, ranges from 80m to 560m in front of the runway threshold (x-direction) and from 300m to 1300m perpendicular to the runway (y-direction). In total eleven locations were selected. A few combinations were omitted because results indicated that these locations would not provide additional valuable data. Last, the obstacle is given two heights H: (1) according to "Annex 14" regulations and (2) according to the "1:35" rule. Figure 6-42 displays an overview of the obstacle locations and restrictions according to both regulations. In summary, 22 scenarios (11 × 2) are analyzed, plus the baseline scenario where no building is present, so 23 situations in total. The width of the obstacle is fixed to 200m.

Table 6–12: *Test matrix for B747 Monte Carlo simulation*

		Obstacle x position [m]			
		-80	**-240**	**-400**	**-560**
Obstacle y position [m]	**-300**	H = 9m *(1:35)* H = 21m *(annex 14)*	H = 9m *(1:35)* H = 21m *(annex 14)*	H = 9m *(1:35)* H = 21m *(annex 14)*	H = 9m *(1:35)* H = 21m *(annex 14)*
	-700	H = 20m *(1:35)* H = 45m *(annex 14)*	H = 20m *(1:35)* H = 45m *(annex 14)*	H = 20m *(1:35)* H = 45m *(annex 14)*	××××××××××××
	-1000	H = 29m *(1:35)* H = 45m *(annex 14)*	H = 29m *(1:35)* H = 45m *(annex 14)*	H = 29m *(1:35)* H = 45m *(annex 14)*	××××××××××××
	-1300	H = 37m *(1:35)* H = 45m *(annex 14)*	××××××××××××	××××××××××××	××××××××××××

Each scenario was repeated 300 times for random turbulence conditions to obtain sufficient statistical data. Evaluation of the results pointed out that more than 100 runs were required to allow adequate convergence of the statistical parameters, as shown in Figure 6-43. This figure shows the history of the mean and standard deviation lateral off-set at touchdown over the total range of 300 runs for the approach scenario disturbed by the wake from the "Annex 14" approved obstacle positioned at x = 80 and, y = 300m indicated short as (80,300).

For the analysis of the Monte Carlo experiment 45 parameters were recorded with a sample rate of 10 Hz. Data acquisition occurred from the moment that the aircraft passed 1000 ft until touchdown.

Relevant performance indicators as indicated in section 5 were selected to quantify the disturbance of the wake on the aircraft approach trajectories:

1. The position of the touchdown point in terms of the lateral deviation from the centerline "XteTD" (cross-track-error) and the longitudinal position "XTD",
2. The maximum bank angle that was initiated during the last 500 ft of the approach,
3. The maximum wind shear hazard index or F-factor encountered.

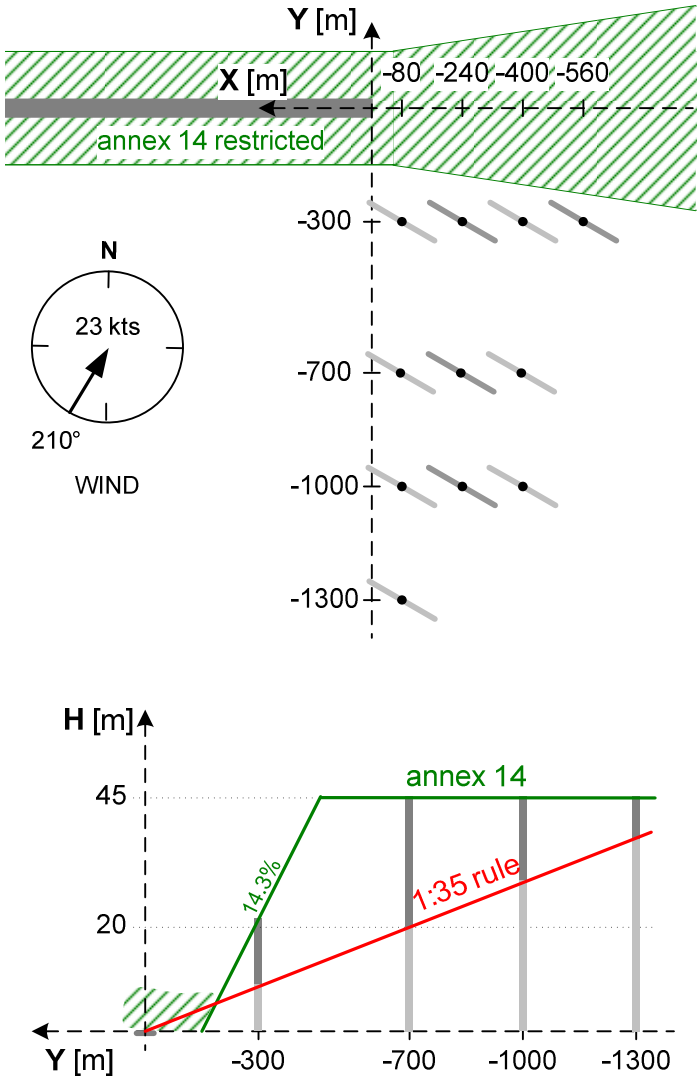

Figure 6-42: *Obstacle locations from test matrix and the obstacle restrictions*

A full-factorial model Analysis of Variance (ANOVA) was conducted to evaluate the effects of the independent measures on these performance indicators. Box plots were created to visualize

the centre and spread of the results. The box plots also reveal ‘weak’ and ‘extreme’ outliers in the data which are presented in the plots with a circle and a star, respectively. These outliers are large deviations and were caused by high gust peaks, possibly combined along multiple axes of the aircraft equations of motion.

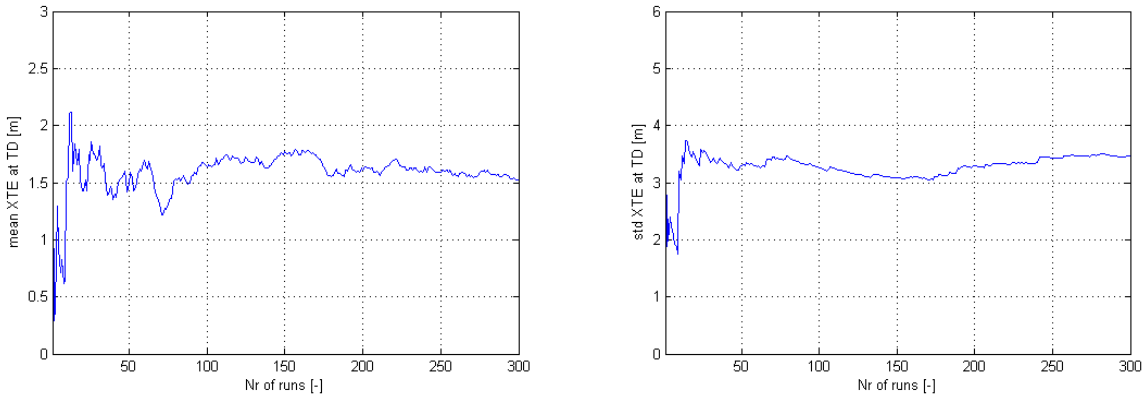

Figure 6-43: *Mean and standard deviation lateral off-set at TD as function of number of runs*

6.5.5 Test matrix results and discussion

The turbulent wind conditions make every simulation run unique. An example of the wind and gust velocities encountered during the baseline scenario (i.e. no wake) and the situations where an obstacle has been set at 80m in front of the threshold with a lateral offset of 300m (80,300) is presented in Figure 6-44. It presents a wind profile encountered over the last 2.5 km for the obstacle-free scenario and scenarios with the mentioned building location in the 210/23 wind condition.

The mean and standard deviations are, respectively, the red and green lines. The horizontal gray line indicates the runway threshold. The logarithmic mean wind profile and the contribution and strength of the different wakes become very clear. Notice that during a few runs, severe gust peaks were created. These rare atmospheric extremes can cause very large trajectory deviations and consequently have a direct impact on the mean and standard deviations of the performance indicators. Figure 6-43 demonstrates this effect with a few relatively large jumps in the history of the mean and standard deviation of the lateral off-set at touchdown over the number of simulation runs. Therefore, visualization with box plots that indicate the center and spread of the results is preferred for the comparison of the test matrix scenarios. The probability (p) value from the ANOVA analysis provides a quantitative measure for the comparison of the disturbed approach trajectories with respect to the nominal, obstacle-free approach. If the probability p is smaller or equal .01 a highly significant difference is found. When the probability p lies between 0.01 and 0.05 the compared scenarios differ significantly. The range between 0.05 and 0.1 indicates borderline significance. No significant discrepancy can be distinguished when the probability is larger than .01.

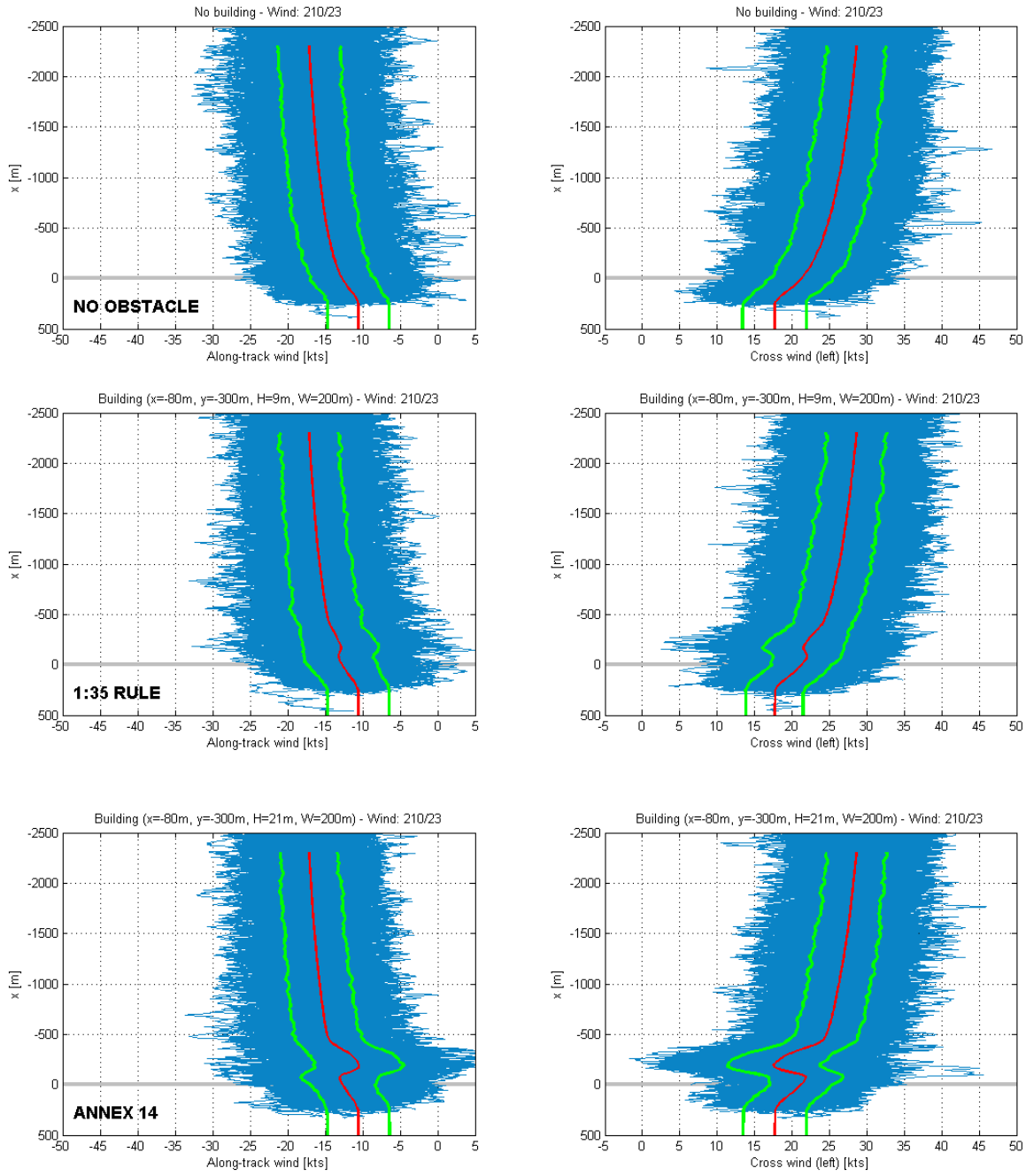

Figure 6-44: *Wind profile encountered over the last 2.5 km for 3 scenarios in the 210/23 wind condition*

6.5.5.1 The main gear touch down point

The most important criterion for the evaluation of a landing procedure is the position of the main gear touchdown point within the desired touchdown zone of the runway (section 5.2). The 300 touchdown points for the baseline scenario and the two evaluated obstacles at position (80,300) are demonstrated in Figure 6-45 for the 210/23 wind condition. The red cross indicates the mean touchdown point. The green rectangle shows the lateral and longitudinal standard

deviation. It stands out that all touchdowns occurred at the very beginning of the desired touchdown zone. When disturbed by the wake of the obstacles, the B747 even 'lands' before the runway which is not acceptable. This is caused by the limited functionality of the used autopilot which had an insufficient sensitive glide slope control law and fails an auto-flare system. In the upcoming evaluation of the longitudinal touchdown point and glide slope error, these imperfections will be neglected and the discussion will be confined to a general comparison of the variation between all scenarios.

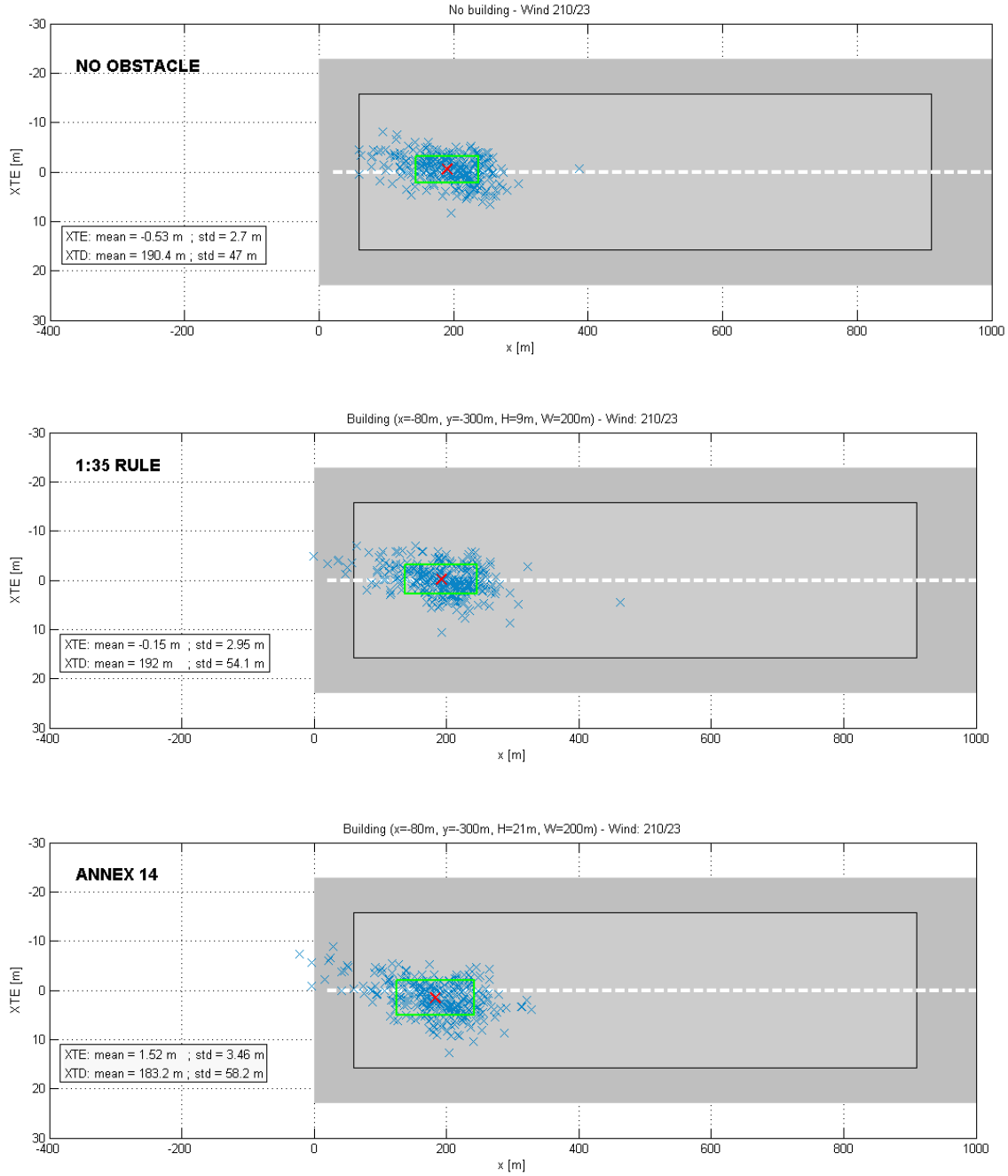

Figure 6-45: The touchdown locations (XTD, XteTD) for the obstacle-free scenario and scenarios for building location (80,300)

The distribution of the lateral deviation “XteTD” of the touchdown point for every scenario of the test matrix is shown in Figure 6-46. The dashed line in the figure indicates the edges of the desired touchdown zone. The vertical size of the figure corresponds with the runway width. As can be expected, the median lateral touchdown and spread of “XteTD” is larger when “Annex 14” obstacles disturbed the approach than in case of “1:35” obstacles. An increasing standard deviation can also be observed in the example of Figure 6-45.

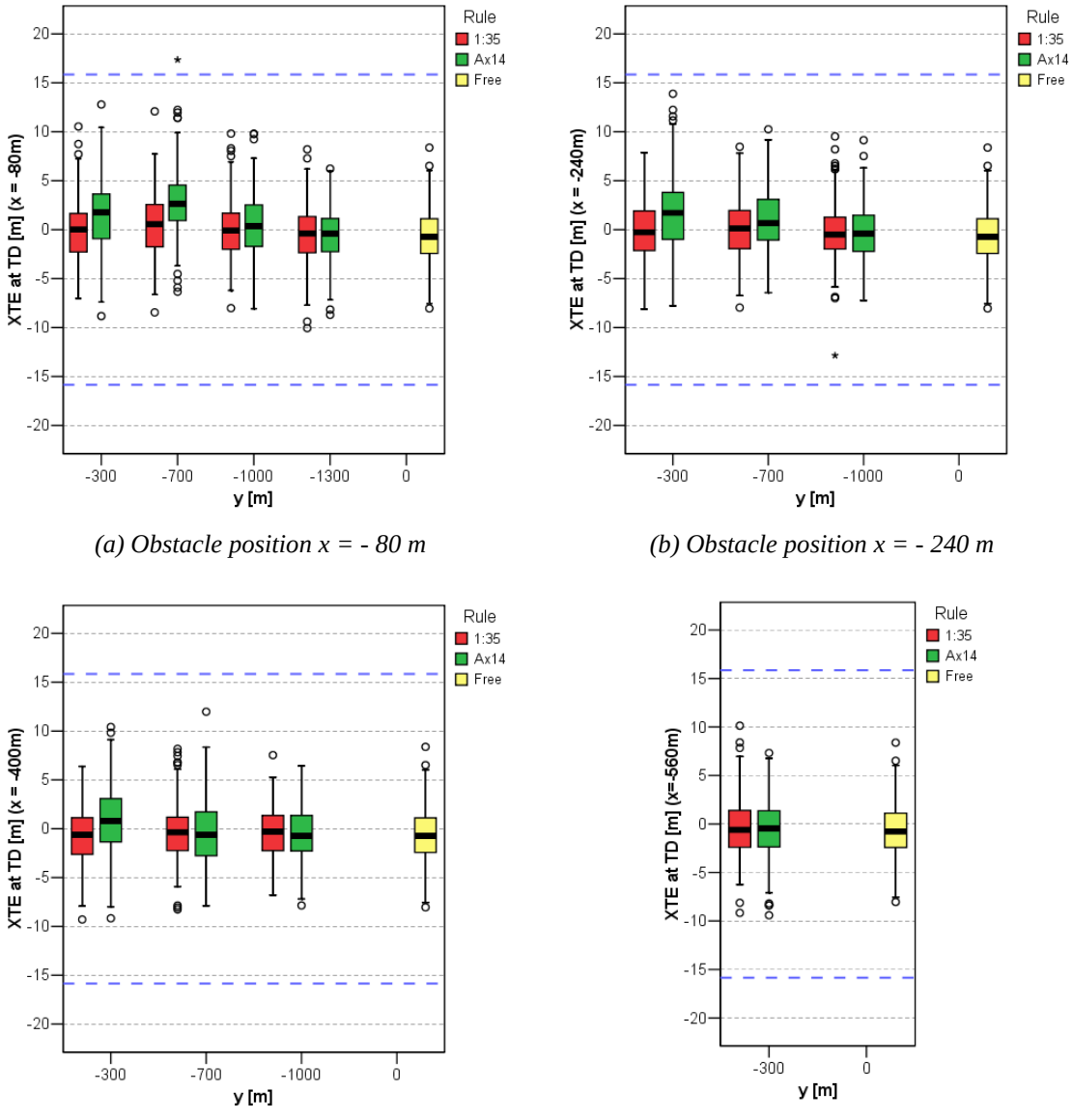

(a) Obstacle position x = - 80 m

(b) Obstacle position x = - 240 m

(c) Obstacle position x = - 400 m

(d) Obstacle position x = - 560 m

Figure 6-46: Lateral deviation at touchdown “XteTD” for various obstacle locations (x, y) and the obstacle-free scenario

The “Annex 14” obstacles even pushed a number of approaches to the side edge of the touch down zone which is certainly not desirable. Naturally the wake impact on the cross-track error diminished when the buildings were positioned further away from the threshold both in x- and y- direction. Since the aircraft encountered the disturbance of the wake earlier in the approach, they had more time to recover and re-stabilize the approach. For the most remote obstacles analyzed here, similar variation for both the “Annex 14” and “1:35” planes can be noticed as with the baseline approach. This suggests that both regulations are sufficiently strict at those locations.

An ANOVA analysis can quantify which buildings still have a relevant effect on “XteTD”. With these results a position perimeter of the obstacles could be marked out for the two investigated regulations.

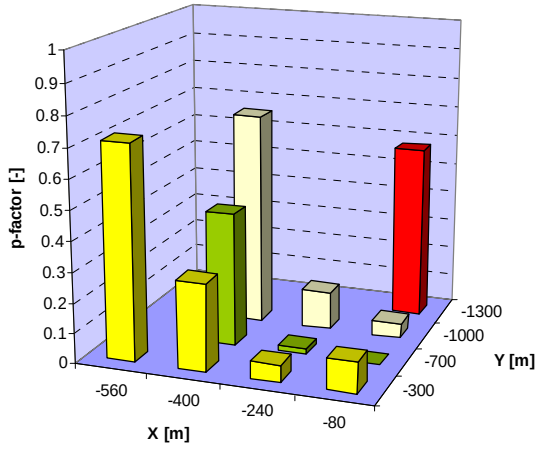

(a) 1:35 rule vs. obstacle-free

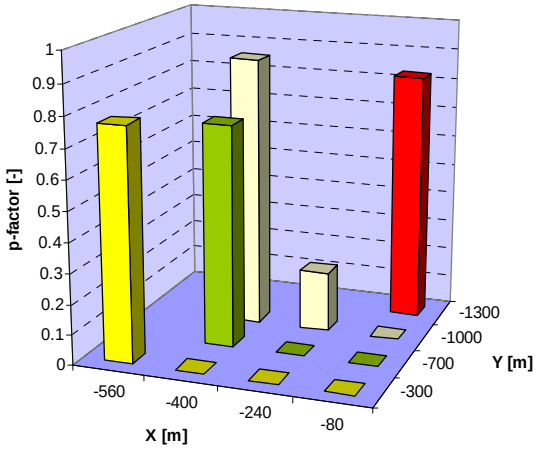

(b) Annex 14 vs. obstacle-free

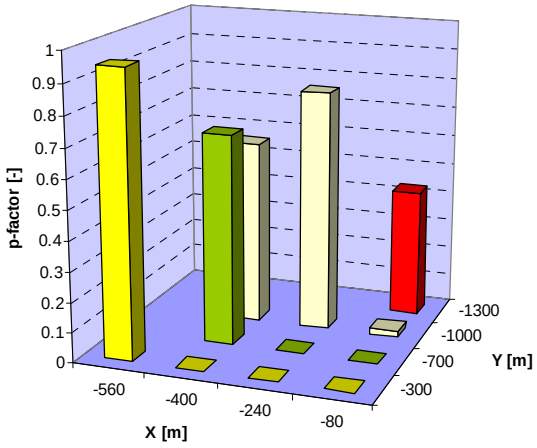

(c) 1:35 rule vs. Annex 14

Figure 6-47: The p-value from “XteTD” comparison using ANOVA analysis

A mutual comparison between "1:35" plane obstacles, "Annex 14" obstacles and the baseline scenario of "XteTD" is visualized in Figure 6-47.
The height of the bars indicates the level of significant difference (p-factor) of "XteTD" between the two scenarios. The actual p-values are listed in Table 6–13. The evaluation primarily indicates that "Annex 14" approved obstacles, i.e. the least strict regulation, tended to have no noticeable disturbance on the lateral offset of the touchdown point when these buildings were located outside a triangular area with a short side of 400-560m along the x-axis and a long side of 1000-1300m along the y-axis. Outside this perimeter hardly any difference can be observed between obstacles with an "Annex 14" and "1:35" rule approved height. Inside this triangle, a few "1:35" obstacles also induce (highly) significant differences, but the discrepancy is clearly less pronounced in the distributions of Figure 6-46. Apart from a few outliers, the extremes and variation of "XteTD" for "1:35" structures were quite similar to the obstacle-free scenario. Notice that the largest differences were found for obstacles that are set around 700m from the runway centerline rather than the one close to the approach trajectory.

Table 6–13: The p-values from ANOVA comparison of "XteTD" between 1:35 rule, Annex 14 obstacles and obstacle-free condition

		Obstacle x position [m]				**Obstacle x position [m]**			
		-80	**-240**	**-400**	**-560**	**-80**	**-240**	**-400**	**-560**
Obstacle y position [m]	**-300**	0.101	0.057	0.290	0.713	0	0	0	0.770
	-700	0	0.019	0.443		0	0	0.736	
	-1000	0.049	0.126	0.709		0	0.200	0.899	
	-1300	0.577	**1:35 rule vs. obstacle-free**			0.826	**Annex 14 vs. obstacle-free**		
Obstacle y position [m]	**-300**	0	0	0	0.949				
	-700	0	0	0.703					
	-1000	0.020	0.806	0.616					
	-1300	0.432	**1:35 rule vs. Annex 14**						

	Highly significant $p \leq 0.01$
	Significant $0.01 < p \leq 0.05$
	Borderline significant $0.05 < p \leq 0.1$
	Not significant $p > 0.1$

The longitudinal position of the touchdown point "XTD" appears to be less dependent on the obstacle conditions than "XteTD" as shown with the box plots of Figure 6-48. The solid line is the threshold of the runway. The dashed line indicates the front of the desired touchdown zone.

Obstacles located close to the runway do cause a number of early touchdowns when strengthened by a severe gust combination, but in general the disturbance of the wake on the vertical approach profile is relatively small at touchdown. The ANOVA analysis confirms these observations as demonstrated in Figure 6-49 and Table 6–14.

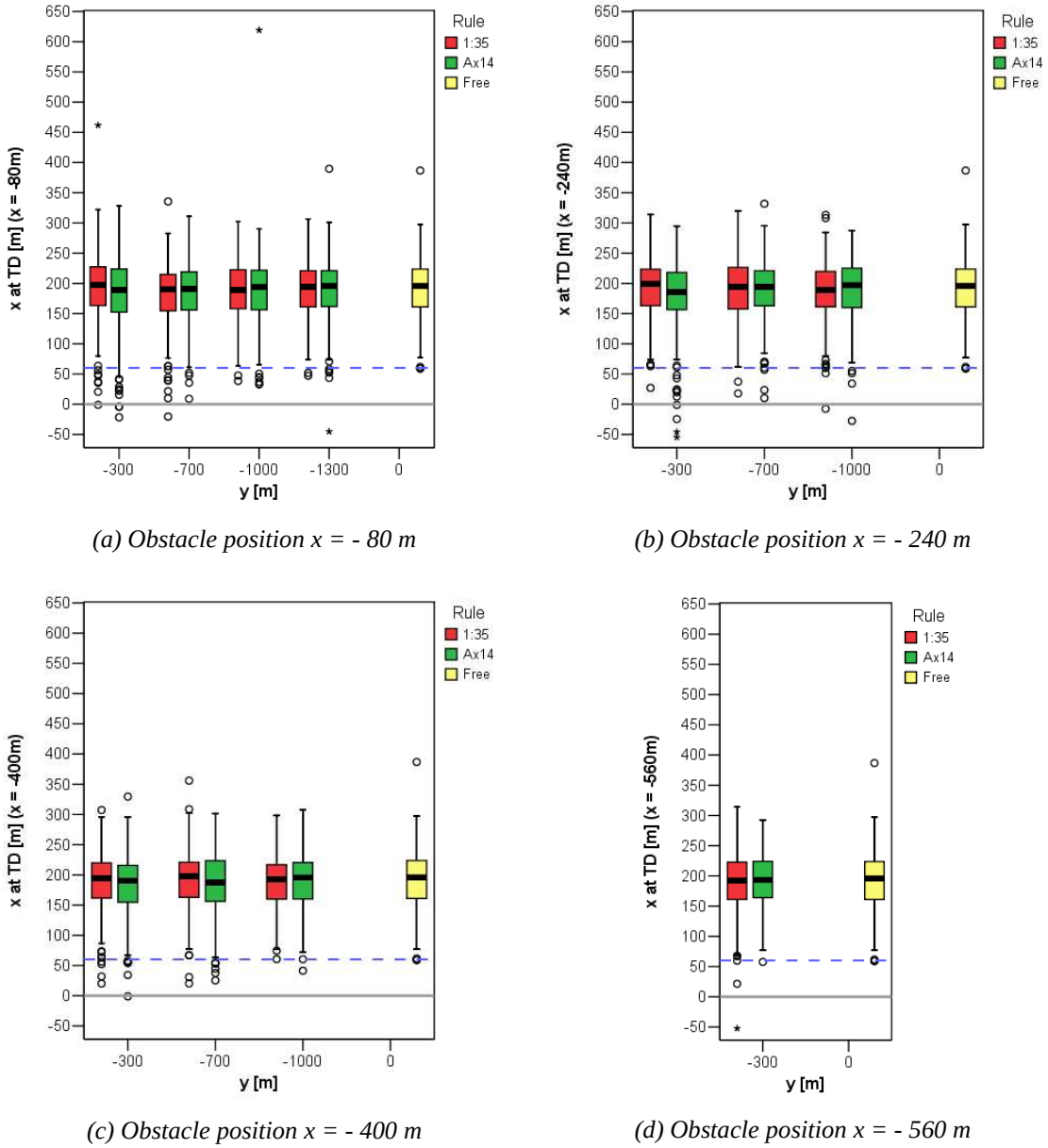

(a) Obstacle position x = - 80 m

(b) Obstacle position x = - 240 m

(c) Obstacle position x = - 400 m

(d) Obstacle position x = - 560 m

Figure 6-48: Longitudinal touchdown point "XTD" for various obstacle locations (x, y) and obstacle-free scenario for the 210/23 wind condition

Obstacles conform the "1:35" plane do not create a significant disturbance on XTD, except obstacle position (80,700).

This obstacle generated an even smaller touchdown spread (probably causing the small p-value), but with more outliers towards the runway threshold. “Annex 14” approved buildings positioned within 400m from the runway tend to have a (just) significant effect. For these cases the variation is somewhat larger with several early touch down’s. Although the autopilot is limitedly capable of performing adequate landings in the vertical plane, it can still be concluded that the obstacles only have a relatively small influence on “XTD”. But when considering the results from the “Annex 14” obstacles located at position (80,300) and (240,300), it might be valuable to limit their heights at least to the “1:35” rule.

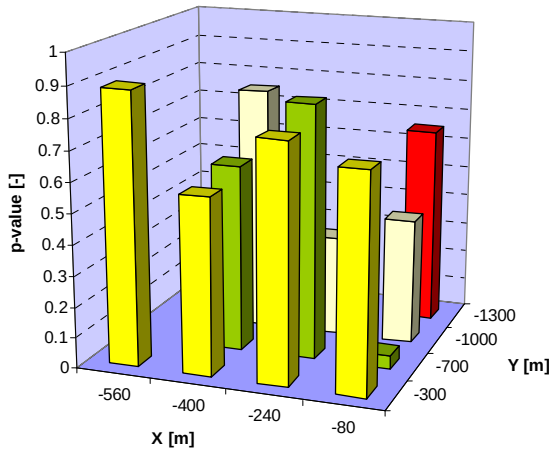

(a) 1:35 rule vs. obstacle-free

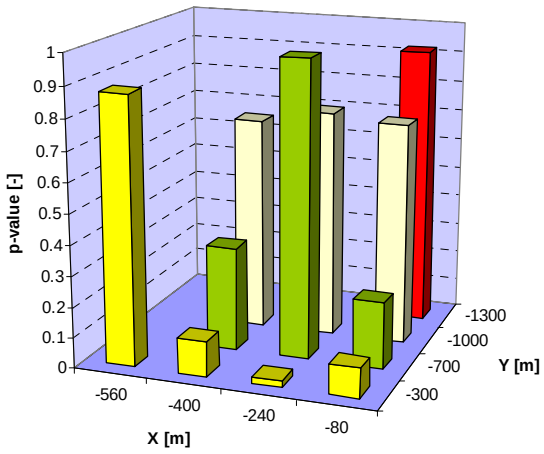

(b) Annex 14 vs. obstacle-free

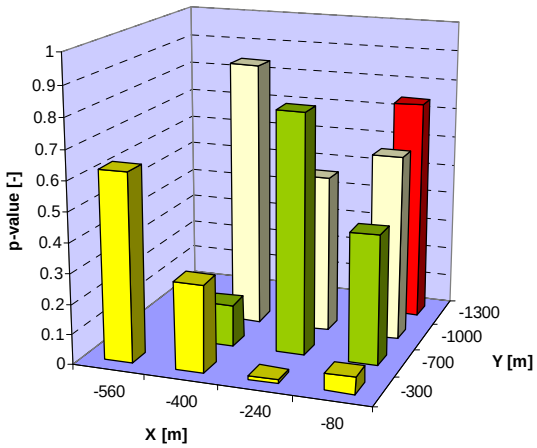

(c) 1:35 rule vs. Annex 14

Figure 6-49: The p-value from “XTD” comparison using ANOVA analysis

Table 6–14: The p-values from ANOVA comparison of "XTD" between 1:35 rule, Annex 14 obstacles and obstacle-free condition

		Obstacle x position [m]				Obstacle x position [m]			
		-80	**-240**	**-400**	**-560**	**-80**	**-240**	**-400**	**-560**
Obstacle y position [m]	**-300**	0.702	0.770	0.576	0.886	0.096	0.022	0.116	0.874
	-700	0.042	0.827	0.610		0.219	0.971	0.340	
	-1000	0.412	0.328	0.802		0.729	0.750	0.705	
	-1300	0.651	**1:35 rule vs. obstacle-free**			0.921	**Annex 14 vs. obstacle-free**		
Obstacle y position [m]	**-300**	0.056	0.011	0.290	0.626				
	-700	0.430	0.800	0.140					
	-1000	0.619	0.526	0.887					
	-1300	0.741	**1:35 rule vs. Annex 14**						

Highly significant $p \leq 0.01$

Significant $0.01 < p \leq 0.05$

Borderline significant $0.05 < p \leq 0.1$

Not significant $p > 0.1$

6.5.5.2 The roll response

The maximum absolute roll angle encountered during the approach appeared to be another interesting parameter when comparing the different wakes. As can be expected, the "Annex 14" obstacles induced (much) larger roll angles to correct for the lateral deviations from the localizer track as presented in Figure 6-50. An example of the roll angles that were required to keep the aircraft on track for obstacle position (80,300) is depicted in Figure 6-51. The figure shows histories of the roll angle over the last 2.5 km (~500 ft descend) for the obstacle-free scenario and scenarios with building location (80,300) in the 210/23 wind condition. The mean and standard deviations are, respectively, the red and green lines. The vertical gray line indicates the runway threshold. The vertical black line reflects the center of the wake when crossing the approach path. The orange edges bound the zones wherein bank angles are considered hazardous. (Note: these lines are constructed assuming that the aircraft perfectly moves along the 3° ILS descend trajectory.)

The large disturbance of the "Annex 14" approved obstacle with a height of 21m strikes immediately. Notice in the baseline scenario that also a single detrimental gust combination can cause the B747 to respond with a maximum roll angle of 10 degrees. "Annex 14" obstacles located closer than 400-560m in front of the threshold and 700-1000m laterally, caused the aircraft to roll more than 10 degrees during several runs. At touchdown this would cause an

engine strike with the ground. However none of the scenarios resulted into an actual engine strike or bank angle warning.

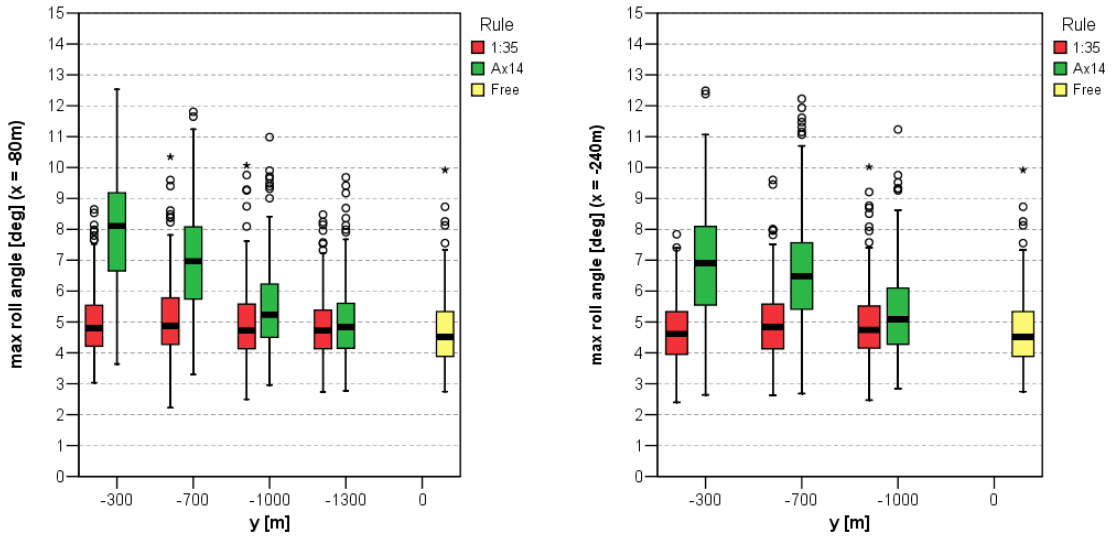

(a) Obstacle position x = - 80 m

(b) Obstacle position x = - 240 m

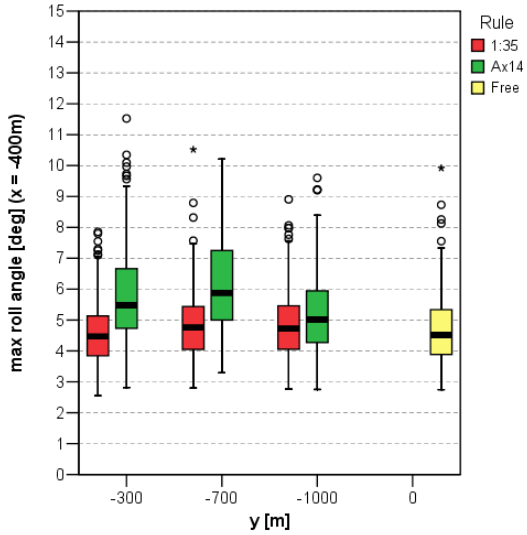

(c) Obstacle position x = - 400 m

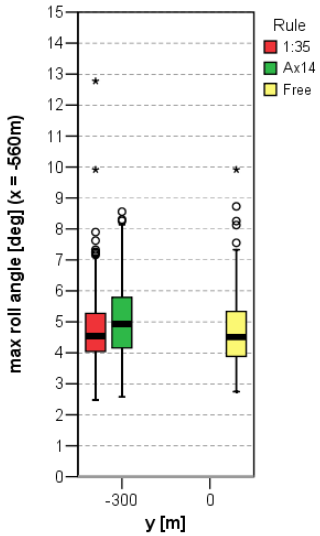

(d) Obstacle position x = - 560 m

Figure 6-50: Maximum absolute roll angle for various obstacle locations (x, y) and obstacle-free scenario for the 210/23 wind condition

Secondly, almost all of these high maximum roll angles occur very close to the ground, as depicted in Figure 6-52, which shows the altitude at which the maximum absolute roll angle occurred, for various obstacle locations (x, y) and obstacle-free scenario for the 210/23 wind condition. An ANOVA analysis indeed reveals highly significant distinctions for the altitude within the mentioned perimeter (Figure 6-53 and Table 6–15). Large rolling maneuvers at final

approach and close to the ground can not be accepted. When applying the criterion for hazardous bank angles (Figure 5-9), hazardous bank angles occurred in almost 10% and more of the approaches with “Annex 14” obstacles located in the mentioned area, as shown in Table 6–16. This table shows the percentage of runs where hazardous bank angles were encountered according to the “1:35” rule and “Annex 14” obstacles. As a reference the baseline turbulent atmosphere in the obstacle-free scenario caused hazardous bank angles in 1% of the runs.

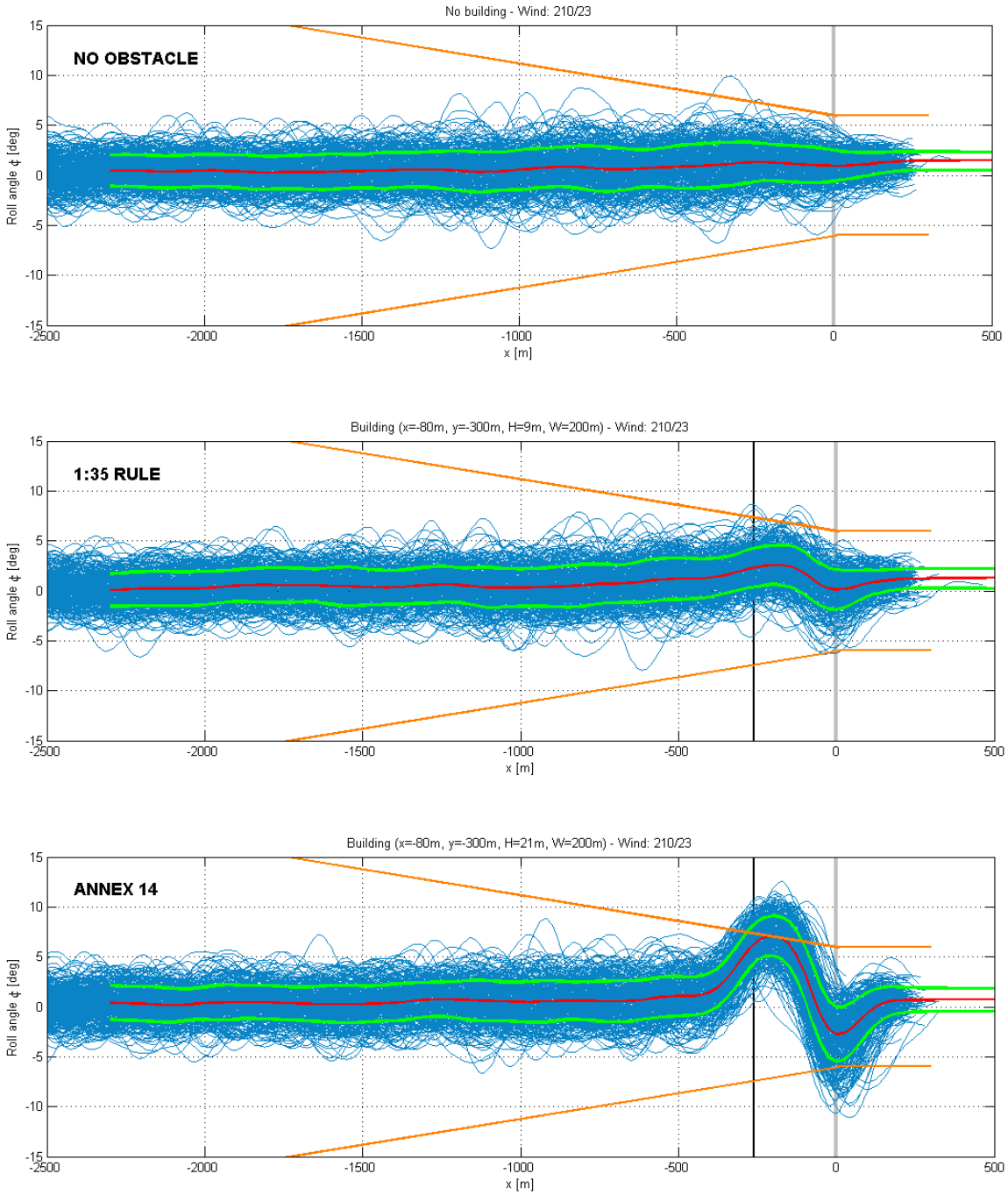

Figure 6-51: Histories of the roll angle over the last 2.5 km

This suggests that “Annex 14” approved obstacles should not be allowed there. Outside this boundary, the difference in the number of runs with hazardous bank angles between “Annex 14” and the “1:35” rule is relatively small.

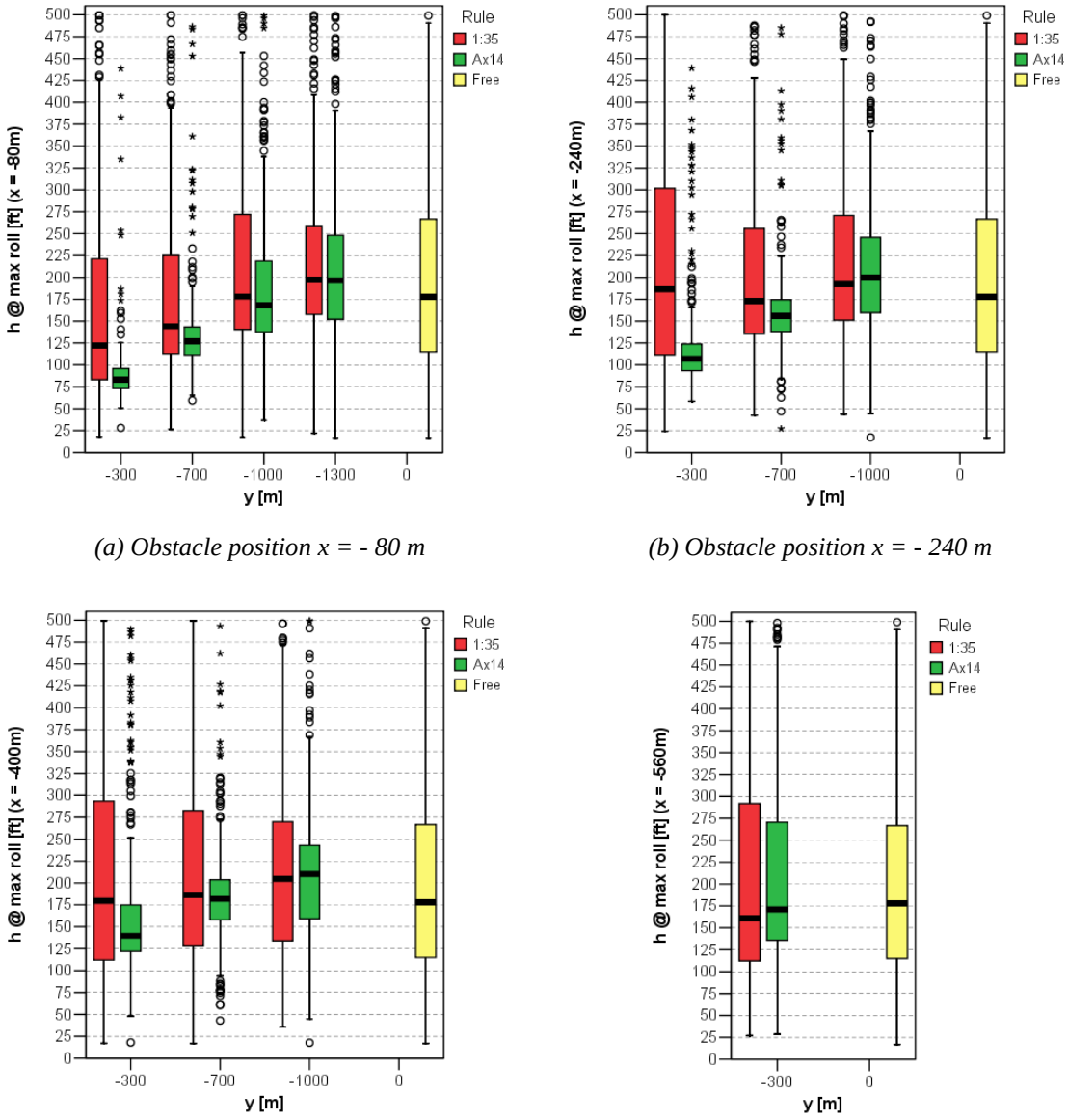

(a) Obstacle position x = - 80 m

(b) Obstacle position x = - 240 m

(c) Obstacle position x = - 400 m

(d) Obstacle position x = - 560 m

Figure 6-52: The altitude at which the maximum absolute roll angle occurred

On the other hand all obstacles according to the “1:35” rule have a very similar maximum roll angle with respect to the obstacle-free scenario (Figure 6-50). Despite the visual similarity, (highly) significant differences were calculated for most “1:35” obstacles. Indeed, the distributions of the maximum roll angle are slightly larger. This could be expected since the

wake naturally provides some extra lateral deviation at a certain point during the approach, demanding stronger roll maneuvers. Nevertheless, it can be concluded that the difference in maximum roll angle is in most cases negligible. Additionally, the corresponding altitudes of the maximum roll ($h@\varphi_{max}$) with 1:35 obstacles are comparable to the baseline condition (Figure 6-52), except for the first two obstacles along the position line of 80m in front of the threshold. The calculation of the probability value confirms these observations (Figure 6-53): only the obstacles at position (80,400) and (80,700) significantly cause maximum roll angles occurring at lower altitude than when no wake is generated. Yet, the bank angles only appeared to be hazardous in maximum 3% of the runs (Table 6–16), which is just a small discrepancy with respect to the obstacle-free reference condition where the aircraft responded with hazardous bank angles in 1% of the approaches.

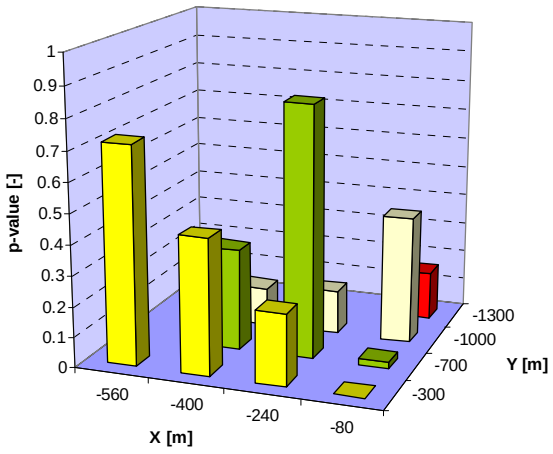

(a) 1:35 rule vs. obstacle-free

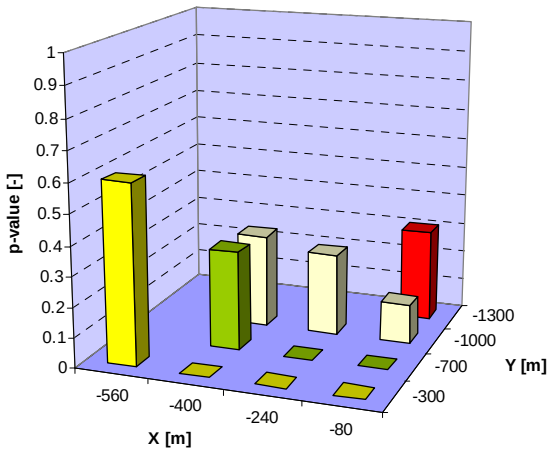

(b) Annex 14 vs. obstacle-free

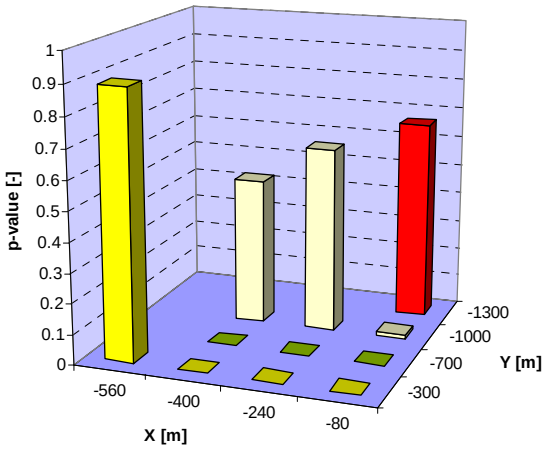

(c) 1:35 rule vs. Annex 14

Figure 6-53: The p-value from $h@\varphi_{max}$ comparison using ANOVA analysis

The analysis of the roll response indicated that within the rectangle with a length in x-direction of approximately 500m and width in y-direction of around 1000m annex 14 obstacles induced too large bank angles. Limiting the heights to the 1:35 rule in this area is expected to be acceptable. However this should be validated with subjective opinions in the piloted simulator experiment. Outside the mentioned area, the annex 14 regulations appear to be well applicable.

Table 6–15: The p-values from ANOVA comparison of $h@\varphi_{max}$ between 1:35 rule, Annex 14 obstacles and obstacle-free condition

		Obstacle x position [m]				Obstacle x position [m]			
		-80	**-240**	**-400**	**-560**	**-80**	**-240**	**-400**	**-560**
Obstacle y position [m]	**-300**	0	0.234	0.446	0.717	0	0	0	0.559
	-700	0.021	0.829	0.334		0	0	0.330	
	-1000	0.421	0.144	0.126		0.130	0.273	0.310	
	-1300	0.159	**1:35 rule vs. obstacle-free**			0.305	**Annex 14 vs. obstacle-free**		
Obstacle y position [m]	**-300**	0	0	0	0.891				
	-700	0	0	0.001					
	-1000	0.013	0.621	0.491					
	-1300	0.668	**1:35 rule vs. Annex 14**						

Highly significant $p \leq 0.01$

Significant $0.01 < p \leq 0.05$

Borderline significant $0.05 < p \leq 0.1$

Not significant $p > 0.1$

Table 6–16: The percentage of runs where hazardous bank angles were encountered for the 1:35 rule and Annex 14 obstacles

		Obstacle x position [m]				Obstacle x position [m]			
		-80	**-240**	**-400**	**-560**	**-80**	**-240**	**-400**	**-560**
Obstacle y pos. [m]	**-300**	3.0%	1.7%	1.0%	1.3%	69.0%	38.3%	9.0%	2.0%
	-700	2.7%	1.3%	1.7%		27.7%	10.7%	4.3%	
	-1000	1.7%	0.7%	1.0%		3.3%	2.3%	2.0%	
	-1300	0.0%	**1:35 RULE**			1.3%	**ANNEX 14**		

6.5.5.3 The wind shear hazard index

The presence of the wakes from an obstacle did not appear to have any major influence on the maximum encountered wind hear hazard index or F-factor during the approaches, as presented in Figure 6-55. This figure shows the maximum wind shear hazard index encountered for various obstacle locations (x, y) and the obstacle-free scenario for the 210/23 wind condition. A "must alert" threshold is set at 0.13 ([36], indicated by the dashed line.

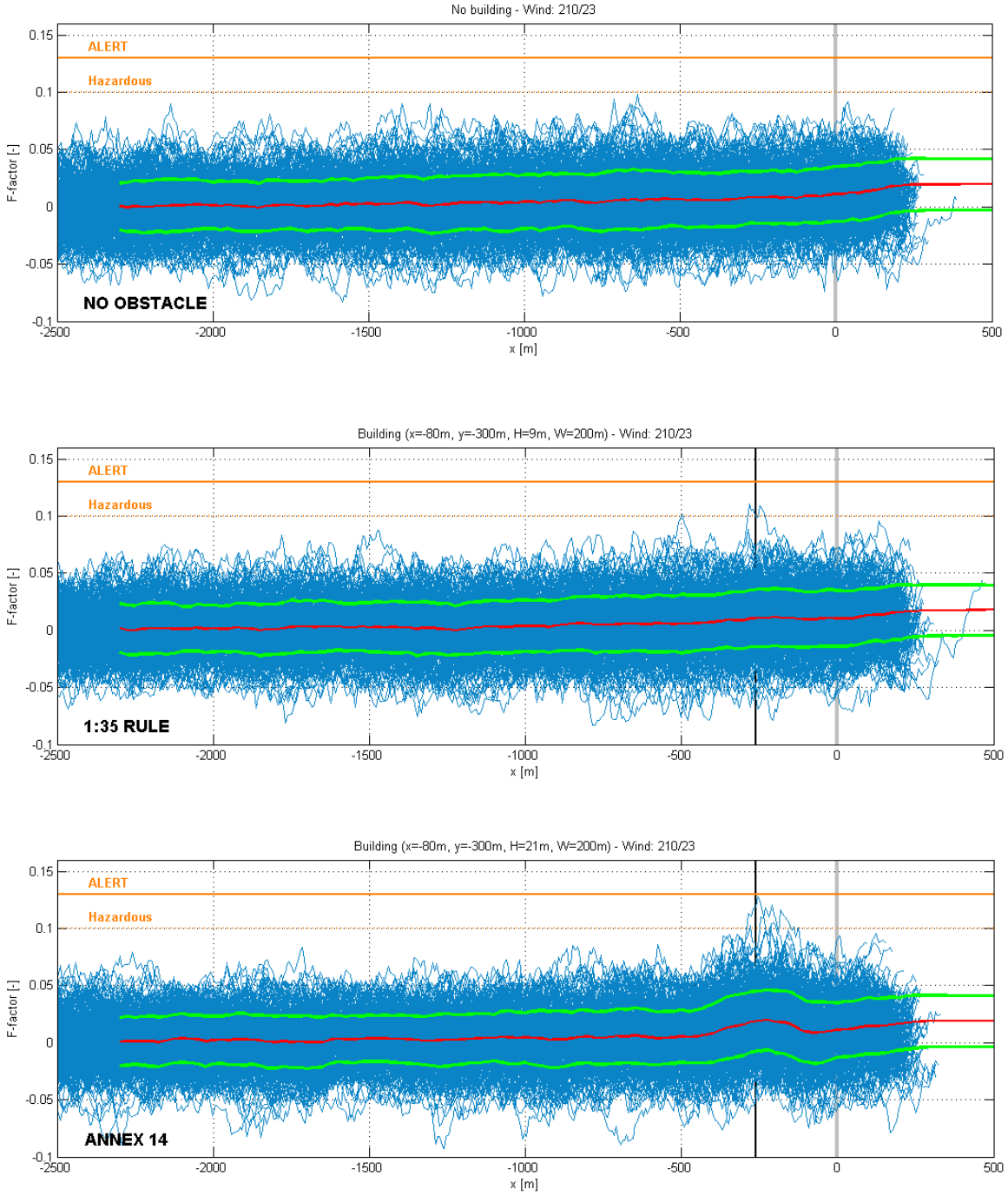

Figure 6-54: The wind shear hazard index or F-factor experienced over the last 2.5 km

Only a very few extremes were reported, like in the example of Figure 6-54, which shows the wind shear hazard index or F-factor experienced over the last 2.5 km (~500 ft descend) for the obstacle-free scenario and scenarios with building location (80,300) in the 210/23 wind condition.

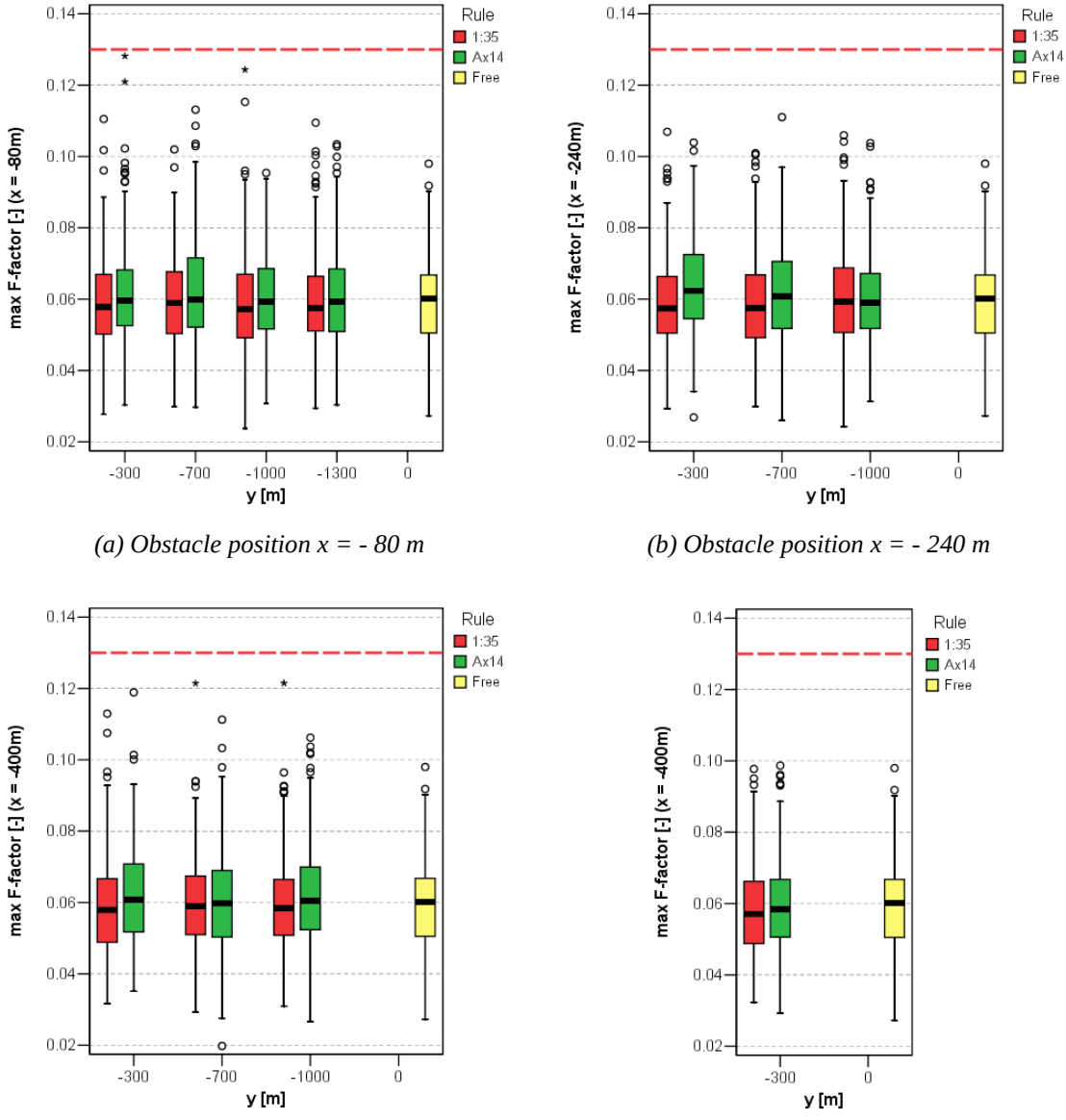

(a) Obstacle position x = - 80 m

(b) Obstacle position x = - 240 m

(c) Obstacle position x = - 400 m

(d) Obstacle position x = - 560 m

Figure 6-55: The maximum wind shear hazard index encountered (F-factor)

The mean and standard deviations are, respectively, the red and green lines. The vertical gray line indicates the runway threshold. The black line reflects the center of the wake when crossing the approach path. From the plots it appears that the wind shear alert was never

triggered. Especially for “1:35” obstacles, the generated wake did not significantly increase the F-factor as the high p-values prove in Figure 6-56 and Table 6–17. A few “Annex 14” approved obstacles positioned near the threshold tended to increase the risk of wind shear slightly but significantly. In the area up to 400m in front of the threshold and 700m in lateral direction also a significant difference in wind shear hazard is found with respect to the “1:35” rule.

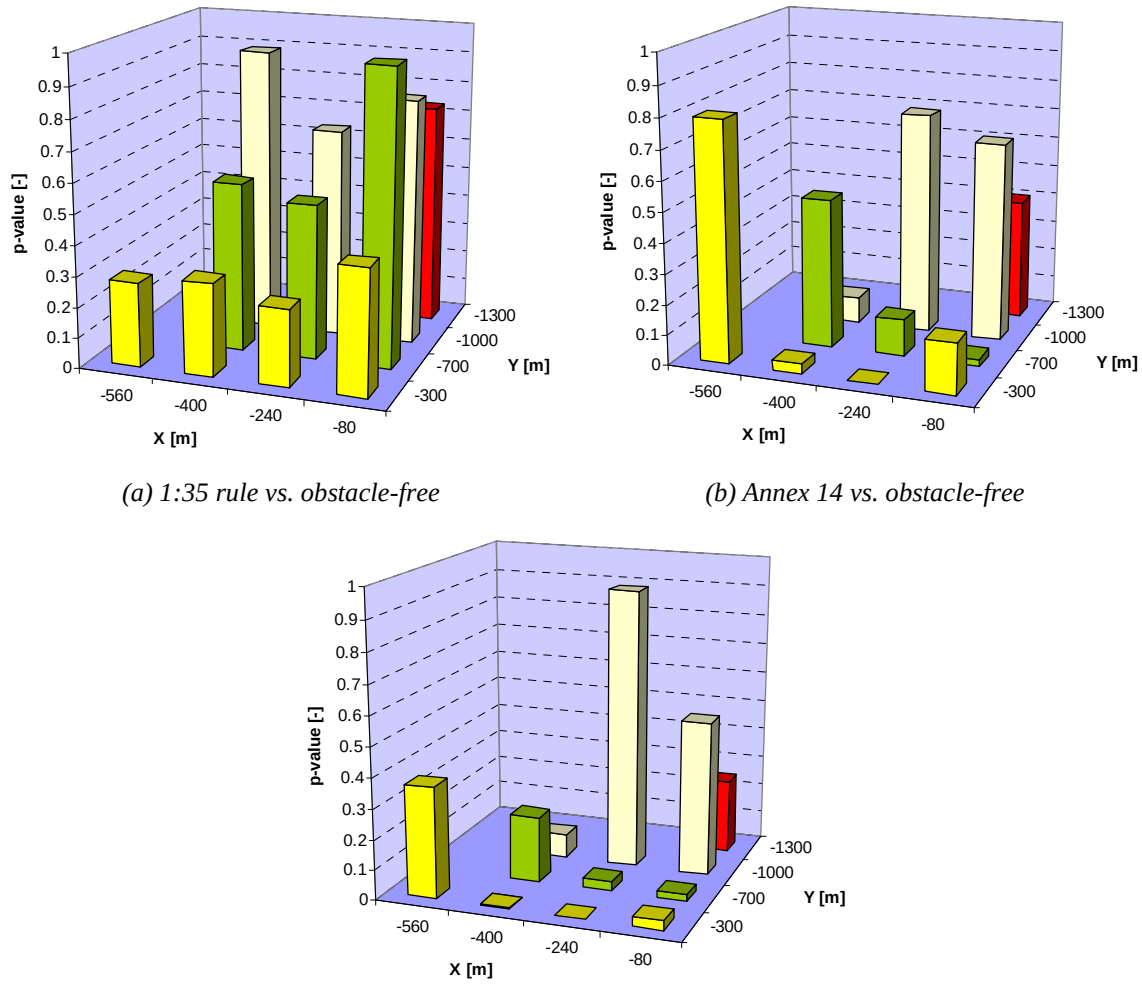

(a) 1:35 rule vs. obstacle-free

(b) Annex 14 vs. obstacle-free

(c) 1:35 rule vs. Annex 14

Figure 6-56: The p-value from F-factor comparison using ANOVA analysis

For the “Annex 14” obstacle located at position (80,300), the mean of the wind shear hazard measure over all the runs definitely increase, as can be seen in Figure 6-54. Although this is undesirable, no strong conclusions on the decline of flight safety by “Annex 14” obstacles can be drawn.

The non-significant effect of the presence of “1:35” obstacles on the F-factor also supports an observation from the data that showed an insignificant disturbance on the maximum downward

glide slope deviation. So in general, several results propose that the 1:35 rule might form a good regulation for the maximum height of obstacles positioned closely to the runway.

Table 6–17: The p-values from ANOVA comparison of F-factor between 1:35 rule, Annex 14 obstacles and obstacle-free condition

		Obstacle x position [m]				Obstacle x position [m]			
		-80	**-240**	**-400**	**-560**	**-80**	**-240**	**-400**	**-560**
Obstacle y position [m]	**-300**	0.411	0.251	0.303	0.277	0.169	0	0.033	0.559
	-700	0.965	0.509	0.553		0.023	0.123	0.493	
	-1000	0.808	0.687	0.933		0.66	0.738	0.086	
	-1300	0.732	**1:35 rule vs. obstacle-free**			0.305	**Annex 14 vs. obstacle-free**		
Obstacle y position [m]	**-300**	0.031	0	0.002	0.368				
	-700	0.020	0.032	0.219					
	-1000	0.515	0.931	0.078					
	-1300	0.247	**1:35 rule vs. Annex 14**						

Highly significant $p \leq 0.01$

Significant $0.01 < p \leq 0.05$

Borderline significant $0.05 < p \leq 0.1$

Not significant $p > 0.1$

6.5.6 Extension for "worst case" obstacles

The influence of a wake generated by "regular" block-shaped obstacles has been evaluated in the previous paragraphs. However, not all obstacles have a nice rectangular shape. They might have a special form, like for example the net-shape of the engine test facility (PDP). A wind tunnel experiment demonstrated that the PDP creates a much stronger wake as its shape withholds more wind (section 4). Therefore, the offline B747 simulations have been extended with an investigation on the disturbance caused by such "worst case" obstacles with heights according to "Annex 14" and the "1:35" rule. In order to model the worsening wake characteristics of the obstacle, its porosity factor *p* has been set to -1, just like the PDP. This can be physically interpreted as the creation of a more than impenetrable wind shield. Figure 6-57 illustrates the consequential difference in wake strength. The figure shows scenarios with a "regular" block-shaped building (p = 0.1) and a "worst case" obstacle (p = -1), both located at position (240, 1000) and for a 210/23 wind condition. The mean and standard deviations are, respectively, the red and green lines. The horizontal gray line indicates the runway threshold. With the results of the test matrix in mind, a few particular obstacle locations have been selected for analysis, as shown in Table 6–18. The results give an idea of the effect of a "worst case"

shape on the “1:35” rule on one hand. On the other hand, again a rough indication should be found of the area where “Annex 14” regulations should not be applied for these “worst case” conditions, in comparison to the boundary assigned for the “regular” shaped obstacles. Again, Monte Carlo simulations with 300 runs per scenario have been conducted in a 210/23 wind environment with surface roughness of 0.03, as was done for the test matrix evaluation.

Table 6–18: Additional scenarios of non-regular Annex 14 and 1:35 rule obstacles

	x position [m]	y position [m]	height (H) [m]	width (W) [m]
1:35 rule	-80	-300	9	200
	-240	-1000	29	200
Annex 14	-240	-1000	45	200
	-80	-1300	45	200
	-560	-1000	45	200
	-760	-700	45	200
	-560	-300	21	200

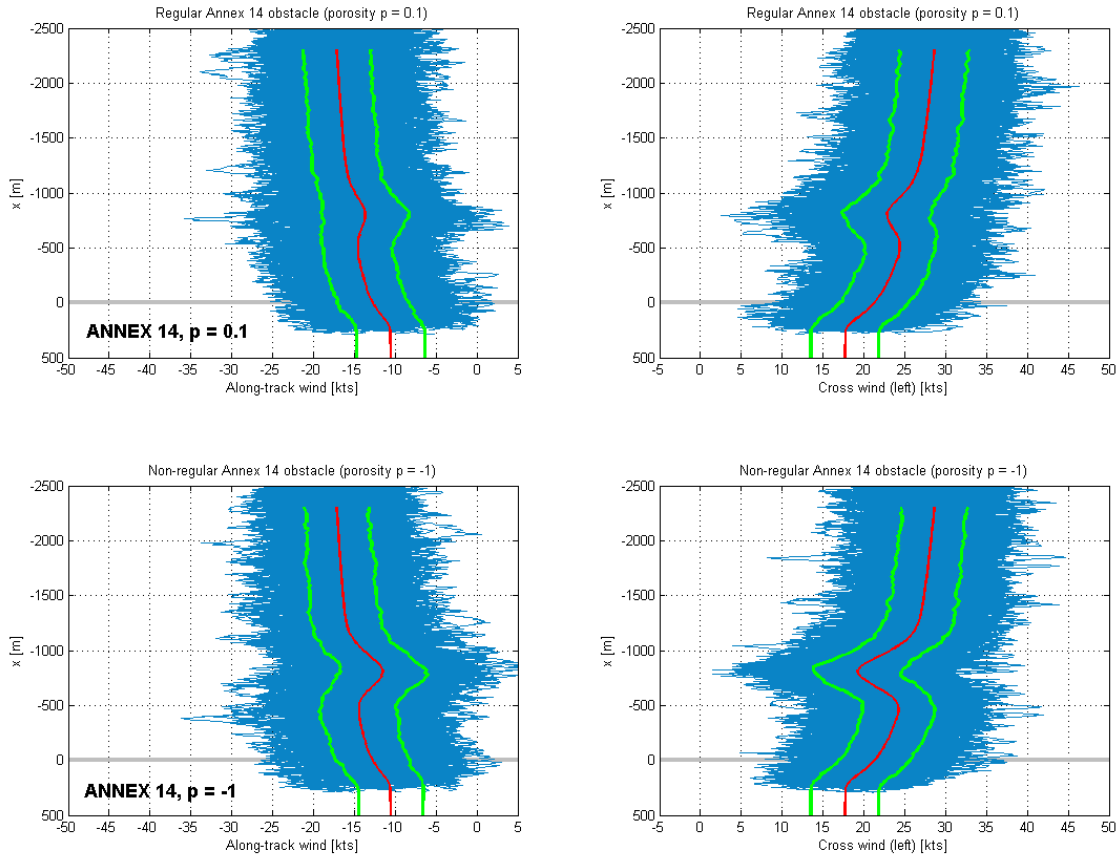

Figure 6-57: The wind profile encountered over the last 2.5 km for the two “Annex 14” scenarios

The previous evaluation of the test matrix demonstrated that the most interesting performance indicators were the position of the touchdown point, the roll response of the aircraft and the encountered wind shear hazard defined by the F-factor. A statistical analysis will be presented for these parameters.

6.5.6.1 Results for "Annex 14" "worst case" obstacles

A comparison of the scenarios with a "regular" and "worst case" "Annex 14" obstacle located at position (240, 1000) with respect to the obstacle-free condition reveals that much more disturbance is generated on the B747 approach trajectory.

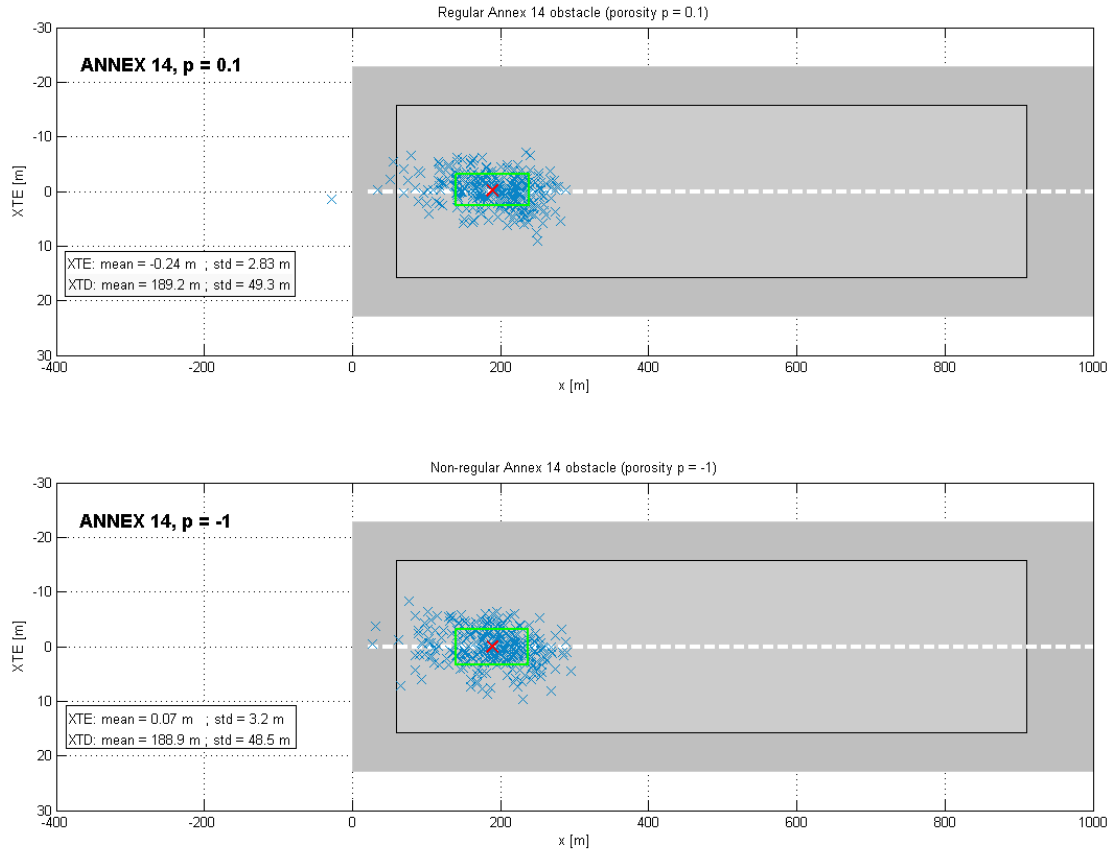

Figure 6-58: The touchdown locations (XTD, XteTD) for the Annex 14 scenarios with "regular" block-shaped building (p = 0.1) and "worst case" obstacle (p = -1)

Figure 6-58 shows the touch down dispersion of an "Annex 14" "regular" shaped obstacle and an "Annex 14" "worst case" obstacle both located at position (240,1000) for the 210/23 wind condition. The red cross indicates the mean touchdown point. The green rectangle shows the lateral and longitudinal standard deviation. A somewhat larger although not significantly larger touch down dispersion can be observed for the "worst case" obstacle.

The largest effect can be seen in the roll response of the aircraft, as shown in Figure 6-59. The plot applies to an obstacle that for both scenarios is located at position (240, 1000) in the 210/23 wind condition. The mean and standard deviations are, respectively, the red and green lines. The

vertical gray line indicates the runway threshold. The vertical black line reflects the center of the wake when crossing the approach path. The orange edges bound the zones wherein bank angles are considered hazardous. (Note: these lines are constructed assuming that the aircraft perfectly moves along the 3° ILS descend trajectory) Hazardous bank angles responses were encountered more frequently, i.e. in 18.3 % of the approaches as listed in Table 6–19. In the table the grey-scales indicate the level of significant difference as previously defined in Table 6–17.

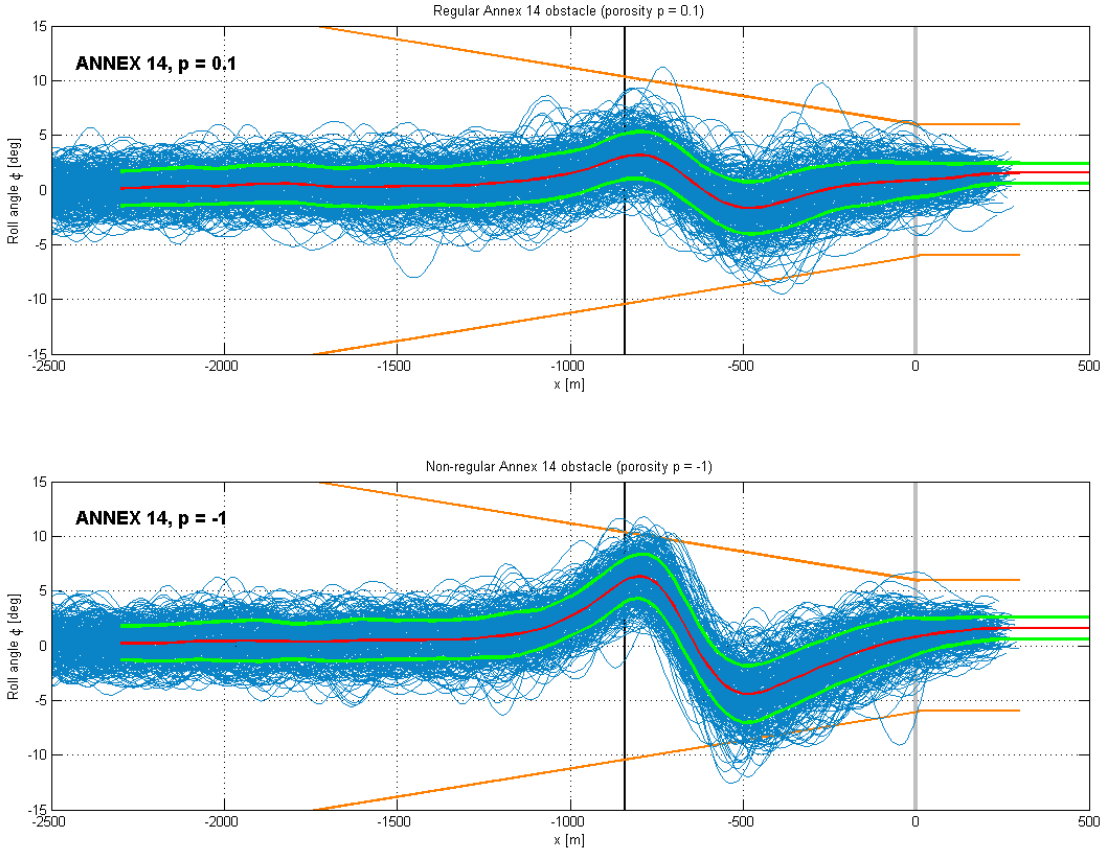

Figure 6-59: The histories of the roll angle for the Annex 14 scenarios with regularly block-shaped building (p = 0.1) and a special-shaped obstacle (p = -1)

Table 6–19: Statistical comparison between "regular" and "worst case" Annex 14 obstacles

		Regular (p = 0.1) vs. obstacle-free	**Non-regular (p = -1)** vs. obstacle-free	**Regular (p = 0.1) vs. non-regular (p = -1)**
p-values	xte_{TD}	0.200	0.014	0.211
	x_{TD}	0.750	0.702	0.951
	$\overline{F}$	0.738	0.047	0.093
Percentage runs with hazardous bank angle		2.3%	18.3%	

Consequently significantly higher maximum roll angles were reported (Figure 6-61 (b)). On the other hand, the wake of regular obstacles only demanded bank inputs comparable to the situation without the presence of the obstacle. An ANOVA analysis of the other relevant performance indicators proved that also the lateral deviation of the touchdown point “XteTD” and the maximum wind shear hazard significantly differ for the less-porous obstacle, as listed in Table 6–19. Figure 6-61 illustrates these calculations with a larger spread and higher mean of “XteTD” and the maximum F-factor. Also the mean of the F-factor over all the runs visibly increases at the moment that the wake crosses the approach path, as can be seen in the histories of Figure 6-60 . No relevant effect on the longitudinal touchdown position was observed. Again, the generated wakes do not influence the vertical descend profile much.
The analysis of this particular obstacle location suggests that the previously defined perimeter wherein “Annex” 14 height limitations were not acceptable for “regular” obstacle should be enlarged if “worst case” obstacles are built near the runway. Such structures could for example be buildings with a U- or V-shape oriented transverse on the direction of the wind (like the PDP).

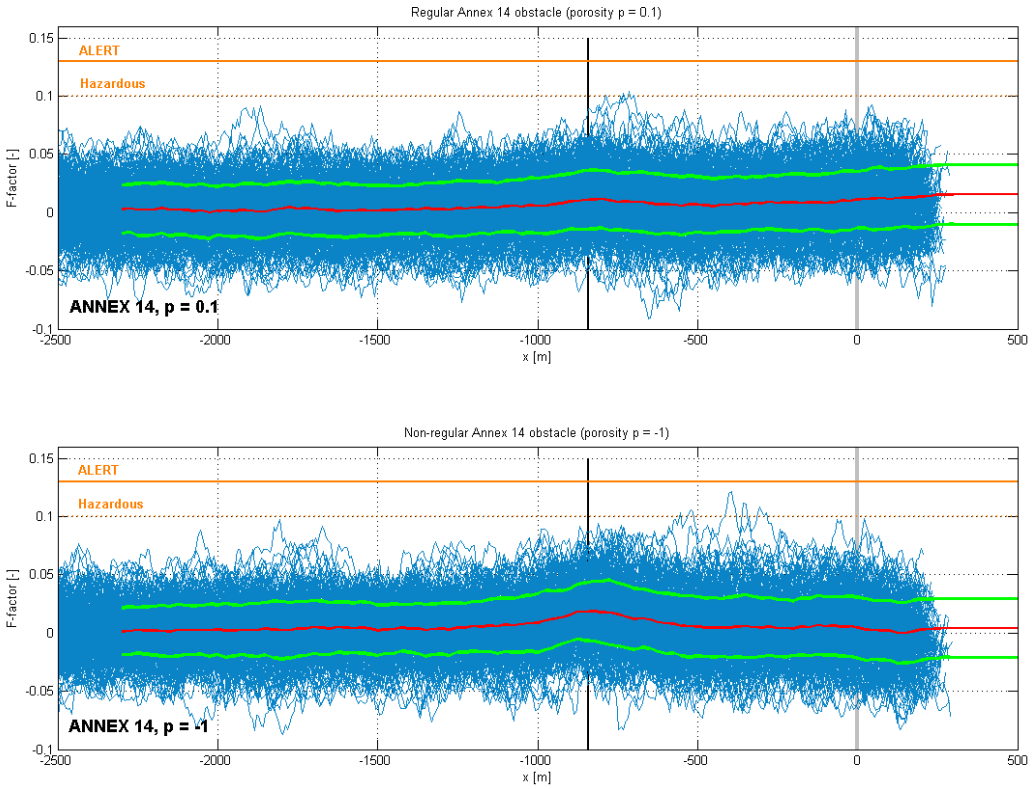

Figure 6-60: The wind shear hazard index or $\overline{F}$ -factor for the Annex 14 scenarios with regularly block-shaped building (p = 0.1) and a special-shaped obstacle (p = -1)

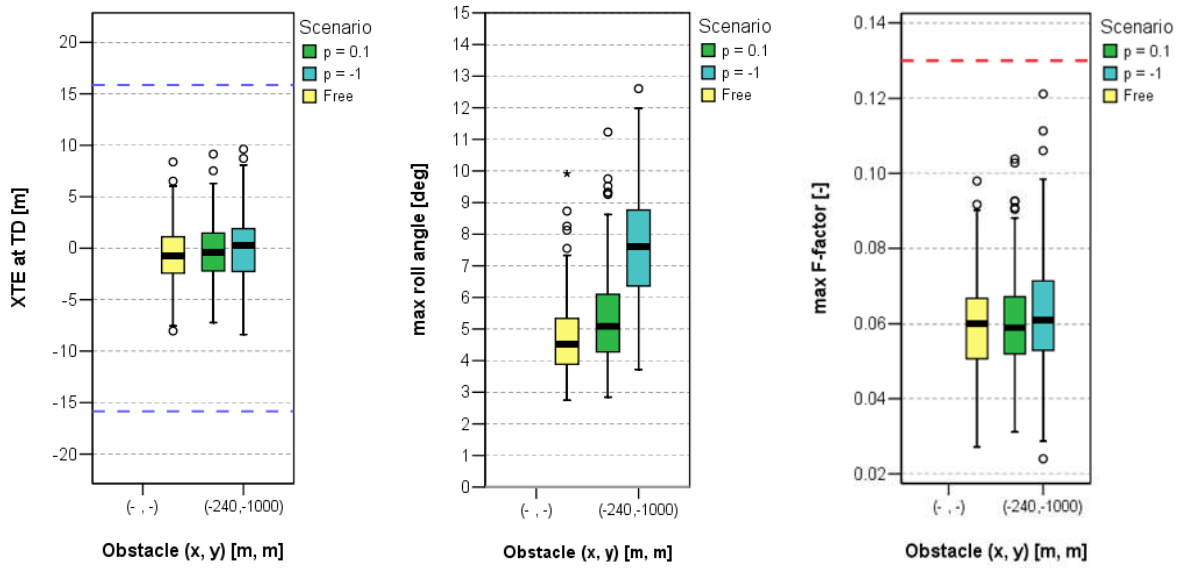

(a) xte_{TD} *(b) φ_{max}* *(c) maximum $\bar{F}$ -factor*

Figure 6-61: Lateral deviation at touchdown (XteTD), maximum roll angle and maximum wind shear hazard index encountered (F-factor), for a non-regular Annex 14 obstacle (p = -1)

A selection of four 'more-than-impenetrable' obstacles (Table 6–18), positioned around the area where "Annex 14" is undesired for a "regular" block-shaped obstacle, was made to come up with a rough indication of a second 'worst-case' boundary of acceptance of "Annex 14" applicable to "worst case" obstacles. The most important results of the statistical analysis for the additional "Annex 14" obstacles are presented in Table 6–20.

Table 6–20: Statistical comparison of a series of non-regular Annex 14 obstacles with respect to the obstacle-free scenario

		Obstacle location			
		(-80,-1300)	**(-560,-1000)**	**(-760,-700)**	**(-560,-300)**
p-values w.r.t obstacle-free	xte_{TD}	0.039	0.931	0.421	0.028
	x_{TD}	0.748	0.124	0.821	0.883
	$\bar{F}$	0.819	0.052	0.010	0.149
Percentage runs with hazardous bank angle		3.7%	2.7%	9%	9%

A distribution of the cross-track-error, maximum roll angles and maximum wind shear index is presented in Figure 6-62 to Figure 6-64.

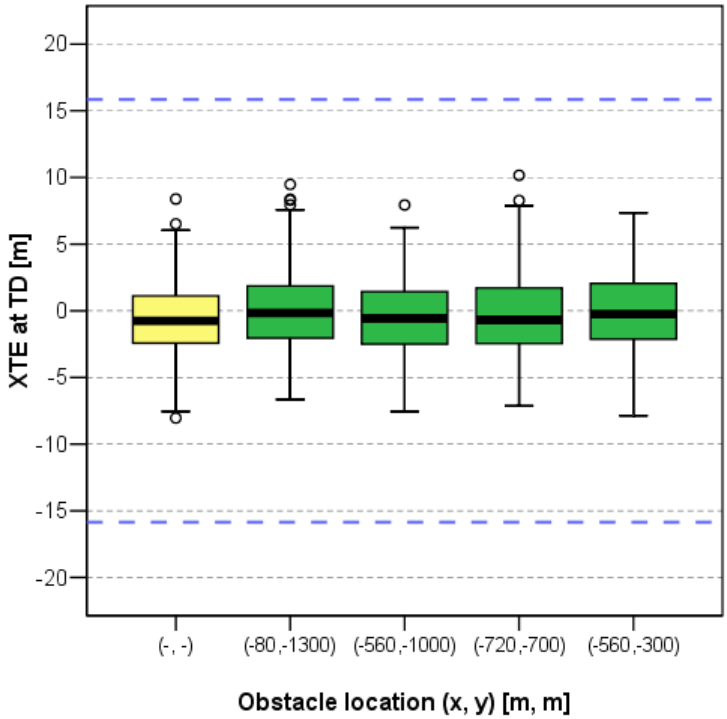

Figure 6-62: Lateral deviation at touchdown (xte_{TD}) for a range of non-regular Annex 14 obstacles (p = -1) at position (x, y) and the obstacle-free scenario in the 210/23 wind condition

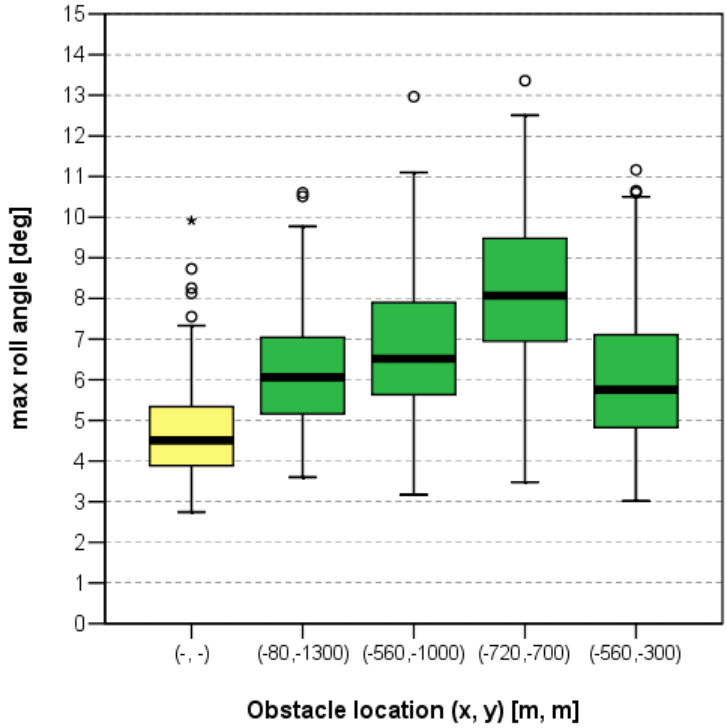

Figure 6-63: Maximum roll angle for a range of non-regular Annex 14 obstacles (p = -1) at position (x, y) and the obstacle-free scenario in the 210/23 wind condition

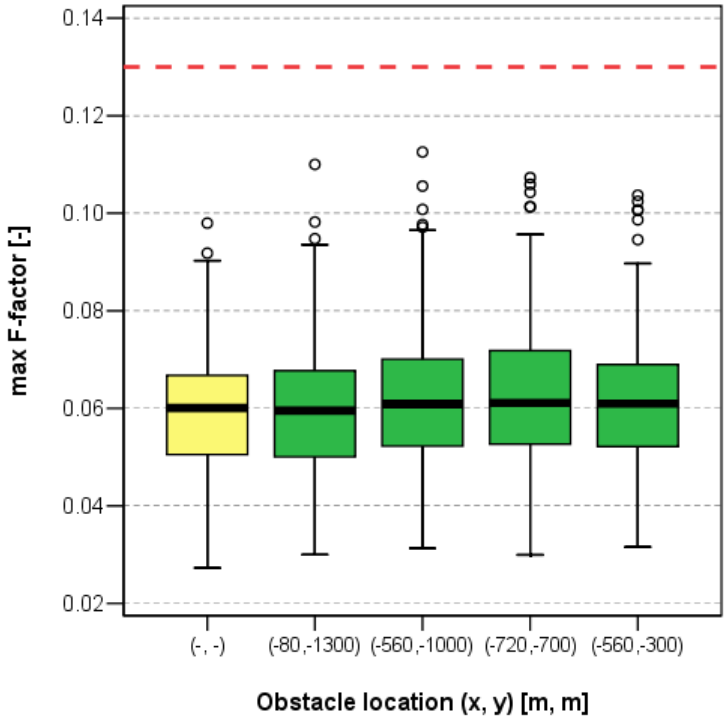

Figure 6-64: Maximum wind shear hazard index (F-factor) for a range of non-regular Annex 14 obstacles (p = -1) at position (x, y) and obstacle-free scenario in the 210/23 wind condition

It is shown that the obstacles located at (560,1000) and (760,700) had no significant influence on the mean area where the aircraft touches the runway, while a just significant effect on "XteTD" was calculated for the test cases positioned at (80,1300) and (560,300). This difference is incontestably present in Figure 6-62, but can be considered relatively small and hence negligible. Similar conclusions can be drawn for the wind shear hazard: a (just) significant, but relatively small increase of the F-factor is observed for "Annex 14" obstacles (560, 1000) and (760, 700). The most important considerable disturbance on the landing operation is found in the roll response of the B747 when the aircraft passes through the wake created by the "worst case" "Annex 14" obstacles with position (760, 700) and (560, 300). The required bank angles to compensate the deviation from the localizer appeared to be hazardous in 9% of the conducted approaches, which is not preferred. Nevertheless, it can be expected that these spots are located close to the transition where "Annex 14" approved heights no longer create an undesired wake that affects the safety of the landing . After all, the percentage of runs with hazardous bank angles tends to converge towards a level similar to the reference wake-free approach scenario (i.e. hazardous bank angles in 1% of the runs). The amount of undesired roll angles found for the other two obstacles is acceptable with respect to the baseline obstacle-free scenario. Note that although larger maximum bank angles were experienced with the (560, 1000) wake, they are less hazardous than in case of the (560,300) scenario.

6.5.6.2 Results for "worst case" obstacles according to the 1:35 rule

It was previously suggested that the "1:35" rule puts an acceptable limitation on the height of obstacles with a "regular" block-shaped form. Only obstacles close to the runway threshold provided a small, but probably acceptable disturbance on the landing. The question is now whether the "1:35" rule would also be an acceptable alternative for limiting the heights of "worst case" structures. A check on two obstacle locations from the test grid has been performed. The one closest to the runway (80, 300) and one further away at (240, 1000) where the "Annex 14" regulation appeared to be insufficient in the previous section, have been selected.

In contrast to the insignificant differences found for a regular "1:35" structure at position (80,300), a wake strengthened by the worsened shape of the obstacle does significantly alter the lateral component of the touchdown point as indicated with the zero probability value in **Error! Reference source not found.**. The grey-scales indicate the level of significant difference as previously defined in Table 6–17.

However a comparison of the spread of "XteTD" in **Error! Reference source not found.** (a) shows that this difference is relatively small and still acceptable, but there is definitely a visible disturbance. As before, no considerable effect is established in the longitudinal direction "XTD". The stronger wake also does not significantly increase the wind shear hazard, although a little more peaks are pointed out in **Error! Reference source not found.** (c). The only adverse effect that can not be tolerated is the major increase of the roll response of the aircraft. Large bank angles were applied close to the ground, comparable with to the roll angles encountered when disturbed by the unacceptable wake of "regular" "Annex 14" obstacles (Figure 6-50). This observation is also reflected in the high percentage of runs with hazardous bank angles of 20.7%. It appears that for this particularly "worst case" obstacle even the 1:35 rule is not stringent enough. The online simulator experiment should validate whether this wake requires unacceptable roll maneuvers in order to bring the aircraft safely on the ground.

Table 6-21: Statistical comparison between "regular" and "worst case" "1:35" obstacles

		Regular (p = 0.1) vs. obstacle-free	**Non-regular (p = -1)** vs. obstacle-free	**Regular (p = 0.1) vs. non-regular (p = -1)**
p-values	xte_{TD}	0.101	0	0.008
	x_{TD}	0.702	0.552	0.353
	$\bar{F}$	0.411	0.378	0.098
Percentage runs with hazardous bank angle		3%	20.7%	

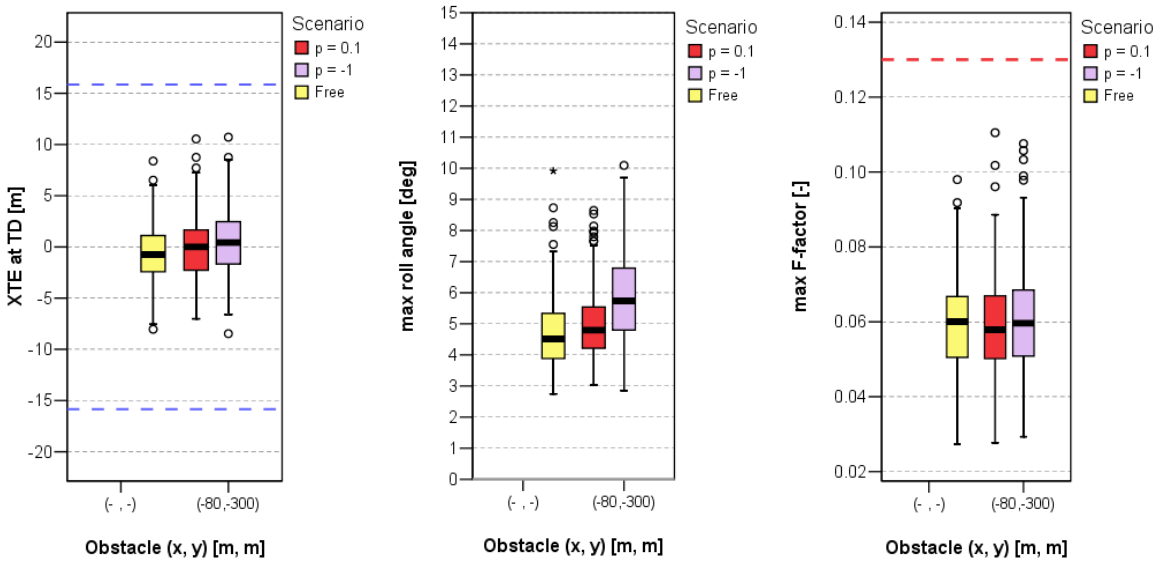

(a) xte_{TD} *(b) φ_{max}* *(c) maximum $\bar{F}$ -factor*

Figure 6-65: Lateral deviation at touchdown (XteTD), maximum roll angle (φ_{max}) and maximum F-factor, for a non-regular 1:35 obstacle (p = -1) at obstacle position (80,300)

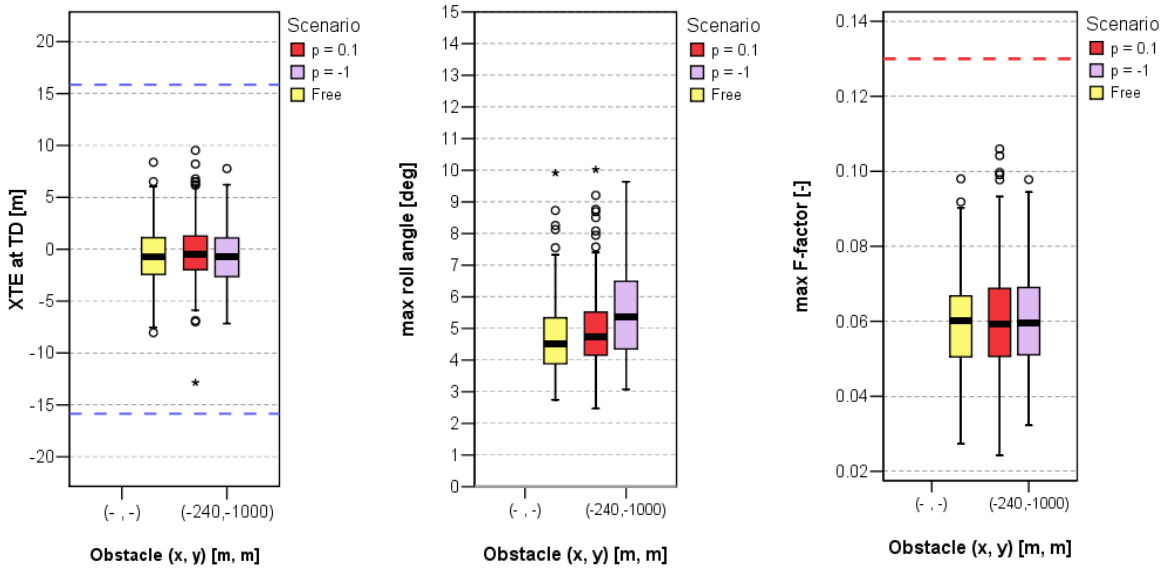

(a) xte_{TD} *(b) φ_{max}* *(c) maximum $\bar{F}$ -factor*

Figure 6-66: Lateral deviation at touchdown (XteTD), maximum roll angle (φ_{max}) and maximum F-factor, for a non-regular 1:35 obstacle (p = -1) at obstacle position (240,1000)

Unlike the above observation, the second “worst case” obstacle analyzed here demonstrates that the “1:35” rule offers an excellent limitation on the height of obstacles with “worst case” characteristics when they are positioned a little further from the threshold. The ANOVA analysis calculates no significant differences in touchdown characteristics or in the wind shear

risk, as listed in Table 6–22. Again the grey-scales indicate the level of significant difference as previously defined in Table 6–17.
On the other hand, **Error! Reference source not found.** indicates that the maximum roll angle increases considerably up to the same level as for the obstacle located at position (80,300) (compare with **Error! Reference source not found.**). However, in this case these bank angles were reported at higher altitudes and appear to be non-hazardous during most approaches: only in 2.3% of the runs which is just a little more than with a "regular" obstacle (p = 0.1).

Finally, it can be remarked that the test engine facility (PDP) was located near position (80,300) and was originally 16m high. This height exceeds the 1:35 rule with approximately 7m, while it has been suggested above that the "1:35" rule would already be unacceptable when considering the amount of hazardous bank angles experienced. Hence, it can be concluded that the original PDP structure was certainly designed too high for that particular location or should have been located further away from the runway threshold. On the other hand, the PDP is currently 8m high which is just a little bit less than allowed by the "1:35" rule. Since no complaints about the remaining wake disturbance during the approach on runway 27 at Schiphol Airport have been reported by pilots, the above interpretation that the "1:35" rule would still allow too high obstacles with worst case characteristics (like the PDP) around the location of (80,300), has to be employed with care. Again, pilot opinions from the online simulator experiment should validate where the boundary of acceptable wake disturbances should be drawn.

Table 6–22: Statistical comparison between "regular" and "worst case" 1:35 obstacles at position (240, 1000) with respect to the obstacle-free scenario

		Regular (p = 0.1) vs. obstacle-free	**Non-regular (p = -1)** vs. obstacle-free	**Regular (p = 0.1) vs. non-regular (p = -1)**
p-values	xte_{TD}	0.126	0.358	0.015
	x_{TD}	0.328	0.329	0.906
	$\bar{F}$	0.612	0.687	0.936
Percentage runs with hazardous bank angle		0.7%	2.3%	

6.5.7 Wind criteria derived from B747 Monte Carlo Simulations

This section looks at the wind conditions that existed during the measurements. Together with the conclusions of the Monte Carlo simulations a wind criterion can be derived.

Figure 6-67 shows the maximum cross wind deficit vs. the height along the approach path where this maximum occurs. Every building from the B747 test is shown in the plot. The meaning of the symbols is:

- Square shaped for worst case buildings with Annex 14 height
- Circular for worst-case buildings with height according the 1:35 rule
- Cross for regular buildings with Annex 14 height
- Triangle for the PDP building with the original and current height

The color of the symbol shows the conclusion from the Monte Carlo simulations:

- Green is an accepted building
- Blue is a border case building
- Red is a disallowed building

The wind scenario used is 23kts from direction 210 with turbulence intensity of 0.178 at 10m.

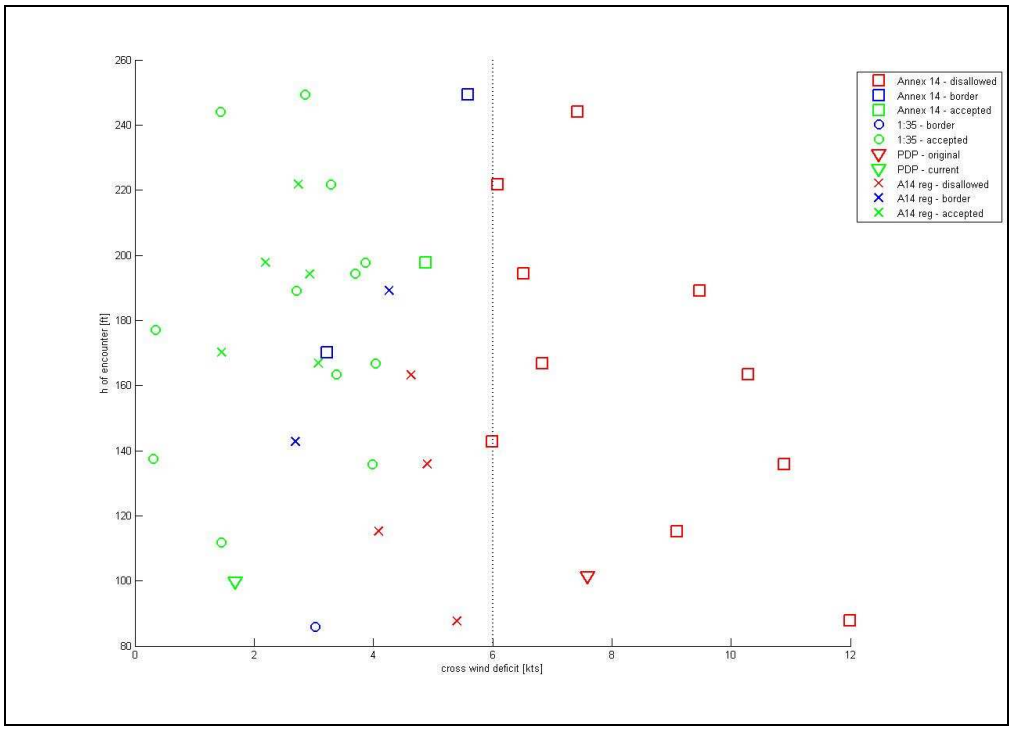

Figure 6-67: Maximum cross wind deficit vs. height

From Figure 6-67 it can be observed that the maximum allowable cross wind deficit for a B747 is 6 knots. Also from the figure it can be seen that this maximum would not disapprove all disallowed buildings.

7 Piloted B747 simulations

7.1 Introduction

In this section the piloted simulator experiment is described which is part of the validation of the offline results.
The Boeing B747 has been selected for the tests as a good representative of a heavy weight aircraft. A heavy weight aircraft is chosen for the piloted experiment because a former study showed that this type of aircraft was more critical in the final approach stage than e.g. the Fokker 100 ([9]. Approaches into a decreasing wind field with gust/turbulence have been executed.

7.2 NLR simulator facility GRACE

The experiment has been carried out on NLR's moving-base research flight simulator GRACE (Generic Research Aircraft Cockpit Environment).
A high level of realism is essential for a flight simulation evaluation with valid results. NLR has achieved a new level of realism in research flight simulation with its newest flight simulator GRACE . GRACE features a unique system of adaptable hardware and software. It employs large displays and masks, modular, exchangeable modules and in-house developed software. GRACE can be configured to simulate Airbus, Boeing and Fokker like aircraft.
A picture of GRACE from the outside is shown in Figure 7-1. The cockpit provides accommodation for two pilots and a number of observers. A picture from the cockpit is shown in Figure 7-2. Both captain and first officer have electronic Primary Flight Displays (PFD) and Navigation Displays (ND) at their disposal.
The primary flight controls are the control wheels and columns, four throttle levers and rudder pedals. Furthermore controls are available to operate the flaps, landing gear, speed brakes, electrical pitch trim switches on the control wheels and toe brakes.
The simulator is provided with an electric motion system controlling six degrees of freedom.

The operator controlling the simulation has available a written start-up and closure procedure, a schedule of the total experimental set-up, the outline planning and timetable as well as ATC communication procedures. Furthermore he is able to perform the role of air traffic controller in the experiment.

For the wind disturbance experiment a generic block shaped building was created by means of in-house software tools. This generic obstacle then was implemented in the visual database. Depending on the test run the dimensions of the obstacle could be adapted. Also the position could be varied per test run. It has enhanced the fidelity of the simulation and it provided the pilots with a visual cue of the dimensions and position of the obstacle.

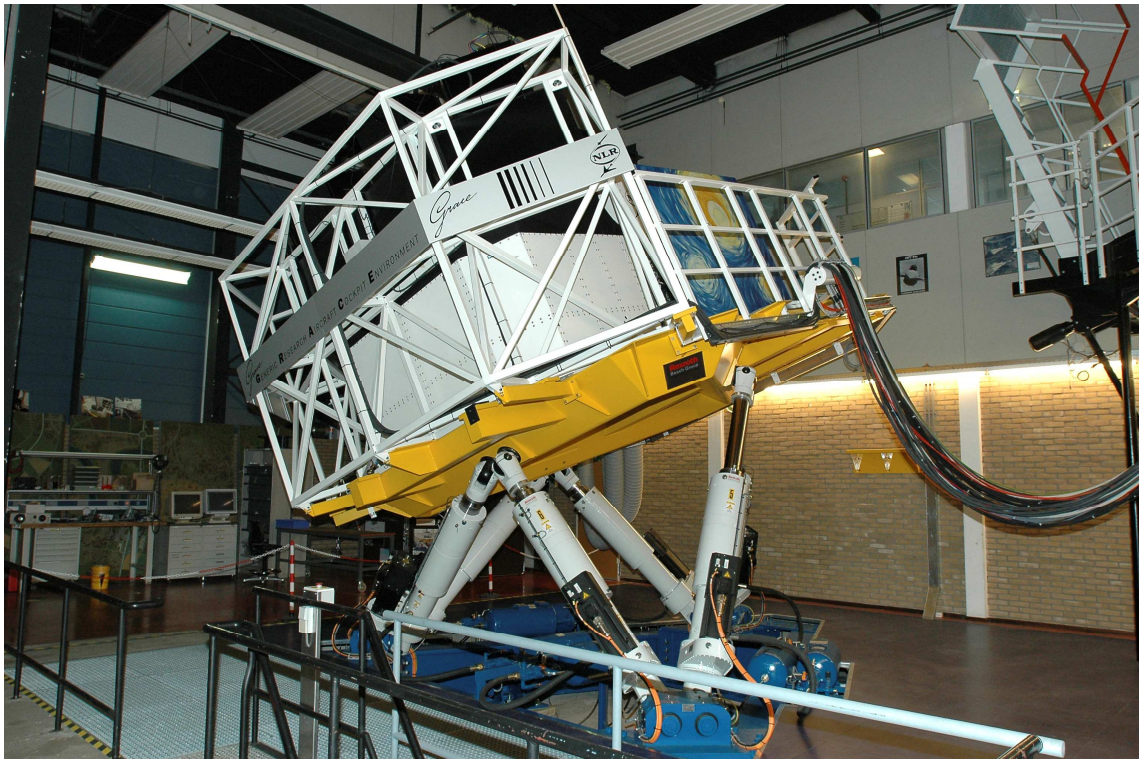

Figure 7-1: NLR's research flight simulator GRACE from the outside

Figure 7-2: Cockpit view of GRACE

7.3 Mathematical models

7.3.1 Related to B747 aircraft

For the experiment the simulator has been programmed with the aerodynamic characteristics of the Boeing 747-200 and the characteristics of the General Electric CF6-50E/-45A jet engine. PFD, NAV and engine digital cockpit displays however corresponded to the latest version of the B747 viz. the 400 series.

The forces and moments as result of the changing wind conditions act on the centre of gravity of the aircraft. In the mathematical model also the span wise distributed turbulence acts on the aircraft's CG through angle of attack and speed dependent contributions. The update rate of the aircraft equations of motions and control system is 50 Hz.

7.3.2 Related to the experiment

The wind climate model employed in the offline simulations was implemented also in the mathematical models of GRACE.

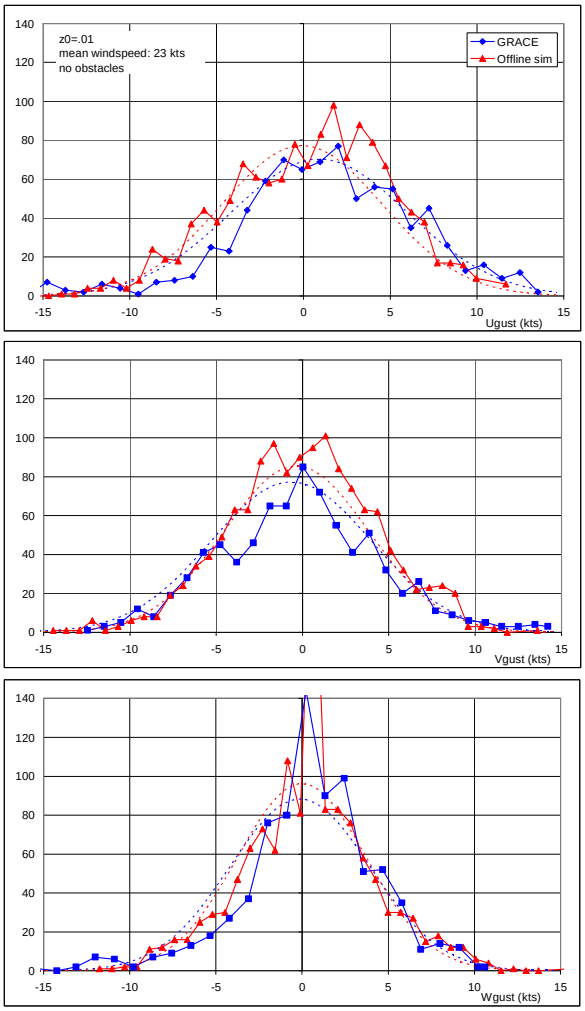

Figure 7-3: Comparison between turbulence in GRACE and offline simulation

Figure 7-3 shows histograms obtained from data corresponding to the turbulence model as imbedded in the F100 offline simulation and as programmed in the computer model of GRACE. Histograms are presented for the longitudinal turbulence (Ugust), lateral turbulence (Vgust) and vertical turbulence (Wgust). For comparison the best fitted normal distribution for each data set is given as well. A good correlation between the two data sets can be observed.
To compensate for the lack of periphery and to assist the pilot to control the bank angle during landing and flare a bank angle warning as function of height above the runway has been incorporated. If a critical bank angle which depends on the height above the ground is exceeded an aural alert is presented to the pilot. To take into account the amount of roll rate that is evoked also a phase advance feature proportional to roll rate is incorporated. Above 100 ft the alert is inhibited. Because of the wing-mounted engines the bank angle aural limit for the B747 at touch down is 7 degrees.

7.4 Test procedure

Before the actual start of the experiment a checkout of the complete test set-up has been performed with a pilot that did not participate in the experiment. The purpose of the checkout is to investigate whether the simulator models in combination with the wind climate models is implemented correctly in the simulator computer and to test the feasibility of the proposed procedures and evaluation objectives. On March 8 2006 the checkout of the B747 experiment set up has been performed successfully.

In the experiment at first the project pilots executed a number of approaches and landings with increasing difficulty. These test runs allowed the pilot to familiarize himself with the simulator cockpit, experiment set-up and procedures.
Every approach in the experiment to runway 27 started with the aircraft positioned at an initial altitude of 1000ft, on the ILS path, under VMC conditions, with landing flaps selected and gear down. Autopilot and auto throttle were engaged. After stabilization of the aircraft the autopilot (A/P) was disconnected. Then until touch down or at the initiation of a go-around the aircraft was flown manually with the recommended crosswind technique for the aircraft.
The wind correction on the final approach airspeed (FAS) in the experiment is based on the Boeing 747 Flight crew training manual:

- Use an approach speed wind correction of ½ the steady headwind component plus the entire gust increment above the steady wind, based on tower reported winds. The maximum wind correction should not exceed 20kts.

The auto throttle (A/T) initially was engaged. However, if deemed necessary it was disconnected and manually operated by the pilot. This because of the under-wing engine position of the B747 the auto throttle has difficulty to control the aircraft speed accurately in high turbulent conditions.

The approach and landings in the experiment were made under ILS flight director guidance. In addition PAPI was available to assist the pilot.

Runway length was no parameter of concern in this experiment. Simulated runway width is 150ft.

The pilot was asked to continuously judge the safety situation by controlling and monitoring height, speed and glide slope and localizer deviations. If a go-around decision was taken only the initiation of a go-around procedure was required. As soon as the aircraft was stabilized the simulation was stopped.

Ground spoilers were armed at the start of the test run and deployed automatically upon touch down of the main gear. Because of the loss of fidelity in the modeling of the ground tire reactions under high crosswind conditions the simulation automatically was ended at main gear touch down plus 3 seconds.

7.5 Validation matrix

Five pilots took part in the evaluation and all are experienced B747 captains from KLM. Obviously also less experienced crews should be able to operate within the severe gusting conditions without requiring exceptional skills. However for this experiment it was considered more worthwhile to use the expertise of highly experienced pilots.

Table 7–1: Online test matrix for 1:35 plane

Session 2 Landing **rwy 27** **With obstacles 1:35** **worst case obstacles**

nr	mean wind speed (kts) excl gust	wnddir. (dg)	X-wind (kts)	Hd-wind (kts)	Turb (on/off)	Appr. spd flps 30 (kts)	LND/TO	Hobst (m)	Z0 (m)	Width (m)	XRW/YRW-position (m)	Remarks
1	23	210 (L)	20	12	on	156	LND	9	0.01	250	-80/-300	210/23 gusting 32
2	23	330 (R)	20	12	on	156	LND	20	0.01	250	-400/700	330/23 gusting 32
3	23	210 (L)	20	12	on	147	LND	20	0.001	250	-400/-700	210/23
4	23	330 (R)	20	12	on	156	LND	37	0.01	250	-720/1300	330/23 gusting 32
5	23	330 (R)	20	12	on	147	LND	43	0.001	250	-720/1500	330/23
6	23	210 (L)	20	12	on	156	LND	29	0.01	250	-240/-1000	210/23 gusting 32
7	28	225 (L)	20	20	on	161	LND	9	0.01	250	-80/-300	225/29 gusting 41
8	28	315 (R)	20	20	on	161	LND	20	0.01	250	-400/700	315/29 gusting 41
9	28	225 (L)	20	20	on	151	LND	20	0.001	250	-400/-700	225/29
10	28	315 (R)	20	20	on	161	LND	37	0.01	250	-720/1300	315/29 gusting 41
11	28	315 (R)	20	20	on	151	LND	43	0.001	250	-720/1500	315/29
12	28	225 (L)	20	20	on	161	LND	29	0.01	250	-240/-1000	225/29 gusting 41

Table 7–2: Online test matrix Annex 14

Session 3 Landing **rwy 27** **With obstacles annex 14** **worst case obstacles**

nr	mean wind speed (kts) excl gust	wnddir. (dg)	X-wind (kts)	Hd-wind (kts)	Turb (on/off)	Appr. spd flps 30 (kts)	LND/TO	Hobst (m)	Z0 (m)	Width (m)	XRW/YRW-position (m)	Remarks
1	23	210 (L)	20	12	on	156	LND	21	0.01	250	-80/-300	210/23 gusting 32
2	23	330 (R)	20	12	on	156	LND	45	0.01	250	-400/700	330/23 gusting 32
3	23	210 (L)	20	12	on	147	LND	45	0.001	250	-400/-700	210/23
4	23	330 (R)	20	12	on	156	LND	45	0.01	250	-240/500	330/23 gusting 32
5	23	330 (R)	20	12	on	156	LND	36	0.01	250	-80/400	330/23 gusting 32
6	23	210 (L)	20	12	on	147	LND	45	0.001	250	-240/-500	210/23
7	28	225 (L)	20	20	on	161	LND	21	0.01	250	-80/-300	225/29 gusting 41
8	28	315 (R)	20	20	on	161	LND	45	0.01	250	-400/700	315/29 gusting 41
9	28	225 (L)	20	20	on	151	LND	45	0.001	250	-400/-700	225/29
10	28	315 (R)	20	20	on	161	LND	45	0.01	250	-240/500	315/29 gusting 41
11	28	315 (R)	20	20	on	161	LND	36	0.01	250	-80/400	315/29 gusting 41
12	28	225 (L)	20	20	on	151	LND	45	0.001	250	-240/-500	225/29

Furthermore it was explicitly not the purpose of the simulator experiment to obtain a statistically significant data set. Within the scope of the project it should lead to a sufficient indication regarding the fly ability of approaches in the presence of gust/turbulence with and without the presence of “stand alone” obstacles.

The validation matrix relevant for the experiment is depicted in Table 7–1and Table 7–2 and was flown by each project pilot.
In each approach a randomly different sample of the gust/turbulence profile was presented to the pilot leading to a variety of possible gust/turbulence conditions within the wind model boundaries presented in section 3 and 4.

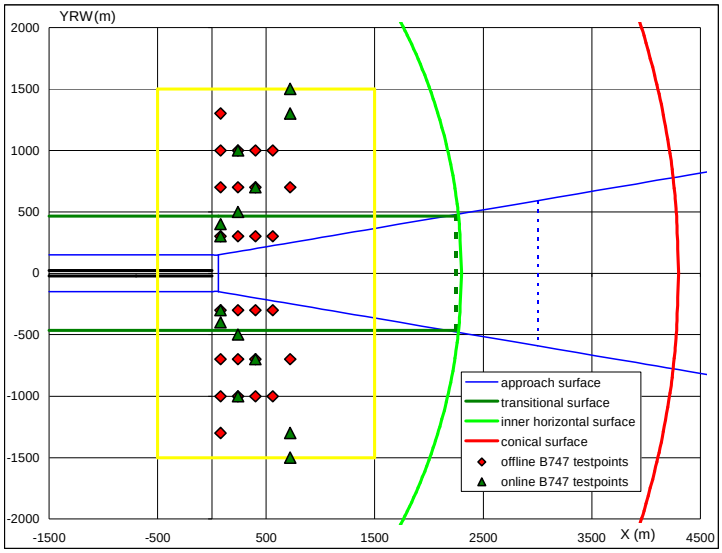

Figure 7-4: Test points of online validation matrix

To prevent habituation, approaches were made alternatively with both left and right crosswind. The position of the stand alone obstacle test points of the validation matrix are shown in Figure 7-4 projected on the offline B747 test points.

7.6 Experiment

Approximately two weeks before the experiment pilot briefing guides were sent to the project pilots ([38]. The briefing guide contained all the relevant aspects of the experiment.

The experiment on NLR's GRACE simulator consisted of five days in total. The simulator tests took place on March 13th, 16th, 20th, 21st and 22nd of 2006.

7.7 Results

7.7.1 Data examples

Just as for the F100 offline simulations presented in Figure 6-22 and Figure 6-23, Figure 7-5 and Figure 7-6 yield time histories from two B-747 piloted approaches to runway 27. The same conditions as for the offline simulation are valid i.e. a reference wind speed of 23kts in combination with a surface roughness of .01m. Also the same stand alone obstacle dimensions and positions have been used.

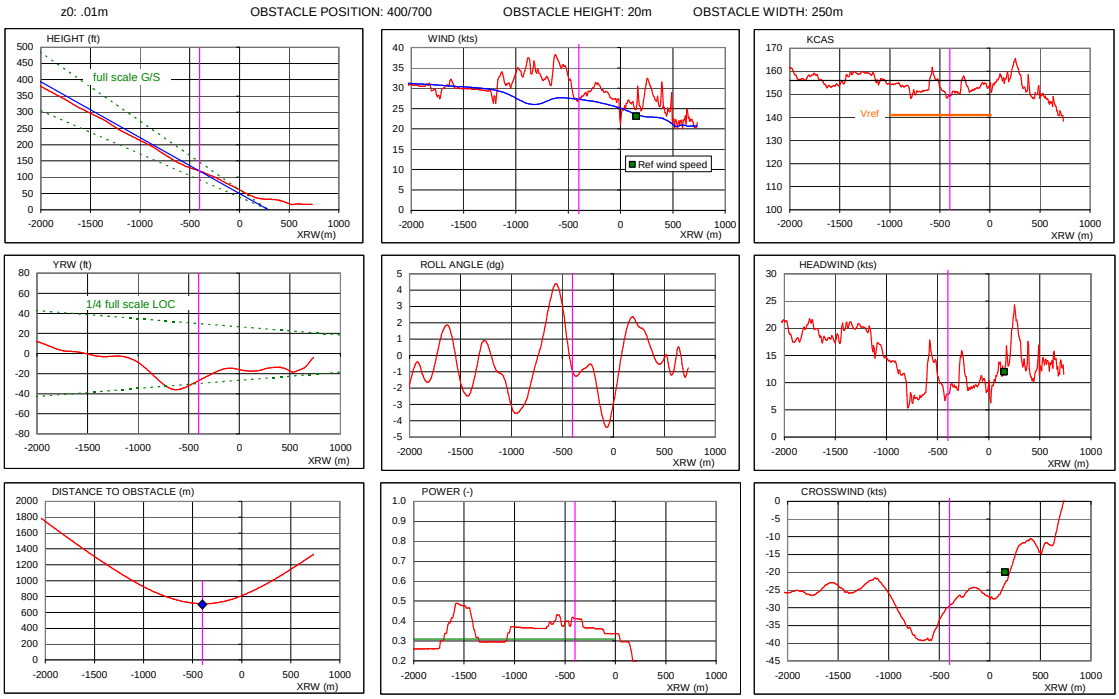

Figure 7-5: Time histories of parameters recorded during piloted B747 simulation wind speed: 23kts z0:.01m (medium turbulence)

Figure 7-5 shows the results for an approach and landing with a “stand alone” obstacle positioned at 400m in front of the runway threshold and an offset of 700m from the runway centreline (in short 400/700). Obstacle height is 20m (according to “1:35” plane) and obstacle width is 250m. Figure 7-6 shows the results of an approach with an obstacle position of 240m in front of the threshold and a lateral offset of 500m (in short 240/500). Obstacle height in this case is 45m according to the obstacle clearance plane and width is identical; 250m. In the simulator the latter approach resulted in a go-around.

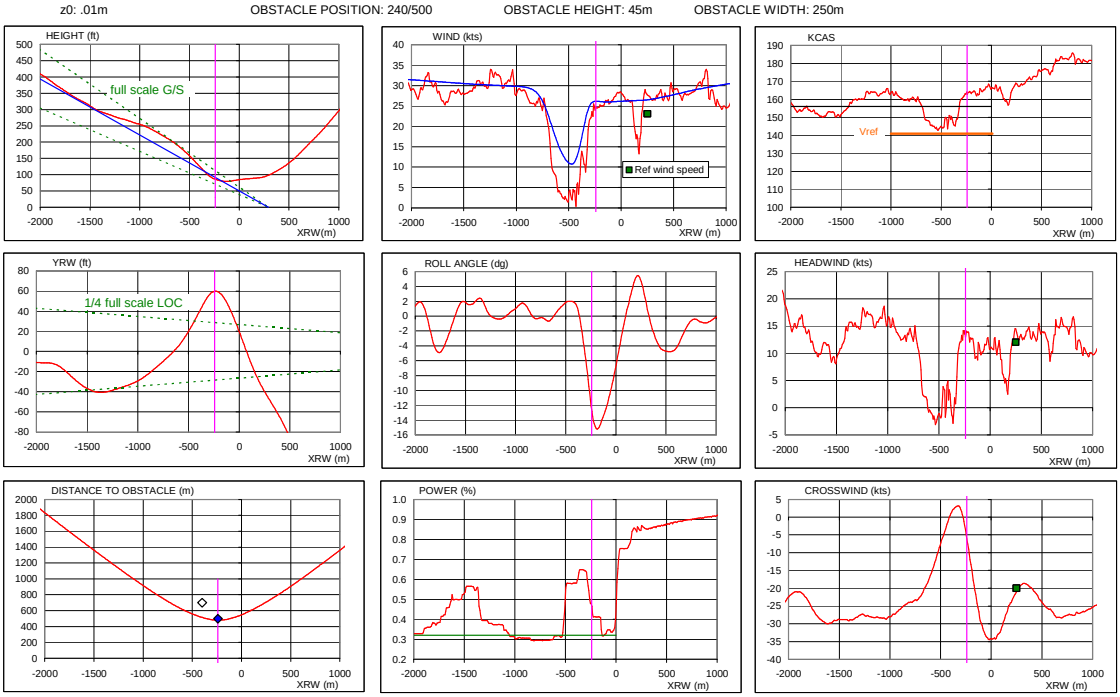

Figure 7-6: Time histories of parameters recorded during piloted B747 simulation wind speed: 23kts z0:.01m (medium turbulence)

Between the parameters corresponding to the F100 offline auto land approach (Figure 6-22 and Figure 6-23) and the online piloted simulation (Figure 7-5 and Figure 7-6) an interesting similarity can be observed. Wind, wake and airspeed traces show similar trends. Also the increase in power due to the drop off of airspeed as result of the obstacle shading and the ascent as result of this above the glide path can be noted.
However a major difference can be found in the large roll angle deflection applied by the pilot when the aircraft traverses the obstacle wake. Corrections for the developing lateral offset as result of the suddenly decreasing/increasing crosswind and headwind component are destabilizing the flight path in such a way that a go-around is initiated.

7.7.2 Objective results

Figure 7-7 presents results of snapshots of the sink rate, roll angle and main gear position at the moment of touch down of all piloted approaches presented in the validation matrix (Table 7–1 and Table 7–2).

The left part of the figure shows data applicable for obstacles with height according to the "1:35" plane, whereas the right hand plots show data corresponding to obstacles meeting "Annex 14" height. It appears from these snap shots that also for the piloted approaches the dispersion found in the landing performance along the runway as well in lateral direction is much larger for the "Annex 14" cases than for the "1:35" cases. Three touchdowns that fall outside the defined touch down zone for the Annex 14 data can be noted. However roll angles remain at or within the 6 degree boundaries for both cases.

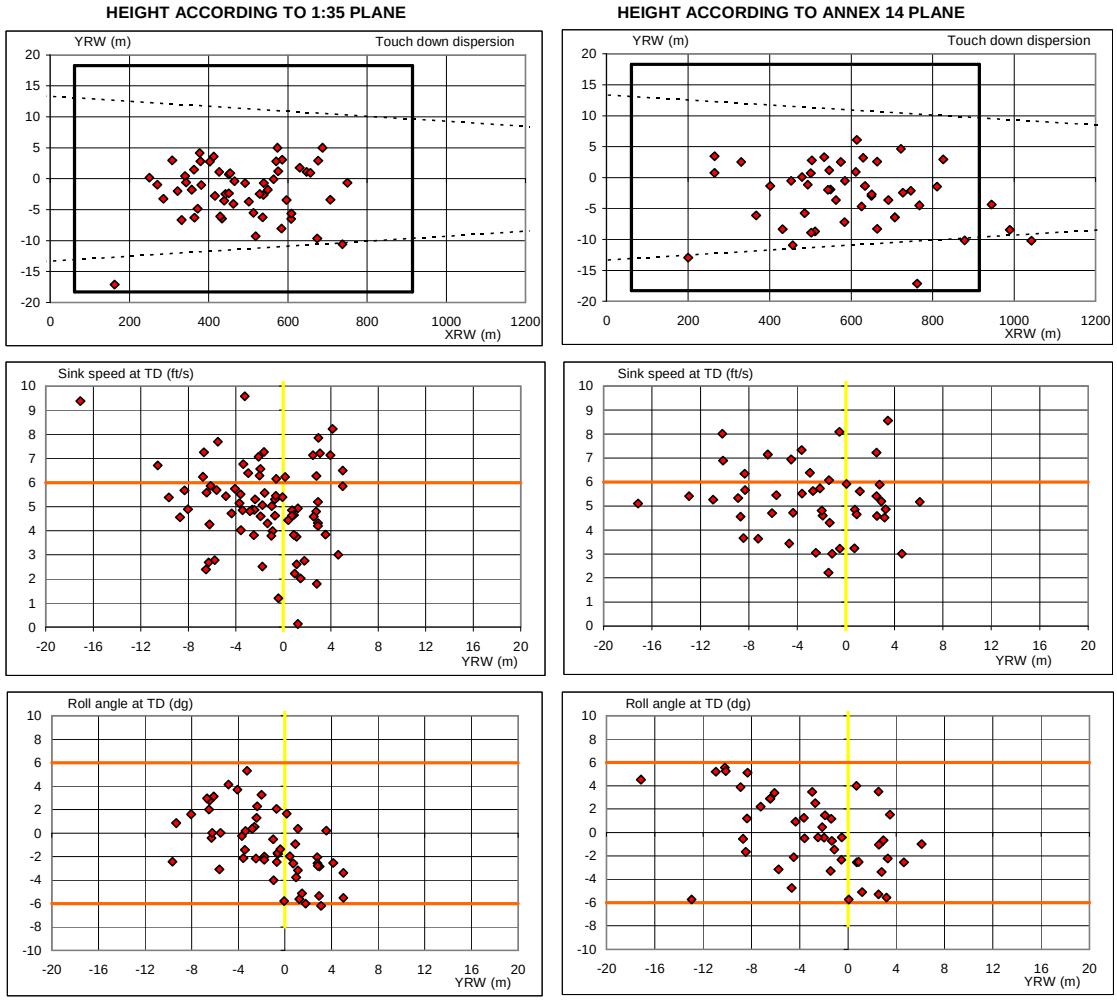

Figure 7-7: Piloted B747 touch down data

Finally Table 7–3 and Table 7–4 give a survey of the number of landings made during the experiment days corresponding to the validation matrix given in Table 7–1 and Table 7–2. In

addition the number of initiated go-around's and the number of landings which were considered unsafe by the pilots are presented. It must be mentioned that the data corresponding to **set1** up to **set5** are not given in chronological sequence.

The data presented in Table 7–3 apply to a reference wind speed of 23kts in combination with a surface roughness of .01m. According to Figure 6-9 this means that during the approaches RMS turbulence intensity values of 3.3-3.8 knots are encountered below 300ft. Expressed in JAR-AWO definitions the aircraft has experienced "medium turbulence" during these runs.

The data presented in Table 7–4 apply to a reference wind speed of 28kts in combination with a surface roughness of .01m. According to Figure 6-9 this means that during these approaches RMS turbulence intensity values of 4.0-4.7 knots are encountered below 300ft. Expressed in JAR-AWO definitions the aircraft has experienced "heavy turbulence" during these runs.

Table 7–3: Percentage go-around/unsafe landing during piloted B747 simulations wind speed: 23kts z0:.01m (medium turbulence)

	height according to 1:35 plane				height according to annex 14 plane			
	nr of landings	nr of GA	unsafe landings	total GA+ unsafe landings	nr of landings	nr of GA	unsafe landings	total GA+ unsafe landings
set1	6	0	0	0	6	3	0	3
set2	6	0	0	0	7	2	1	3
set3	5	1	1	2	4	1	0	1
set4	6	1	0	1	7	2	2	4
set5	7	0	0	0	6	1	0	1
Total	30	2	1	3	30	9	3	12
				10.0%				**40.0%**

Table 7–4: Percentage go-around/unsafe landing during piloted B747 simulations wind speed: 28kts z0:.01m (heavy turbulence)

	height according to 1:35 plane				height according to annex 14 plane			
	nr of landings	nr of GA	unsafe landings	total GA+ unsafe landings	nr of landings	nr of GA	unsafe landings	total GA+ unsafe landings
set1	6	1	0	1	6	1	0	1
set2	6	0	0	0	6	1	5	6
set3	4	1	0	1	6	1	1	2
set4	8	3	0	3	7	3	0	3
set5	9	1	1	2	6	1	1	2
Total	33	6	1	7	31	7	7	14
				21.2%				**45.2%**

From the two tables the following observations can be made for the approaches flown with "stand alone" obstacles limited in height by the 1:35 plane:

- For the approaches flown in "medium turbulence" conditions with RMS turbulence intensities of 3.3-3.8 knots still 3 out of the 30 approaches resulted in a go-around or unsafe landing.

- For the approaches flown in “heavy turbulence” conditions with RMS turbulence intensities of 4.0-4.8 knots the number of go-arounds/unsafe landings increased to 7 out of 33 approaches.

These data show the impact of the overall surface roughness on the aircraft handling and landing performance. Apparently a surface roughness that leads to turbulence intensities with a standard deviation of more than 4 knots is capable of producing wind climate samples which result in a go-around/unsafe landing. From Table 7–4 it can be observed that the increase of the turbulence level to “heavy” doubles the number of go-arounds/unsafe landings.
As can be observed from the tables the approaches made in presence of obstacles meeting “Annex 14” heights experience a much higher number of go-around’s/unsafe landings. This applies in particular to the approaches performed in medium turbulence conditions. The number is quadrupled for approaches flown in conjunction with “Annex 14” obstacles with respect to approaches flown with obstacles with heights according to the “1:35 plane”. The approaches flown in heavy turbulence and annex 14 height limited obstacles lead to a redoubling of the amount of go-arounds/unsafe landings. The explanation for this is that in this wind climate the effects of the “stand alone” obstacle become partly overshadowed by the turbulent nature of the atmosphere.

7.7.3 Subjective results

In this section subjective data obtained from pilot comments and pilot ratings during the B747 experiments on GRACE are presented.
In Table 7–5 a survey is given of the mean values and corresponding standard deviations of “*Cooper/Harper ratings*” and “*workload assessment*”. Also presented in the table is the “*effort to control*” a number of significant parameters such as *airspeed*, *roll angle* and *pitch angle* and related parameters *glide slope tracking / vertical speed* and *localiser tracking / heading*. An overview of the type of questionnaires involved is presented in Appendix C.

Table 7–5: Summary of pilot ratings

	approach				landing			
	1:35		annex14		1:35		annex14	
	mean	stdev	mean	stdev	mean	stdev	mean	stdev
C/H rating	4.4	0.5	4.3	0.4	5.5	0.9	6.8	1.2
Workload	5.8	0.4	5.5	0.3	6.7	0.5	7.4	0.7
Effort to control:								
speed	4.2	0.7	4.2	0.5	5.1	0.6	6.3	0.7
bank	3.3	0.4	3.5	0.3	3.9	0.5	4.9	1.2
pitch	4.1	0.7	4.1	0.4	5.3	0.9	6.3	0.7
g/s	4.1	0.8	4.0	0.4	5.3	1.0	6.3	0.8
loc	3.3	0.4	3.3	0.3	4.0	0.8	4.8	1.0

As has been postulated in section 5.3 two phases in the approach have been distinguished viz. the approach to approximately 200ft height and the landing from 200ft until main gear touch down. In the table this distinction is made also. The left part of the table represents the approach phase. The right part yields the data for the landing phase. Furthermore for both phases the ratings are presented for the case in which an obstacle was present with a height according to the “Annex 14” plane and an obstacle with a height in accordance with the “1:35” plane limit. Not surprisingly the table shows that in the approach phase the Cooper/Harper ratings (both mean value and standard deviation) are in the same order for the “1:35”case and “annex 14” case. For the landing phase it can be observed that for all considered parameters the mean value of the “Annex 14” ratings is substantially higher than the “1:35” ratings. The standard deviation however shows similar magnitudes for the two cases.

The numerical values of workload and control effort appearing in Table 7–5 are visualised on their respective scales in Figure 7-8 and Figure 7-9. Shown are the mean values and the one sigma range encountered. The **blue** lines represent the landing phase and the **red** lines apply for the approach phase. The **solid** lines in the figure represent the results applying to obstacles with height according to “Annex 14” planes. The **dotted** lines represent the data corresponding to obstacles with height according to the “1:35” plane. It can be observed from Figure 7-8 that for the “approach phase” both the “Annex 14” and “1:35” data are assessed as “*demanding of pilot attention, skill or effort”*. Standard deviation for the two cases is similar and relatively small.

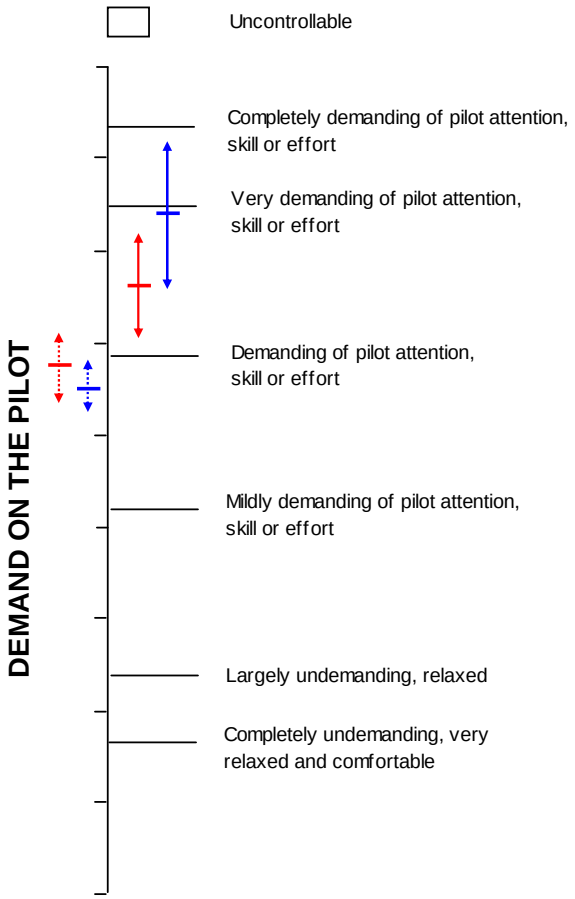

Figure 7-8: Pilot workload

Not surprisingly standard deviations in the landing phase are larger. For the "1:35" data a range between "*demanding of pilot attention, skill or effort*" and "*very demanding of pilot attention, skill or effort*" can be observed. The landing data for the "Annex 14" case has a mean value at a level corresponding to "*very demanding of pilot attention, skill or effort*". However situations are possible which may reach a level up to "*completely demanding of pilot attention, skill or effort*".

The data plotted in the pilot control effort scales (Figure 7-9) show the same trend as for the workload scales. It can be observed that the longitudinal control effort of airspeed, pitch angle and glide slope/vertical speed is assessed more difficult than the lateral/directional parameters; bank angle and localiser/heading.

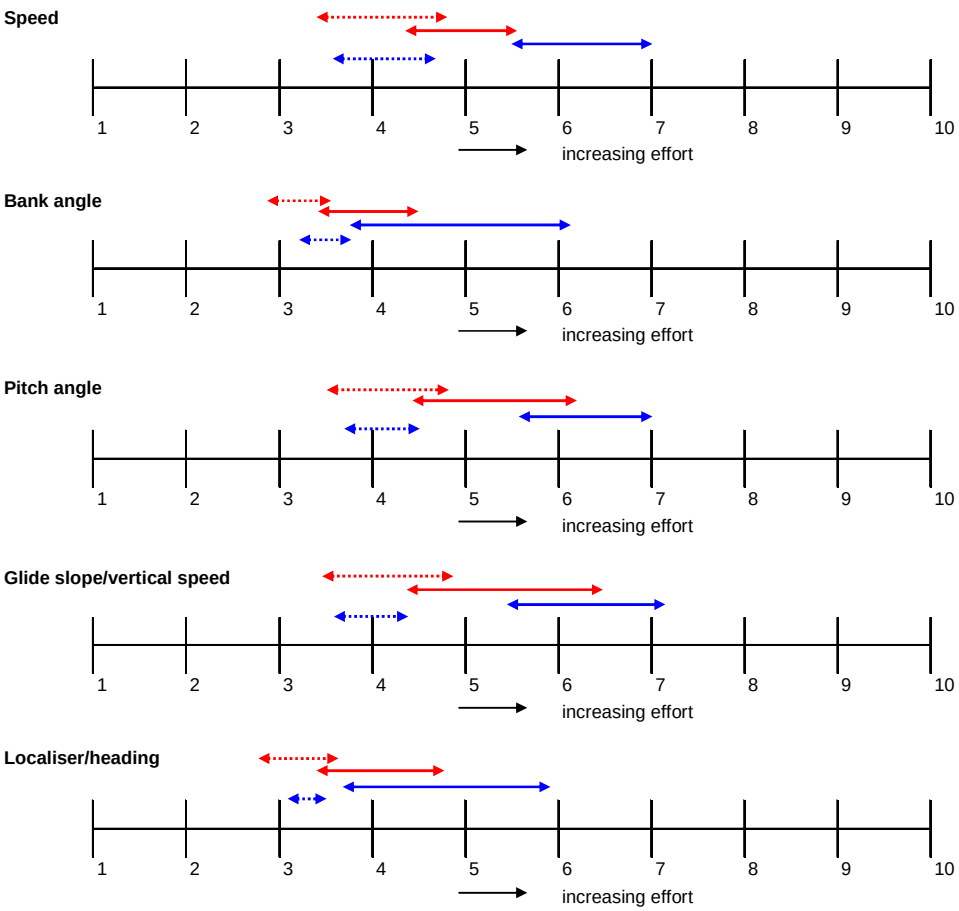

Figure 7-9: Pilot control effort

Finally Figure 7-10 presents the mean values including the standard deviation range of all pilot ratings. In the Cooper/Harper plot shown in the upper left graph the subjective C/H criterion of 5 is shown. This criterion is postulated in section 5.3 and corresponds to the following C/H assessment with respect to flight handling:

- "*Aircraft characteristics have moderately objectionable deficiencies*".
- "*The demands upon the pilot in the required operation are such that considerable pilot compensation is needed for adequate performance*".

From the C/H plot it follows that the approach phase in both cases is acceptable. When looking at the C/H ratings applicable for the "1:35" in the landing phase it can be substantiated that this is just acceptable taken into account the turbulent conditions involved. However this does not hold for the "Annex 14" data, because the mean C/H rating certainly does not meet the criterion. Peaks values up to a C/H rating of 8 can be observed. In the workload plot in the upper right of Figure 7-10 the "*demanding of pilot attention, skill or effort"* (light brown) and *"very demanding of pilot attention, skill or effort*" (brown) levels are indicated. Approaches in both cases are labelled "*demanding of pilot attention, skill or effort"*. Landing workload for the "Annex 14" cases is assessed significantly higher than for the "1:35" data. Finally in lower part

of Figure 7-10 the control effort ratings for the parameters indicated in Table 7–5 are visualised. They are in line with the observations and conclusions taken from the C/H and workload ratings.

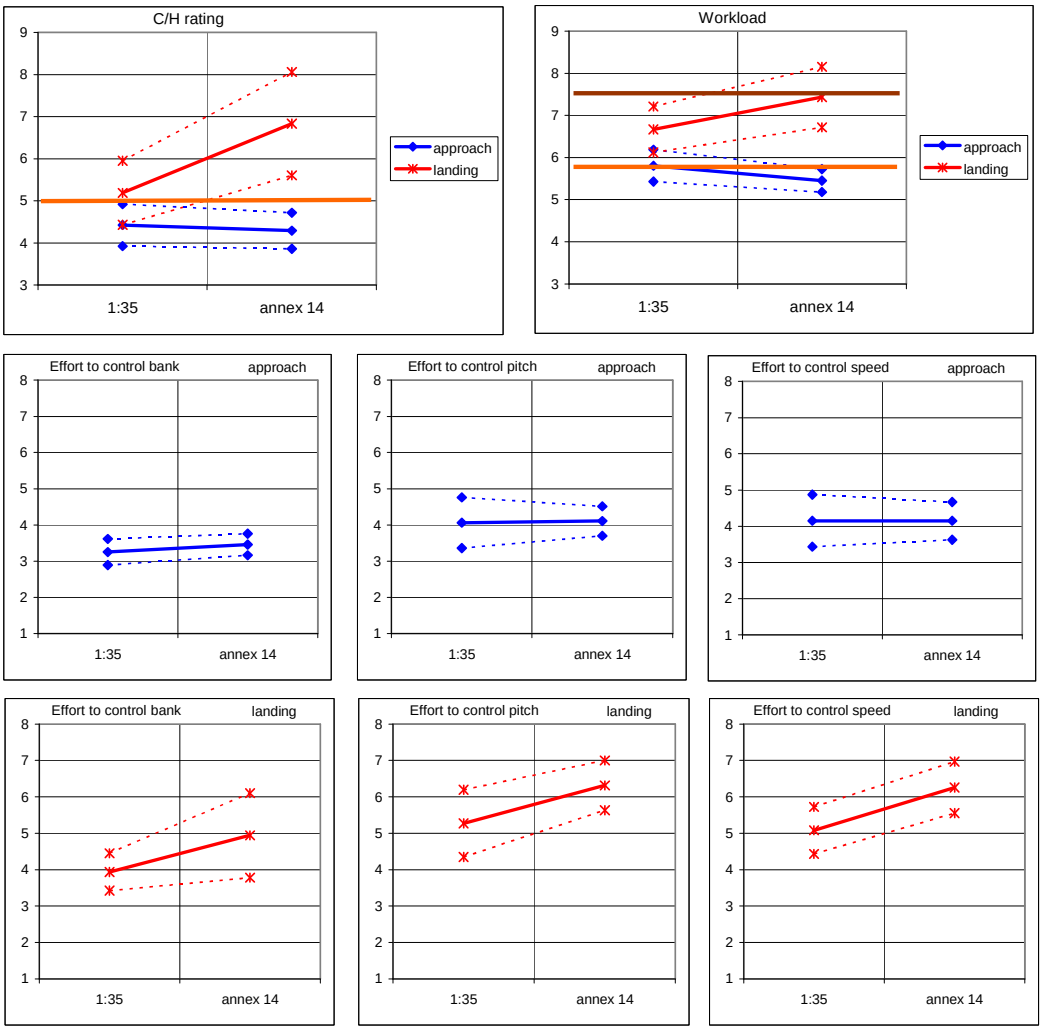

Figure 7-10: Pilot ratings of 1:35 plane and annex 14 obstacle heights

8 Wind disturbance criteria

8.1 Introduction

In this section the results of the offline Fokker F100 simulation and the results of the offline and online Boeing B747 simulation are summarized. Based on this, a wind disturbance criterion is defined. This will be done by means of wind disturbance planes applicable for “stand alone” obstacles and the definition of RMS values of the turbulence intensities that will affect the aircraft handling and landing performance substantially. The wind disturbance planes are considered as a first safety net when stand alone buildings or structures are planned near landing areas. If the structure height protrudes the wind disturbance plane additional requirements are necessary which are discussed in paragraph 8.3. The defined RMS turbulence intensities are intended as a reference for the overall surface roughness and can be tailored to specific areas in the vicinity of the runway.

8.2 Main observations from the performed simulations

The main observations from the offline F100 simulations are:

1. The variation in mean wind speed due to a stand alone obstacle must remain below 7 knots along the aircraft trajectory at heights below 200ft. The horizontal gust/turbulence levels caused by a stand alone obstacle in combination with the meso-scale surface roughness must remain below a RMS value of 4 knots.
2. The cross track touch down dispersion for “Annex 14” and “1:35” obstacles is of the same magnitude.
3. For nearby obstacles the along track touch down dispersion of landings corresponding to “Annex 14” obstacles and “1:35” obstacles is different. Landings with “Annex 14” obstacles touched down further on the runway than landings with “1:35” obstacles.
4. For far away obstacles the along track main gear touch down dispersion of “Annex 14” obstacles and “1:35” obstacles is of the same magnitude. Consequently obstacles positioned further than approximately 750m do not significantly affect the touch down landing performance anymore.
5. All landings are within the defined touch down box for the F100 (see section 5.2).
6. Roll angle dispersion at the threshold is such that occasionally the roll angle criterion (see section 5.2.5) is exceeded for nearby “Annex 14” obstacles. Touch down dispersion however remains within the roll angle criterion.
7. Critical F-factor crossings are of the same order for the reference condition (no obstacle) and obstacles with a height according to the “1:35” plane.
8. A substantial increase of critical F-factor crossings is observed for “Annex 14” obstacles positioned in a disk-shaped segment of 750m x 1200m (Figure 6-40).

9. The encountered turbulence level and wind shearing in the lower atmosphere contributed substantially to the dispersion of the landing performance.
10. The mathematical model for the RMS turbulence intensity is a function of surface roughness, height and reference wind speed. Models for this parameter are derived by ESDU in ([25] and in Appendix B. However, in order to avoid the additional step from surface roughness to turbulence intensity, the standard deviation of the turbulence itself was taken as relevant parameter during the simulations. For the latter in literature (MILSPEC, JAR-AWO and ICAO) criteria can be found in relation to handling qualities issues. Therefore in the evaluations with respect to turbulence reference is made to this RMS turbulence intensity parameter and not to the surface roughness itself.

The main observations from the non-piloted (offline) B747 simulations are:

1. The variation in mean wind speed due to a stand alone obstacle must remain below 6 knots along the aircraft trajectory at heights below 200ft. The horizontal gust/turbulence levels caused by a stand alone obstacle in combination with the meso-scale surface roughness must remain below a RMS value of 4 knots.
2. It appeared that already basic rectangular obstacles located close to the threshold with an "Annex 14" approved height had a significant disturbance on the approach trajectory of the B747. High roll angles were required at very low altitudes in order to land the aircraft on the runway in the touchdown zone. These bank angles violated the hazardous bank criterion in approximately 10 to 70% of the approaches disturbed by the nearby "Annex 14" obstacles. Nevertheless, roll angles at touchdown were within the roll angle criterion.
3. Even with the severe roll maneuvers, most touchdowns occurred a few meters from the runway center line with a few extremes close to the edge of the touchdown zone, and closer to the runway threshold. In general, the touch down deviation for nearby "Annex 14" obstacles is larger than for "1:35" obstacles.
4. The wake strength of the close by "regular" "Annex 14" obstacles slightly increased the wind shear hazard. However no wind shear alerts were triggered.
5. In the vertical trajectory profile, the wakes appeared to have only little effect both for "Annex 14"and "1:35"obstacles.
6. In summary, for "regular" block-shaped obstacles, the offline B747 simulations suggest that the "Annex 14" regulation allows too high obstacles in the area between the runway and up to roughly 500m before the threshold and 1000m laterally next to the runway.
7. The evaluations of five Annex 14 "worst case" obstacles showed that the above perimeter wherein "Annex 14" height limitations are not desired, should be enlarged for "worst case" obstacles (e.g. the PDP) to 750m before the runway and 1200m laterally. Figure 8-1 gives an impression of the estimated location of the boundary of this restriction. The red hatched

perimeter applies to the height of “regular” block-shaped obstacles. The orange hatched zone applies for “worst case” obstacles like the PDP.

8. The results indicate that most obstacles with a height according to the “1:35” rule added no significant additional disturbance to the approach trajectory. Consequently, the “1:35” rule might be an acceptable alternative to the inadequate “Annex 14” regulations close to the runway. However, “1:35” obstacles positioned within 300m from the runway had a small effect on the landing characteristics which can not be neglected.

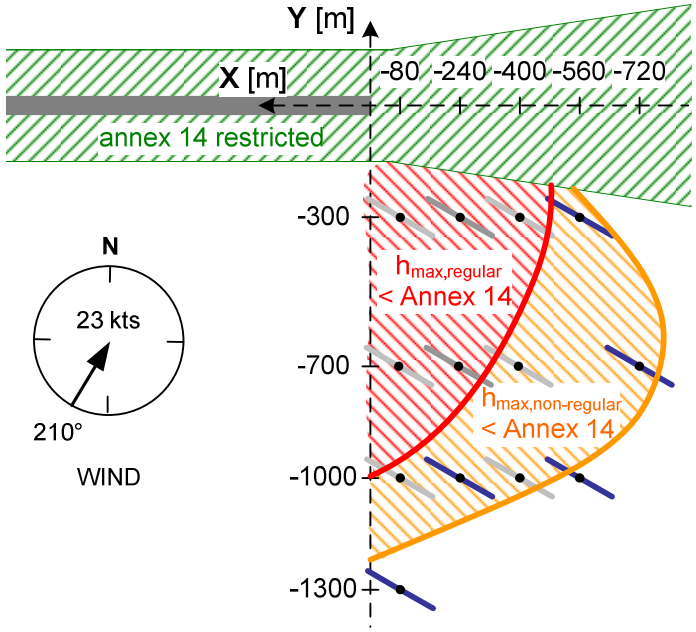

Figure 8-1: Area for B747 where more stringent limitations than approved by Annex 14, should be applied to obstacle heights

The main observations from the piloted B747 simulations are:

- Objective results
  1. Cross track touch down deviation for nearby “Annex 14” obstacles is larger than for “1:35” obstacles.
  2. The same applies for the along track touch down dispersion. Also here a trend was observed of a delayed touch down when nearby “Annex 14” obstacles were included. A number of touch downs corresponding to “Annex 14”obstacles were outside the defined touch down box.
  3. Roll angles at main gear touch down were within the roll angle criterion both for “Annex 14”and “1:35”obstacles.
  4. No wind shear algorithm was available in the piloted simulations. However according to the project pilots in some cases they had expected a wind shear caution or alert.

5. Approaches made in presence of nearby obstacles meeting “Annex 14” heights experienced a much higher number of go-around’s/unsafe landings than approaches made in presence of obstacles meeting “1:35” heights.
6. Gust/turbulence and wind shear phenomena as result of the general surface characteristics (thus not created by a “stand alone” obstacle) contributed substantially to the touch down dispersion.
7. The variation in mean wind speed due to a stand alone obstacle must remain below 7 knots along the aircraft trajectory at heights below 200ft. The horizontal gust/turbulence levels caused by a stand alone obstacle in combination with the meso-scale surface roughness must remain below a RMS value of 4 knots.

- Subjective ratings
  1. C/H rating: For the approach phase (1000ft-200ft) C-H ratings were of the same order for “Annex 14”obstacles and “1:35” obstacles. They are mainly affected by the amount of gust/turbulence encountered during the approach. A mean value of approximately 4.5 was obtained, which is within the C-H criterion of 5. For the height range below 200ft C-H mean value ratings slightly above 5 were obtained for landings with “1:35”obstacles. Also here the turbulence level played a significant role in the pilot judgement. However landings including “Annex 14” obstacles showed ratings with 1-sigma values of 8. This can not be attributed to the turbulence level alone but is the result of the combined effects of the “stand alone” obstacle (speed deficit) and the gust/turbulence disturbing the glide path. Considering the C-H criterion it can be concluded that “Annex 14” obstacles are not acceptable.
  2. Workload: The pilot workload ratings confirm the above observations. In the approach phase the amount of workload for the “Annex 14” and “1:35” obstacles are of the same order: “*Demanding of pilot attention, skill or effort*”. For the landing phase “Annex 14” workload ratings are in a range up to “*Completely demanding of pilot attention, skill or effort*” whereas “1:35”obstacle ratings remain in between “*Demanding of pilot attention, skill or effort*” and “*Very demanding of pilot attention, skill or effort*”.

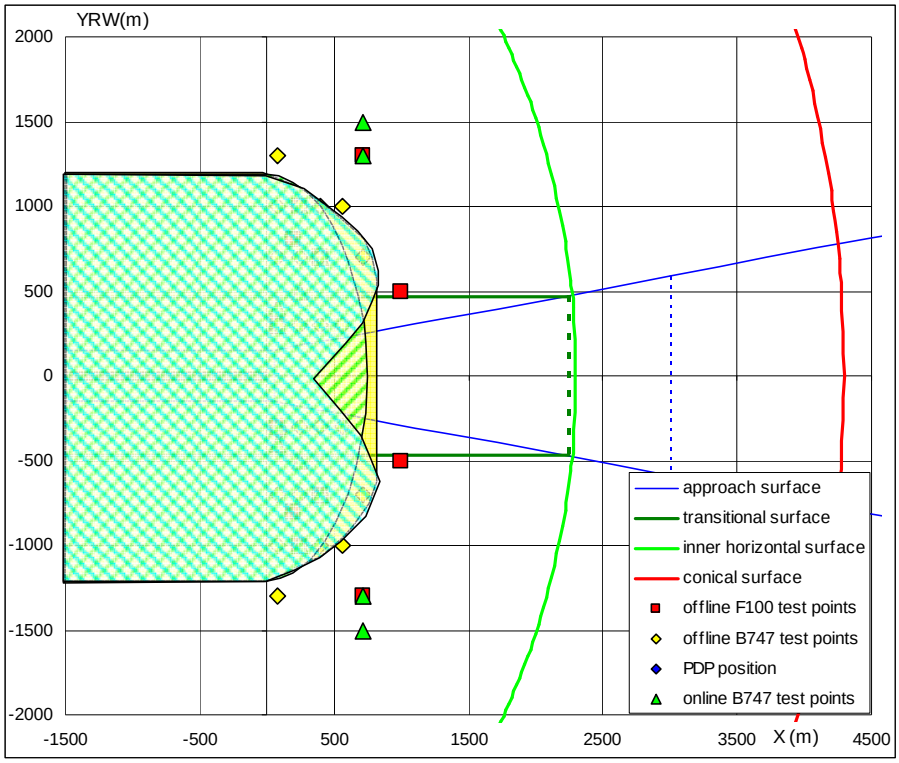

Figure 8-2: Areas with more stringent height limitations than approved by Annex 14

Furthermore it can be concluded that the results from the piloted simulations are in line with the results found from the offline simulations. However the large roll angle excursions found in the B747 offline simulations do not match completely the findings of the piloted B747 evaluations.

Based on the above mentioned observations the following wind disturbance criteria are defined:

- **The variation in mean wind speed due to wind disturbing structures must remain below 7 knots along the aircraft trajectory at heights below 200ft. The speed deficit change of 7 knots must take place over a distance of at least 100m.**
- **The variation in mean wind speed due to wind disturbing structures must remain below 6 knots <u>across the aircraft trajectory</u> at heights below 200ft. The speed deficit change of 6 knots must take place over a distance of at least 100m.**

Resulting in the following guidelines for planned structures in the vicinity of runways:

1. **The glide path segment that covers the approach above 1000ft AGL**.
   For this part of the glide path wind disturbances due to a “stand alone” obstacle and gust/turbulence created by the overall surface roughness are not a direct threat to flight safety. Consequently no wind disturbance planes are required for this segment other than the ICAO Annex 14 obstacle clearance planes.

2. **The glide path segment that covers the approach from 1000ft AGL to 200ft AGL**.
   a. "Stand alone" obstacle.
      No distinct effect of a "stand alone" obstacle on aircraft handling and landing performance could be established in this height range. The effect is submerged in the overall surface characteristics. The offline and piloted simulations showed that the obstacle clearance planes defined by ICAO Annex 14 give sufficient protection to wind disturbances as result of "stand alone" obstacles. No specific wind disturbance planes are required for this segment.
   b. Surface roughness.
      In this altitude range wind disturbance acting on aircraft is defined by the turbulence intensity applicable for the build up area affecting the runway threshold zone. It is a function of the surface roughness and reference wind speed.
      The offline and piloted simulations showed that RMS values of the turbulence intensity in excess of 5kts (heavy turbulence) sometimes lead to too large glide path deviations as result of gust and wind shear phenomena.
3. **The glide path segment that covers the landing phase from 200ft AGL to touch down and the high speed roll out.**
   a. "Stand alone" obstacle.
      In this height range a distinct effect of a "stand alone" obstacle on the aircraft handling and performance could be established.
      For this segment wind disturbance criteria are necessary that are more stringent than the ICAO "Annex 14" planes. It appeared that "stand alone" obstacles in a disk-shaped area with origin in the center of the runway threshold and radii of approximately 1200m perpendicular to runway centerline and 900m in front of the runway threshold and not protruding an imaginary plane with a slope of 1:35 with the extended runway centerline as base did not affect the response and performance of the aircraft significantly. In order to cover the high speed ground roll the defined 1:35 plane is also applicable up to 1500m beyond the runway threshold.
   b. Surface roughness.
      In this height range the aircraft handling and performance is affected both by the turbulence intensity applicable for the area affecting the runway threshold zone and the increased turbulence caused by the wake of a "stand alone" obstacle.
      The offline and piloted simulations showed that RMS values of the turbulence intensity less than 4kts (medium/heavy turbulence) due to the surface roughness in front of the landing area in combination with the speed deficit and induced speed gradients of a "stand alone" obstacle limited in height by the 1:35 plane did not lead to unacceptable aircraft handling and landing performance.

The segment where the 1:35 wind disturbance plane becomes restrictive is shown in Figure 8-2. It encompasses both the B747 and F100 defined areas and is valid for “worst case” obstacles.

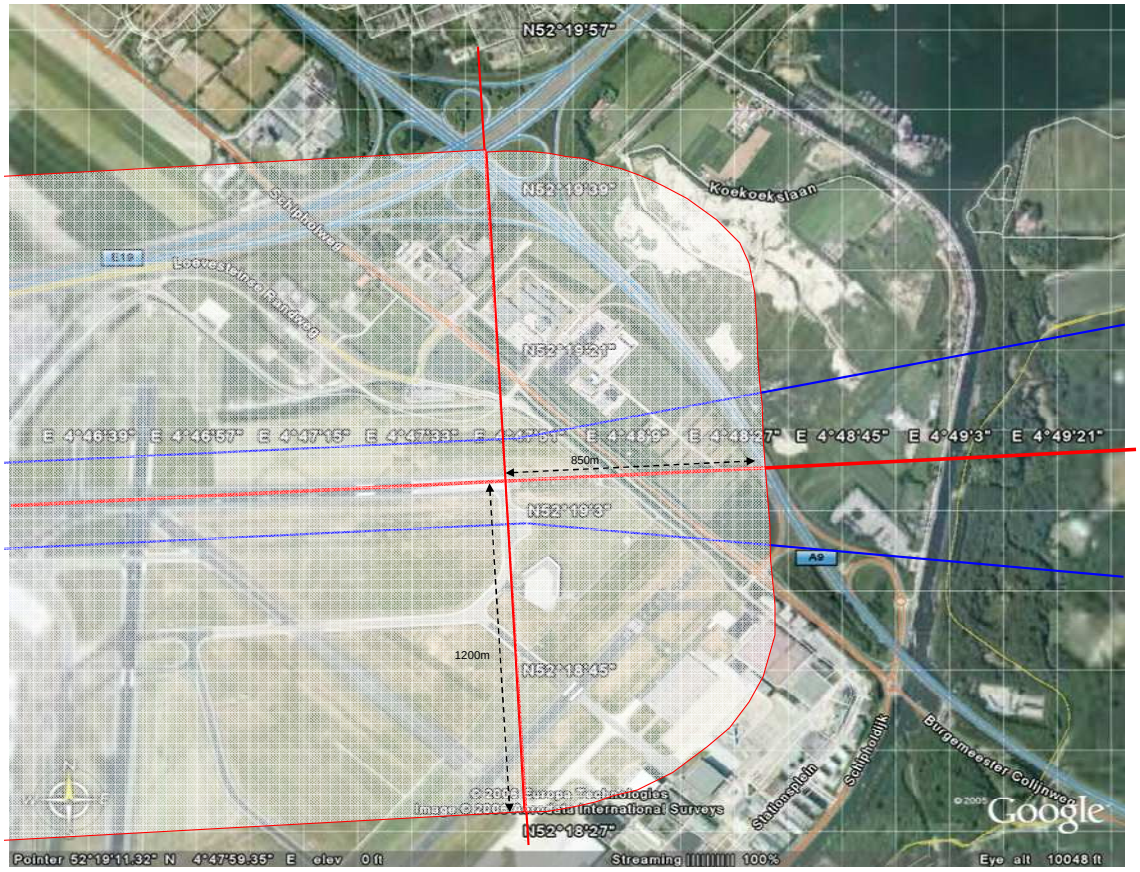

Figure 8-3: Area around runway 27 of Schiphol Airport where more stringent limitations than approved by Annex 14, should be applied to obstacle heights

An illustration of the area in which the wind disturbance plane becomes restrictive is shown in Figure 8-3 and Figure 8-4 for runway 27 and runway 36R respectively. The semi permeable area indicates where the “1:35” wind disturbance plane must be applied. Outside this area, the “Annex 14” limitations are satisfactory.

Figure 8-4: Area around runway 36R of Schiphol Airport where more stringent limitations than approved by Annex 14, should be applied to obstacle heights

8.3 Acceptance procedures

In this paragraph acceptance criteria are presented for proposed "stand alone" buildings or structures that protrude the wind disturbance plane. The criteria are based on simulations executed with the F100 aircraft. The following requirements are defined:

- **Minimum obstacle width for which the wind disturbance plane applies**.
  A rough estimation is presented of the minimum width for an obstacle that still leads to significant wind disturbance to aircraft on the glide path below 200ft. The F100 aircraft is decisive in this respect because it has a lower approach speed than the B747. In strong head wind conditions it is possible that this leads to ground speeds of approximately 50-55m/s during the final approach. As is shown in paragraph 5.2.2.1 and paragraph 5.2.5.2 wakes lasting approximately 4 seconds or more are required before they have a significant effect on the aircraft. This means that with a ground speed of 50m/s the wake distance must be 200m or more. Figure 8-5 shows the wake distance as function of obstacle width during final approach. The simulated "worst case" obstacle with a height of 18m is positioned relative close to the runway threshold (80/330). The maximum strength of the wake affects the aircraft at 100ft AGL.

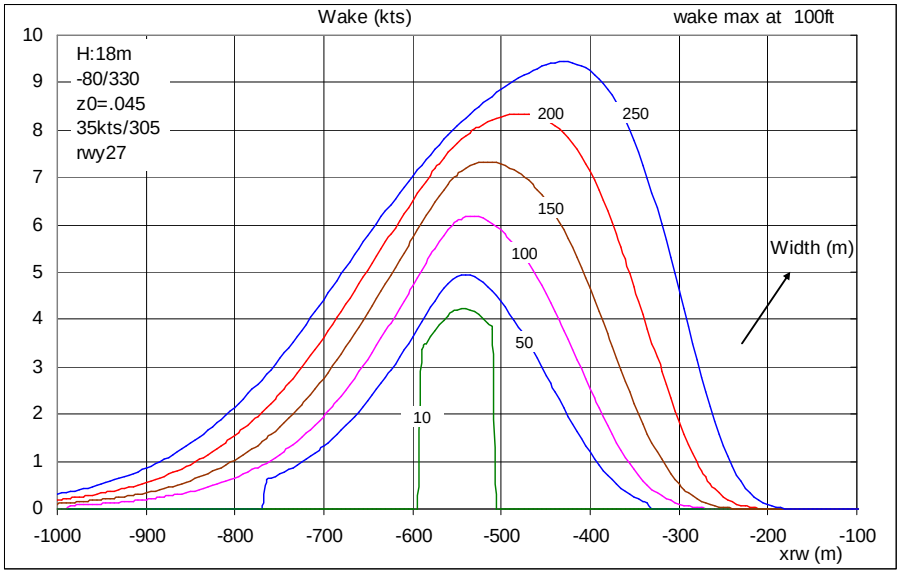

Figure 8-5: Wake distance as function of obstacle width

If the calculated ground distance of 200m is plotted into Figure 8-5 it appears that this corresponds to an obstacle width of approximately 30m. Therefore it is stated that obstacles with a width less than 30m and producing a maximum speed deficit less than 8kts are allowed to protrude the 1:35 wind disturbance plane. Obviously the height may never exceed the Annex 14 obstacle clearance requirements.

- **Requirements with respect to the maximum speed deficit that can be allowed**.
  - Along track: As is evaluated in paragraph 5.2.2.1 the maximum speed defect that is allowed in longitudinal direction may not exceed 8kts.
  - Cross track: As is evaluated in paragraph 5.2.5.2 the maximum speed defect in lateral direction may not exceed 12kts.

The postulated 7kts criterion is a conservative interpretation of the above observations and therefore is also recommended as criterion for structures protruding the 1:35 plane.
Horizontal gust/turbulence levels caused by a stand alone obstacle protruding the 1:35 plane in combination with the meso-scale surface roughness must remain below a RMS value of 4 knots.

9 Conclusions and recommendations

The investigation described in this report deals with the performance, controllability and safety of an aircraft under the influence of wind effects of buildings or obstacles.
In order to focus the study a number of constraints were required. The most relevant are:

- The wind direction is perpendicular towards a “stand alone” obstacle. Thus effects due to a non-perpendicular wind flow are no part of this investigation.
- The simulations address generic “worst-case” block-shaped obstacle characteristics in which variations in the wind field at the two corners of the obstacle are taken into account.
- No mechanical failures (e.g. engine) are introduced to the aircraft during the approach/landing.
- Maximum cross wind in the investigation is limited to 20 knots.
- Only dry runway conditions are considered.
- Good visual conditions prevailed during the piloted simulations. Low visibility has not been addressed.
- The results apply to a neutral atmosphere including strong winds in excess of 15 knots. Convective effects as result of the local heating of the earth surface by the sun have not been taken into account.
- The work is tailored to two jet aircraft equipped with conventional controls. Propeller driven aircraft and Fly-By-Wire aircraft as well as Very Large Aircraft have not been evaluated.
- Tail wind components are not present.
- High speed roll out, take-off and go-around were no part of the investigation.

The main conclusions of the study for the considered segments can be summarized as follows.

A. The segment that covers the approach flight phase from 1000ft AGL to 200ft AGL.

a. <u>“Stand alone” obstacle.</u>

No distinct effect of “stand alone” obstacles on the aircraft handling and performance could be established in this height range. The effect is submerged in the overall surface characteristics of the build up area affecting the runway. The offline and piloted simulations showed that the obstacle clearance planes defined by ICAO Annex 14 give sufficient protection to wind disturbances as result of “stand alone” obstacles. No specific wind disturbance planes are required for this segment.

b. <u>Surface roughness.</u>

In this altitude range the wind disturbance effect on the aircraft is defined by the turbulence intensity applicable for build up area affecting the runway. It is a function of the surface roughness and a reference wind speed.

The offline and piloted simulations showed that RMS values of the turbulence intensity of the horizontal components in excess of 5kts (heavy turbulence) sometimes lead to too large glide path deviations as result of gust and wind shear phenomena. In this height range the horizontal scale lengths used in the gust/turbulence simulation varied from 200m to 300m.

B. The segment that covers the landing phase from 200ft AGL to touch down and the high speed roll out.

a. <u>"Stand alone" obstacle.</u>

It was established that for this segment wind disturbance criteria are necessary that are more stringent than the "Annex 14" planes. It appeared that stand alone obstacles in this area not protruding an imaginary plane with a slope of 1:35 with the extended runway centerline as base did not affect the response and landing performance of the aircraft significantly.

The segment where the wind disturbance plane is restrictive is bounded by a disk-shaped segment with origin in the center of the runway threshold and radii of approximately 1200m (perpendicular to runway centerline) and 900m in front of the runway threshold.

Although it was not a part of the study it is proposed to cover the high speed roll out by extending the 1:35 plane up to 1500m aft of the runway threshold.

For "stand alone" block shaped structures the following <u>criteria</u> have been derived:

> **<u>Along the aircraft track</u> the speed deficit due to a wind disturbing structure must remain below 7 knots. The speed deficit change of 7 knots must take place over a distance of at least 100m.**
>
> **<u>Across the aircraft track</u> the speed deficit due to a wind disturbing structure must remain below 6 knots. The speed deficit change of 6 knots must take place over a distance of at least 100m.**

The criteria are depicted schematically in the next figure:

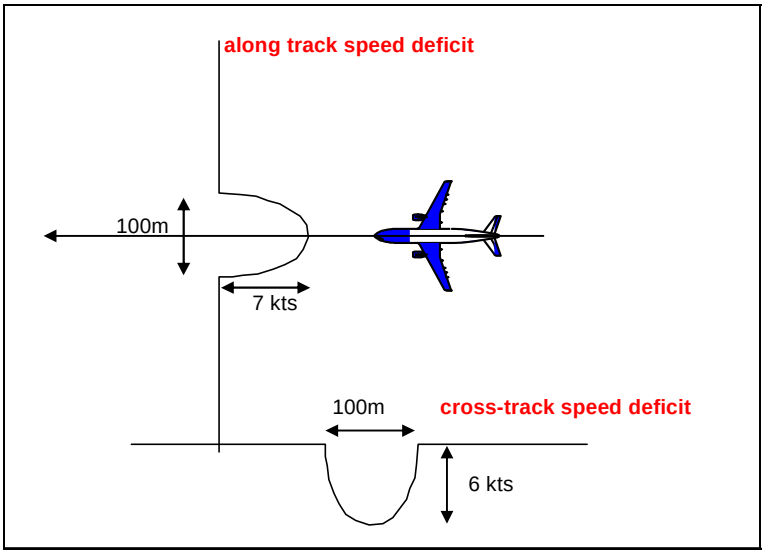

b. <u>Surface roughness.</u>

In this altitude range the wind disturbance effect on the aircraft is defined by the turbulence intensity applicable for build up area affecting the runway and the additional turbulence intensity created by the stand alone structure. It was found that the gust/turbulence components in horizontal direction caused by a wind disturbing structure in combination with the meso-scale surface roughness must remain below RMS values of 4 knots. In this height range the horizontal scale lengths used in the gust/turbulence simulation varied from 50m to 200m.

However the study also revealed a strong relation between surface roughness and the mean wind profiles. Surface roughness and reference wind speeds selected for the simulations lead to gust and turbulence levels varying from medium to severe.

In addition the investigation led to the following conclusions:

- The study showed that pilot's acceptance of a stand alone obstacle is significantly influenced by the effects of gusts and turbulence.
- From tests on the NLR moving base simulator it was observed that a surface roughness length of more than .1m in combination with reference wind speeds higher than 23kts was not realistic from a pilot's point of view because this leads to RMS values of the turbulence intensity of more than 6kts. For low altitudes these magnitudes are unrealistic according to ICAO and JAR-AWO standards and may lead to large structural loads on the airframe. Therefore the encountered turbulence levels in the simulations are defined in terms of their RMS turbulence intensity values.
- On essential points the results of the offline F100 and B747 simulations are in line with each other. However the observed very large roll angles (in excess of 10dg) were not

confirmed by the piloted evaluation on the moving base simulator. During the latter pilots had more difficulty with pitch attitude and vertical speed control.

- Based on the above observation it is stated that the criterion is valid for all aircraft weight classes (Citation-Airbus A380). In the study two extremes have been chosen with respect to size and inertia. Extrapolation to A380 aircraft and small business Citation like aircraft is possible because the aircraft motions and response than is determined more by the relationship between weight, span, wing area and the like.
- It can be made plausible that propeller-driven aircraft are not more critical than jet-propelled aircraft. In fact it can be put forward that because of the fluctuating wind fields and the fact that propeller-driven aircraft have much better engine response times to throttle lever movements this class of aircraft is able to react faster to fluctuating conditions. Also the increased prop wash over the wing in general gives such an aircraft a faster and better control in varying wind conditions. Although accidents with propeller aircraft are known in the past in which wind shear played a role the number is far less than the amount of incidence/accidents with jet engine aircraft.
- Fly-by-wire control systems are fed by inertial and pressure sensors. These sensors are able to sense deviations from a desired state much faster than a human being. In addition the response is univocal and reproducible. Manual control often shows lags because the deviation has to be recognized at first, where after the correct action has to be taken. Consequently it can be stated that FBW aircraft are less sensible for wind disturbances as discussed in this report.
- Aerodynamics during the high speed landing ground roll play a significant part down to an airspeed of approximately 80kts. For adverse weather and runway conditions the high speed ground roll can absorb up to 1500m of runway length. Therefore the proposed 1:35 wind disturbance plane has been extended aft of the runway threshold up to 1500m. If the runway is used on both sides for landing this in fact means that the 1:35 plane is applicable for most of the runway length.
- From previous studies in relation with wind breaks it appeared that take off in comparison with the landing phase is less critical. Certainly in strong head winds aircraft quickly ascend to heights where wind disturbance due a stand alone obstacle is submerged in the overall surface characteristics. Therefore the defined 1:35 plane also is valid for take off conditions including the high speed take off ground roll.

The investigation led to the following observations:

- The amount of gust and turbulence present in the lower earth boundary layer is a large contributing factor in the response and landing performance of an aircraft. It may cover up or aggravate the wake characteristics of a stand alone obstacle.

- In this study “regular” block-shaped obstacles and “worst case” obstacles have been analyzed. From a safety point of view is has been preferred to base the wind disturbance planes on the characteristics of a “worst case” obstacle.
- Surface roughness lengths applicable for runways on airports in general vary from .001m (airport at sea ([9]) to .003m (ESDU ([24]). However for Schiphol KNMI in ([45] presents a surface roughness of .03m for the landing area. However z0 values up to .15m are applicable for the landing area of runway 27 as result of the build up area at or outside the airport when winds come from a south western direction.
- The simulations were executed with an x-wind component of 20kts (excluding gust). If the cross wind limit is increased to 25kts (excluding gusts) obviously flight handling and landing performance will deteriorate even further. However within the framework of this study the gust/turbulence level is a function of the ***total*** wind speed and thus independent of the distribution between x-wind and head wind component. However from a wind disturbance point of view higher crosswinds are not advised.
- During the piloted simulations it appeared that in general pilots also visually assessed the effect of a stand alone obstacle if this obstacle was positioned in the direct scan of the pilot.
- The alertness of the pilot to possible wind effects due to stand alone obstacles plays an important role. This was observed during the piloted simulations. During highly turbulent and gusting approaches requiring much effort of the pilot the effect of the stand alone structure was considered less critical than during smooth weather approaches, where the upset of the stand alone structure was not expected.

In conjunction with the above conclusions the following recommendation is proposed:

- Because of the strong non-linear relation between gust/turbulence and surface roughness in combination with wind speed further research into the effects of this parameter may be worthwhile.

10 References

[1] Boom, v.d. R.P., "*Offerte aanvraag voor het faciliteren en uitwerken van onderzoeksopdracht inzake wind criteria*", DGTL/05.004809, July 2005

[2] Nieuwpoort, A.M.H., "*Proposal for the formulation of wind disturbance criteria due to buildings planned at and around airports*", NLR-memorandum ATSF-2005-071, August 2005.

[3] Nieuwpoort, A.M.H., "*Dynamics of crosswind operations*", NLR-CR-98494, November 1998.

[4] Es, v G.W.H., Geest, v/d P.J. and Nieuwpoort, A.M.H., "*Safety aspects of aircraft operations in crosswind*", NLR-TP-2001-217, May 2001.

[5] Gooden, J.H.M. , "*Reduction of the wind disturbance along the approach to runway 27 on AAS by lowering the test run facility from 16 to 6 m, a wind tunnel investigation*", NLR-CR-98427, October 1998.

[6] Willemsen, E., Gooden, J.H.M. and Marsman, A.P.L.A., "*Study on the aerodynamic characteristics in relation to aircraft behaviour of the test run facility at Amsterdam Airport Schiphol*", DNW CR-96002L, 1996

[7] Takens, J. and Willemsen, E., "*Wind tunnel investigation on the wind effects of a test run. facility at Schiphol airport with regard to the approach paths of runway 27 and 22*", DNW CR-95002C, 1995

[8] Nieuwpoort, A.M.H. "*The effect of wind disturbances due to an obstacle on aircraft*", NLR-CR-99482, September 1999.

[9] Nieuwpoort, A.M.H. and Gooden, J.H.M., "*Exploratory investigation into the effects of a windbreak on the flyability of aircraft during landing and take-off at an airport situated at sea*", NLR-CR-2002-370, July 2002.

[10] Anon, "*JAR-AWO All weather operations*", Joint Aviation Requirements, Change 2, August 1996

[11] Anon, "*International standards and recommended practices*", AERODROMES ANNEX 14, Volume 1 aerodrome design and operations, July 1995, Chapter4: Obstacle restriction and removal.

[12] Vicroy, D.D., Bowles, R.L. and Passman, R.H., "Airborne wind shear detection and warning systems", NASA-CP-1010S-PT-1, September 1992.

[13] Anon, "*Airborne windshear warning and escape guidance systems for transport planes"*, TSO-C117a, FAA,1996

[14] Rossow, V.J., "*Research on aircraft/vortex- wake interactions to determine acceptable level of wake intensity*", Journal of aircraft, vol. 25, no 6, June 1988.

[15] Luckner, R., Hoehne, G. and Fuhrman, M.,"*Hazard criteria for wake vortex encounters during approach*", Airbus Deutschland GmbH, Hamburg.

[16] Sammonds, R.I. and Stinnett, G.W., "*Criteria relating wake vortex encounter hazard to aircraft response*", Journal of aircraft, vol. 14, no 10, October 1977.

[17] Perera, M.D.A.E.S., "*Shelter behind two-dimensional solid and porous fences*", J. Wind Eng. Industr. Aerodyn., vol.8, pp. 93-104, 1981.

[18] Tucker J., "*Estimation of shelter provided by solid and porous fences*", ESDU Freeman, B.C., 97031, 1998.

[19] Counihan, J., Hunt, J.C.H. and Jackson, P.S., "*Wakes behind two-dimensional surface obstacles in turbulent boundary layers*", J. Fluid Mech., Vol.64, pp. 529-563, 1974.

[20] Castro, I.P. and Garo, L., "*Flow through porous fences in thick boundary layers*". Part II – Laboratory experiments. Report ME-FD/98.91, School of Mechanical & Materials Engineering, University of Surrey, 1998.

[21] Freeman, B.C., "*Longitudinal turbulence intensities over terrain with roughness changes*", ESDU 84030, 1984.

[22] Anon., "*Flight handling certification F28 mk070*", Fokker report no. V-28-174, May 1995

[23] Wieringa, J. and Rijkoort, P.J., "*Windklimaat van Nederland*". KNMI, 1983.

[24] Anon, "*Strong winds in the atmospheric boundary layer, Part 1: mean-hourly wind speeds*", ESDU 82026, March 1990.

[25] Anon, "*Strong winds in the atmospheric boundary layer, Part 2: discrete gust speeds*", ESDU 83045, august 1984.

[26] Anon, "*Wind environment around buildings, Aerodynamic concepts*", Proceedings of the fourth international conference, Heathrow, 1975

[27] Tacken,M., "*Windhinder, een literatuurstudie"*, Memo no 14, TUD, February 1977

[28] Voorden, M v/d.,"*Windhinder"*, Stichting Bouw Onderzoek, 1982

[29] Castro, I.P., "*Wake characteristics of two-dimensional perforated plates normal to an air-stream*", J. Fluid Mech., vol.46, pp.599-609 (1971)

[30] Nieuwpoort, A.M.H., "Offline 6 degree of freedom simulation programme of F100". Fortran 77 software programme.

[31] Anon, "*Military specification of flying qualities of piloted airplanes*", MIL-F-8785C, August 28, 1996

[32] Hanke, C. and Nordwall, D., "*The Simulation of a Jumbo Jet Transport Aircraft. Volume II: Volume II: Modeling Data*", Tech. Rep. NASA CR-114494/D6-30643, The Boeing Company, 1970

[33] Hanke, C., "*The Simulation of a Large Jet Transport Aircraft. Volume I: Mathematical Model*", Tech. Rep. NASA CR-1756, The Boeing Company, 1971

[34] Mulder, J.A., van der Vaart J.C. and van Staveren J.W., "*Aircraft Responses to Atmospheric Turbulence*", Lecture Notes AE4-304, TU Delft, 1998

[35] Heffley, R. and Wayne, F., "*Aircraft Handling Qualities Data*", Tech. Rep. NASA CR-2144, Systems Technology, Inc., 1972

[36] Proctor, F.H., Hinton, D.A. and Bowles, R.L., "*A Windshear Hazard Index*", Preprints of 9th Conference on Aviation, Range and Aerospace Meteorology, 11-15 September 2000, Orlando Florida, p. 482-487

[37] Barnes, T., Defiore, T. and Micklos, R., "*Video landing parameter survey-Washington National Airport*", DOT/FAA/AR-97/106, June 1999.

[38] Nieuwpoort, A.M.H., "*Simulator test programme for the obstacle wind disturbance experiment*", to be published, March 2006.

[39] Anon, "*Addendum bij eindrapport 97-75/A-26*", PH-TKC- Boeing 757, 24 december 1997, Amsterdam Airport Schiphol.

[40] Anon, "*Wind environment around buildings, Aerodynamic concepts*", Proceedings of the fourth international conference, Heathrow, 1975

[41] Bovenkamp, vd N., "*Non-aerodynamic data related to the Fokker 100 aero database*", Fokker report L-28-586, January 1995.

[42] Anon, "*Flight simulator data for the Fokker F28 Mk100*", Fokker Report L-28-336, issue 8.5, July 1992.

[43] Nelson, R.C. and McCormick, B.W., "*The dynamic behavior of an aircraft encountering aircraft wake turbulence*", AIAA paper no. 74-774, August 5-9, 1974.

[44] Stewart, E.C., "*A study of the interaction between a wake vortex and an encountering airplane*", AIAA paper no. 93-3642-CP, August 1993

[45] Anon, "*Wind study Amsterdam Airport Schiphol*", KNMI, August 1997.

[46] Geest, van der P.J., "*Effects of FMS F2A software changes with respect to the Fokker 100 Wind shear detection Function*", Fokker report VS-28-30, December 1990.

[47] Anon, "*Windverstoring onder invloed van bebouwing*", DGL/IVW-DL version 0.2, Juli 2004

[48] Es, van G.W.H., Geest, van der P.J., "*A study of normal operation landing performance on subsonic civil narrow body jet aircraft during ILS approaches*", NLR-CR-2006-049, 2006

Appendix A RMS of turbulence in relation to normal load

Definitions:

n_z: Normal load
L: Lift
g: Gravitational acceleration
W: Weight = aircraft mass x g
ρ: Air density
VA: Airspeed
S: Wing area
C_L: Lift coefficient
α: Angle of attack
w_{B_g}: Gust velocity in z direction
σ_w: Standard deviation of turbulence in z direction

The normal load can be defined as:

$$n_z = \frac{L}{W}$$

For the aerodynamic lift it applies:

$$L = C_L \cdot \tfrac{1}{2} \cdot \rho \cdot VA^2 \cdot S$$

From this it follows for the increment/decrement of the angle of attack as result of a normal load deviation:

$$\Delta\alpha = \frac{2 \cdot m \cdot g}{C_{L_\alpha} \cdot \rho \cdot VA^2 \cdot S} \cdot \Delta n_z$$

Also valid is:

$$\Delta\alpha = \frac{w_{B_g}}{VA}$$

which leads to the following expression for the gust velocity in vertical direction:

$$w_{B_g} = \frac{2 \cdot m \cdot g}{C_{L_\alpha} \cdot \rho \cdot VA \cdot S} \cdot \Delta n_z$$

Now it is assumed that: $w_{B_{g_{\lim}}} = 3 \cdot \sigma_w$

Then it applies for the standard deviation in z-direction:

$$\sigma_{w_{\lim}} = \frac{2 \cdot m \cdot g}{3 \cdot C_{L_\alpha} \cdot \rho \cdot VA \cdot S} \cdot \Delta n_{z_{\lim}}$$

Or written explicitly in $\Delta n_{z_{\lim}}$:

$$\Delta n_{z_{\lim}} = \frac{3 \cdot C_{L_\alpha} \cdot \rho \cdot VA \cdot S}{2 \cdot m \cdot g} \cdot \sigma_{w_{\lim}} = \frac{1.5 \cdot C_{L_\alpha} \cdot \rho \cdot VA}{W/S} \cdot \sigma_{w_{\lim}}$$

It can be observed that the normal load increases linearly with the airspeed, decreases with height and is inversely proportional to the wing loading.

For the F100 and B747 the following relation between standard deviation and normal load deviation can be derived:

F100:

$$\sigma_{w_{\lim}} = \frac{2 \cdot 33000 \cdot g}{3 \cdot 5.73 \cdot 1.2 \cdot 70 \cdot 93.5 \cdot .5144} \cdot \Delta n_{z_{\lim}} = 9.3 \cdot \Delta n_{z_{\lim}} \text{ kts}$$

B747:

$$\sigma_{w_{\lim}} = \frac{2 \cdot 240000 \cdot g}{3 \cdot 5.73 \cdot 1.2 \cdot 82 \cdot 511 \cdot .5144} \cdot \Delta n_{z_{\lim}} = 10.6 \cdot \Delta n_{z_{\lim}} \text{ kts}$$

As is shown in Figure 3-6 the vertical and horizontal turbulence components are related. For the JAR-AWO model it applies at approximately 200ft:

$$\sigma_{u_{\lim}} = \sigma_{v_{\lim}} = 1.5 \cdot \sigma_{w_{\lim}}$$

Consequently:

F100: $\sigma_{u_{\lim}} = \sigma_{v_{\lim}} = 14. \cdot \Delta n_{z_{\lim}}$ **B747**: $\sigma_{u_{\lim}} = \sigma_{v_{\lim}} = 16. \cdot \Delta n_{z_{\lim}}$

Heavy turbulence in horizontal direction according to Table 3–3 is 5 kts. This results in normal load variations as follows:

F100: $\Delta n_{z_{\lim}} = .36g$ **B747**: $\Delta n_{z_{\lim}} = .32g$

Appendix B Description wind model 3D building and PDP

The variables related to the wind climate model are expressed in the "***wake axes system***" as defined in section 6.4.1.6. In the derivation of the mathematical wind model the following notations are used:

x, y, z	XPATHN, YPATHN, ZPATHN coordinates (see section 6.4.1.6) [m]
C_Γ	Vorticity constant, $\frac{\Gamma_0}{4\pi V_H H}$ [-]
H	(Effective) height of wind screen [m]
p	(Effective) porosity of wind screen [m]
V	(time averaged) wind speed [m/s]
V_H	Undisturbed wind speed at z=H [m/s]
V_y , V_z	Velocity components in y, resp. z-direction [m/s]
V_t	Magnitude of the tangential velocity component, perpendicular to x [m/s]
V_{10}	Undisturbed wind speed at z=10 m [m/s]
W	(Effective) width of obstacle [m]
y_n , z_n	Grid coordinates in PDP wake transformation [m]
y_{vortex}, z_{vortex}	Position of vortex core (y>0) [m]
z_0	Surface roughness [m]
Γ	Vortex strength, index 0 at x=0 [m^2/s] ($\Gamma < 0$ for PDP)
κ	Von Kármàn constant [-]
η	Dimensionless parameter voor z [-]
σ_u	RMS turbulence intensity in x-direction, idem σ_v , σ_w in y and z-direction [m/s]
ζ	Dimensionless wake mixing area parameter [-]

index:

a	Undisturbed atmospheric boundary
b	Behind 2-D wind screen
ab	Behind 3-D wind screen
x, y, z	Component in x, y en z-direction

The calculation of the wind field behind an obstacle with finite width in principal is based on the calculation of the wake behind a 2-D infinitely wide wind screen. Consequently the computation consists of three parts, which are discussed hereafter. The first part yields a description of a coordinate transformation required for the modelling of the PDP wind climate.

For a “regular” obstacle, without vorticity this transformation is not required and applies: $(y_n, z_n) = (y, z)$.

1. Coordinate transformation for a wake deformed by vortices (PDP situation):

The initial vortex strength is assumed to be proportional with the wind speed and screen height according to:

$$\Gamma_0 = 4\pi C_\Gamma V_H H$$

in which C_Γ is a constant of proportionality.
With increasing distance behind the wind screen the vortex strength becomes less. This is mainly a function of turbulence intensity and scale length. Here a relation ship derived from PDP wind tunnel measurements is used:

$$\Gamma = \Gamma_0 . \exp\left(-\frac{x/H}{w_0} \right) \qquad (w_0 = 27)$$

According to potential theory both vortices approach each other asymptotically to a certain minimum distance. However this does not occur in practice because the vortices “eat” each other as result of viscous effects. At some distance the lateral vortex position does not change very much behind the screen and even starts to increase again. Therefore the in-between vortex distance is assumed to be constant and equal to the width of the rear wall (55m). This leads to; y_{vortex} of 27.5m.
The mutually induced vertical displacement velocity of the vortices at some height above ground level (where the influence of mirrored “underground” vortices is reduced) amounts to:

$$W_{vortex} = \frac{-\Gamma}{4\pi y_{vortex}}$$

From this the vertical position of the vortices can be modeled, assuming V_H is a characteristic horizontal displacement velocity of the vortex and that the vortices don’t loose their strength (which is acceptable within this approximation):

$$\frac{z_{vortex}}{H} = 1 - \frac{w_2 C_\Gamma x}{y_{vortex}} \qquad (w_2 = 0.54)$$

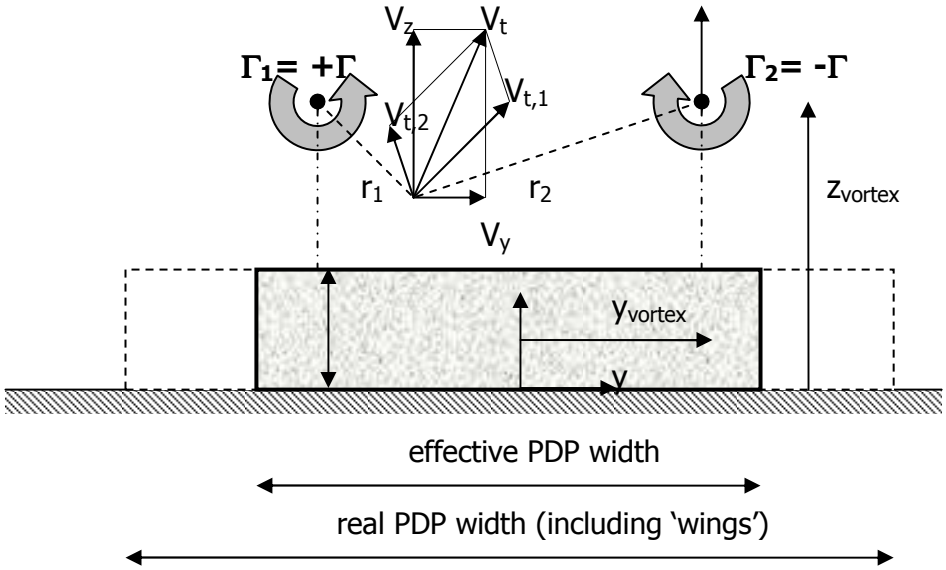

In case of a wind oriented vortex pair the velocity components normal to the wind direction have to be calculated. This is done using the Lamb-Oseen vortex description including a viscous core. The diameter of the viscous core is set to:

$$r_c = \frac{z_{vortex}}{2}$$

For each of the two vortices (j=1, 2) the induced velocity at position (y,z) results from:

$$\Delta y_j = y - (-1)^j y_{vortex}$$
$$\Delta z = z - z_{vortex}$$
$$r_j = \sqrt{\Delta y_j^{\,2} + \Delta z^2}$$
$$\frac{V_{t,j}}{V_H} = (-1)^j \frac{1}{2\pi} \frac{(\Gamma / V_H)}{r_j} \left[1 - \exp\left\{ -\left(\frac{r_j}{r_c} \right)^2 \right\} \right]$$

Summation over both vortices gives the horizontal and vertical lateral velocity components:

$$\frac{V_y}{V_H} = \sum_{j=1}^{2} \frac{-\Delta z_j}{r_j} \frac{V_{t,j}}{V_H}; \quad \frac{V_z}{V_H} = \sum_{j=1}^{2} \frac{\Delta y_j}{r_j} \frac{V_{t,j}}{V_H}$$

These lateral velocities induce by the vortices create a deformation of the wake. The direction of the rotation of the vortices is such that the wake becomes narrower and in addition is transported upwards. The wake deformation is described in this model by a grid transformation.

The wake at a point (x,y,z) in the field including vorticity is then found by the transformation of that point to a position (x, y_n, z_n) in the field without vorticity. Wake information at position (x, y_n, z_n) behind a 3D-screen without vorticity then is used to compute the wake at position (x,y,z). Obviously the transformation only applies to values of x > 0.

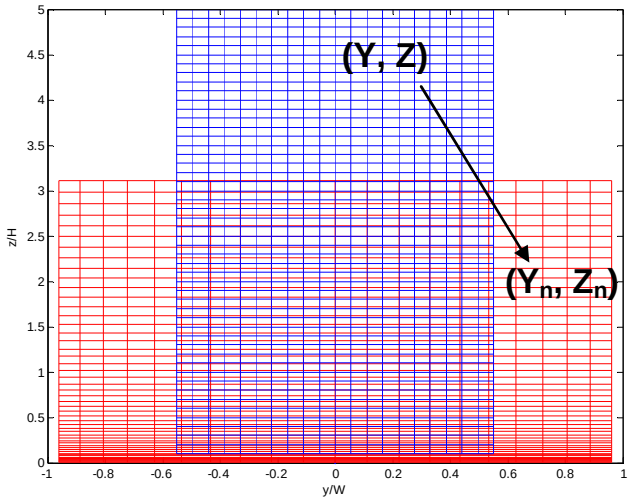

The description of the transformation starts with the definition of a so-called "amplification factor", which makes sure that the transformation has no effect at small and large values of x and also when the vorticity decreases. The factor is at maximum at a (arbitrary chosen) value of x/H=20:

$$af = -g_1 \frac{40(x/H)}{(x/H)^2 + 400} C_\Gamma \qquad (g_1=4.6)$$

The horizontal grid deformation (normal to the wind direction) results from:

$$\frac{y_n}{W} = \left[1 + w_1.af.\exp\left\{-\left(\frac{y}{W}\right)^2\right\}\right].\frac{y}{W} \qquad (w_1 = 1.0)$$

The vertical grid deformation results from:

$$a_1 = m_0 - 1$$

$$\frac{z_n}{H} = \left[1 + a_1.af.\exp\left\{-a_2\left(\frac{z}{z_{vortex} - H}\right)^2\right\}\right].\frac{z}{H} \qquad (m_0 = 0.1,\ a_2 = 0.08)$$

From this it follows for the derivatives:

$$\frac{dy_n}{dy} = 1 + w_1.af\left\{1 - 2\left(\frac{y}{W}\right)^2\right\}.\exp\left\{-\left(\frac{y}{W}\right)^2\right\}$$

$$\frac{dz_n}{dz} = 1 + a_1.af\left\{1 - 2a_2\left(\frac{z}{z_{vortex} - H}\right)^2\right\}.\exp\left\{-a_2\left(\frac{z}{z_{vortex} - H}\right)^2\right\}$$

Summarized the transformation procedure consists of:

1. Determination of the x, y, z of the aircraft in the "wake axes system",
2. Transformation of this position using the relations above to x, y_n and z_n
3. Use these new values of x, y and z to calculate the local wind using the equations in the next sections.

These relations are developed for the PDP and a wind direction of 210°.
Hereafter the general equations are presented, both valid for the PDP and a "regular" generic building.

2. Calculation of the wake behind an infinitely long wind screen (2D wind break)

For a given surface roughness z_0 and assuming an undisturbed atmospheric boundary layer it applies for the wind velocity at height z (V_a) relative to the wind velocity at a reference height of 10m (V_{10}):

$$\frac{V_a}{V_{10}} = \frac{\log(z/z_0)}{\log(10/z_0)}$$

This gives the undisturbed wind speed at screen top height V_H / V_{10} by substitution of $z=H$
For the vertical velocity gradient it follows that:

$$\frac{d\left(V_a/V_H\right)}{d\left(z/H\right)} = \frac{-1}{z/H.\log\left(z_0/H\right)}$$

Behind a wind screen the following empirical relations apply:

$$K = -\frac{2\kappa^2}{\log\left(z_0/H\right)}; \qquad (\kappa = 0.41)$$

$$\eta = \frac{z/H}{\sqrt{K.x/H}}$$

$$f_{dV} = \eta^{0.4}\left(7.8 - 2.2\eta\right)\cdot\exp\left(-0.1\eta^2\right)$$

$$\frac{\Delta V_b(z_n)}{V_H} = \frac{1-p}{x/H}\cdot f_{dV}$$

$$\frac{V_b(z)}{V_{10}} = \frac{V_a(z)}{V_{10}} - \frac{\Delta V_b(z_n)}{V_H}\cdot\frac{V_H}{V_{10}}$$

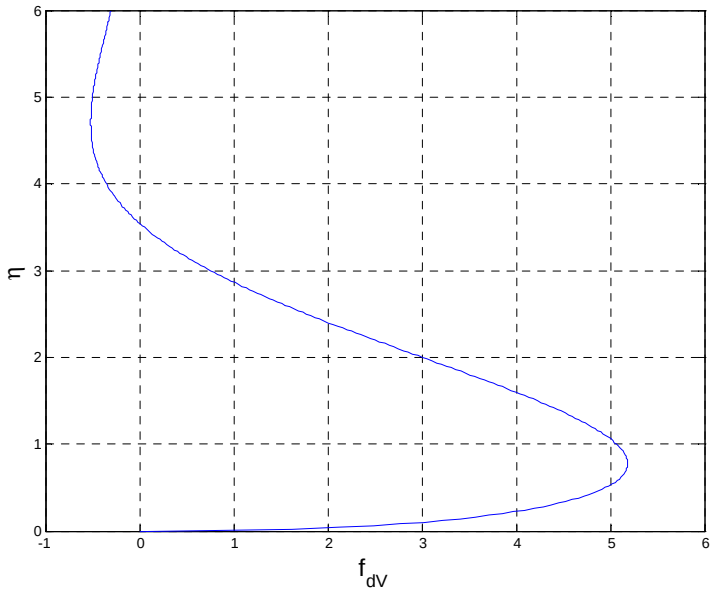

The vertical gradient behind a wind screen can be found from:

$$\frac{d\left(\Delta V_b / V_H\right)}{d\left(z_n / H\right)}\cdot(z_n) = \frac{1-p}{\left(x/H\right)^{1.5}\cdot\sqrt{K}}\cdot\left(3.12\eta^{-0.6} - 3.08\eta^{0.4} - 1.56\eta^{1.4} + 0.44\eta^{2.4}\right)\cdot\exp\left(-0.1\eta^2\right)$$

In the not-transformed grid this can be written as:

$$\frac{d\left(V_b/V_H\right)}{d\left(z/H\right)}\cdot(z) = \frac{d\left(V_a/V_H\right)}{d\left(z/H\right)}\cdot(z) - \frac{d\left(\Delta V_b/V_H\right)}{d\left(z_n/H\right)}\cdot(z_n)\cdot\frac{dz_n}{dz}\cdot(z)$$

The turbulence levels in the undisturbed atmospheric boundary layer follow from:

$$z_s = 100 z_0^{0.25}$$

$$\lambda = 0.125\{10 + \log(z/z_s)\}.\exp\left[-0.000225\{5 + \log(z/z_s)\}^4\right]$$

$$\frac{\sigma_{u,a}}{V_{10}} = \frac{\lambda}{\log(10/z_0)}$$

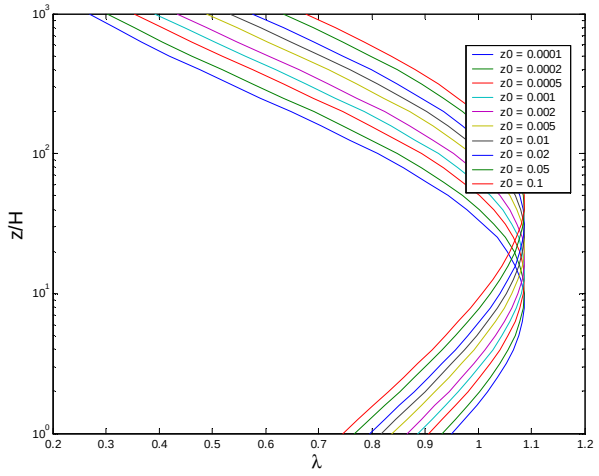

The turbulence levels behind the wind screen can be modelled empirically by:

$$f_1 = \left\{(\eta+2)^{2.75} - 2^{2.75}\right\}.\exp\left\{-0.08(\eta+1)^{2.5}\right\}$$

$$f_2 = 1.04\exp\left(-3.25p^{1.85}\right) - 0.04 \qquad (p \geq 0)$$

$$f_2 = 1 \qquad (p < 0)$$

$$\frac{\Delta(\sigma_u^2)}{V_H^2} = \frac{K}{x/H}.f_1.f_2$$

$$\frac{\sigma_{u,b}}{V_{10}}\cdot(z) = \sqrt{\left(\frac{\sigma_{u,a}}{V_{10}}\cdot(z)\right)^2 + \frac{\Delta(\sigma_u^2)}{V_H^2}\cdot(z_n)\cdot\left(\frac{V_H}{V_{10}}\right)^2}$$

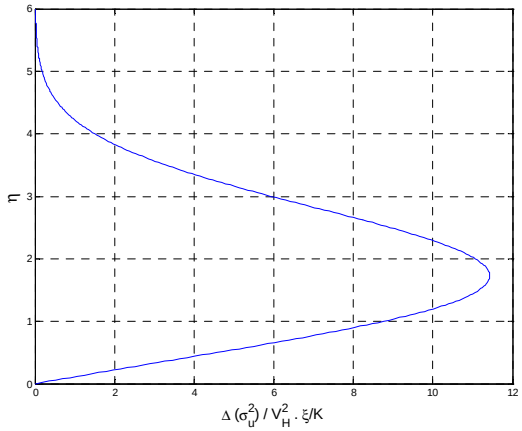

3. Correction of the 2D-wake to one including the end effects of a finite width wind screen.

The lateral proportion of the mixing area behind a single, 2D wake edged boundary can be described by mixing length theory as follows:

$$c_e = 7$$

$$\xi_{se} = c_e \cdot \frac{|y_n| - W/2}{x}$$

This relation is taken as a starting point for modelling the finite sharp-edged boundaries of an obstacle limited in height. Eventually the effects of both edges of the screen submerge into each other in the centre behind the obstacle. A better description of the wake conditions behind an obstacle with a limited W/h including edge effects can be obtained when the above formula is somewhat modified. In this way also a smoother transition in the screen centre can be achieved. The modification results in:

$$\zeta = c_e \frac{\sqrt{y_n^{\,2} + H^2} - \sqrt{\left(\tfrac{1}{2}W\right)^2 + H^2}}{x}$$

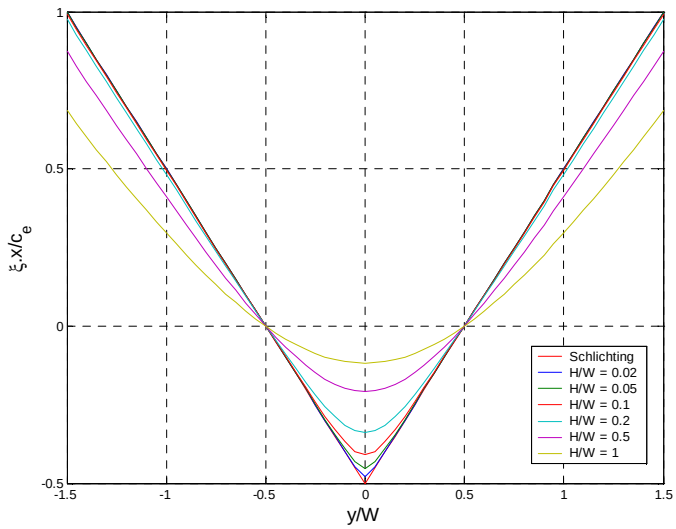

At the borders of the screen both left and right still applies ξ=0. In the centre of the screen ζ becomes les negative, depending on the relation W/H. For large values of y ζ approaches the above relationship.

The time averaged wind velocity behind a finite wind screen follows from a description in which the transition is described by the error-function in ζ:

$$erf(\zeta) = \frac{2}{\sqrt{\pi}} \int_0^{\zeta} e^{-t^2} dt$$

leading to:

$$V_{ab} = \frac{V_a + V_b}{2} + \frac{V_a - V_b}{2} . erf(\zeta)$$

In line with the "mixing length" theory it is assumed that the local turbulence can be scaled with the maximum local average wind gradient in any lateral direction.
The horizontal and vertical gradients are:

$$\frac{dV_{ab}}{dy} = \frac{1}{\sqrt{\pi}} \frac{c_e}{x} \frac{V_a - V_b}{\exp(\zeta^2)} \frac{y_n}{\sqrt{y_n{}^2 + H^2}} . \frac{dy_n}{dy}$$

$$\frac{dV_{ab}}{dz} = \frac{dV_a/dz + dV_b/dz}{2} + \frac{dV_a/dz - dV_b/dz}{2} . erf(\zeta)$$

The maximum gradient in any lateral direction the can be found from:

$$\left(\frac{dV_{ab}}{dr} \right)_{\max} = \sqrt{\left(\frac{dV_{ab}}{dy} \right)^2 + \left(\frac{dV_{ab}}{dz} \right)^2}$$

To avoid problems at low values of dV_a/dz and in particular dV_b/dz the turbulence intensities are not directly scaled with these gradients. A damping correction is applied through a factor g_1. The local turbulence intensity then follows from:

$$\sigma_{u,a_c} = \sqrt{\frac{\left(dV_{ab}/dr\right)_{\max}^2 + \left(g_1 . V_H / H\right)^2}{\left(dV_a/dz\right)^2 + \left(g_1 . V_H / H\right)^2}} . \sigma_{u,a}$$

$$\sigma_{u,b_c} = \sqrt{\frac{\left(dV_{ab}/dr\right)_{\max}^2 + \left(g_1 . V_H / H\right)^2}{\left(dV_b/dz\right)^2 + \left(g_1 . V_H / H\right)^2}} . \sigma_{u,b} \qquad (g_1 = 0.25)$$

$$\sigma_{u,ab} = \frac{\sigma_{u,a_c} + \sigma_{u,b_c}}{2} + \frac{\sigma_{u,a_c} - \sigma_{u,b_c}}{2} . erf(\xi)$$

The turbulence intensities in y en z-direction follow from the hereafter presented relations. The vertical turbulence intensity is scaled as function of height in a way that it is damped near the earth surface:

$$\frac{\sigma_{v,ab}}{V_{10}} = \frac{\sigma_{u,ab}}{V_{10}}$$

$$\frac{\sigma_{w,ab}}{V_{10}} = att(z) \cdot \frac{\sigma_{u,ab}}{V_{10}} = \sqrt[4]{\frac{z-5}{350}} \cdot \frac{\sigma_{u,ab}}{V_{10}}$$

Finally some typical parameter values for a “regular” block-shaped obstacle and the values to be applied for the PDP 210 dg wind direction configuration are presented in the following table:

AAS	H [m]	W [m]	P [-]	x [m]	C_Γ [-]
EH310	40	300	0.1	400	0
PDP, 210°	16	145	-1.0 **	350	-0.22

** A negative porosity seems strange, but is due to the fact that the shape of the PDP generates a deep wake and sweeps the wake together behind a small part of the wind screen. The resulting wake does not resemble that of a porous screen but looks in fact more than solid screen. The negative porosity, gives a deeper wake. The choice of the porosity above is based on a comparison with wind tunnel results. Note that a surface roughness of 0.1 is fairly large for Schiphol, but this value was chosen as the wind tunnel test was performed at this value of z_0.

Appendix C Pilot ratings

- **Cooper-Harper rating scale for flight handling**

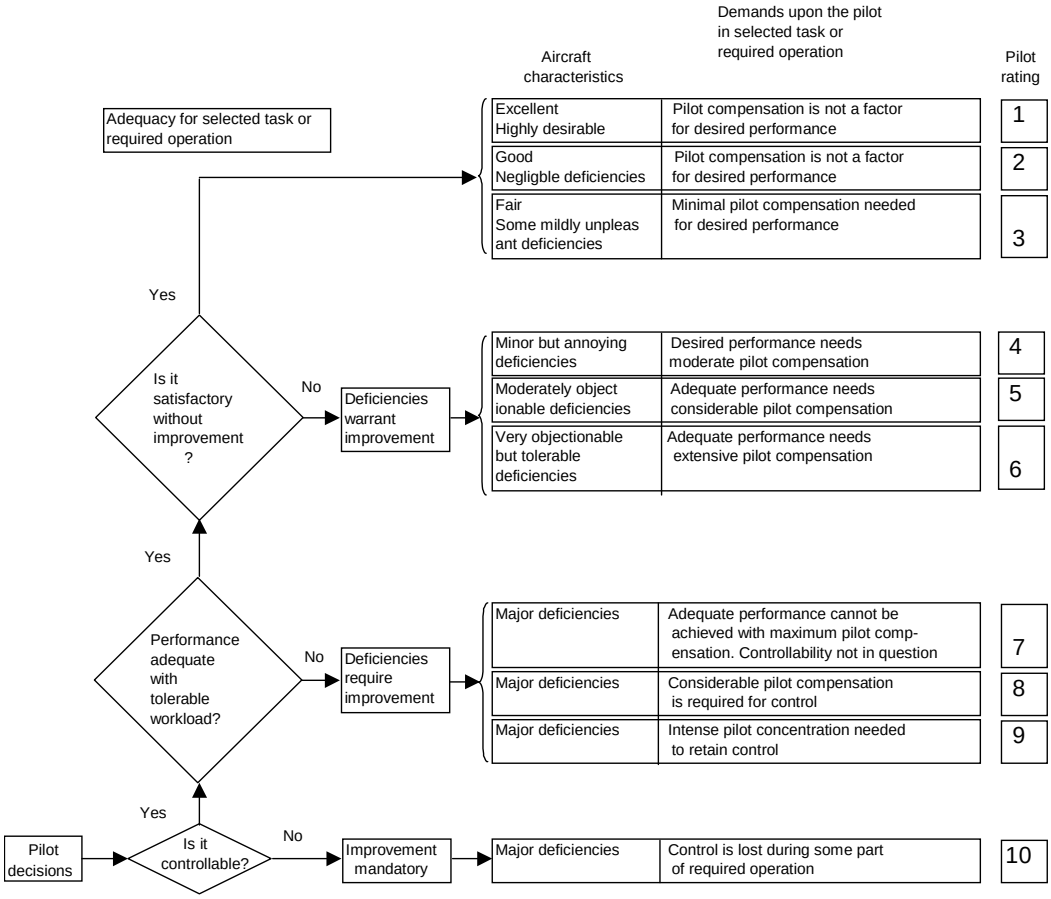

- **Overall work load rating**

On the scale below, indicate by a circle (approach) or cross (landing) your level of workload experienced during the landing segment:

1. Indicate the hazard of the crosswind experienced during this run:

☐ none ☐ light ☐ moderate ☐ heavy ☐ extreme ☐ very extreme (crash)

2. Was a landing made? ☐ Yes ☐ No (goto 5)

3. If 'yes' was it a safe landing? ☐ Yes (goto 5) ☐ No

4. If NOT a safe landing, why not? (choose MORE than ONE category if appropriate):

☐ Exceeding bank angle limits
☐ Too high a speed at touchdown
☐ Too high a sink rate
☐ Landed too short
☐ Landed too long
☐ Other (specify):

……

5. Using the scales below, rate your effort to control: Approach/TO: O Land: X

a. speed

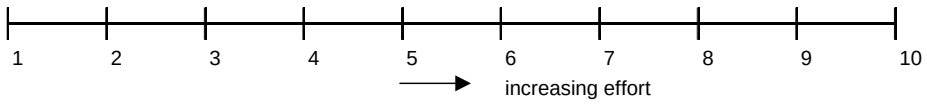

b. bank angle

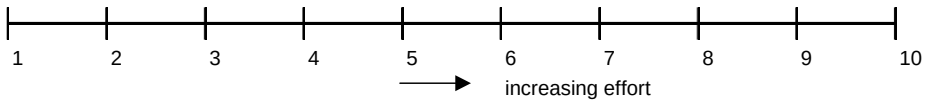

c. pitch angle

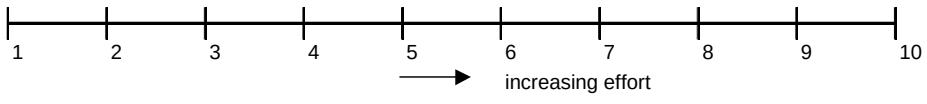

d. glide slope/vertical speed

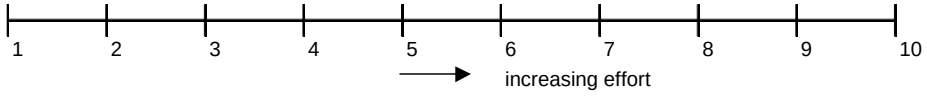

e. Localiser/heading

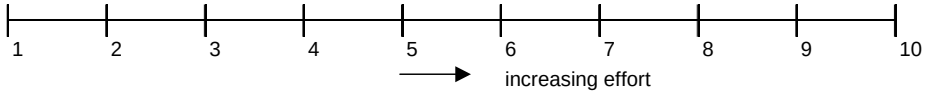

6. Rate below the overall (mental) workload Approach/TO: O Land: X

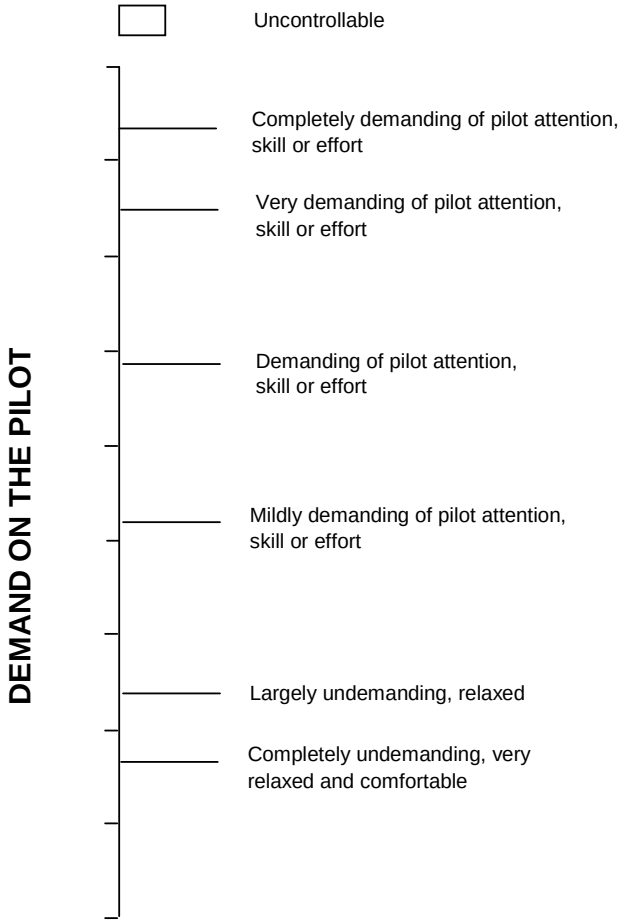

Appendix D Atmospheric model

The effect of turbulent air on aircraft behavior can be modeled as additional aerodynamic forces (X_g, Y_g, Z_g) and moments (L_g, M_g, N_g) acting on the aircraft. These extra forces and moments are then functions of the gust velocities u_g, v_g and w_g.

$$\begin{bmatrix} X \\ Y \\ Z \end{bmatrix}_{total} = \begin{bmatrix} X \\ Y \\ Z \end{bmatrix}_{non-linear\ aircraft} + \begin{bmatrix} X \\ Y \\ Z \end{bmatrix}_{g}$$

$$\begin{bmatrix} L \\ M \\ N \end{bmatrix}_{total} = \begin{bmatrix} L \\ M \\ N \end{bmatrix}_{non-linear\ aircraft} + \begin{bmatrix} L \\ M \\ N \end{bmatrix}_{g}$$

For aircraft flight dynamics it is common practice to express these forces and moments in non-dimensional coefficients as follows,

$$C_{X_g} = \frac{X_g}{\frac{1}{2}\rho \mathrm{V}^2 \mathrm{S}} \quad C_{Y_g} = \frac{Y_g}{\frac{1}{2}\rho \mathrm{V}^2 \mathrm{S}} \quad C_{Z_g} = \frac{Z_g}{\frac{1}{2}\rho \mathrm{V}^2 \mathrm{S}}$$

$$C_{L_g} = \frac{L_g}{\frac{1}{2}\rho \mathrm{V}^2 \mathrm{S}\overline{\mathrm{c}}} \quad C_{M_g} = \frac{M_g}{\frac{1}{2}\rho \mathrm{V}^2 \mathrm{S}\overline{\mathrm{c}}} \quad C_{N_g} = \frac{N_g}{\frac{1}{2}\rho \mathrm{V}^2 \mathrm{S}\overline{\mathrm{c}}}$$

Similarly, non-dimensional equivalents are used for describing the dependency of these flight dynamics on the turbulence field (u_g, v_g, w_g), assuming that these gust velocities are relatively small with respect to V. The non-dimensional parameters are $\hat{u}_g = \frac{u_g}{V}$, the gust slip angle $\beta_g = \frac{v_g}{V}$ and the gust angle of attack $\alpha_g = \frac{w_g}{V}$. For simplicity, the dependency of the gust forces an moments on these variables using series expansion will be limited to linear terms only, giving a linear aircraft gust response model.

The aircraft response to atmospheric turbulence can be split up in a symmetric motion component and an asymmetric motion component. The symmetric response of the aircraft, defined by the longitudinal forces X_g and Z_g, and the longitudinal moment M_g, only depends on the varying longitudinal gust components $\hat{u}_g$ and α_g acting in the centre of gravity.

Consequently, the longitudinal non-dimensional force and moment coefficients can be expressed as follows,

$$C_{X_g} = C_{X_{u_g}} \hat{u}_g + C_{X_{\dot{u}_g}} \frac{\dot{\hat{u}}_g \overline{c}}{V} + C_{X_{\alpha_g}} \alpha_g + C_{X_{\dot{\alpha}_g}} \frac{\dot{\alpha}_g \overline{c}}{V}$$

$$C_{Z_g} = C_{Z_{u_g}}\hat{u}_g + C_{Z_{\dot{u}_g}}\frac{\dot{\hat{u}}_g\bar{c}}{V} + C_{Z_{\alpha_g}}\alpha_g + C_{Z_{\dot{\alpha}_g}}\frac{\dot{\alpha}_g\bar{c}}{V}$$

$$C_{m_g} = C_{m_{u_g}}\hat{u}_g + C_{m_{\dot{u}_g}}\frac{\dot{\hat{u}}_g\bar{c}}{V} + C_{m_{\alpha_g}}\alpha_g + C_{m_{\dot{\alpha}_g}}\frac{\dot{\alpha}_g\bar{c}}{V}$$

where $C_{X_{u_g}}$ $C_{X_{\dot{u}_g}}$, etc. represents the partial derivatives of the force/moment with respect to the listed non-dimensional gust parameter. These coefficients are called 'gust derivatives' and are aircraft dependent. The values of the gust derivatives depend on the stability derivatives of the aircraft and can be approximated with the formulas presented in Table C-1. Approximated values for the B747-200 are derived from literature ([34] and ([35] or estimated through evaluation of the B747-200 model.

What remains to be defined are the turbulence field inputs and their derivatives ($\hat{u}_g$, $\dot{\hat{u}}_g$, α_g and $\dot{\alpha}_g$) acting in the aircraft's centre of gravity.

Table C-1: Calculation of the symmetric gust derivatives

$C_{X_{u_g}} = C_{X_u}$ = -0.42	$C_{Z_{u_g}} = C_{Z_u}$ = -2.98	$C_{m_{u_g}} = C_{m_u}$ = -0.185
$C_{X_{\dot{u}_g}} = 0$	$C_{Z_{\dot{u}_g}} = 2C_{m_{ac}} = 0$	$C_{m_{\dot{u}_g}} = -2C_{m_h}\frac{l_h}{\bar{c}}$ = 0.74
$C_{X_{\alpha_g}} = C_{X_\alpha}$ = 1.59	$C_{Z_{\alpha_g}} = C_{Z_\alpha}$ = -5.293	$C_{m_{\alpha_g}} = C_{m_\alpha}$ = -0.1
$C_{X_{\dot{\alpha}_g}} = 0$	$C_{Z_{\dot{\alpha}_g}} = C_{Z_\alpha} - C_{Z_q}$ = 13.36	$C_{m_{\dot{\alpha}_g}} = C_{m_\alpha} - C_{m_q}$ = 21.4

A gust velocity field that is encountered along the aircraft's flight path, can be described with a one-dimensional turbulence model characterized by the known Dryden spectral densities. The general state-space description for the corresponding forming filters can be written as,

$$\dot{u}_g(t) = -\frac{V}{L_g}u_g(t) + \sigma_{u_g}\sqrt{\frac{2V}{L_g}}\omega_1(t)$$

$$\begin{bmatrix}\dot{v}_g(t)\\ \dot{v}_g^*(t)\end{bmatrix} = \begin{bmatrix}0 & 1\\ -\frac{V^2}{L_g^2} & -2\frac{V}{L_g}\end{bmatrix}\begin{bmatrix}v_g(t)\\ v_g^*(t)\end{bmatrix} + \begin{bmatrix}\sigma_{v_g}\sqrt{\frac{3V}{L_g}}\\ \left(1-2\sqrt{3}\right)\sigma_{v_g}\sqrt{\left(\frac{V}{L_g}\right)^3}\end{bmatrix}w_2(t)$$

$$\begin{bmatrix} \dot{w}_g(t) \\ \dot{w}_g^*(t) \end{bmatrix} = \begin{bmatrix} 0 & 1 \\ -\frac{V^2}{L_g^2} & -2\frac{V}{L_g} \end{bmatrix} \begin{bmatrix} w_g(t) \\ w_g^*(t) \end{bmatrix} + \begin{bmatrix} \sigma_{w_g}\sqrt{\frac{3V}{L_g}} \\ \left(1-2\sqrt{3}\right)\sigma_{w_g}\sqrt{\left(\frac{V}{L_g}\right)^3} \end{bmatrix} w_3(t)$$

where $w_1(t)$, $w_2(t)$ and $w_3(t)$ are three independent white noise inputs driving the turbulence generating filters. The integral scale of length L_g is a measure that reflects the scale of the turbulence. For landing, an average L_g of 150 m can be chosen. The standard deviations σ of the turbulence components are calculated with the applicable wind climate model of section 4. Dividing the generated turbulence velocities by V gives the desired non-dimensional equivalents.

The asymmetric aircraft motion is more complicated since the gust velocities u_g and w_g vary along the lateral axis resulting in a span wise distributed turbulence field that effects the rolling and yawing moments of the aircraft. Consequently, atmospheric turbulence now has to be considered as a two-dimensional process. The contribution of the side gust velocity v_g can still be evaluated in the center of gravity of the aircraft. Another gust model is required that include the average relations between longitudinal and vertical gust velocities in two different points on the aircraft's body. New shaping filters for the turbulence input of the asymmetric rolling and yawing moments are created,

$$\begin{bmatrix} \dot{\hat{u}}_g(t) \\ \dot{\hat{u}}_g^*(t) \end{bmatrix} = \begin{bmatrix} 0 & 1 \\ -\frac{1}{\tau_1\tau_2}\left(\frac{V}{L_g}\right)^2 & -\frac{\tau_1+\tau_2}{\tau_1\tau_2}\frac{V}{L_g} \end{bmatrix} \begin{bmatrix} \hat{u}_g(t) \\ \hat{u}_g^*(t) \end{bmatrix} + \begin{bmatrix} \frac{\tau_3}{\tau_1\tau_2}\sqrt{\frac{V}{L_g}I_{\hat{u}_g}(0,B)} \\ \left(1-\frac{\tau_3(\tau_1+\tau_2)}{\tau_1\tau_2}\right)\frac{1}{\tau_1\tau_2}\sqrt{\left(\frac{V}{L_g}\right)^3 I_{\hat{u}_g}(0,B)} \end{bmatrix} w_1(t)$$

$$\begin{bmatrix} \dot{\alpha}_g(t) \\ \dot{\alpha}_g^*(t) \end{bmatrix} = \begin{bmatrix} 0 & 1 \\ -\frac{1}{\tau_4\tau_5}\left(\frac{V}{L_g}\right)^2 & -\frac{\tau_4+\tau_5}{\tau_4\tau_5}\frac{V}{L_g} \end{bmatrix} \begin{bmatrix} \alpha_g(t) \\ \alpha_g^*(t) \end{bmatrix} + \begin{bmatrix} \frac{\tau_6}{\tau_4\tau_5}\sqrt{\frac{V}{L_g}I_{\alpha_g}(0,B)} \\ \left(1-\frac{\tau_6(\tau_4+\tau_5)}{\tau_4\tau_5}\right)\frac{1}{\tau_4\tau_5}\sqrt{\left(\frac{V}{L_g}\right)^3 I_{\alpha_g}(0,B)} \end{bmatrix} w_3(t)$$

In the above equations, the variables $I_{\hat{u}_g}(0,B)$, $I_{\alpha_g}(0,B)$ and τ_1 till τ_6 are part of the so-called effective one-dimensional power spectral densities which approximates the actual power

spectral densities of the rolling and yawing moments due to turbulence. The values of these parameters (Table C-2) depend on the factor $B = \frac{b}{2L_g} = \frac{59.64}{2 \cdot 150} = 0.1988$ for a B747-200.

Table C-2: The variables of the approximated effective power spectral density function of the horizontal and vertical gust velocity for B = 0.1988 ([34]

$I_{\hat{u}_g}(0,B)$ = 0.2519903 $\sigma^2_{\hat{u}_g}$	τ_1 = 0.288690	τ_2 = 0.747955	τ_3 = 0.590821
$I_{\alpha_g}(0,B)$ = 0.1794823 $\sigma^2_{\alpha_g}$	τ_4 = 0.218703	τ_5 = 0.488882	τ_6 = 0.390730

The filter that generates the gust side slip angle β_g is identical to the Dryden turbulence filter which is valid in the centre of gravity,

$$\begin{bmatrix} \dot{\beta}_g(t) \\ \dot{\beta}^*_g(t) \end{bmatrix} = \begin{bmatrix} 0 & 1 \\ -\left(\frac{V}{L_g}\right)^2 & -2\frac{V}{L_g} \end{bmatrix} \begin{bmatrix} \beta_g(t) \\ \beta^*_g(t) \end{bmatrix} + \begin{bmatrix} \sigma_{\beta_g}\sqrt{\frac{3V}{L_g}} \\ \left(1-2\sqrt{3}\right)\sigma_{\beta_g}\sqrt{\left(\frac{V}{L_g}\right)^3} \end{bmatrix} w_2(t)$$

Again, a linear aircraft response model can be created that reflects the contribution of these asymmetric gust inputs on the flight dynamics [3],

$$C_{Y_g} = C_{Y_\beta}\beta_g + C_{Y_{\dot{\beta}_g}}\frac{\dot{\beta}_g b}{V}$$

$$C_{l_g} = C_{l_{u_g}}\hat{u}_g + C_{l_{\beta_g}}\beta_g + C_{l_{\dot{\beta}_g}}\frac{\dot{\beta}_g b}{V} + C_{l_{\alpha_g}}\alpha_g$$

$$C_{n_g} = C_{n_{u_g}}\hat{u}_g + C_{n_\beta}\beta_g + C_{n_{\dot{\beta}_g}}\frac{\dot{\beta}_g b}{V} + C_{n_{\alpha_g}}\alpha_g$$

The asymmetric gust derivatives can be calculated as indicated in Table C-3. Approximated values for the B747-200 are derived from literature ([34] and ([35] or estimated through evaluation of the B747-200 model. Note: index ‘w’ indicates that only the contribution of the wing is taken.

The contribution of $\dot{\beta}_g$ has been omitted for the Boeing 747-200 since the values of the corresponding gust derivatives could not be retrieved adequately. Usually the effect of $\dot{\beta}_g$ may be neglected when considering an aircraft with a straight wing and relatively small tail planes. This is however not applicable for a Boeing 747-200. However, it is expected that this simplification is not essential for the goal of this research project.

Table C-3: Calculation of the asymmetric gust derivatives

$C_{Y_{u_g}} = 0$	$C_{l_{u_g}} = -C_{l_{r_w}} = -0.7C_{l_r}$ = 0.137	$C_{n_{u_g}} = -C_{n_{r_w}} = -0.2\,C_{n_r}$ = 0.072
$C_{Y_{\beta_g}} = C_{Y_\beta}$ = -1.08	$C_{l_{\beta_g}} = C_{l_\beta}$ = -0.281	$C_{n_{\beta_g}} = C_{n_\beta}$ = 0.184
$C_{Y_{\dot{\beta}_g}} = C_{Y_{\dot{\beta}}} + \frac{1}{2} C_{Y_{r_{f+v}}}$ = 0	$C_{l_{\dot{\beta}_g}} = C_{l_{\dot{\beta}}} + \frac{1}{2} C_{l_{r_{f+v}}}$ = 0	$C_{n_{\dot{\beta}_g}} = C_{n_{\dot{\beta}}} + \frac{1}{2} C_{n_{r_{f+v}}}$ = 0
$C_{Y_{\alpha_g}} = 0$	$C_{l_{\alpha_g}} = C_{l_{p_w}} = 0.8\,C_{l_p}$ = 0.402	$C_{n_{\alpha_g}} = C_{n_{p_w}} = 0.9\,C_{n_{p_w}}$ = -0.1998